Numerical Well Testing of Coalbed Methane (CBM) Reservoir

Lili Xue

Submitted for the degree of Doctor of Philosophy

Heriot-Watt University

Institute of Petroleum Engineering

September 2012

ABSTRACT

Numerical experiments and field applications proved that there exist percolation non-linearity and fluid multi-variability in low permeability CBM reservoirs. The percolation of fluid needs to overcome threshold pressure gradient, and klinkenberg effects will restrict the gas permeability. In addition, production enhancement and ultimate recovery improvement have given multi-branch horizontal wells the advantage over the vertical wells in many CBM marginal reservoirs. Moreover, Enhance Coalbed Methane (ECBM) recovery through injection of gases has been publicly proven, and can increase gas resources, however, its application in some actual field failed to address the good history matching.

In this thesis, the numerical simulation and well testing problems encountered in the reservoir exploration and production are investigated. Firstly, a new dual porosity, single permeability model was developed, which reflects the high velocity non-Darcy flow that considers the threshold pressure, gas slippage and matrix shrinkage effects. It is solved using the fully implicit numerical method, a computer programme called COAFOR has been developed for this purpose.

Secondly, an advanced non-analytical coupled CBM model is developed for predicting the flux in the CBM reservoir and single or multi-branch wellbore simultaneously. Thirdly, a coupled compositional triple porosity horizontal wellbore model for CBM reservoir considering the gas slippage and threshold pressure gradient effects is proposed with a newly developed permeability model. The simulator, called TRIPLE-COAL, was developed for this model.

Finally, the new models developed in this thesis are validated by applying them into Heshun block, Yanchun South block and Zhijin block respectively. The history matching results checked the reasonability and accuracy of the models built in this thesis. The coupled multi-branch horizontal triple porosity model shows better matching result in Zhijin block than the coupled multi-branch horizontal dual porosity model in Yanchuan South block.

To my parents,
who gave me endless love and support.

Acknowledgements

I would like to express my sincere gratitude to my supervisor Professor Shiyi Zheng in London South Bank University, originally works for Heriot-Watt University for providing me with the opportunity to study as a PhD student in the Institute of Petroleum Engineering of Heriot-Watt University, and also for his guidance and constant support throughout my course of PhD study. I would also like to extend my appreciation to my second supervisor James M. Somerville for his help to my study.

I would like to thank BG group, Wintershall Holding AG and Petro China for their financial support that providing me with tuition fees. Schlumberger is gratefully thanked for providing with the simulation and numerical well testing analysis software.

I am also very grateful to the academics, research staff, secretaries, librarian and those who helped during the course of this study in the Institute of Petroleum Engineering at Heriot-Watt University. Many thanks to the committee members, friends, and colleagues in the PRIME project group, especially my group mates: Wenbin Xu, Fei Wang, Fuyong Wang, Yiqun Zhang and Haiyun Yan.

Special thanks would like to be given to my friend Prof. Dorrik Stow, Prof. Mike Christie, Prof. Colin MacBeth, Dr. Peter Olden, Dr. Min Jin, Alison Proud, Dr. Dan Arnold, Prof. Eric Mackay, Dr. Jingsheng Ma, Dr. Kejian Wu and Dr. Zeyun Jiang. Their advice, suggestions, and help are gratefully appreciated.

In separate, my dedication goes to my parents for their constant support and encouragements throughout all my school years. I send you all my love and warm hugs from the distance. I could not survive without your constant guidance, support and love.

ACADEMIC REGISTRY

Research Thesis Submission

Name*:*	**LILI XUE**		
School/PGI:	**Institute of Petroleum Engineering (IPE)**		
Version: *(i.e. First, Resubmission, Final)*	**Final**	Degree Sought (Award **and** Subject area)	**PhD**

Declaration

In accordance with the appropriate regulations I hereby submit my thesis and I declare that:

1) the thesis embodies the results of my own work and has been composed by myself
2) where appropriate, I have made acknowledgement of the work of others and have made reference to work carried out in collaboration with other persons
3) the thesis is the correct version of the thesis for submission and is the same version as any electronic versions submitted*.
4) my thesis for the award referred to, deposited in the Heriot-Watt University Library, should be made available for loan or photocopying and be available via the Institutional Repository, subject to such conditions as the Librarian may require
5) I understand that as a student of the University I am required to abide by the Regulations of the University and to conform to its discipline.

* *Please note that it is the responsibility of the candidate to ensure that the correct version of the thesis is submitted.*

Signature of Candidate*:*		Date:	

Submission

Submitted By *(name in capitals):*	**LILI XUE**
Signature of Individual Submitting:	
Date Submitted:	

For Completion in the Student Service Centre (SSC)

Received in the SSC by *(name in capitals):*			
Method of Submission *(Handed in to SSC; posted through internal/external mail):*			
E-thesis Submitted (**mandatory for final theses)**			
Signature:		Date:	

TABLE OF CONTENTS

LISTS OF FIGURES

LISTS OF TABLES

Nomenclature

Symbols:

k_l : Permeability, md

k_{lrg} : Relative permeability to gas phase, fraction

k_{lrw} : Relative permeability to water phase, fraction

k_0 : Fracture permeability at initial time, md

B_{lg} : Gas phase FVF, rm^3 /sm^3 or rb /Mscf

B_{lw} : Water phase FVF, rm^3 /sm^3 or rb /stb

p_{lg} : Gas pressure, MPa or Psi

p_{lw} : Water pressure, MPa or Psi

p_{wf} : Well bottom-hole pressure of the coal seam, MPa or Psi

p_{Li} : Langmuir pressure of component i, MPa or Psi

Δp_{fric_i} : Wellbore friction pressure drop, MPa or Psi

Δp_{acc_i} : Wellbore acceleration pressure drop, MPa or Psi

$p^{'}$: Net output pressure squared difference, MPa or Psi

s_{lg} : Gas phase saturation, fraction

s_{lw} : Water phase saturation, fraction

D_l : Diffusion coefficient, fraction

q_{afg} : Gas cross flow from macro-pore system to the cleat system, m^3/day or Mscf/day

q_{afw} : Water cross flow from macro-pore system to the cleat system, m^3/day or Mscf/day

q_{mag} : Volumetric gas transfer from coal surface to macro-pore system, m^3/day or Mscf/day

q_{fvg} : Volumetric gas production rate in cleat system, m^3/day or Mscf/day

q_{fvw} : Volumetric water production rate in cleat system, m^3/day or stb/day

Q_i : Gas flux from branch to the main stream, m^3/day or Mscf/day

Q_{Ri} : Gas flux from the wellbore adjacent upstream segment flow into the current segment, m^3/day or Mscf/day

q_i : Gas flux of the formation flow, $q_i = q_{wi} + q_{gi}$, m^3/day or Mscf/day

$Q_{\max}$: Hoped maximal gas flow rate, m^3/day or Mscf/day

x_f : Half fracture length, m or ft

h : Thickness of the coal seam, m or ft

r_w : Well radius, m or ft

r_e : Drainage area radius, m or ft

r_b : Well segment length in the grid system, m or ft

D : Wellbore diameter, m or ft

V_0 : Gas molar volume under standard condition, 22.4L/mol, m^3/t or scf/cu ft

V_{Li} : Langmuir volume of component i, m^3/t or scf/cu ft

y_i : Mole fraction of the component i, fraction

c_f : Rock compressibility, 1/MPa or 1/Psi;

c_t : Total compressibility, 1/MPa or 1/Psi;

V_{im} : Average matrix gas concentration for component i, kg/ m^3 or scf/ft^3

$V_{iE}(p_{ag})$: Equilibrium methane concentration for component i, kg/ m^3 or scf/ft^3

τ : Sorption time, d

z : Gas compressibility factor, dimensionless

V_H : Henry adsorption, constant

K_c : Henry constant

V_p : Freudlich coefficient, fraction

E : Young's modulus of coal, MPa or Psi

K : Bulk modulus of coal, MPa or Psi

M : Constrained axial modulus, md

T_g : Conductivity coefficient, dimensionless

T_D : Diffusivity coefficient, dimensionless

A : Main stream cross-section area, m^2/ft^2

S : Skin factor, $S = -\ln(\frac{x_f}{2r_w})$, dimensionless

T_D : Diffusivity coefficient

V_{vi} : Segment well velocity, m^3/h or ft^3/h

V_{Ri} : Velocity from branch to the main stream, m^3/h or ft^3/h

$\overline{V_i}$: Average fluid velocity within corresponding segment, m^3/h or ft^3/h

K_i : Equivalent isotropic permeability, md

f_0 : Initial fraction factor, fraction.

N_{Re} : Reynolds number, constant

R : Universal gas constant, 8.3143 J/(mol.K)

T : Absolute temperature, K

r_{sw}: Ratio of the dissolved gas in the water phase, fraction

Greek:

∇: Vector factor

β_1, β_2 : Gas slippage effect experimental factor, fraction

$\alpha_1, \alpha_2, \alpha_3, \alpha_4$: Threshold pressure gradient effect experimental factor, fraction

ν : Poisson ratio, fraction

μ_{lg} : Gas-phase viscosity, mPa·s

μ_{lw} : Water-phase viscosity, mPa·s

μ_i: Fluid viscosity in corresponding wellbore segment, mPa·s

ϕ_l : Porosity, fraction

$\Delta\phi_f$: Fracture porosity variation induced by the matrix shrinkage, fraction

ϕ_{fr} : Critical fracture porosity, fraction

λ_g : Gas phase effective mobility, fraction

λ_w: Water phase effective mobility, fraction

λ_t: Total effective mobility, fraction

σ : Effective horizontal stress, MPa or Psi

γ_0 : Coal surface energy under vacuum condition, J/ft^3 or J/m^3

γ : Coal surface energy after gas is adsorbed, J/ft^3 or J/m^3

$\Delta\gamma$: Variation of surface energy, J/ft^3 or J/m^3

ε_s : Relative deformation factor, fraction

φ : Angle between main stream and branch, degree

ω : Angle between main stream and branch, degree

Γ : Outer boundary of the CBM reservoir

ρ_{lg} : Gas phase density, kg/m^3 or scf/ft^3

ρ_{lw} : Water phase density, kg/m^3 or scf/ft^3

Subscripts:

$l = a, f$: Macro-pore system and cleat system respectively.

a : Macro-pore system

f : Cleat system

i : Integer from 1 to n

w : Wellbore or water

t : Total

c : Capillary

g : Gas

sw : Solved gas in water phase

LIST OF PUBLICATIONS

Zheng, S.Y. and Xue, L.L.. Modelling and simulation of a new dual porosity CBM reservoir model with an improved permeability model through horizontal wells. SPE141118, SPE Middle East Unconventional Gas Conference and Exhibition, 31 January-2 February 2011, Muscat, Oman.

Zheng, S.Y. and Xue, L.L.. An advanced multi-lateral horizontal well coupled CBM Simulation model and its application in Qinshui Basin of China. SPE 149956, SPE/EAGE Unconventional resources conference and exhibition, 20-22 March 2012, Vienna, Austria.

Xue, L.L. and Zheng, S.Y.. A New Coupled Coalbed Methane (CBM) Reservoir Model and its application in the field, accepted (19/03/2012), in press, International Journal of Mining Science and Technology.

Xue, L.L. and Zheng, S.Y.. Novel insights for enhanced coalbed methane technology, submitted to 'Journal of Petroleum Science and Engineering'.

Xue, L.L. and Zheng, S.Y.. Calibration of coalbed methane reservoir models through sensitivity analysis and their application in the field, submitted to 'Journal of Canadian Petroleum Technology'.

Hu, X.H., Xue, L.L., Long S.X. and Zheng, S.Y.. Application of a novel Flowing Material Balance Technique During gas-water flow for Unsaturated coalbed methane (CBM) Reservoirs, submitted to 'Journal of Petroleum Science and Engineering'.

Chapter 1 Introduction

1.1 Background

1.1.1 Development of CBM reservoir abroad

The main component of CBM is CH_4, known as the self-storage and non-conventional natural gas present in CBM reservoirs, and similar to the conventional natural gas, it is a very clean fossil energy. And its reserve is approximately the same order of magnitude as that of oil and natural gas together. But due to the limit of the available technology in the exploration and evaluation technology, the huge CBM reserve has not been effectively found.

Several workers analyzed 985 samples of 1380 CBM wells in American, and concluded that the average composition of CBM is: 93.2% CH_4, 2.6% heavy hydrocarbons, 3.1% CO_2, 1.1% N_2. Some Chinese scholars also studied the component of 358 Chinese samples, and found that the composition is: 85%-93% CH_4, less than 2% CO_2, less than 10% N_2.

The current global energy structure is: 36% oil, 26% coal, 23% natural gas, 15% others (hydropower, nuclear power etc). The shares of unconventional gas among the global energy structure will be more than natural gas around 2013, and it will be more than oil around 2020, which means the unconventional gas will have a leading role among the future world energy.

Nowadays, CBM is gradually being widely focused by every country in the world as the alternative energy resource of oil and conventional natural gas in the next few decades. The main drivers for this move are the continuously reducing cost of coal seam gas production and the depleting conventional energy resources. The estimated largest amount of CBM reserves are as follows (**Table 1.1**).

Country	Estimated largest amount of CBM	Country	Estimated largest amount of CBM
Russia	113	Poland	3
Canada	37	England	2
China	30—35	Ukraine	2
America	21.4	Kazakhstan	1
Australia	8.6—14	India	0.8
Germany	3	South Africa	0.8

Table 1.1 CBM Reserve of Major Coal-Producing Country in the World ($10^{12}m^3$)

American, Canada, Australia and United Kingdom are in the forefront of the world in the development and study of CBM reservoirs, especially America which started the industry for CBM fields with an annual production less than 100 million cubic meters since 1970s, while it began its commercial extraction phase in the early 80s owing to the improvement of drilling and exploration technology. The annual production has been around 350 million cubic meters since 1990s, and Coalbed Methane accounted for 8.8% of the gas reserves and 9.2% of the annual output at the end of 2000. In addition, its production reached 452.8 million cubic meters in 2003, 500 million cubic meters in 2004. The United States has drilled more than 8200 Coalbed Methane wells at the end of 2005, and the Coalbed Methane production is 10% of the total natural gas production.

The development of CBM reservoirs has been very fast in Canada. There were only 250 CBM wells before 2001 in Canada. However, the CBM wells increased by more than 1000 from 2002 to 2003 with daily methane production 3000-7000 cubic meters per well. European countries had a long history in methane drainage and usage, but the surface development of CBM is still in its infancy. The total CBM resources are about 20 thousand million cubic meters in the four British coalfields (South, central, north and Scotland area). In addition, 45% CBM wells in UK are horizontal wells due to its low permeability characteristics.

The CBM exploration in Australia began in 1976, mainly concentrated in the Queensland BaoEn basin. And the Coalbed Methane had been produced successfully through drilling from 1987 to 1988, its production increased year by year since 1996. 277 CBM wells were increased in 2004 with production rate going to 13.56 million cubic meters per year; 78% comes from Queensland, meeting 31% of the state's gas needs.

1.1.2 Development of CBM reservoir in China

Underground mining is the main exploration method in China, the world's largest coal production countries. The development and utilization of CBM has risen to a high strategic level in China as the energy supplies are being tight and the environmental protection requirement is being higher.

Currently, the problem is that it is difficult to form the stable industrial gas currents for the CBM reservoir in many blocks. This is because it has its own disadvantages:

1) There are mainly three 'low' characteristics for the CBM reservoir in China: low pressure (pressure coefficient is lower than 0.8), low porosity (lower than 70%) and low permeability. The permeability is generally around 0.001-0.0001 μm^2.

2) The coal reservoir characteristic test, fracturing and exploitation technologies that are suitable for the complex geological conditions of China are not perfect, and they are still in development.

3) The area that has industrial exploitation value mainly distributes in the middle rank coal seam, while low rank coal seam and high rank coal seam occupies the biggest proportion in China, which is a serious problem for the exploration. Theoretically, the gas production ability for low rank coal seam is very low, and the high rank coal seam even doesn't have gas production ability, this is caused by the extremely low permeability and low desorption ability respectively.

4) The stimulation technology that is suitable for the Chinese CBM reservoir characteristics is not perfect in the CBM exploitation and enhancement of low permeability CBM production. This is because the coal mine experts are not familiar with the exploitation of natural gas, and the natural gas experts are not familiar with the exploitation of Coalbed Methane (conventional natural gas is mainly free gas, while Coalbed Methane is mainly the adsorption gas CH_4). Presently, most of the basic theories for CBM reservoir development come from the conventional natural gas exploitation idea and can't completely adapt to the special characteristics of CBM reservoir in China.

From this point of view, the large scale development of CBM reservoir in China is limited, thus there are still a lot of tasks for the oil and gas experts to do for the CBM reservoir exploration and development.

1.2 Exploration mechanism and production characteristics

1.2.1 Models used in CBM reservoir simulation

Reservoir model typically utilized for desorption-controlled reservoirs is dual porosity/single permeability model. In this case dual porosity means that two in-situ locations exist that can be used for gas storage and gas adsorption: matrix system and cleat system. Single-permeability, which refers to the cleat system, is the only

permeability network that gas or water must flow to reach the wellbore. The model is shown in (**Figure 1.1)**. It is the idealized Warren & Root sugar-cube model.

This approach to model coals and shale has become accepted practice. Experience has shown that the models can frequently be in gross error when forecasting well or field performance based on limited reservoir; gas production is usually over-predicted and water production under-predicted. While performing reservoir studies in shale and low-rank coal plays throughout the world, it became clear that the accepted assumption of gas desorbing directly from the coal matrix into the cleat system is not entirely valid. In practice, gas production occurs much later than the models predict, and cannot be adequately explained though the normal parameters of sorption time, permeability, relative permeability, etc. Analysis of core and other data suggests that another porosity and permeability system is required to account for this effect, especially within the matrix blocks themselves. An advanced, triple-porosity/dual permeability model (**Figure 1.2**) has therefore been developed, in which gas desorbs from the internal matrix block surfaces, migrates via conventional Darcy flow through micro-permeability matrix, and into the cleat system where it then flows to the wellbore. Water can also be stored both within the matrix blocks and in the cleat system.

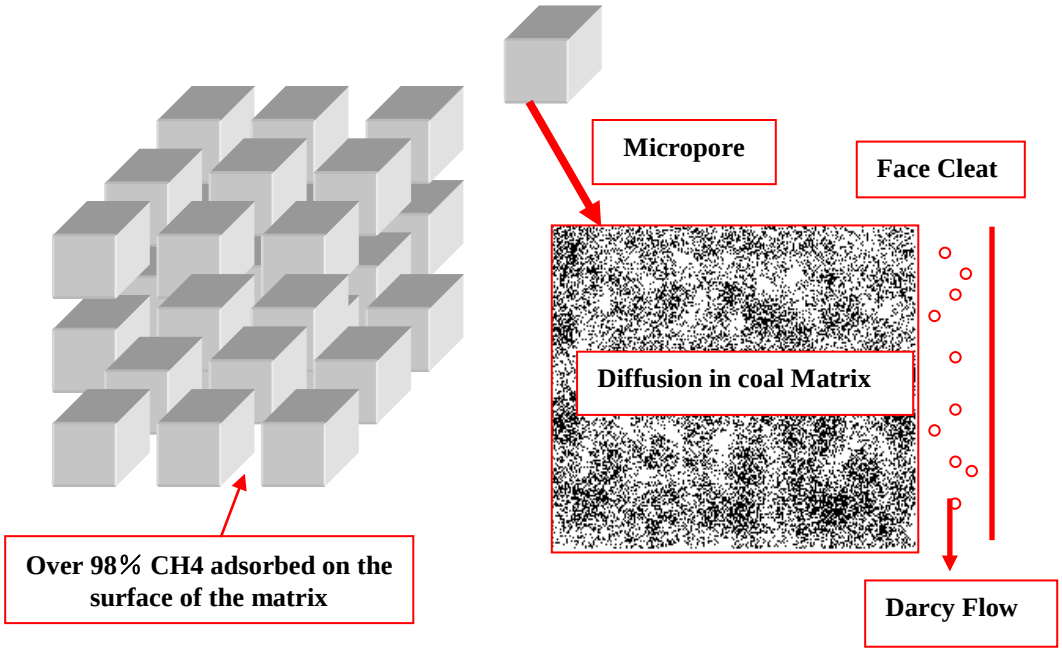

Figure 1.1 Warren & Root Reservoir Model Idealization

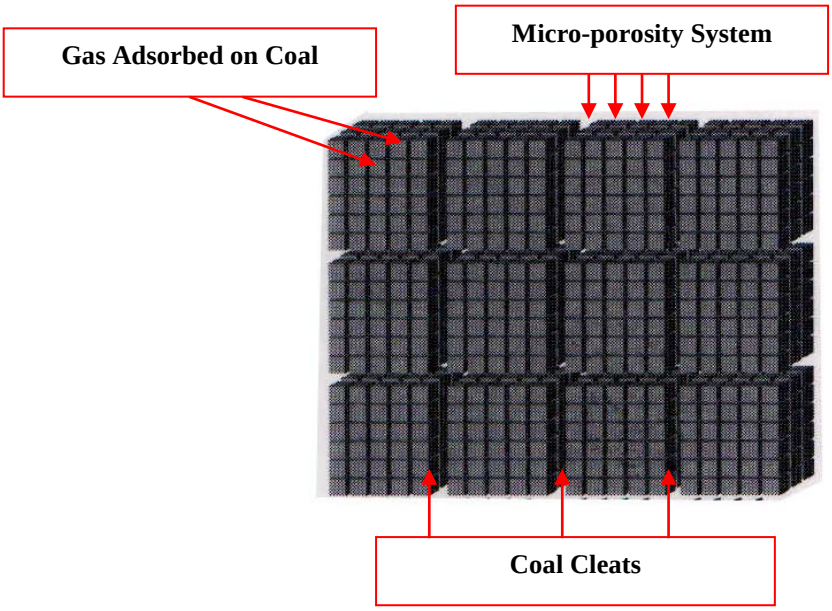

Figure 1.2 Representation of Triple-Porosity/Dual-Permeability System

1.2.2 Exploration mechanism

The methane is stored in the cleat and matrix system in the CBM reservoir as free state, dissolved state and adsorbed state.

(1) Free state

CH_4 performed as gas status that existed in the macro-pore system and cleat system in the CBM reservoir, and its content depends on the free space of the coal as well as the gas pressure and temperature. Free state CH_4 can move freely in the pore of the coal. This mechanism is accordance with the real gas state **Equation (1.1)**.

$$\rho = \frac{pM}{zRT} \tag{1.1}$$

For the isothermal process, z is only a function of Coalbed Methane pore pressure p, and $z = 1$ represents ideal gas.

(2) Dissolved state

There is a portion of Coalbed Methane dissolved in the water of coal seam under certain conditions. Its solubility can be described through Henry's law:

$$p_b = K_c C_b \tag{1.2}$$

In cases where there is little dissolved gas, **Equation (1.2)** is not commonly used.

(3) Adsorbed state

Adsorption is the main storage method for CBM. The CBM adsorption ability is related to temperature and pressure: it increases with the increasing of pressure, while decreases with the increasing of temperature.

Adsorption capacity of coal is measured by the adsorption, which is defined as the adsorbed coal gas volume (or mass) per unit coal volume under standard condition. When the temperature is a constant, adsorption and pressure type curve is called isotherm adsorption curve. This isotherm adsorption type curve can be used to determine the initial maximum content of CH_4 and critical desorption pressure.

There are mainly three types of mathematical model considering the adsorption of coal seam:

(1) Henry isotherm adsorption model

$$V = V_H p \tag{1.3}$$

Equation (1.3) indicates that the adsorption is simply proportion to pressure in the Henry isotherm adsorption curve (**Figure 1.3** (a)).

(2) Langmuir isotherm adsorption model

For most coals, the Langmuir isotherm theory (**Langmuir, I., 1916[1]**) is adequate for simple, single-layer adsorption:

$$V = \frac{V_L bp}{1 + bp} \tag{1.4}$$

Equation (1.4) can describe the coal seam single layer adsorption characteristic more accurately as shown in **Figure 1.3** (b). There is a linear relationship between $1/p$ and $1/V$.

(3) Freudlich isotherm adsorption model：

$$V = V_p p^N \tag{1.5}$$

Equation (1.5) describes the multilayer adsorption characteristic, and there exists a straight line on the $\log V - \log p$ plot (**Figure 1.3** (c)).

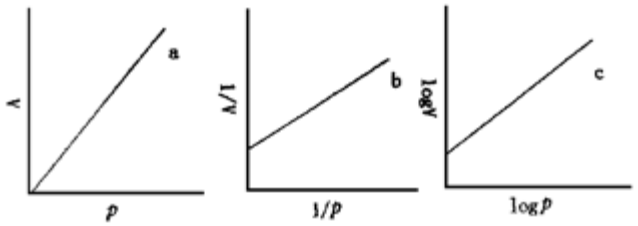

Figure 1.3 Isotherm adsorption law
a: Henry adsorption law； b: Langmuir adsorption law ； c: Freudlich adsorption law

Statistics from most samples of the world show that the Coalbed Methane adsorption characteristics are in line with Langmuir adsorption law.

1.2.3 Production characteristic

Conventional gas reservoirs consist of matrix and pore-space (**Figure 1.4**). The gas is stored in the pore space and the gas in place is a function of the formation porosity, pressure, temperature, and water saturation. There is usually no or little mobile water associated with conventional gas reservoirs. Therefore, relative permeability is not a significant factor in managing conventional gas reservoirs. When production begins and the reservoir pressure declines, usually small or no changes are observed in the formation permeability. Gas production gradually decline while water production slowly increase during the whole production stage for conventional gas (**Figure 1.5**).

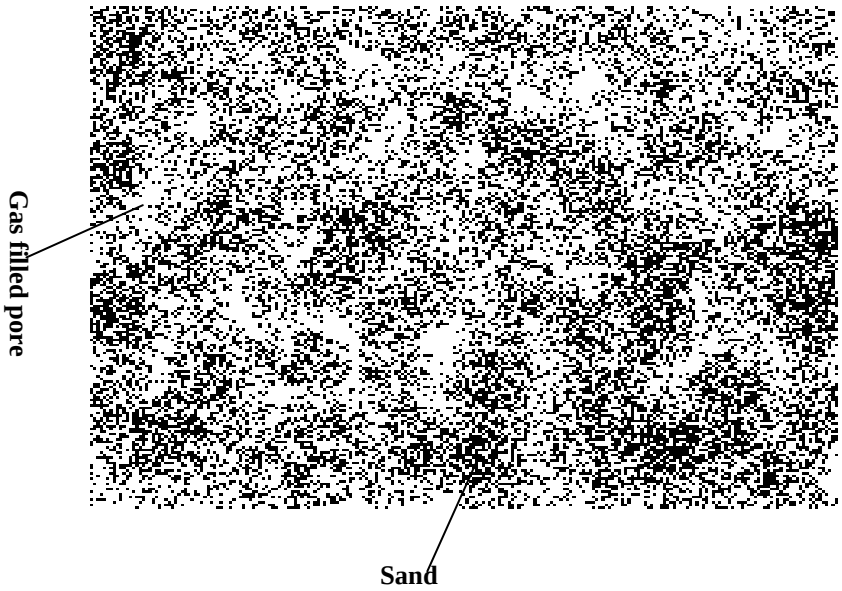

Figure 1.4 Structure for Conventional Gas Sands

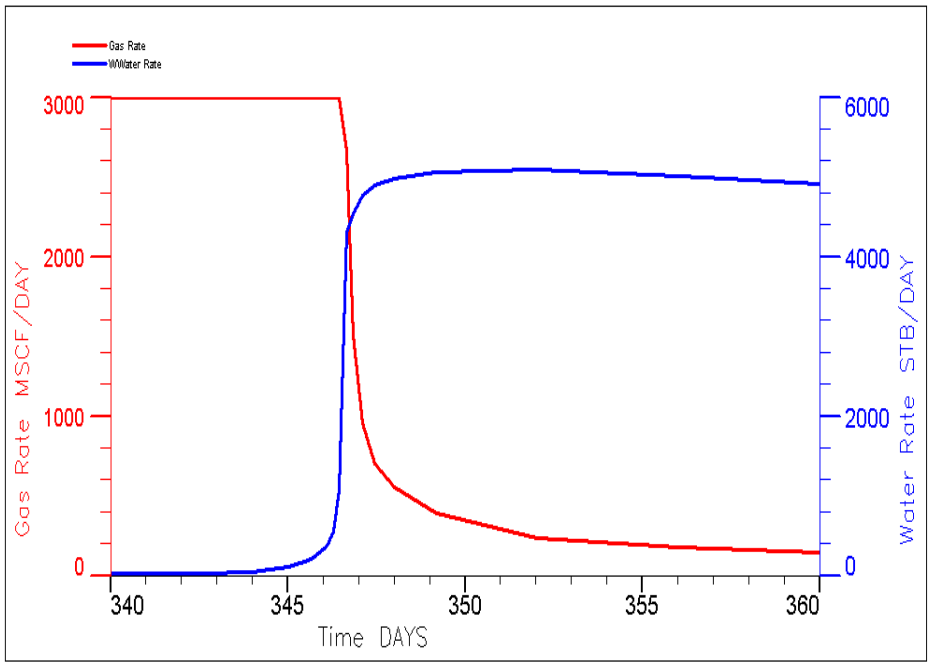

Figure 1.5 Production curve for Conventional Gas Sands

On the other hand, CBM reservoirs consist of coal matrix blocks that contain micropores. The matrix blocks are separated by cleats (**Figure 1.6**), in addition, there are two kinds of cleats, one is the butt cleat and the other is the face cleat, which are typically perpendicular to each other. The gas is adsorbed on the coal and the gas in place is a function of the coal adsorptive capability, which is usually described by an adsorption isotherm, the reservoir pressure and temperature. The cleat system is generally 100% saturated with water at virgin conditions. The transport process of CBM reservoir is shown in **Figure 1.8**.

It can be seen that (red curve represents gas production and blue curve represents water production) the gas and water production of CBM experiences a relatively complicated process. There are typically three stages in coal dewatering process (**Figure 1.7**):

Stage 1: dewatering and depressurization

A huge amount of water is produced at the initial drainage because water initially occupies the cleat porosity in the reservoir, which controls the flow to the production well.

Stage 2: Stable production

At this stage, the gas production rate reaches at its maximum while the water production rate is considerably being reduced. The reservoir flow condition is almost stabilized until the beginning of the third stage.

Stage 3: Gas production rate declines

At this stage, the gas production rate is being to decline, and the water production rate is very low and even can be negligible. Additionally, the variations of the relative permeability to both gas and water are very little.

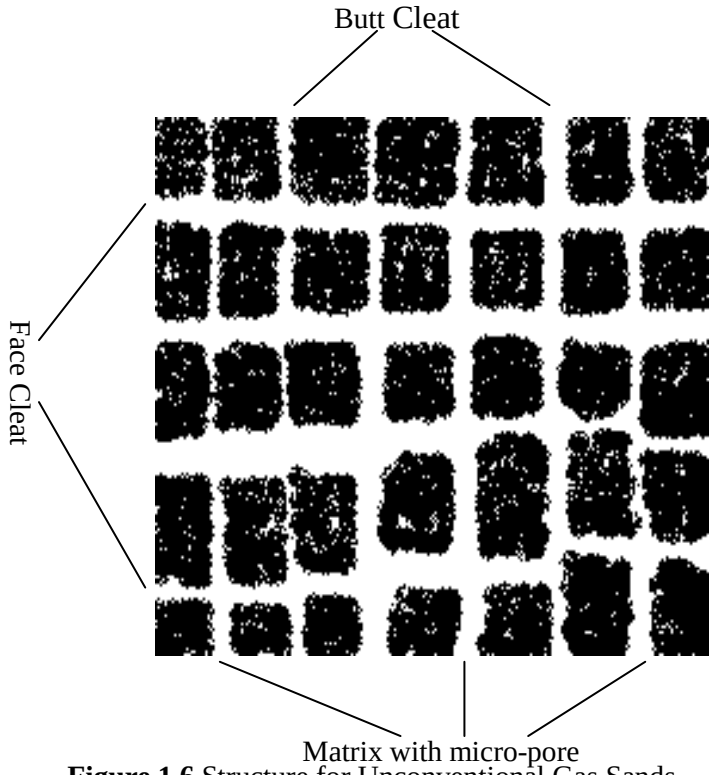

Figure 1.6 Structure for Unconventional Gas Sands

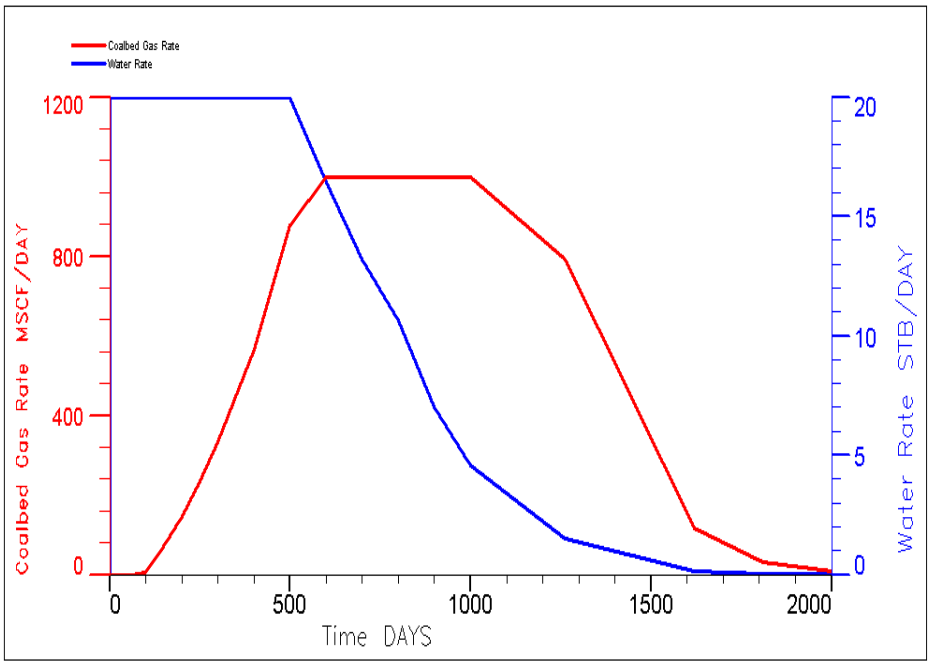

Figure 1.7 Production curve for Unconventional Gas Sands

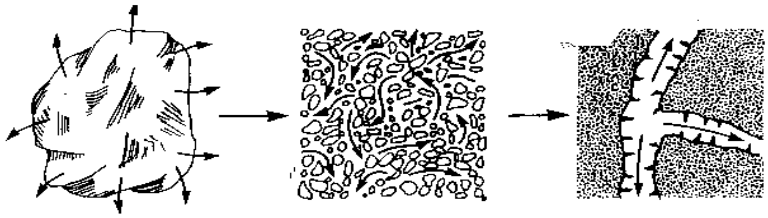

Figure 1.8 The Transport Process of CBM Reservoir

1.3 Main conflicts in the development of CBM reservoir

Three types of CBM reservoir models are used currently to simulate CBM/ECBM processes on the basis of the evolution of CBM reservoir simulation techniques.

Conventional Black Oil and Compositional Models, such as GEM (Computer Modelling Group (CMG) Ltd., Calgary), and GCOMP (BP-Amoco, Houston) are actually single porosity models that ignore the gas diffusion in the micro-pores (**Manik, J., 1999[2]; Manik, J., et al., 2000[3]**). This approach is apparently not valuable for the description of the CBM recovery process because of the lack of a supporting theory.

The models, such as COALGAS, COMET (Advanced Resources International, Arlington, Virginia) and SIMED Ⅱ (Commonwealth Scientific and Industrial Research Organization, Kinnoull Grove, Syndal, Victoria, Australia and the Netherlands Institute of Applied Geoscience TNO, Utrecht, The Netherlands) are specially developed to simulate CBM recovery processes. These types of model are now widely used in modelling CBM/ECBM (**Law, D.H.-S, et al., 2002[4]**), the fluid flow is described by a two phase, water and gas flow according to Darcy's law. The non-equilibrium formations (pseudo-steady-state method) are added to the gas equation as a source or sink term. The diffusion process in the micro pores affects the gas sorption rate. Additionally, various adsorption models can be used to simulate the multi-components gas adsorption gas adsorption equilibrium.

However, COALGAS, being a single component model, is capable of modeling only the primary CBM recovery process. The modelling of ECBMR by N_2 or CO_2 injection

cannot be performed with the single component two phase models because such a problem description requires compositional formulation in both the diffusion and the flow equations. Although the COMET2 and SIMED Ⅱ models are able to describe mixed gas diffusion and flow in coals, the gas diffusion rate in these models was modelled using a pseudo steady state method, which has been proved inaccurate for describing early stage diffusion, and for coals with multiscale pore structures. Therefore, such models still need to be improved for describing ECBMR processes.

More recently, many attempts have been made to improve the CBM/ECBMR simulation with alternative models, such as the unsteady state model, the bidisperse pore diffusion model, and the triple-porosity simulation model [e.g. COMET3 (Advanced Resources International, 2002, Arlington, Virginia)] (**Clarkson, C.R. and Bustin, R.M., 1999[5]; Shi, J.Q. and Durucan, S., 2003[6]; Cui, X.J., et al., 2004[7]; Siemons, N., et al., 2003[8]**). The fluid flow through fractures was simulated with a two-phase compositional model. Gas diffusion in the coal matrix was described as bidisperse diffusion (or two step diffusion): micro-pore diffusion and macro-pore diffusion. Additionally, several empirical equations were incorporated in the simulator to describe the variation of coal properties because of coal matrix shrinkage. The simulators used for the CBM reservoir simulation is summerized (**Table 1.2**).

CBM Simulators	CMG	ECLIPSE	COMET3	SIMED II	GCOMP	METSIM2
Mutiple Gas Components (3 or more)	Yes	Yes	Yes	Yes	Yes	Yes
Dual Porosity Approach	Yes	Yes	Yes	Yes	No	Yes
Triple Porosity/Dual Perm	No	No	Yes	Yes	No	No
Mixed Gas Diffusion	Yes	Yes	Yes	Yes	NO	Yes
Mixed Gas Adsorption	Yes	Yes	Yes	Yes	Yes	Yes
Gas water Rel. Perm Adjustment	No	No	Yes	No	No	Yes
Global Perm Adjustment	No	No	Yes	Yes	No	Yes
Dynamic Perm. Model	Yes	No	Yes	Yes	No	No
Stress Dependent Perm. And Porosity	Yes	Yes	Yes	Yes	Yes	Yes
Coal Shrinkage/Swelling	Yes	No	Yes	Yes	Yes	Yes

Table 1.2 Characteristics Comparison of CBM Simulators

1.3.1 Review of the traditional CBM reservoir simulation

1.3.1.1 Production forecast method

The evaluation of reserves has great significance in the reservoir engineering, and it is crucial for the development of production strategy, design of facilities and evaluation of the productivity. Currently, there are various studies on how to evaluate it, and they can be typically classified into two types:

The first type is developed (**King, G.R., 1993[9]; Seidle, J.P., 1999[10]; Ahmed, T., et al., 2006[11]; Xue, ChengGang, et al. 2000[12]; Chen, YuanQian and Hu, JiangGuo, 2008[13]**) based on the material balance methods for conventional reservoir, and it considered the special storage and transportation mechanism of CBM reservoir. However, it can't be used until the average formation pressure data is got, even worse, it is not feasible to get the average formation pressure data through build up well test for the low permeable CBM reservoir during production. This is because it is not only time consuming but also hard to interpret when there is two phase flow in the reservoir. Thus it is difficult to apply this kind of method to fields.

The second type is the flowing material balance method. It's initially proposed for the analysis of the production data for conventional reservoir at stable production rate (**Mattar, L. and McNeil, R., 1998[14]; Agarwal, R.G., et al., 1998[15]**), and it is independent of the shut in pressure. Following that models, the method under varied flowing rate was developed (**Mattar, L. and Anderson, D., 2005[16]**) and was introduced into CBM reservoir (**Gerami, S., et al., 2007[17]; Clarkson, C.R., et al., 2008[18]; Morad, K. and Clarkson, C.R., 2008[19]**). However, the Morad's method can only be applied to dry CBM reservoirs; Moreover, it is inconvenient to determine the pseudo-pressure for the flowing material balance method proposed by Clarkson. Because it is impossible to get the relationship between well-bottom pressure (or reservoir pressure) and water saturation during gas-water production period, which has already been mentioned by Clarkson for further discussion.

There are some empirical formulas to determine their relationship (**Handy, L.L., 1957[20]; Fetkovich, M.J., 1973[21]; Al-Khalifah, A-J.A., et al., 1987[22]**), and they are extended from condensate reservoir to CBM reservoir (**Kamal, M.M. and Six, J.L., 1989[23]**). These empirical formulas will be valid only if it is assumed that the volumes of free gas and adsorbed gas keep in a balance. However, it is only effective for very limited conditions (**Jochen, V.A., et al., 1994[24]**).

1.3.1.2 Review of well testing technology

The well testing technology for CBM reservoir is different from the conventional gas reservoir. The difference lies in three aspects: well testing fluid, fluid characteristics, different well test object and analyzing method in different stages.

1) Well test fluid

Water occupied the cleat system initially in the CBM reservoir, so the well testing fluid for CBM reservoir is the water in the initial stage. While the natural gas that existed in the sandstone is the testing object for the conventional gas reservoir.

2) Fluid characteristics

Coal seam composes of matrix system and cleat system. The Coalbed Methane is adsorbed on the surface of matrix pore system, and water filled in the cleat system. The adsorbed gas begins to desorb once the CBM reservoir pressure is lower than the critical desorption pressure; the gas diffusion in the matrix system accords with the Fick's law. And the two phase (water and gas) flow accords with the Darcy's law when the diffused gas comes into the cleat system. Thus although there is double structure in the CBM reservoir, it doesn't have the double flowing condition.

However, the conventional natural gas structure can not only provide the dual structure but can also provide the dual flowing condition for the gas, this means that the gas flows from matrix system to cleat system and it accords with the Darcy flow in the cleat system. The dual flowing characteristics differentiate it from CBM reservoir.

3) Different well test object and analyzing method

There exist three stages for the production of Coalbed Methane: dewatering process, gas and water production stage and only gas production stage. Only the water is produced during the dewatering process, which is the main well testing stage for CBM reservoir. After that is the two phase flow process, the multiphase well testing method needs to be developed. Finally, the single phase well testing method needs to be proposed for the well testing interpretation. Differently, the conventional reservoir only produce gas, so only the single gas phase well testing method should be applied for it.

The mathematical well testing methods that are being used currently are summarized as:

1) P-M method

It is assumed that gravitational effects and capillary pressure can be neglected, the pressure gradient variation and saturation gradient variation is supposed to be ignored. In addition, the total mobility is proposed by Perrine (**Perrine, R.L, 1956[25]**). The pressure equation can be written as:

$$\frac{1}{r}\frac{\partial}{\partial r}(r\frac{\partial p}{\partial r}) = \frac{\phi C_t}{\lambda_t}\frac{\partial p}{\partial t} \tag{1.6}$$

Martin (**Martin, J.C., 1959[26]**) proved the validity of the pressure method from theory. Only the total mobility value λ_t can be interpreted if the total mobility method is applied to the CBM reservoir for multiphase well testing interpretation. This is because the accurate relative permeability data is very difficult to get for the CBM reservoir.

2) Pseudo pressure method

Some worker use the psedudo pressure method for interpretating the conventional oil and gas reservoir (**Ayan, C. and Lee, W.J., 1988[27]; Raghavan, R., 1975[28], 1989[29]**). A new analysis method for pressure transient testing in coal degasification projects was proposed by **Kamal, M.M. and Six, J.L., 1989[23]**. The two phase coal degasification pseudo pressure function is defined as:

$$p_{pcd} = 2\int_{p_{ref}}^{p}(\frac{k_{rg}}{\mu_g Z_g} + \frac{k_{rw}}{\mu_w Z_w})pdp \tag{1.7}$$

In addition, the pseudo pressure seepage flow equation for the CBM reservoir is:

$$\frac{1}{r}\frac{\partial}{\partial r}(r\lambda_t\frac{\partial p_{pod}}{\partial r}) = \phi C_t\frac{\partial p_{pod}}{\partial t} \tag{1.8}$$

Moreover, the gas and water permeability, volume factor and viscosity have the following relationship:

$$\frac{k_{rw}}{k_{rg}} = \frac{V_w}{V_g}\frac{\mu_w}{\mu_g} \tag{1.9}$$

This equation is only suitable for the case when the desorption speed is fast enough. What is more, the isothermal adsorption data and relative permeability data are needed. However, the isothermal adsorption data for CBM reservoir are difficult to get for its

special characteristic, and the relative permeability data can only be got through history matching.

3) Pressure square method

The pressure square method for the multiphase well test analysis was firstly proposed in 1987 (**AI-Khalifah, A-J.A., et al., 1987[22]**). The flow equations for the multiphase flow can be shown as:

$$\nabla^2 p + \nabla p.\nabla[\ln[\frac{k_0}{\mu_0 B_0}]] = \frac{\phi c_t}{\lambda_t}\frac{\partial p}{\partial t} \tag{1.10}$$

The $\frac{k_0}{\mu_0 B_0}$ term can be assumed to vary linearly with the pressure as reported by Handy (**Handy, L.L., 1957[20]**) and applied by Fetkovich (**Fetkovich, M.J., 1973[21]**). Thus, **Equation (1.10)** can be arranged as:

$$\nabla^2 p^2 = \frac{\phi c_t}{\lambda_t}\frac{\partial p^2}{\partial t} \tag{1.11}$$

It can be easily seen that **Equation (1.11)** is similar with the single phase diffusivity equation.

In case that CBM reservoir is different from the common oil reservoir, the pressure squared method proposed by AI-Khalifah can't be directly applied to the gas and water two phase CBM reservoirs. Thus the pressure square method has to be modified for the well testing interpretation of CBM reservoir.

All the stated above, the current published well testing methods had its strengths and at the same time they also had their limitations. For example, only the total mobility value λ_t can be interpreted if the modified P-M method for CBM reservoir is used due to the difficulty in getting accurate relative permeability data; pseudo pressure method can only limited to the situation when the gas desorption is very fast, and also need the isothermal adsorption data for the interpretation, which is very difficult to get. Thus more appropriate well testing method for CBM reservoir needs to be investigated.

1.3.1.3 Review of gas slippage and threshold pressure gradient

Gas slippage is a phenomenon associated with non-laminar gas flow effects in porous media, if the slip effect is not considered correctly, the gas relative permeability will

vary with test pressures and may be greater than one at some water saturations. This phenomenon is especially significant in low permeability or tight gas sands characterized by small pore throats. However, few researches regarding the gas slip effect in two phase flow have been published. On the other hand, the gas has to overcome the threshold pressure before it flow through the media in the CBM reservoir, which is defined as the minimum pressure needed to initiate the displacement of a wetting phase by a non-wetting phase from a porous medium that is 100 percent saturated with the wetting phase.

The gas slippage effect was firstly studied and documented in porous media (**Klinkenberg, L.J., 1941[30]**), and showed that the observed gas permeability is a function of the mean core pressure. It can be shown as the following equation forms:

$$k = k_{\infty}(1 + b / \overline{p}) \tag{1.12}$$

Later, the two phase gas slippage phenomenon is also studied (**Rushing, J.A., et al., 2003[31]; Li, K. and Horne, R.N., 2001[32]**), they define the gas relative permeability $k_{rg}(S_w, p_m)$ at any mean pressure as:

$$k_{rg}(S_w, p_m) = k_{rg\infty}(S_w)(1 + \frac{bs_w}{p_m}) \tag{1.13}$$

Then the study on the gas slippage effect for the low permeability reservoir was carried out through numerical or experimental method (**Ertekin, T.K., et al., 1986[33]; Estes, K.R. and Fulton, F.P., 1956[34]; Jones, F.O. and Owens, W.W., 1980[35]); Sampath, K. and William, K.C., 1982[36]); Rushing, J.A., et al., 2004[37]**). The basic gas slippage factor is defined as:

$$b = 0.86 k_{\infty}^{-0.33} \tag{1.14}$$

And the correlative power function can be substituted by b in Klinkenberg's equation:

$$k_a = k_{\infty}(1 + \frac{0.86 k_{\infty}^{-0.33}}{\overline{p}}) \tag{1.15}$$

Sampath and William's (**Sampath, K. and William, K.C., 1982[36]**) slippage factor is:

$$b = 0.0955(k_{\infty g} / \phi)^{-0.53} \tag{1.16}$$

Rushing, J.A.'s (**Rushing, J.A., et al., 2004[37]**) gas slippage factor is:

$$b = 38(k_K / \phi_g)^{-0.45} \tag{1.17}$$

The threshold pressure phenomena in porous media were firstly studied in the early 1970s (**Thomas, L.K., et al., 1968[38]; Wu, F., et al., 2001[39]**). They concluded that the equations of threshold pressure gradient for gas and water phase are:

$$\lambda_{bg} = (\alpha_1 / (k_f k_{rg\infty}) + \alpha_2 \tag{1.18}$$

$$\lambda_{bw} = (\alpha_3 \mu_w / (k_f k_{rw\infty})^{\alpha_4} \tag{1.19}$$

Unfortunately, a comprehensive CBM reservoir simulation model that considering both the effects of threshold pressure and gas slippage has not been developed yet.

1.3.1.4 Review of Mathematical methods for CBM reservoir simulation

In the early 1970s, an iterative method is proposed for the inversion of sparse band-structured matrices of the type that are common in numerical reservoir simulators (**Vinsome, P.K.W., 1976[40]**). An analysis of the coalbed degasification process was presented later based on the iterative method (**Ancell, K.L., et al., 1980[41]**). The mathematical model is:

$$\nabla.\{\frac{\rho_w k k_{rw}}{\mu_w}(\nabla p_w - \rho_w g \nabla h)\} - q_{wv} = \frac{\partial}{\partial t}(\phi \rho_w s_w) \tag{1.20}$$

$$\nabla.\{\frac{\rho_g k k_{rg}}{\mu_g}(\nabla p_g - \rho_g g \nabla h)\} + N_v - q_{gv} = \frac{\partial}{\partial t}(\phi \rho_g s_g) \tag{1.21}$$

Equation (1.20) and **Equation (1.21)** are solved by accompanying with other auxiliary, initial and boundary equations

The transient and semi-steady state solutions of the radial diffusivity equation for CBM reservoirs are presented then (**Bayles, G.A. and Reznik, A.A., 1986[42]**). The modified radial diffusivity equation is:

$$\frac{\partial(\rho\phi)}{\partial t} - q_r - \frac{1}{r}\frac{\partial}{\partial r}(r_D \frac{K}{\mu}\frac{\partial p}{\partial r}) = 0 \tag{1.22}$$

The mathematical and numerical developments for a series of finite difference models that simulate the simultaneous flow of water and gas through dual porosity coal seam

during the degasification process (**King, R.G., et al., 1986[43]**) are studied and described. The macro pore gas and water transport equations in this study are:

$$\nabla.[\frac{\alpha\lambda_g p_{ag}}{Z}\nabla p_{ag} + D_a\nabla(\frac{S_{ag}p_{ag}}{Z})] + \frac{p_{sc}T}{T_{sc}}q_{ai} = \frac{\partial}{\partial t}(\frac{\phi_a S_{ag} p_{ag}}{Z}) \tag{1.23}$$

$$\nabla.(\frac{\alpha\lambda_w}{B_w}\nabla p_{aw}) = \frac{\partial}{\partial t}(\frac{\phi_a S_{aw}}{B_w}) \tag{1.24}$$

At the same period, a mathematical formulation, applicable to both numerical simulation and transient well analysis, that describes the flow of gas in very tight ($k_\infty < 0.1md$) porous media and includes a dual-mechanism transport of gas is proposed (**Ertekin, T.K., et al., 1986[33]**). This provides the new idea about the numerical simulation and transient well testing for low permeability CBM reservoir. Followed that an approximate analytical solution for single phase gas flow is derived (**Bumb, A.C. and McKee, C.R., 1988[44]**), the governing equation is:

$$\phi\frac{\partial\rho_g}{\partial t} + \alpha c_m\rho_g\frac{\partial p_g}{\partial t} + \rho_{gsc}\frac{\partial V_E}{\partial t} = \frac{1}{r}\frac{\partial}{\partial r}(r\frac{k}{\mu_g}\rho_g\frac{\partial p_g}{\partial r}) \tag{1.25}$$

Later on, a pressure transient analysis technique for Coalbed Methane is proposed (**Ertekin, T. and Sung, W., 1989[45]**). The equation in this study is:

$$\frac{1}{r_a}\frac{\partial}{\partial r_a}(r_a\frac{p}{\mu z}\frac{\partial p}{\partial r_a}) = \frac{\phi}{\alpha}\frac{c_g}{k}\frac{p}{z}\frac{\partial p}{\partial t} + \frac{p_{sc}T}{\alpha k T_{sc}}\frac{\partial V}{\partial t} \tag{1.26}$$

As an extension, an analytical solution for transient pressure response of a horizontal well in CBM reservoir is addressed (**Sarkar, P.S. and Rajtar, J.M., 1994[46]**). Wellbore storage and skin effects are illustrated in the study, the flowing equation is:

$$\frac{k_x}{k_y}\frac{\partial^2 p^2}{\partial x^2} + \frac{k_z}{k_y}\frac{\partial^2 p^2}{\partial z^2} + \frac{\partial^2 p^2}{\partial y^2} = \frac{(\phi\mu c_t)_f}{k_y}\frac{\partial p^2}{\partial t} + \frac{2p_{sc}T\mu z}{T_{sc}k_y}\frac{\partial V}{\partial t} \tag{1.27}$$

Then, a new analysis method for pressure transient testing in coal degasification projects is presented (**Kamal, M.M. and Six, J.L., 1993[47]**). The diffusivity equation for the system is shown as:

$$\nabla(\frac{\lambda_g}{z_g} + \frac{\lambda_w}{z_w})\nabla p + q = \phi c_t\frac{\partial p}{\partial t} \tag{1.28}$$

Recently, the two phase mathematical model that integrated the matrix shrinkage effect (**Zhang, X.M. and Tong, D.K., 2008[48]; Zheng, S.Y. and Xue, L.L., 2011[49]**) was proposed. The transport equations in fracture system for two phases are as follows:

$$\begin{aligned}\nabla\cdot\left(\alpha\frac{k_{rg}k_f}{\mu_g B_g}\nabla\Phi_g+D_f\nabla(\frac{s_g}{B_g})\right)+q_{vm}-q_{vg}&=\frac{\partial}{\partial t}\left(\frac{\phi_f s_g}{B_g}\right)\\ \nabla\cdot\left(\alpha\frac{k_{rw}k_f}{\mu_w B_w}\nabla\Phi_w\right)-q_{vm}&=\frac{\partial}{\partial t}\left(\frac{\phi_f s_w}{B_w}\right)\end{aligned}\tag{1.29}$$

The relationship between porosity and permeability in this study is given by:

$$\begin{aligned}\phi_f&=\phi_{f0}e^{c_f(p-p_0)}+\phi_{fr}(1+2/\phi_{fr})\Delta\varepsilon\\ \frac{k_f}{k_{f0}}&=(\frac{\phi_f}{\phi_{f0}})^3\end{aligned}\tag{1.30}$$

Followed that a mathematical model to predict the CBM reservoir production and carbon dioxide (CO_2) sequestration in a coal seam was developed (**Ozdemir, E., 2009[50]**). The mathematical model is described as:

For CO_2 in the gas phase

$$\begin{aligned}-\frac{1}{r}\frac{\partial}{\partial r}\{r[\frac{(1-y_1)\alpha\alpha_1 kk_{rg}}{\mu_g B_g}\frac{\partial p_g}{\partial r}+(1-y_1)D_a\frac{\partial}{\partial r}(\frac{s_g}{B_g})+R_{SW1}\frac{\alpha kk_{rw}}{\mu_w B_w}\frac{\partial(p_g-p_{cgw})}{\partial r}]\}\\ \pm(q_{ai})_2=\frac{\partial}{\partial t}(\frac{(1-y_1)\phi s_g}{B_g}+R_{SW1}\frac{\phi(1-s_g)}{\alpha_1 B_w})\end{aligned}\tag{1.31}$$

For CH_4 in the gas phase

$$\begin{aligned}-\frac{1}{r}\frac{\partial}{\partial r}\{r[\frac{(1-y_1)\alpha\alpha_1 kk_{rg}}{\mu_g B_g}\frac{\partial p_g}{\partial r}+(1-y_1)D_a\frac{\partial}{\partial r}(\frac{s_g}{B_g})+R_{SW2}\frac{\alpha kk_{rw}}{\mu_w B_w}\frac{\partial(p_g-p_{cgw})}{\partial r}]\}\\ \pm(q_{ai})_2=\frac{\partial}{\partial t}(\frac{(1-y_1)\phi s_g}{B_g}+R_{SW2}\frac{\phi(1-s_g)}{\alpha_1 B_w})\end{aligned}\tag{1.32}$$

Later, worker (**Scott, R. and Larry, P., 2001[51]**) found that the dual porosity single permeability model can frequently be in gross error when forecasting well or field performance based on limited reservoir and/or production data. Thus, an advanced, triple porosity dual permeability model is developed, in which gas desorbs from the internal matrix block surfaces, and migrates via conventional Darcy flow through

micro-permeability matrix, and into the cleat system where it then flows to the wellbore. Water can also be stored within the matrix blocks and in the cleat system.

Then some alternative models that describe the multi-component gas diffusion and flow in bulk coals were investigated (**Douglas, M.S. and Williams, F.L., 1984[52]; Wei, X.R., et al., 2007[53]; Shi, J.Q. and Durucan, S., 2008[54]**). Also, a single phase, 1D mathematical formation in radial/cylindrical coordinates to examine unsteady state micr-opore sorption for the composite micro-pore/fracture Coalbed Methane transport problem was developed (**Kolesar, J.E., et al., 1990[55]**).

1.3.1.5 Review of Matrix shrinkage/swelling effect

Different models were developed to describe the variation in CBM reservoir properties, especially permeability. The effect of matrix shrinkage on CBM reservoir permeability was first quantified by Gray (**Gray, I, 1987[56]**). Since then, a number of theoretical and empirical permeability models have been put forward. A brief review of the most popular models is given below.

(1) Somerton, et al., Model (**Somerton, W.H., et al., 1975[57]**)

They developed a model that describes the variation of coal core permeability with confining stress. The model is provided as follows:

$$k = 1.013x10^{-0.31\sigma} \tag{1.33}$$

Later, the effect of methane desorption on gas flow in coal was investigated (**Harpalani, S. and Schraufnagel, A.R., 1990[58]**).

(2) Gray Model (**Gray, I, 1987[56]**)

The shrinkage of coalbed matrix and its effect on reservoir permeability were first quantified by Gray's Model. The effective horizontal stress variation in CBM reservoir is given by:

$$\sigma - \sigma_0 = \frac{v}{1-v}(p - p_0) + \frac{E}{1-v}\frac{\Delta\varepsilon_s}{\Delta p_s}\Delta p_s \tag{1.34}$$

(3) McKee, et al., Model (**McKee, C.R., et al, 1988[59]**)

The fundamental relationships for permeability, porosity, and density as a function of effective stress for both constant and variable pore compressibility are given as:

$$\phi = \phi_0 \frac{e^{-\overline{C_p}}\Delta\sigma}{1-\phi_0(1-e^{-\overline{C_p}\Delta\sigma})} \tag{1.35}$$

$$k = k_0 \frac{e^{-3\overline{C_p}}\Delta\sigma}{1-\phi_0(1-e^{-\overline{C_p}\Delta\sigma})} \tag{1.36}$$

The correlated effective stress is given as:

$$\sigma = 0.572D \tag{1.37}$$

Here, the effective stress gradient is 0.572 psi/ft under lithostatic condition for coal seams.

(4) Seidle, John P. and Huitt, L.G. Model (**Seidle, J.P. and Huitt, L.G., 1995[60]**)

Their development of equations relating matrix shrinkage, cleat porosity and permeability can be shown as:

$$\begin{aligned} &\frac{\phi_f}{\phi_{fi}} = 1+(1+\frac{2}{\phi_{fi}})c_m(1E-6)V_m(\frac{bp_i}{1+bp_i}-\frac{bp}{1+bp}) \\ &\frac{k_f}{k_{fi}} = (\frac{\phi_f}{\phi_{fi}})^3 \end{aligned} \tag{1.38}$$

(5) Palmer, I. and Mansoori, J. (P&M) Model (**Palmer, I. and Mansoori, J., 1998[61]**)

Assume that the matrix shrinkage effect can be fitted to a Langmuir type curve by ignoring the grain compressibility, and suppose a cubic relationship between porosity and permeability. The P&M Model was developed as follows:

$$\begin{aligned} &\phi-\phi_0 = \frac{1}{M}(p-p_0)-(1-\frac{K}{M})\varepsilon_l(\frac{p}{p+p_\varepsilon}-\frac{p_0}{p_0+p_\varepsilon}) \\ &\frac{k}{k_0} = \frac{\phi^3}{\phi_0^{\,3}} \end{aligned} \tag{1.39}$$

(6) Shi, J.Q. and Durucan, S. Model (**Shi, J.Q. and Durucan, S., 2005[62]**)

This model was developed based on a bundled-matchstick geometry representation of CBM reservoir to describe the variation of permeability during primary production. The corresponding mathematical equations are shown as follows:

$$\sigma - \sigma_0 = \frac{v}{1-v}(p - p_0) + \frac{E}{1-v}\frac{\Delta\varepsilon_s}{\Delta p_s}\Delta p_s$$
$$k = k_0 \exp\{-3C_f(\sigma - \sigma_0)\} \quad (1.40)$$

Comparison of P&M Model (**Palmer, I. and Mansoori, J., 1998[61]**) to Shi & Durucan model (**Shi, J.Q. and Durucan, S., 2005[62]**) reveals that the two models are very similar in concepts and derivation, except that Shi & Durucan model has a matrix shrinkage term from 1.5 to 3 which is stronger than P&M model. This is because of different Poisson ratio in the model. In addition, both models assumed and used cubic form of permeability porosity relationship (**Equation (1.39)** and **Equation (1.40)**).

Later on, a theoretical model (**Pan, Z.J. and Connell, D.L., 2007[63]**) is derived to describe adsorption induced coal swelling at adsorption and strain equilibrium. After that, a new equation that can be used to model the permeability behavior of a fractured, sorptive elastic medium, such as coal, under variable stress conditions was proposed (**Robertson, E.P. and Christiansen, R.L., 2008[64]**). An improved mixed gas adsorption isotherm model based on the extended Langmuir theory was also proposed (**Robertson, E.P., 2008[65]**).

In addition, the influence of net stress on porosity, permeability, and reservoir quality index of Australian Coalbed Methane formation was investigated through experimental study (**Shedid, A.S. and Rahman, K., 2009[66]**). Recently, a new model from basic thermodynamic principles that is more predictive than the empirically based approaches was developed (**Clarkson, C.R., et al., 2010[67]**). The coupled permeability model in this study is shown as follows:

$$\frac{k_a}{k_{a,i}} = \left(\frac{\varphi}{\varphi_i}\right)^3 = \left[1 + \frac{c_f}{\varphi_i}(p - p_i) + \frac{1}{\varphi_i}\left(\frac{K}{M} - 1\right)(\Delta\varepsilon)\right]^3 \quad (1.41)$$

As stated above, these methods can give a good evaluation of the matrix shrinkage effect for the middle rank CBM reservoir. However, there exists a big gross error for the high rank or low rank CBM reservoir, especiall for the low rank CBM reservoir. Thus, this drives for the development of more accurate permeability models that can evaluate the matrix shrinkage effect for different ranks of CBM reservoir.

1.3.1.6 Review for the development of horizontal wells

Horizontal wells are widely used in many new oil and gas fields. Productivity of a horizontal well can usually be greater than that of vertical well for several reasons.

Firstly, horizontal wells can be opened to a larger portion of the reservoir than vertical wells. A larger contact area allows lower drawdown to recover more oil and gas. Secondly, horizontal wells can be drilled perpendicular to oriented natural fractures and therefore intersect with more fractures. Also it may be possible to induce multiple hydraulic fractures. Increased productivity is not the only benefit of horizontal wells: improved sweep efficiency, reduced coning of water or gas and increased drainage area are other advantages of horizontal wells over vertical wells. Therefore, horizontal wells are believed to perform better than their vertical counterparts in thin reservoirs.

Recent interest in horizontal wells has been accelerating owning to the improved drilling and completion technology, which has resulted in the increased efficiency and economics in oil and gas recovery. The increases in oil and gas production rate and improvement in ultimate recovery have given horizontal wells the edge over vertical wells in many margin reservoirs. The disadvantages here are that it is relatively much more expensive to drill and complete a horizontal well than a vertical one. From this point of view, engineers need reliable methods to estimate its expected productivity to determine the economical feasibility of drilling a horizontal well,.

It has long been recognized the advantage of the fully implicit strongly coupled reservoir/wellbore model. Many reservoir simulators had been proposed for this purpose (**Bansal, P.P., et al., 1979[68]; Cheshire, M.I., et al., 1980[69]**). Some scholars (**Folefac, A.N., 1988[70];** (**Folefac, A.N., et al., 1991[71]; Arshad, A.M., 1990[72]**) noticed the inflow performance of horizontal wells and realized that hence their deliverability may be affected by pressure drop along the wellbore, which has serious implications on perforated well length because the productivity index is no longer directly proportional to the well length..

Later, a modular, comprehensive modeling of well and reservoir was proposed (**Brekke, K., et al., 1993[73]; Al, Attas, M.O., 1996[74]**). In an effort to improve wellbore simulation, the introduction of two extra variables (liquid and gas flow fraction) in wellbore model was proposed (**Holmes, J.A., 1983[75]**).

Then, the application of a multi-segment well model to simulate the flow in advanced wells was proposed (**Holmes, J.A., et al., 1998[76]**) using a commercial black oil simulator. And an analytical model that used to couple the flow in the horizontal wellbore with the inflow model in the reservoir was firstly developed (**Dikken, J.B., 1990[77]**).

Analytical equation based reservoir models are able to calculate reservoir pressure drop or inflow rate for well/reservoirs with some prescribed geometry, without having to rigorously work with the governing diffusivity equation. Examples of such models are: (**Borisov, J.P., 1964[78]; Joshi, S.D., 1991[79]; Babu, D.K., et al., 1991[80]; Goode, P.A. and Wilkinson, D.J., 1991[81]; Mutalik, P.N., et al., 1988[82]**). These models are presented in **Table 1.3** (note that the Babu and Odeh model presented in this table is for a semi-steady state case with a fixed wellbore length).

Borisov	$J_0 = \dfrac{2\pi K_h h/(\mu_0 B_0)}{\ln(4\frac{r_e}{L}) + \frac{h}{L}\ln(\frac{h}{2\pi r_w})}$
Joshi	$J_0 = \dfrac{2\pi\beta k_h h}{\mu_0 B_0[\ln\{\frac{a+\sqrt{a^2-(L/2)^2}}{L/2}\} + \frac{\beta h}{L}\ln(\frac{(\frac{\beta h}{2})^2+\beta^2\delta^2}{\beta h r_w/2})]}$
Babu and Odeh	$J_0 = \dfrac{2\pi b\sqrt{k_y k_v}/(\mu_0 B_0)}{\ln(\sqrt{ah}/r_w) + \ln C_H - 0.75 + S_R}$
Goode and Wilkinson	$J_0 = \dfrac{2\pi k_h h/(\mu_0 B_0)}{P_{wD} + S_m}$
Mutalik et al	$J_0 = \dfrac{2\pi k_h h/(\mu_0 B_0)}{\ln(r_e'/r_w) - A' + s_f + s_m + s_{CA,h} - c' + Dq}$

Table 1.3 Horizontal Inflow Equations

The priority of the horizontal well over the vertical well was questioned (**Zhang, L. and Dusseault, M.B., 1994[83]**) later. Then a comprehensive, three dimensional, transient semi-analytical models for infinite conductivity and finite conductivity wellbores in isotropic or anisotropic reservoirs was proposed (**Penmatcha, V.R. and Aziz, K., 1998[84]**). Also, the simple analytical solutions based on the assumption of infinite drain-hole conductivity (**Giger, F.M., 1984[85]; Furui, K.J. and Hill, A.D., 2003[86]; Hagoort, J., 2009[87]**) were derived.

Following that, the effect of wellbore pressure drop on horizontal well productivity through using the general semi-analytical model was discussed (**Ozkan, E., et al., 1999[88]**). A coupled reservoir/wellbore simulation tool which is based on lumped parameter was developed (**Vicente, R., et al., 2003[89]; Augustine, R.J., 2002[90]; Ouyang, L.-B. and Huang, B., 2005[91]**). Recently, a method for inflow profile prediction using a coupled reservoir/wellbore simulator based on an algorithm originally proposed by Kabir (**Kabir, A., 2006[92]**) was addressed (**Kabir, A. and**

Sanchez, G., 2009[93]; Kabir, A. and Jose, A. V., 2010[94]; Gui, P., et al., 2006[95]).

The study of the fractured horizontal well was also implemented (**Chen, C.-C. and Raghavan, R., 1997[96]; Wan, J. and Aziz, K., 2002[97]; Guo, B.Y. and Yu, X.C., 2008[98]; Lin, J.J. and Zhu, D., 2010[99]**). After that, the horizontal well fracturing technology for reservoirs with low permeability was studied (**Cai, W.B., et al., 2009[100]**). Then, a method that can predict horizontal well performance as well as that can be applied for fractured horizontal wells was developed (**Lin, J.J. and Zhu, D., 2010[99]; Belyadi, A., et al., 2010[101]**).

The summary of the methodology was developed to analyze pressure build up (PBU) tests in the single lateral horizontal wells (**Briceno, M., et al., 2002[102]**). In addition, the grid system requirements for the numerical modeling of pressure transient tests regarding both fractured and non fractured reservoir through horizontal wells were discussed (**Al-Mohannadi, N., et al., 2004[103]; Al-Thawad, F., et al., 2004[104]**).

What is more, the horizontal well technology is also widely used for unconventional gas reservoir (**Ertekin, T., et al., 1988[105]; Osisanya, O.S. and Schaffitzel, F.R., 1996[106]; Mutalik, P.N. and Magness, W.D., 2006[107]; Clarkson, C.R., et al., 2009[108]; Meszaros, G., 2007[109]; Lehocky, N. and Jonkers, J., 2008[110]; Soliman, M.Y., et al., 2010[111]; Sani, M.A. and Ejefodomi, A.E., 2011[112]**). Great finding had been proposed through their study. Unfortunately, they did not extend the technology in the presence of matrix shrinkage, gas slippage and threshold pressure gradient effects.

1.3.1.7 Review of multi-branch horizontal wellbore

Coal seams perform its unusual reservoir rock due to its highly complex reservoir characteristics. One of the major differences between CBM reservoir and conventional gas reservoir is that coal represents both the source and the reservoir rock at the same time. The methane is adsorbed in the internal of the coal, which allows the most of the gas to be stored in the coal rock (**Maricic, N., et al., 2005[113]**), while the gas is found as free state in the conventional sandstone reservoirs.

Multi-branch horizontal well technology is a fast developed oil and gas exploitation technology. If the multi-branch horizontal well technology is combined with the CBM reservoir characteristic, it can be used for the CBM reservoir exploitation. The

difference of multi-branch horizontal well technology between conventional low permeability gas and CBM reservoir is that the multi-branch horizontal well for CBM reservoir needs longer horizontal displacement and more branches.

The horizontal well development has a great improvement in the oil and gas field. In vertical well plane, it is typically divided into five types: clustered branch horizontal well; radial branch horizontal well; reverse branch horizontal well; folder branch horizontal well; pinnate horizontal well. While there are three types of horizontal well configuration in horizontal plane, and the pinnate horizontal well configuration is the most popular one among them.

Many achievements had been proposed for the multi-branch horizontal well technology until now (**Konopczynski, M.R., et al. 1995[114]; Vo, D.T. and Madden, M.V., 1995[115]; Winton, J.A.C., et al., 1998[116]; Ross, B., 1996[117]; Zhu, D., et al., 2002[118]; DeMong, K. and Rivenbark, M., 2000[119]**). Multi-branch horizontal well technology is widely used for the oil recovery (**Hembling, D., et al., 2006[120]; Mohamed, M.G. and Monhamed, B.E., 2008[121]; Salameh, A.L., 2001[122]**), the novel strategy, completion method applied to the oil well showed a good result and can give the guidance for the field production. The multi-branch well modelling for the optimization of the well was also investigated (**Yurkiw, F.J., et al., 1996[123]; Retnanto, A., et al., 1996[124]; Lee, S.S., et al., 2001[125]**).

The horizontal and multi-branch well performance analysis is made lately (**Joshi, S., 2000[126]; Tabatabaei, M. and Ghalambor, A., 2009[127]**). Recent research found that CBM reservoir can be drained through small diameter horizontal holes (**Maricic, N., et al., 2005[113]; Thomas, E. and Suhy, P.E., 2009[128]**). One of the merits of the horizontal well is that the well direction, shape and position can be controlled (**Ertekin, T., et al., 1988[105]**). Later on, the challenges, lessons learned and successful implementations of multi-branch completion technology offshore Abu Dhabi are proposed (**Kikuchi, S. and Fada'q, S.A., 2006[129]**).

As illustrated above, many mathematical simulation models both with vertical well types and horizontal well types that are used in the CBM reservoir have been developed. They can simulate the gas and water production rate for CBM reservoir in some extent. The gas slippage and threshold pressure gradient effects are both considered in the simulation for some conventional oil and gas reservoir. The matrix shrinkage effect is also taken into consideration for some specified CBM reservoir. However, the gas

slippage and threshold pressure gradient effects as the whole part are not studied in CBM reservoir yet, which sometimes results in overestimating gas production rate and underestimating the water production rate, and can't exactly be used for the history matching of field data. In addition, the permeability model developed currently has a lot of limitations and shortcomings. Thus this drives me to find the novel and comprehensive mathematical models with vertical well production type as well as coupled horizontal well types for the simulation of CBM reservoir.

1.3.1.8 Review of Enhanced technology

Unlike conventional gas reservoirs, methane in coalbeds is stored primarily as a sorbed gas, at near liquid densities, on the internal surface area of the microporous coal. The surface area of the coal on which the methane is adsorbed is very large (20 to 200 m^2 /kg) (**Patching, T.H., 1970[130]**). And, if saturated, CBM can have five times the volume of gas contained in a conventional sandstone gas reservoir of comparable size. Thus the exploitation of CBM reservoir has great significance, especially the implementation of enhanced technology on it for the recovery of the gas rate.

The basic simulation models utilized for the CBM reservoir is characterized as dual porosity (**King, G.R., et al., 1986[43]**) and triple porosity models (**Scott, R., and Larry, P., 2001[51]**). An advanced Coalbed Methane transport model is proposed by considering the effect of stress and matrix shrinkage in a permeability model (**Zhang, X.M. and Tong, D.K., 2008[47]**). And the compositional dual porosity CBM reservoir model is also developed for the purpose of CO_2 sequestration (**Ozdemir, E., 2009[50]**). The problem is that they didn't extend the novel idea into the triple porosity CBM reservoir model.

Moreover, the most popular enhanced CBM recovery technology is injecting gas (CO_2 /N_2). There are mainly two types of ECBM recovery methods: one is numerical simulation method, and the other is experiment method.

The ECBM models are proposed to investigate the parameters that affect the recovery of CBM reservoir (**Smith, H.D., et al., 2005[131]; Balan, H.O. and Gumrah, F., 2009[132]**). They investigate the effects of permeability anisotropies, diffusion time constant, physical properties and operational parameters of coal on the ECBM process.

The multi-scale model (**Wang, G.X., et al., 2009[133]**) and one dimensional mathematical model (**Ronny, P., et al., 2011[134]**) is also developed for the ECBM

production and CO_2 sequestration. However, although they also consider the effect of matrix shrinkage/swelling on the recovery of Coalbed Methane, the permeability model comes from the extended Palmer/Mansoori (**Palmer, I. and Mansoori, J., 1998[61]**) model hasn't already novel.

On the other hand, the laboratory experiments for the ECBM recovery by gas injection have been successfully done (**Shimada, S., et al., 2005[135]; Mazumder, S., et al., 2006[136]**). Some people even combined experiments with numerical simulation to study the injecting process and how the injection of mixture affects the recovery of gas (**Jessen, K., et al., 2008[137]; Shi, J.Q., et al., 2008[138]**).

In addition, the sorption induced permeability change of coal and the effects of matrix shrinkage and swelling on the ECBM production are widely studied (**Gorucu, B.F., et al., 2007[139]; Mitra, A. and Harpalani, S., 2007[140]; Lin, W., et al., 2008[141]; Mazumder, S. and Wolf, K.H., 2008[142]**). They use different kinds of permeability changes and matrix swelling/shrinkage models through experiment and simulation to study their effect on the gas production during the gas injection process. They found that the injectivity of CO_2 decreases when swelling occurs, coal swelling can have significant effects on injection and production rate, and, hence, profitability.

Interestingly, the characterization and simulation of ECBM for the particular field are investigated (**Jessen, K., et al., 2007[143]; Sinayuc, C. and Gumrah, F., 2008[144]; Calderon, C.E., et al., 2010[145]**). Different simulation models are used for this purpose. Firstly, the implementation of the ISA model into the dual porosity simulator was described for the prediction of displacement performance in ECBM processes (**Jessen, K., et al., 2007[143]**). Then CMG-GEM module was used to simulate the ECBM process (**Sinayuc, C. and Gumrah, F., 2008[144]**). Recently, A commercial simulator is used for the modeling of ECBM process, and two coal seams (Pittsburgh and Upper Freeport) are chosen for the study of CO_2 sequestration (**Calderon, C.E., et al., 2010[145]**).

As discussed above, a lot of achievements and improvements have been got in enhancing the CBM reservoir production. However, the gas slippage effect and threshold pressure gradient effect are not being considered for the advanced triple porosity dual permeability model in these studies. Also the permeability models published are not good enough to simulate the enhancing production process.

1.3.2 Case studies

1.3.2.1 Conventional CBM simulation

The case studies are conducted by using black oil model and compositional model in Eclipse simulation software respectively, which belongs to Schlumberger.

(1) Numerical model

The dual porosity single permeability gas water two phase radial geological model is developed according to the mechanism of CBM exploration. Assuming that gas is adsorbed on the surface of matrix system, water existed in the cleat system, and water can't enter into the matrix system (**Figure 1.9**).

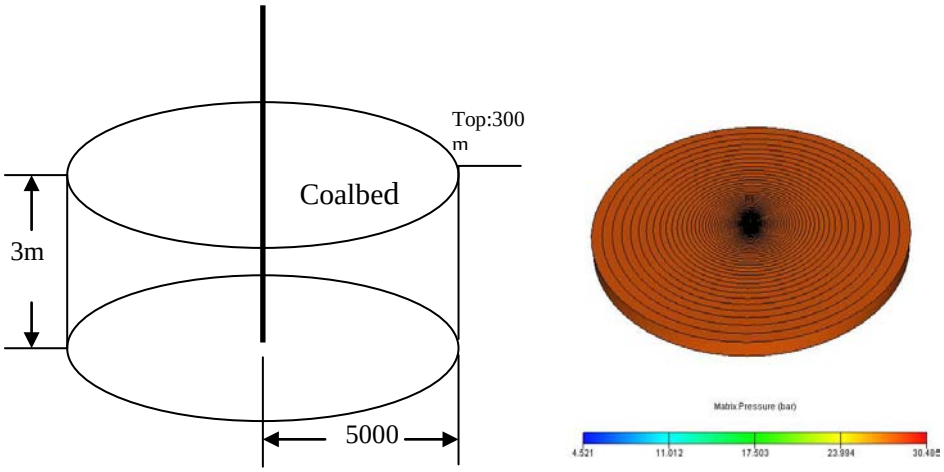

Figure 1.9 Radial Numerical model of CBM reservoir

The matrix permeability of the model is 0, cleat permeability is 5000md. Matrix porosity is 0.08 and cleat porosity is 0.01.

(2) Relative permeability curve

Consider the gas, water capillary effect in the relative permeability curve, and the initial immobile water saturation is 0.2. The relative permeability and capillary pressure curve is shown in **Figure 1.10**.

(3) Initialize the model

The initial pressure at reference surface 300m is 30 Bar; the fracture pressure is generally lower than the matrix pressure to prevent the water in the cleat system flowing into the matrix system. In addition, the initial pressure in the cleat system and matrix system are all 30 Bar.

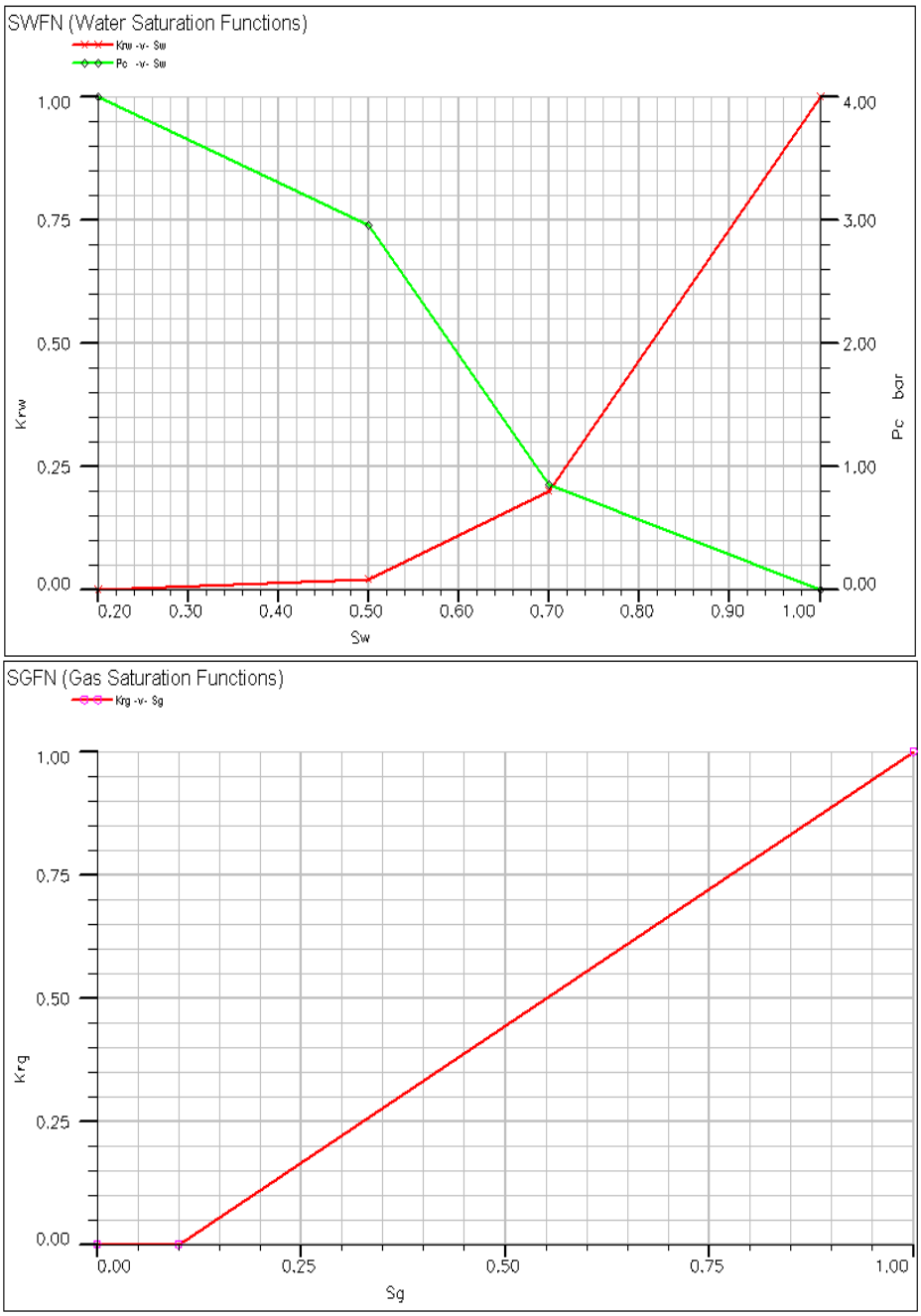

Figure 1.10 Relative permeability and capillary pressure curves for two phase CBM reservoir

(4) Simulation results by black oil model

As known to all, the immobile oil phase in the conventional black oil model is considered as the matrix system of coal seam, the gas desorbed from the oil is achieved through the dissolved gas oil ratio and pressure curve, which approximately represents the isothermal adsorption curve. Thus, the black oil model can approximately simulate the production process of CBM reservoir (**Figure 1.11, Figure 1.12, Figure 1.13 and Figure 1.14**).

As shown in the figure, the first stage is dewatering process, only the water is produced at this stage, the pressure gradually drops with the production time going on. Then the

adsorbed gas began to desorb once the pressure decreases into the critical pressure, this is gas water two phase flow stage, and the gas relative permeability increases while water relative permeability decreases, thus the water production continuously decreases, gas production gradually increases until it reaches its maximum. After that is the third stage, the gas production began to decrease with the simulation time going on, and the water production rate is nearly zero.

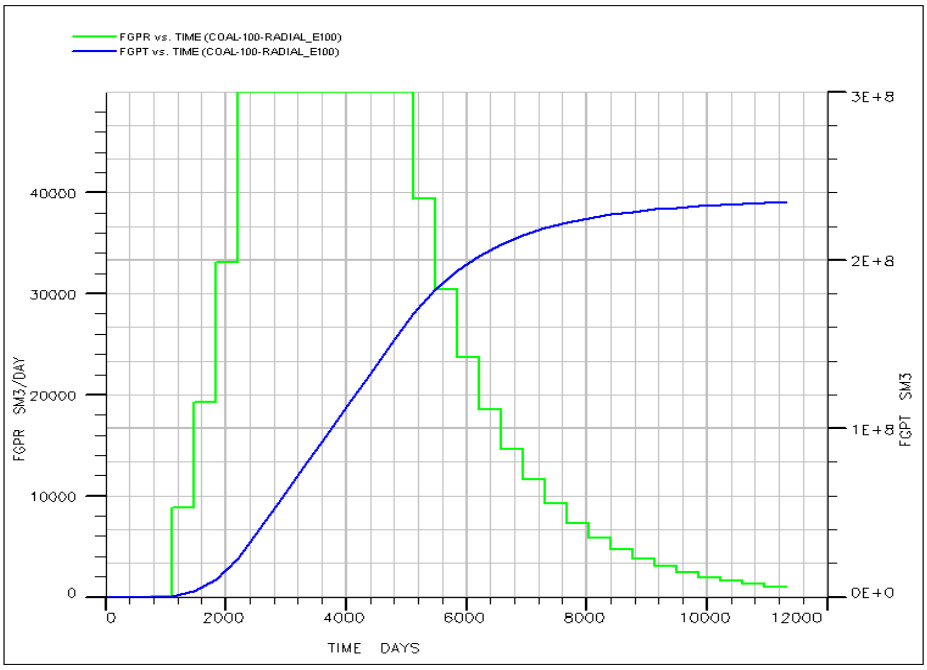

Figure 1.11 Daily gas and total gas production of CBM reservoir

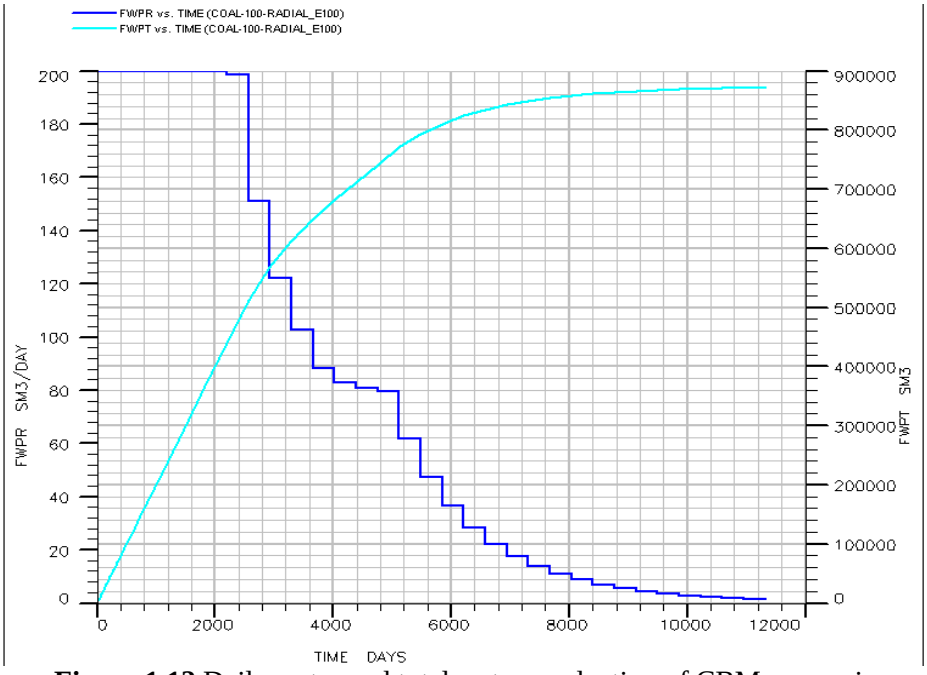

Figure 1.12 Daily water and total water production of CBM reservoir

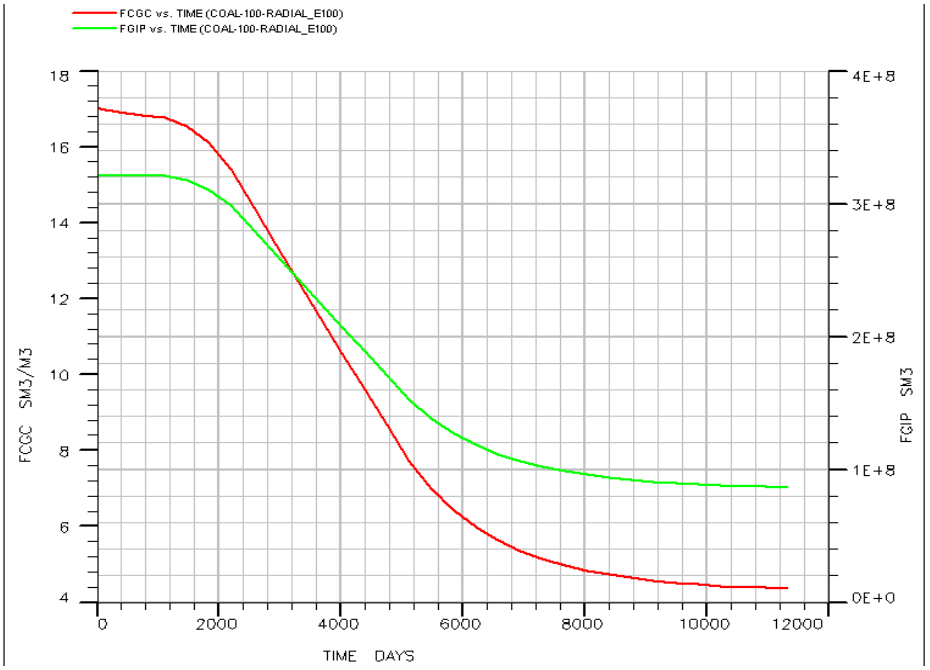

Figure 1.13 Gas concentration and gas in place of CBM reservoir

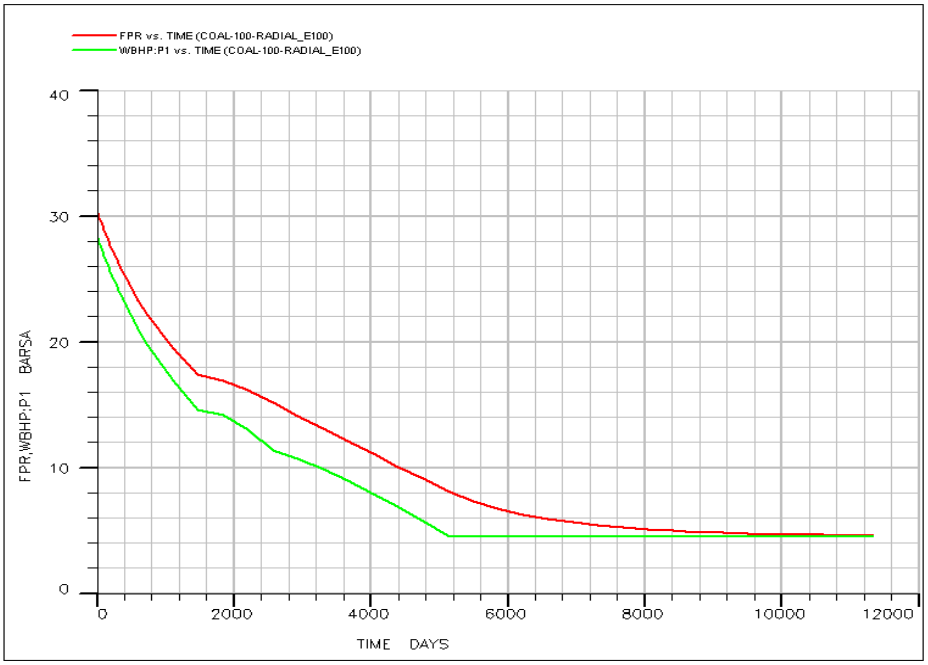

Figure 1.14 Average pressure and WBHP in CBM reservoir

(5) Simulation results using compositional model

The simulation results from compositional model are similar to the results from black oil model (**Figure 1.15, Figure 1.16, Figure 1.17 and Figure 1.18**). The only difference between them is the calculation of K.

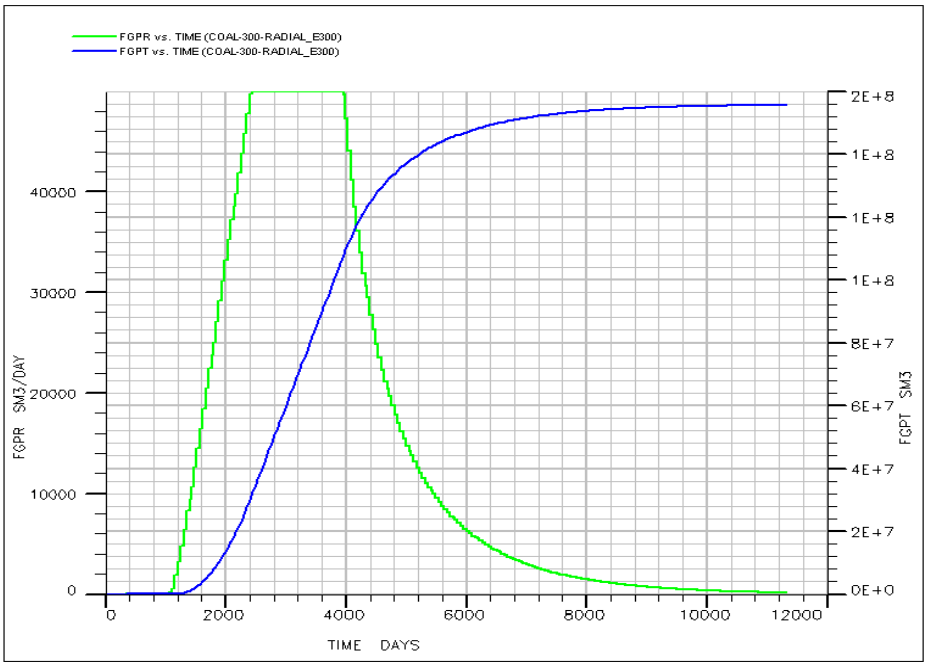

Figure 1.15 Daily gas and total gas production in CBM reservoir

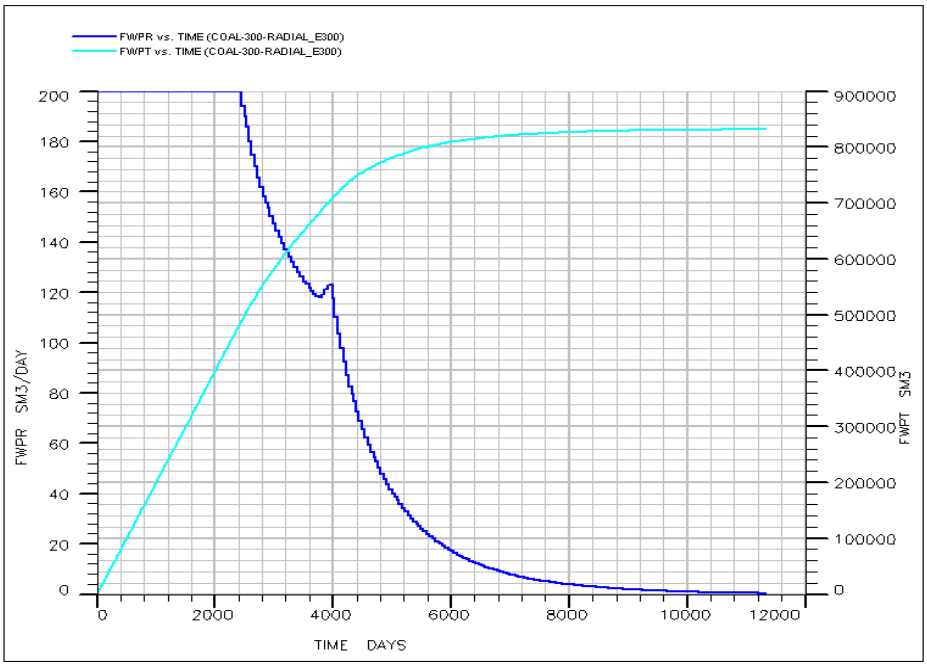

Figure 1.16 Daily water and total water production in CBM reservoir

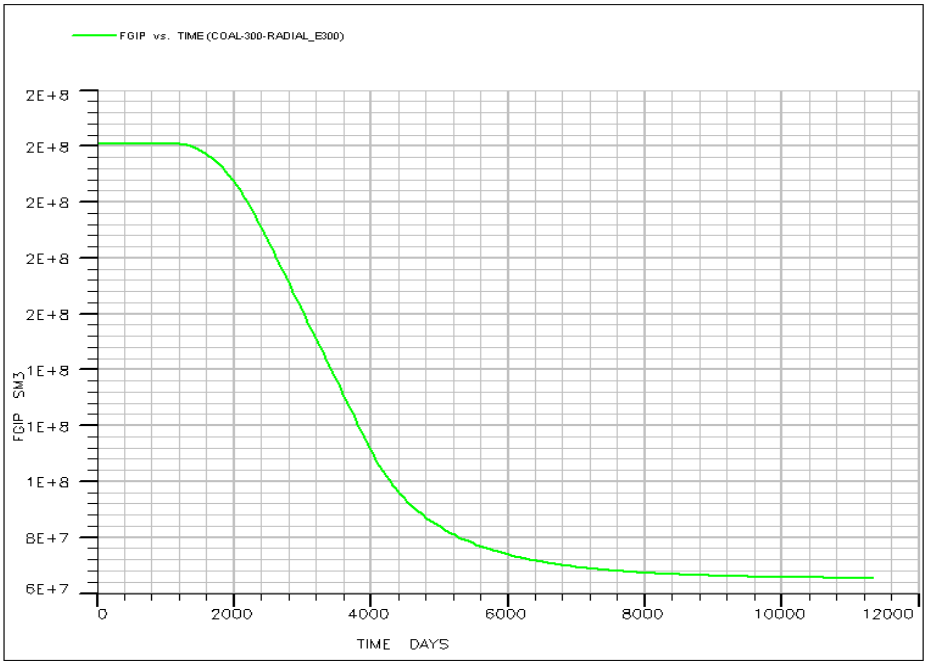

Figure 1.17 Gas in place of the CBM reservoir

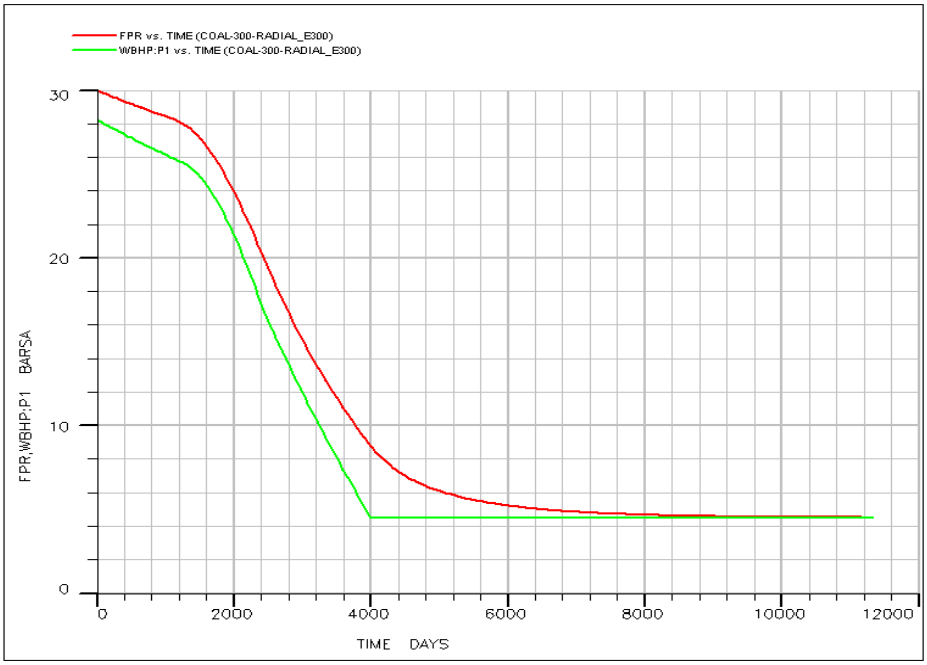

Figure 1.18 Average pressure and WBHP in the CBM reservoir

1.3.2.2 CO_2 displacement simulation

CO_2, N_2 or flue gas (mixture of CO_2 and N_2) can be injected during the early or late CBM development stage according to the different gas adsorption ability in the coal seam. It can not only improve the coal seam pressure but also can make the most of the adsorbed gas in the coal seam being displaced through injection of multiple gases. Thus it can increase the gas production.

The black oil model and compositional model in Eclipse can both consider the injection of CO_2 for displacement. But the black oil model can only consider the single gas injection (single CO_2 or single N_2), while the compositional model can also consider the multiple gas injection. So the compositional model in Eclipse is used for the simulation.

(1) Numerical model

Different from the conventional dual porosity single permeability radial model, the multiple gas injection model uses the rectangular coordinates. The grid for the geological model (**Figure 1.19**) is 11*11*2, the injection CBM well is located in one corner, and the production CBM well is located in the opposite corner.

(2) Simulation result

The injection of flue gas started once the production of Coalbed Methane begins (**Figure 1.20**). The Coalbed Methane production rate decreases initially, then increases and decreases again as shown in the figure. In addition, the drop scale of the methane is not very obvious before the flue gas breakthrough, while the Coalbed Methane production rate suddenly drops quickly and the flue gas production rate gradually increases once the flue gas starts to produce.

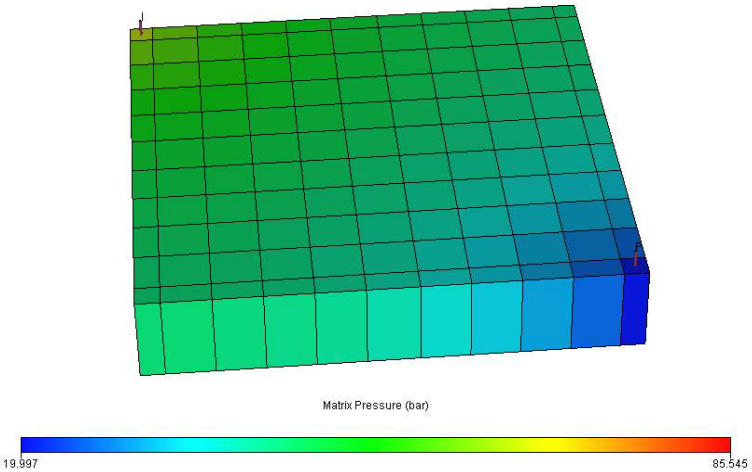

Figure 1.19 Multiple displacement CBM reservoir simulation model

The variation trend of the molar fraction for CH_4 and flue gas (**Figure 1.21**) is very similar to the CH_4 and flue gas production rate trend. Also, the injection pressure has the same changing trend with the coal average pressure (**Figure 1.22**), it decreases initially because of the large production rate of the Coalbed Methane, and then grandually increases, which is caused by the flue gas injection.

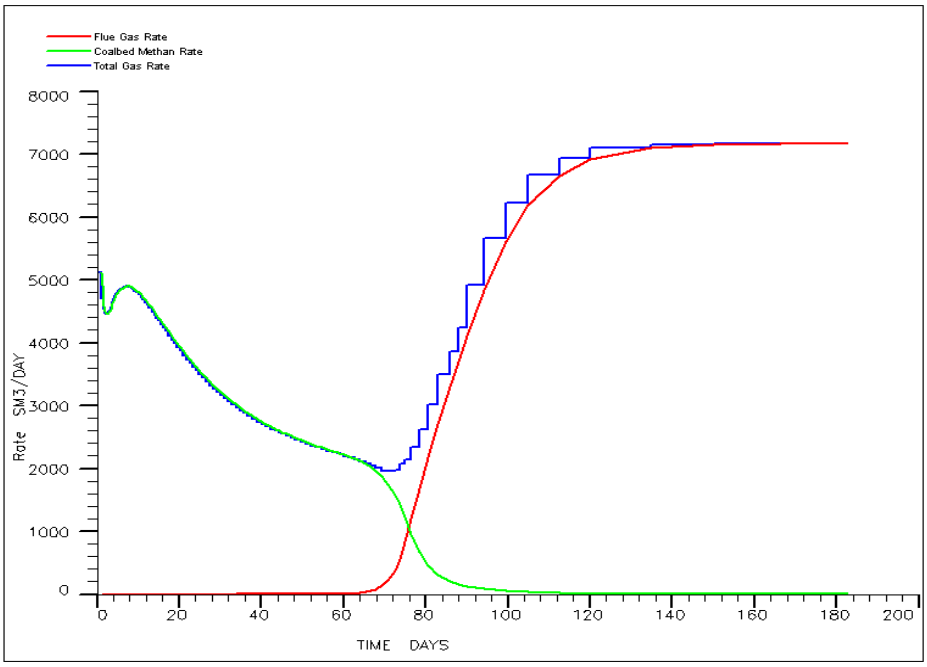

Figure 1.20 Daily Methane, flue gas rate and total gas rate

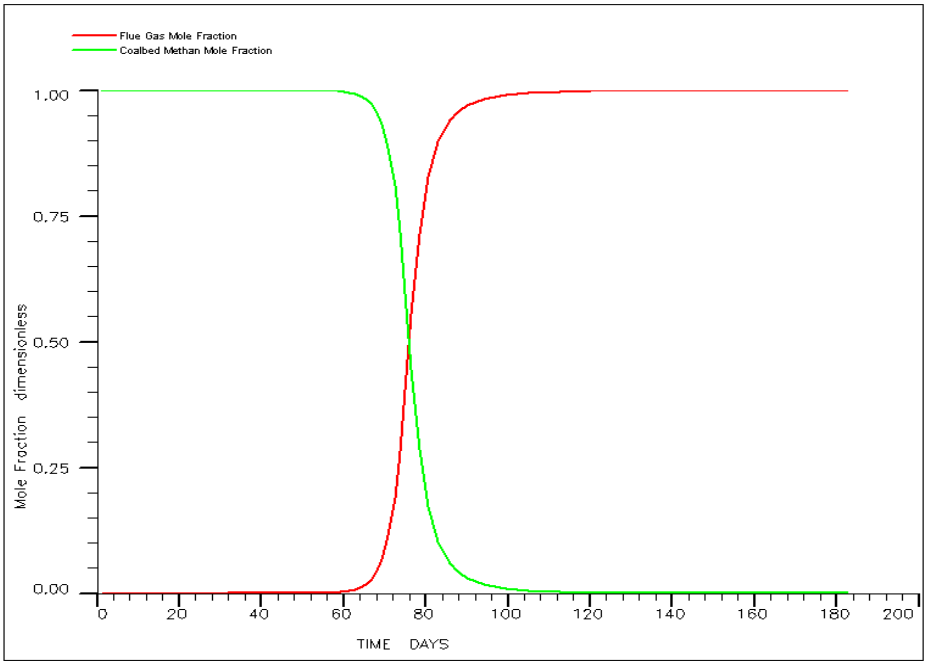

Figure 1.21 Mole fraction of methane and flue gas

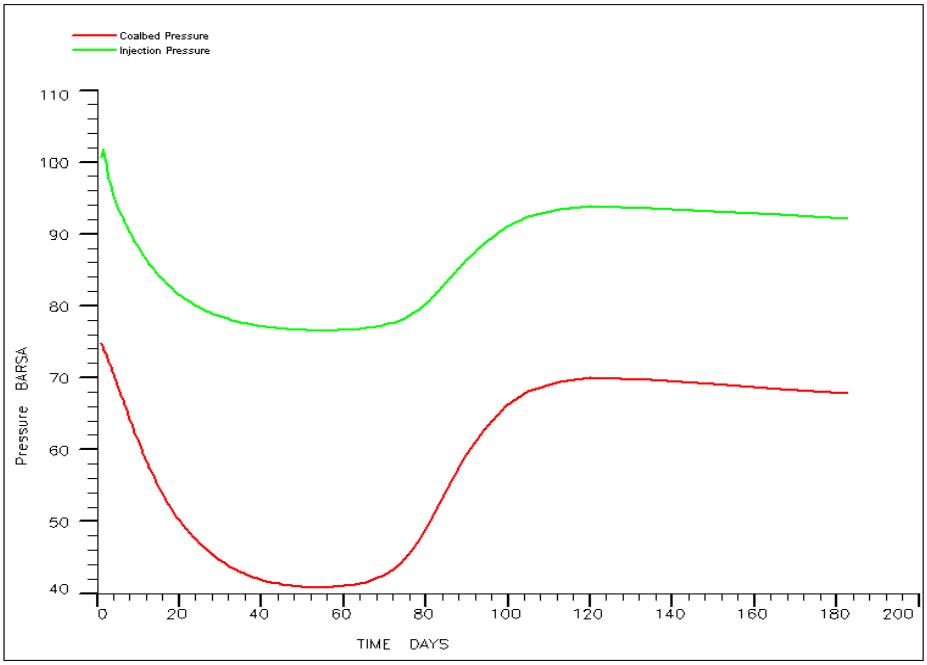

Figure 1.22 Changes of injection pressure and average pressure

1.3.3 Review of the latest development in CBM reservoir simulation

1.3.3.1 CO2 fracture

It is not applicable to all the coal seams through injection of CO_2 to improve the CBM recovery according to most of the experimental study. Because there are many types of coal seams, and the productivity of only a few types' coal seams can be enhanced through the injection of CO_2. In addition, the CO_2 that is not adsorbed on the matrix surface of the coal seam will cause the depletion of the effective fracture porosity, which will hinder the CBM diffusion and flow in the cleat system. Thus, the method that initially fracturing using CO_2 to improve the cleat flow ability, and then displacing the CBM that existed on the surface of the coal seam matrix system by injecting CO_2 to increase the CBM concentration in the cleat system, is very popular in the world.

1.3.3.2 Enhanced gas recovery by Microbial means

The primary recovery of CBM through dewatering process can be 20%-60%, and the secondary recovery through the injection of CO_2 and N_2 can be 60%-80%. Presently, the more forward technique is to continue injecting micro-organisms after the injection of CO_2 and N_2, using the role of nitrogen fixation of N2 and carbon sequestration of CO2 to transfer N2 into ammonia and CO2 into organic polymer carbon. Thus, the adsorption quantity of CBM on the matrix surface can be increased, and most of the CBM can be desorbed from the matrix surface. The final recovery can be increased by 8%-10% by using this method.

1.3.3.3 Coal Gasification

The underground coal seam is not likely to be explored using the underground mining method during the late stage of deep CBM exploration, and the most popular method adopted for this is the coal gasification method. The specific process is shown in **Figure 1.23**.

The coal is ignited by the injection of oxygen or air, the chemical reactions for the degasification process are shown in **Table 1.4**, and the oxygen concentration and burning time is very important during the degasification process. Because there will be too much CO_2 to be produced if completed combustion, which falls short of coal degasification effect. Many countries around the world had done the coal degasification pilot test, while the success report of it is not too much.

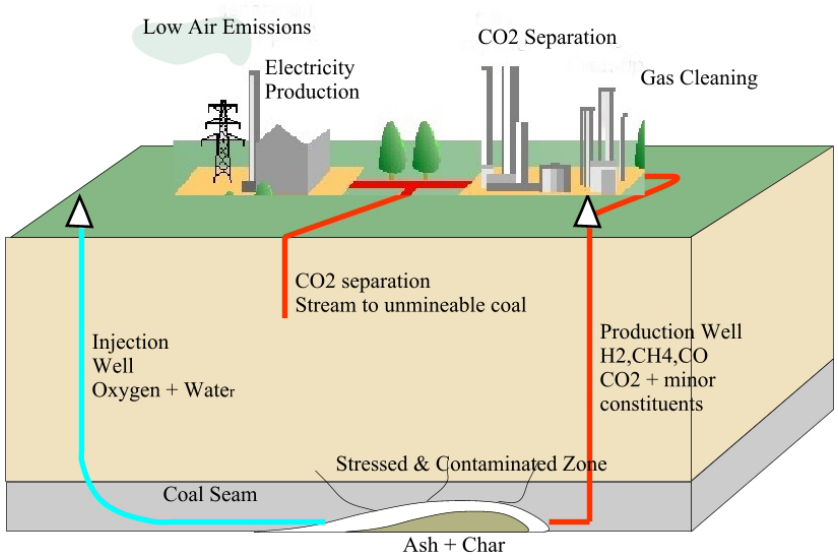

Figure 1.23 Schematic diagram for deep coal gasification process

Reaction		Enthalpy
(1)	Heterogeneous water-gas shift reaction $C + H_2O = H_2 + CO$	$\Delta H = +118.5$ kJ mol-1
(2)	Shift conversion $CO + H_2O = H_2 + CO_2$	$\Delta H = -42.3$ kJ mol-1
(3)	Methanation $CO + 3H_2 = CH_4 + H_2O$	$\Delta H = -206.0$ kJ mol-1
(4)	Hydrogenating gasification $C + 2H_2 = CH_4$	$\Delta H = -87.5$ kJ mol-1
(5)	Partial oxidation $C + 1/2O_2 = CO$	$\Delta H = -123.1$ kJ mol-1
(6)	Oxidation $C + O_2 = CO_2$	$\Delta H = -406.0$ kJ mol-1
(7)	Boudouard reaction $C + CO_2 = 2CO$	$\Delta H = +159.9$ kJ mol-1

Table 1.4 Chemical reaction during the coal degasification process

1.4 Motivation and objective

Many CBM reservoirs have been simulated and studied by scholars. However, the agreement between the simulated result and the field data are not satisfactory due to the limitation of the current developed mathematical model, e.g., the comprehensive effect of gas slippage and threshold pressure gradient as one part are not considered in the model, some of the matrix shrinkage effect model are not reasonable enough. Frequently, the modern CBM reservoir model is highly heterogeneous and low permeability. Thus, some rules of CBM reservoir flow, some accurate and practical CBM reservoir flow model as well as some well testing methods for CBM reservoir are required so that it can be truly and accurately used for the reservoir simulation in real time. It is this demand that motivated the work of this thesis.

The main objective of this thesis is to find some improved mathematical models and well testing methods (based on the published dual porosity, triple porosity CBM reservoir model, the traditional well testing method used for conventional reservoir and unconventional reservoir) for the simulation of low permeability CBM reservoir which are suitable for the history matching of field data. In order to achieve this, the main considerations are as follows:

To develop the advanced dual porosity, single permeability two phase CBM reservoir model, which reflects the concrete influence factors in low permeability CBM reservoirs, such as high velocity non-Darcy flow, threshold pressure and slippage effect. This was followed by a new theoretical formulation of permeability and porosity including the effect of matrix shrinkage.

To develop a new coupled CBM reservoir model to simulate the flow flux and pressure in the CBM reservoir and horizontal wellbore simultaneously. To gain a thorough understanding of vertical well model and coupled horizontal wellbore models by conducting the qualitative comparison of the gas and water production rate.

To develop the triple porosity dual permeability CBM reservoir model that is suitable for the particular field. The gas slippage and threshold pressure gradient effects are both considered, a new permeability and porosity model that reflects both the stress effect and the matrix shrinkage effect is developed. To find the production differences among different well types. The final objective is that this model can be easily used to

guide the reservoir management. What is more, the well testing method is also need to be investigated for this model.

To test the accuracy of the developed advanced models, the validity of understanding and the practicality of procedure, some field examples will be confirmed by these approaches and models.

1.5 Study workflow and outline of the thesis

1.5.1 Study workflow

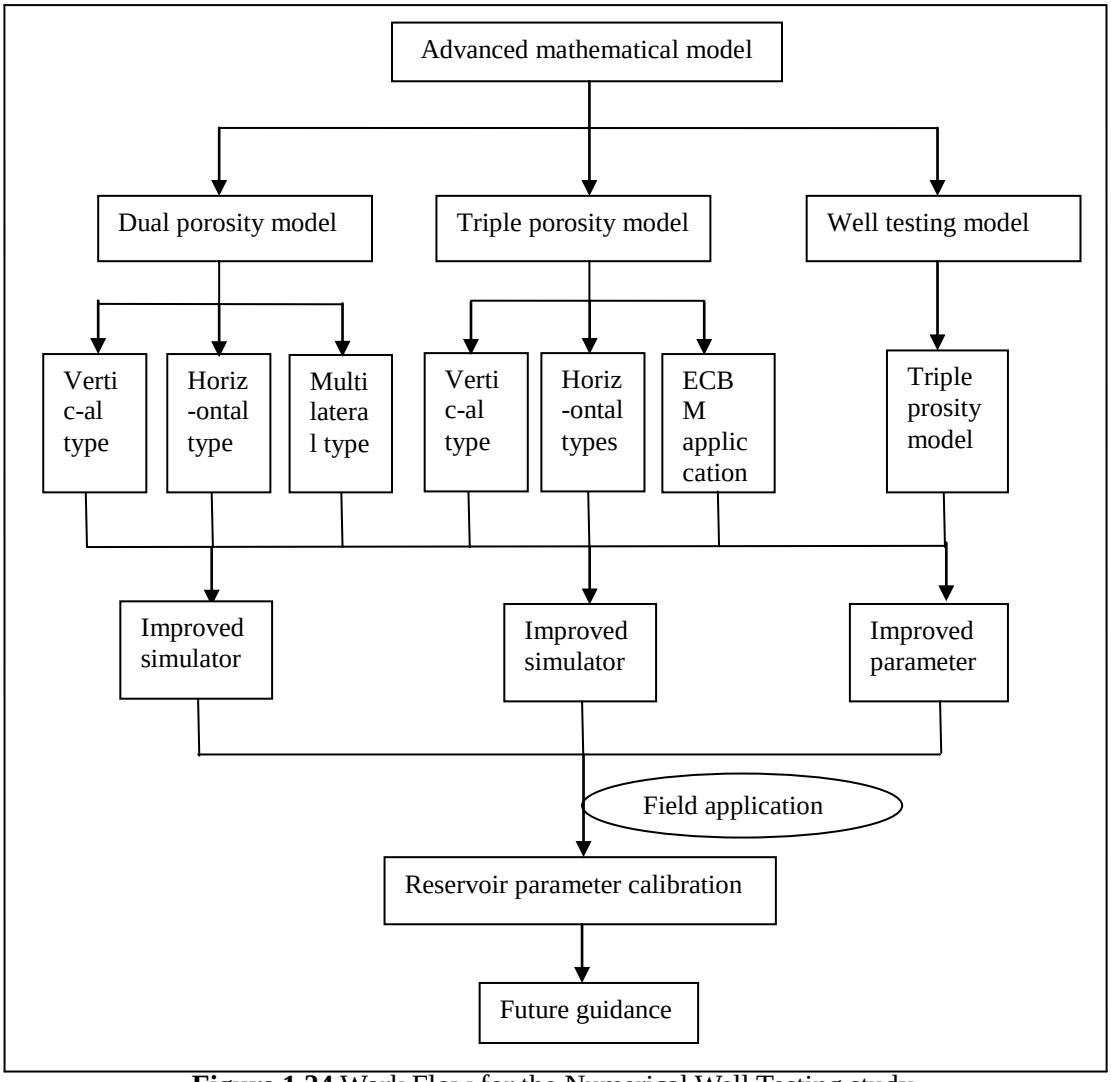

Figure 1.24 Work Flow for the Numerical Well Testing study

In this study, the advanced mathematical models for CBM reservoir with different well types (such as dual porosity vertical well model and horizontal well model, triple porosity vertical well model and multi-branch well model, et al.) are developed based on the published CBM reservoir models. In addition, the well testing model particularly for triple porosity vertical well model is built. The details are summarized (**Figure 1.24**) as follows.

Firstly, building up the advanced mathematical model for low permeability CBM reservoir through vertical well, the gas slippage and threshold pressure gradient effects are considered, the permeability model that reflects the matrix shrinkage effect is also investigated. The IMPES method is modified to get the solution of the model. Then, the corresponding coupled CBM reservoir models are developed.

Secondly, considering the variety of the coal seam types, the triple porosity dual permeability models through vertical, horizontal and multi-branch horizontal well type are developed for the simulation of particular coal seams. The sensitivity analysis as well as the comparison of productivity for different well types is made to guide for the future field application. The corresponding well testing method is then proposed for the validation of the parameter value.

Thirdly, in order to confirm these developed models, three field examples were studied through history matching using the models developed in this thesis. The history matching results validate the accuracy and reasonability of the models proposed. In addition, the calibration for different parameters is made. The calibrated parameters are qualified enough for the accurate simulation of different fields.

1.5.2 Outline of the thesis

This thesis is structured as follows:

Chapter 1 has given a brief background about the development of CBM reservoir: the application of mathematical method in the CBM reservoir and the advantages as well as the disadvantages of the existing well testing technology, production forecast method, matrix shrinkage and swelling technology, ECBM technology in the CBM reservoir. Ultimately, the development of the novel mathematical models and the corresponding well testing methods which are suitable for the accurate simulation and testing of mature field models is determined as the focus of this thesis.

Chapter 2 shows a description of an improved dual porosity, single permeability model of two phase CBM reservoir, this is followed by an newly developed permeability model. The traditional dual porosity single permeability model for CBM reservoir didn’t consider the threshold pressure gradient and gas slippage effects. Also, the permeability that reflects the matrix shrinkage effect is not accurate enough, which will result in the unpractical forecasted field gas and water production rate. Thus the

modified dual porosity mathematical CBM reservoir model in this Chapter is studied for better future field evaluation.

Chapter 3 contains the advanced coupled models to simulate the fluid flow in the low permeability CBM reservoir and horizontal borehole simutaneously. As described in **Chapter2**, the vertical well model can also simulate the fluid flow in the CBM reservoir. However, the recovery of the gas is very low and needs to be improved from the economic view. Thus the finding of much more optimized methods for the simulation of CBM reservoir to enhance the recovery rate is implemented in this Chapter. The study of the single branch and multi-branch horizontal wellbore CBM reservoir models are the focus of this Chapter.

Chapter 4 illustrates the application of ECBM technology in the advanced coupled triple porosity CBM reservoir model. The traditional ECBM reservoir technologies didn't extend the simulation model to the comprehensive compositional triple porosity model that considering the gas slippage and threshold pressure gradient effects which surely has superiority over the conventional dual porosity model as discussed in **Chapter 2** and **Chapter 3**. Also, a novel permeability model based on the surface energy theories is developed to study the matrix shrinkage and swelling effects. In addition, the model is applied to the wells in Yanchuan Southern block for history matching. The calibrated parameters are got through this process which can be used for the guidance of future field application.

Chapter 5 proposed the systematic well testing method for triple porosity CBM reservoir model. Transient testing is a useful tool in managing CBM reservoirs, however, the information from actual field data is not enough to determine the changes of permeability, which is a very important parameter in the forecasting of the production rate for CBM wells. Thus, the pressure squared well testing method is discussed in this Chapter. It neither need the relative permeability curve nor the variation of the pressure gradient for the well interpretation, only the gas saturation gradient of the two phase flow needs to be ignored.

Chapter 6 takes the knowledge described in the previous chapters and applies it to three real field examples. Case studies are designed to test the applicability of the mathematical models for CBM reservoir. These practical applications confirm that the novel mathematical models developed in the thesis can successfully matching the three

real field data by adjusting the reservoir fluid flow parameters and carrying out dynamic management in mature fields.

Chapter 7 concludes by summarizing the thesis, including its major findings and its possible contributions to industry. The outlines for the future work are also listed.

Chapter 2 Modelling and simulation of a new dual porosity, single permeability model of two phase CBM reservoir

2.1 Introduction

Nowadays, CBM is gradually being widely focused by every country in the world as the alternative energy resource of oil and conventional natural gas for the next few decades. The coal with adsorbed gas is shown in **Figure 2.1**. Low permeability CBM reservoirs are characterized by their low porosity and permeability, which in turn induce their complicated permeability characteristics of gas and water during production. Numerical experiments and field applications proved that there exists percolation non-linearity and fluid muti-variability in low permeability CBM reservoirs. The percolation of fluid needs to overcome threshold pressure gradient, and klinkenberg effects will restrict the gas permeability.

Figure 2.1 Coal in the reservoir

Traditionally, the published models for CBM reservoir are classified into three types: empirical, equilibrium, and non equilibrium. Equally, according to the phase diffusivity equation the models are classified into single phase diffusivity equation (**Ertekin, T., et al., 1986[33]; Bayles, G.A. and Reznik, A.A., 1986[42]; Bumb, A.C. and McKee, C.R., 1988[44]; Ertekin, T. and Sung, W., 1989[45]; Sarkar, P.S. and Rajtar, J.M., 1994[46]; Kamal, M.M. and Six, J.L., 1993[47]**) and two phase diffusivity equation (**Ancell, K.L., et al., 1980[41]; King, R.G., et al, 1986[43]; Zhang, X.M. and Tong, D.K., 2008[48]; Ozdemir, E., 2009[50]; Scott, R., and Larry, P., 2001[51]**).

Currently, the two phase diffusivity equation is the most popular one for the simulation of CBM reservoir. Unquestionably, many assumptions are made for the models.

In these models, the single phase models are simple, but they can't truly respond the actual field production of CBM reservoir. Because the well will initially pump the water existed in the reservoir accompanying with the pressure depletion, then the gas will be desorbed from the matrix once the pressure drops below the critical pressure, the gas will be produced together with water during this period, which is known as the water and gas two phase production period.

Some people had studied the production data analysis for single gas phase, water and gas two phase and single water phase in the CBM reservoir (**Clarkson, C.R., et al., 2008[18]**). They focused on the extension of existing PDA techniques to include more complex CBM reservoir behaviour such as changes in effective permeability to gas and evolution of produced gas compositions during depletion. However, they didn't consider the effects of gas slippage and threshold pressure gradient.

This chapter focus on the development of a three dimensional, dual porosity, single permeability, non-equilibrium adsorption, gas-water two phase flow, pseudo-steady state mathematical model, which reflects the concrete influence factors in low permeability CBM reservoirs, such as high velocity non-Darcy flow, threshold pressure gradient and gas slippage effects. This was followed by a new theoretical formulation of permeability and porosity including the effect of matrix shrinkage.

This new model was solved by a fully implicit numerical method and the block pre-conditioning orthogonal minimisation algorithm. A computer programme has been developed for this purpose. Comparison of gas production rate between those from Eclipse software and the current programme was made. A number of synthetic cases were studied, which proved that the developed algorithm works well for solving the problem stated above.

2.2 New developed permeability model

Langmuir isotherms are widely used to describe adsorption/desorption of methane in coal:

$$V_E = \frac{V_L bp}{1+bp} \tag{2.1}$$

Particles on the coal matrix surface possess certain surface energy, resulting in the gas molecules adsorption, and the surface energy will be reduced after gas molecules adsorption (**Wu, J., 1994[146]**). The solid swelling strain is proportional to its surface energy reduction (**Zhang, X.M. and Tong, D.K., 2008[48]**):

$$\varepsilon_s = \rho_c S \Delta\gamma / E \tag{2.2}$$

The surface energy variation of coal matrix caused by gas adsorption is given by Gibbs equation (**Zhang, X.M. and Tong, D.K., 2008[48]**) as follows:

$$\Delta\gamma = \gamma_0 - \gamma = \int_0^p \Gamma RTd \ln p \tag{2.3}$$

Substituting **Equation (2.3)** into **Equation (2.2)**, rearranging:

$$\varepsilon_s(p) = \frac{\rho_c RT}{V_0 E} \int_0^p \frac{V}{p} dp \tag{2.4}$$

The cubic relationship between permeability and porosity to evaluate changes in permeability is used (**Palmer, I. and Mansoori, J., 1998[61]**):

$$\frac{k}{k_0} = (\frac{\phi}{\phi_0})^3 \tag{2.5}$$

The equation for the variation of porosity is described as the following manner (**Palmer, I. and Mansoori, J., 1998[61]**):

$$\phi - \phi_0 = \frac{1}{M}(p - p_0) - (1 - \frac{K}{M})\Delta\varepsilon_s \tag{2.6}$$

Where:

$$M = \frac{E(1-\nu)}{(1+\nu)(1-2\nu)}$$

$$K = \frac{E}{3(1-2\nu)}$$

$$\frac{k}{k_0} = (\frac{\phi}{\phi_0})^3$$

Given that matrix shrinkage is caused by gas desorption from coal during reservoir drawdown, it is reasonable to describe the matrix shrinkage using the above formulation when the reservoir pressure declines from the critical desorption pressure p_r to p:

$$\Delta\varepsilon_s = \varepsilon(p_r) - \varepsilon(p) = \frac{\rho_c RT}{V_0 E}\int_{p_r}^{p}\frac{V}{p}dp \tag{2.7}$$

Substituting **Equation (2.1)** into **Equation (2.7)**, the matrix shrinkage effect under one gas component is given as follows:

$$\Delta\varepsilon_s = \frac{\rho_c V_L RT}{V_0 E}\ln\left(\frac{1+bp_0}{1+bp}\right) \tag{2.8}$$

Substituting **Equation (2.8)** into **Equation (2.6)**, rearranging it:

$$\phi - \phi_0 = \frac{1}{M}(p - p_0) - (1-\frac{K}{M})\frac{\rho_c V_L RT}{V_0 E}[\ln(1+bp_0) - \ln(1+bp)] \tag{2.9}$$

Equation (2.5) and **Equation (2.9)** describe how the permeability in CBM reservoir varies with pore pressure during primary production. The two terms on the right side of **Equation (2.9)** are referred to as the cleat compression and matrix shrinkage terms respectively.

2.3 Modelling of fluid flow in the coal seams

Based on the existing models and field practices, a new dual porosity, single permeability model of CBM reservoir for gas and water two phase production through vertical wells is presented with the following assumptions:

(1) The coal seams are generally characterized as a dual porosity nature composed of a micro-pore system and macro-pore system, and the shape of the reservoir is rectangular.

(2) The coal seams are compressible horizontal reservoir, and

(3) The CBM reservoir system is heterogeneous and anisotropy.

(4) In the original state, coal seams are fully saturated by water, and methane is stored on the internal surface of coal matrix in adsorbed state.

(5) Water is treated as a slightly compressible fluid, and the coal matrix, as a result of its small pore diameter, is inaccessible to water.

(6) The free gas in the fracture system is assumed to behave like a real gas.

(7) The fluid flow in the cleat porosity is a laminar flow due to larger pore sizes and governed by the Darcy's law, the flow in the coal matrix is a diffusion flow due to smaller pores and governed by Fick's first law.

2.3.1 Transport equations in the cleat system

For the gas phase

$$\begin{aligned}&\nabla\cdot\left(\frac{k_f k_{rg\infty}}{\mu_g B_g}(1+\alpha_1(\frac{k_f k_{rg\infty}(s_g)}{\phi_g})^{-\alpha_2}/p_m)(\nabla(p_{fg}-\gamma_g H)-\lambda_{bg})+D_a\nabla(\frac{s_g}{B_g})\right)\\&-q_{vg}+q_{mfg}=\frac{\partial}{\partial t}\left(\frac{\phi_f s_g}{B_g}\right)\end{aligned} \tag{2.10}$$

For the water phase

$$\nabla\cdot\left(\frac{k_f k_{rw\infty}}{\mu_w B_w}(\nabla(p_{fw}-\gamma_w H)-\lambda_{bw})\right)-q_{vw}=\frac{\partial}{\partial t}\left(\frac{\phi s_w}{B_w}\right) \tag{2.11}$$

2.3.2 Auxiliary equations

Equation (2.10) and **Equation (2.11)** is the second order nonlinear partial differential equations which contain four unknowns: p_{fg}、s_g、p_{fw}、s_w . At the same time, p_{fg}、s_g、p_{fw}、s_w satisfy the following state equation:

$$s_g+s_w=1 \tag{2.12}$$

$$p_{cgw}(s_g)=p_{fg}-p_{fw} \tag{2.13}$$

The $p_{cgw}(s_g)$ in the **Equation (2.13)** is called capillary pressure function, which is a given function.

2.3.3 Diffusion/Sorption Formulation

And the desorption rate of gas from coal matrix to fracture is:

$$q_{mfg} = -\frac{\rho_c}{B_g}\frac{\partial V_m}{\partial t} \tag{2.14}$$

Here, the desorbed gas diffusion through the coal matrix system to the cleat system can be described mathematically by Fick'k first law, and the migration velocity of desorbed gas is assumed as a result of concentration gradients in the matrix (**Wu, J., 1994[146]**):

$$\frac{\partial V_m}{\partial t} = -\frac{1}{\tau}[V_m - V_E(p_{fg})] \tag{2.15}$$

The expression of $V_E(p_{fg})$ is shown in **Equation (2.1)**.

2.3.4 Initial conditions of the model

$$p_{fg}(x, y, z, 0) = p_{fg}^0(x, y, z) \tag{2.16}$$

$$s_g(x, y, z, 0) = s_g^0(x, y, z) \tag{2.17}$$

2.3.5 Inner boundary condition

The internal boundary condition at the well can be given as either a pressure constrained or a rate constrained. For the pressure constrained well, the bottom-hole pressure is specified. For rate constrained well, either gas production rate, water production rate, or total production rate can be specified. A more realistic inner boundary condition is that the constant pressure along the open portion of the well-bore resulting in a flux that is not uniform. This is known as the infinite conductivity boundary condition implying that the well-bore pressure is uniform and the integral of the flux over the perforated interval is equal to the constant specified rate. This can be written:

$$q_{vw} = -\int_{p_{wf}}^{p_e} \frac{2\pi hkk_{rw\infty}}{\mu_w B_w} r \frac{dp}{dr}\Big|_{r=r_w} \tag{2.18}$$

$$\frac{\mu_g}{k_g}\frac{q_{vg}}{2\pi rh}\frac{zTp_{sc}}{T_{sc}p} + \beta\rho_g\left(\frac{q_{vg}}{2\pi rh}\frac{zTp_{sc}}{T_{sc}p}\right)^2 = \frac{d(p - \lambda_{bw}r)}{dr}\Big|_{r=r_w} \tag{2.19}$$

2.3.6 External boundary condition

The outer boundary condition can be assumed to be both constant pressure and a no-flow outer boundary due to the symmetrically located wells.

2.3.6.1 Constant pressure external boundary

$$p_{fg}\big|_{x=0} = p_e \qquad p_{fg}\big|_{x=L} = p_e$$

$$p_{fg}\big|_{y=0} = p_e \qquad p_{fg}\big|_{y=W} = p_e \tag{2.20}$$

$$p_{fg}\big|_{z=0} = 0 \qquad p_{fg}\big|_{z=H} = 0$$

$$\frac{\partial s_g}{\partial x}\Big|_{x=0} = 0 \qquad \frac{\partial s_g}{\partial x}\Big|_{x=L} = 0$$

$$\frac{\partial s_g}{\partial x}\Big|_{y=0} = 0 \qquad \frac{\partial s_g}{\partial x}\Big|_{y=W} = 0 \tag{2.21}$$

$$\frac{\partial s_g}{\partial x}\Big|_{z=0} = 0 \qquad \frac{\partial s_g}{\partial x}\Big|_{z=H} = 0$$

2.3.6.2 Closed external boundary

$$\frac{\partial p_{fg}}{\partial x}\Big|_{x=0} = 0 \qquad \frac{\partial p_{fg}}{\partial x}\Big|_{x=L} = 0$$

$$\frac{\partial p_{fg}}{\partial y}\Big|_{y=0} = 0 \qquad \frac{\partial p_{fg}}{\partial y}\Big|_{y=W} = 0 \tag{2.22}$$

$$\frac{\partial p_{fg}}{\partial z}\Big|_{z=0} = 0 \qquad \frac{\partial p_{fg}}{\partial z}\Big|_{z=H} = 0$$

$$\frac{\partial s_g}{\partial x}\Big|_{x=0} = 0 \qquad \frac{\partial s_g}{\partial x}\Big|_{x=L} = 0$$

$$\frac{\partial s_g}{\partial x}\Big|_{y=0} = 0 \qquad \frac{\partial s_g}{\partial x}\Big|_{y=W} = 0 \tag{2.23}$$

$$\frac{\partial s_g}{\partial x}\Big|_{z=0} = 0 \qquad \frac{\partial s_g}{\partial x}\Big|_{z=H} = 0$$

Equation (2.1)-Equation (2.23) consist the complete CBM transport model that in consideration of both gas slippage effect and threshold pressure gradient effect. Moreover, the new developed permeability model is integrated into the transport model of CBM reservoir to study the matrix shrinkage effect.

2.4 Solution for the model

2.4.1 Numerical solutions of transport model for CBM reservoir

The CBM reservoir model developed above can be characterized as the complex non-linear partial differential equations which are difficult to be solved directly, while the numerical method is usually used to solve it. The numerical methods that are generally used in engineering are typically finite difference method, finite element method and finite boundary element method.

Among them, the finite difference method is the most popular one for the oil and gas numerical simulation. This is because it is faster and more mature than any other numerical methods. Thus the fully implicit finite difference method is adopted in this chapter to find the solution for the comprehensive CBM reservoir model.

Firstly, difference the partial differential equation for the gas phase using central block difference method, and then multiply it by $V_{i,j,k} = \Delta x_i \Delta y_j \Delta z_k$, the volume of unit grid block (i, j, k), , there is:

$$\Delta y_j \Delta z_k \left\{ \left(\frac{k_{fx} k_{rg\infty}}{\mu_g B_g} [1 + \alpha_1 (\frac{k_{fx} k_{rg\infty}(s_g)}{\phi_g})^{-\alpha_2} / p_m] \right)_{i+\frac{1}{2},j,k} \left[\frac{p_{fgi+1,j,k} - p_{fgi,j,k}}{\Delta x_{i+\frac{1}{2},j,k}} - \gamma_{gi+\frac{1}{2},j,k} \frac{H_{i+1,j,k} - H_{i,j,k}}{\Delta x_{i+\frac{1}{2},j,k}} - \lambda_{bg} \right] \right.$$

$$+ \frac{D_{fx_{i+\frac{1}{2},j,k}}}{\Delta x_{i+\frac{1}{2},j,k}} \left((\frac{s_g}{B_g})_{i+1,j,k} - (\frac{s_g}{B_g})_{i,j,k} \right) - \left(\frac{k_{fx} k_{rg\infty}}{\mu_g B_g} [1 + \alpha_1 (\frac{k_{fx} k_{rg\infty}(s_g)}{\phi_g})^{-\alpha_2} / p_m] \right)_{i-\frac{1}{2},j,k}$$

$$\left. \left[\frac{p_{fgi,j,k} - p_{fgi-1,j,k}}{\Delta x_{i-\frac{1}{2},j,k}} - \gamma_{gi-\frac{1}{2},j,k} \frac{H_{i,j,k} - H_{i-1,j,k}}{\Delta x_{i-\frac{1}{2},j,k}} - \lambda_{bg} \right] - \frac{D_{fx_{i-\frac{1}{2},j,k}}}{\Delta x_{i-\frac{1}{2},j,k}} \left((\frac{s_g}{B_g})_{i,j,k} - (\frac{s_g}{B_g})_{i-1,j,k} \right) \right\}$$

$$+ \Delta x_i \Delta z_k \left\{ \left(\frac{k_{fy} k_{rg\infty}}{\mu_g B_g} [1 + \alpha_1 (\frac{k_{fy} k_{rg\infty}(s_g)}{\phi_g})^{-\alpha_2} / p_m] \right)_{i,j+\frac{1}{2},k} \left[\frac{p_{fgi,j+1,k} - p_{fgi,j,k}}{\Delta y_{i,j+\frac{1}{2},k}} - \gamma_{gi,j+\frac{1}{2},k} \frac{H_{i,j+1,k} - H_{i,j,k}}{\Delta y_{i,j+\frac{1}{2},k}} - \lambda_{bg} \right] \right.$$

$$+ \frac{D_{fy_{i,j+\frac{1}{2},k}}}{\Delta y_{i,j+\frac{1}{2},k}} \left((\frac{s_g}{B_g})_{i,j+1,k} - (\frac{s_g}{B_g})_{i,j,k} \right) - \left(\frac{k_{fy} k_{rg\infty}}{\mu_g B_g} [1 + \alpha_1 (\frac{k_{fy} k_{rg\infty}(s_g)}{\phi_g})^{-\alpha_2} / p_m] \right)_{i,j-\frac{1}{2},k}$$

$$\left. \left[\frac{p_{fgi,j,k} - p_{fgi,j-1,k}}{\Delta y_{i,j-\frac{1}{2},k}} - \gamma_{gi,j-\frac{1}{2},k} \frac{H_{i,j,k} - H_{i,j-1,k}}{\Delta y_{i,j-\frac{1}{2},k}} - \lambda_{bg} \right] - \frac{D_{fy_{i,j-\frac{1}{2},k}}}{\Delta y_{i,j-\frac{1}{2},k}} \left((\frac{s_g}{B_g})_{i,j,k} - (\frac{s_g}{B_g})_{i,j-1,k} \right) \right\}$$

$$+ \Delta x_i \Delta y_j \left\{ \left(\frac{k_{fz} k_{rg\infty}}{\mu_g B_g} [1 + \alpha_1 (\frac{k_{fz} k_{rg\infty}(s_g)}{\phi_g})^{-\alpha_2} / p_m] \right)_{i,j,k+\frac{1}{2}} \left[\frac{p_{fgi,j,k+1} - p_{fgi,j,k}}{\Delta z_{i,j,k+\frac{1}{2}}} - \gamma_{gi,j,k+\frac{1}{2}} \frac{H_{i,j,k+1} - H_{i,j,k}}{\Delta z_{i,j,k+\frac{1}{2}}} - \lambda_{bg} \right] \right.$$

$$+\frac{D_{fz_{i,j,k+\frac{1}{2}}}}{\Delta z_{i,j,k+\frac{1}{2}}}\left((\frac{s_g}{B_g})_{i,j,k+1}-(\frac{s_g}{B_g})_{i,j,k}\right)-\left(\frac{k_{fz}k_{rg\infty}}{\mu_g B_g}[1+\alpha_1(\frac{k_{fz}k_{rg\infty}(s_g)}{\phi_g})^{-\alpha_2}/p_m]\right)_{i,j,k-\frac{1}{2}}$$
$$\left[\frac{p_{fgi,j,k}-p_{fgi,j,k-1}}{\Delta z_{i,j,k-\frac{1}{2}}}-\gamma_{gi,j,k-\frac{1}{2}}\frac{H_{i,j,k}-H_{i,j,k-1}}{\Delta z_{i,j,k-\frac{1}{2}}}-\lambda_{bg}\right]-\frac{D_{fz_{i,j,k-\frac{1}{2}}}}{\Delta z_{i,j,k-\frac{1}{2}}}\left((\frac{s_g}{B_g})_{i,j,k}-(\frac{s_g}{B_g})_{i,j,k-1}\right)\Bigg\} \quad (2.24)$$
$$+V_{i,j,k}q_{mfgi,j,k}-V_{i,j,k}q_{vgi,j,k}=\frac{V_{i,j,k}}{\Delta t}\left[(\frac{\phi_f s_g}{B_g})^{n+1}_{i,j,k}-(\frac{\phi_f s_g}{B_g})^{n}_{i,j,k}\right]$$

Define the following symbols:

$$F_{i\pm\frac{1}{2},j,k}=\frac{\Delta y_j\Delta z_k}{\Delta x_{i\pm\frac{1}{2},j,k}},F_{i,j\pm\frac{1}{2},k}=\frac{\Delta x_i\Delta z_k}{\Delta y_{i\pm\frac{1}{2},j,k}},F_{i,j,k\pm\frac{1}{2}}=\frac{\Delta x_i\Delta y_j}{\Delta z_{i,j,k\pm\frac{1}{2}}}$$
$$\lambda_{gi\pm\frac{1}{2},j,k}=\left(\frac{k_{fx}k_{rg\infty}}{\mu_g B_g}[1+\alpha_1(\frac{k_{fx}k_{rg\infty}(s_g)}{\phi_g})^{-\alpha_2}/p_m]\right)_{i\pm\frac{1}{2},j,k},\lambda_{gi,j\pm\frac{1}{2},k}=\left(\frac{k_{fx}k_{rg\infty}}{\mu_g B_g}[1+\alpha_1(\frac{k_{fx}k_{rg\infty}(s_g)}{\phi_g})^{-\alpha_2}/p_m]\right)_{i,j\pm\frac{1}{2},k}$$
$$\lambda_{gi,j,k\pm\frac{1}{2}}=\left(\frac{k_{fx}k_{rg\infty}}{\mu_g B_g}[1+\alpha_1(\frac{k_{fx}k_{rg\infty}(s_g)}{\phi_g})^{-\alpha_2}/p_m]\right)_{i,j,k\pm\frac{1}{2}},\lambda_{D_{i\pm\frac{1}{2},j,k}}=\left(D_{fx}\right)_{i\pm\frac{1}{2},j,k},\lambda_{D_{i,j\pm\frac{1}{2},k}}=\left(D_{fy}\right)_{i,j\pm\frac{1}{2},k},\lambda_{D_{i,j,k\pm\frac{1}{2}}}$$
$$=\left(D_{fz}\right)_{i,j,k\pm\frac{1}{2}},T_{gi+\frac{1}{2},j,k}=F_{i+\frac{1}{2},j,k}\times\lambda_{gi+\frac{1}{2},j,k},T_{gi-\frac{1}{2},j,k}=F_{i-\frac{1}{2},j,k}\times\lambda_{gi-\frac{1}{2},j,k};T_{gi,j+\frac{1}{2},k}=F_{i,j+\frac{1}{2},k}\times\lambda_{gi,j+\frac{1}{2},k},T_{gi,j-\frac{1}{2},k}$$
$$=F_{i,j-\frac{1}{2},k}\times\lambda_{gi,j-\frac{1}{2},k},T_{gi,j,k+\frac{1}{2}}=F_{i,j,k+\frac{1}{2}}\times\lambda_{gi,j,k+\frac{1}{2}},T_{gi,j,k-\frac{1}{2}}=F_{i,j,k-\frac{1}{2}}\times\lambda_{gi,j,k-\frac{1}{2}};T_{Di+\frac{1}{2},j,k}=F_{i+\frac{1}{2},j,k}\times\lambda_{Di+\frac{1}{2},j,k},$$
$$T_{Di-\frac{1}{2},j,k}=F_{i-\frac{1}{2},j,k}\times\lambda_{Di-\frac{1}{2},j,k},T_{Di,j+\frac{1}{2},k}=F_{i,j+\frac{1}{2},k}\times\lambda_{Di,j+\frac{1}{2},k},T_{Di,j-\frac{1}{2},k}=F_{i,j-\frac{1}{2},k}\times\lambda_{Di,j-\frac{1}{2},k};$$
$$T_{Di,j,k+\frac{1}{2}}=F_{i,j,k+\frac{1}{2}}\times\lambda_{Di,j,k+\frac{1}{2}},T_{Di,j,k-\frac{1}{2}}=F_{i,j,k-\frac{1}{2}}\times\lambda_{Di,j,k-\frac{1}{2}}$$

Then **Equation (2.24)** becomes:

$$\Bigg\{T_{gi+\frac{1}{2},j,k}\left[(p_{fgi+1,j,k}-p_{fgi,j,k})-\gamma_{gi+\frac{1}{2},j,k}(H_{i+1,j,k}-H_{i,j,k})-\lambda_{bg}\Delta x_{i+\frac{1}{2},j,k}\right]+T_{Di+\frac{1}{2},j,k}\left((\frac{s_g}{B_g})_{i+1,j,k}-(\frac{s_g}{B_g})_{i,j,k}\right)$$
$$-T_{gi-\frac{1}{2},j,k}\left[(p_{fgi,j,k}-p_{fgi-1,j,k})-\gamma_{gi-\frac{1}{2},j,k}(H_{i,j,k}-H_{i-1,j,k})-\lambda_{bg}\Delta x_{i-\frac{1}{2},j,k}\right]-T_{Di-\frac{1}{2},j,k}\left((\frac{s_g}{B_g})_{i,j,k}-(\frac{s_g}{B_g})_{i-1,j,k}\right)\Bigg\}$$
$$+\Bigg\{T_{gi,j+\frac{1}{2},k}\left[(p_{fgi,j+1,k}-p_{fgi,j,k})-\gamma_{gi,j+\frac{1}{2},k}(H_{i,j+1,k}-H_{i,j,k})-\lambda_{bg}\Delta y_{i,j+\frac{1}{2},k}\right]+T_{Di,j+\frac{1}{2},k}\left((\frac{s_g}{B_g})_{i,j+1,k}-(\frac{s_g}{B_g})_{i,j,k}\right)$$
$$-T_{gi,j-\frac{1}{2},k}\left[(p_{fgi,j,k}-p_{fgi,j-1,k})-\gamma_{gi,j-\frac{1}{2},k}(H_{i,j,k}-H_{i,j-1,k})-\lambda_{bg}\Delta y_{i,j-\frac{1}{2},k}\right]-T_{Di,j-\frac{1}{2},k}\left((\frac{s_g}{B_g})_{i,j,k}-(\frac{s_g}{B_g})_{i,j-1,k}\right)\Bigg\}$$
$$+\Bigg\{T_{gi,j,k+\frac{1}{2}}\left[(p_{fgi,j,k+1}-p_{fgi,j,k})-\gamma_{gi,j,k+\frac{1}{2}}(H_{i,j,k+1}-H_{i,j,k})-\lambda_{bg}\Delta z_{i,j,k+\frac{1}{2}}\right]+T_{Di,j,k+\frac{1}{2}}\left((\frac{s_g}{B_g})_{i,j,k+1}-(\frac{s_g}{B_g})_{i,j,k}\right)$$
$$-T_{gi,j,k-\frac{1}{2}}\left[(p_{fgi,j,k}-p_{fgi,j,k-1})-\gamma_{gi,j,k-\frac{1}{2}}(H_{i,j,k}-H_{i,j,k-1})-\lambda_{bg}\Delta z_{i,j,k-\frac{1}{2}}\right]-T_{Di,j,k-\frac{1}{2}}\left((\frac{s_g}{B_g})_{i,j,k}-(\frac{s_g}{B_g})_{i,j,k-1}\right)\Bigg\}$$
$$+V_{i,j,k}q_{mfgi,j,k}-V_{i,j,k}q_{vgi,j,k}=\frac{V_{i,j,k}}{\Delta t}\left[(\frac{\phi_f s_g}{B_g})^{n+1}_{i,j,k}-(\frac{\phi_f s_g}{B_g})^{n}_{i,j,k}\right] \quad (2.25)$$

The following linear difference operator is introduced for simplifying the equation:

$$\Delta A\Delta B = \Delta_x A\Delta_x B + \Delta_y A\Delta_y B + \Delta_z A\Delta_z B$$

$$\Delta_1 C = \Delta_{1x} C + \Delta_{1y} C + \Delta_{1z} C$$

Where:

$$\Delta_x A\Delta_x B = A_{i+\frac{1}{2},j,k}(B_{i+1,j,k} - B_{i,j,k}) - A_{i-\frac{1}{2},j,k}(B_{i,j,k} - B_{i-1,j,k})$$

$$\Delta_y A\Delta_y B = A_{i,j+\frac{1}{2},k}(B_{i,j+1,k} - B_{i,j,k}) - A_{i,j-\frac{1}{2},k}(B_{i,j,k} - B_{i,j-1,k})$$

$$\Delta_z A\Delta_z B = A_{i,j,k+\frac{1}{2}}(B_{i,j,k+1} - B_{i,j,k}) - A_{i,j,k-\frac{1}{2}}(B_{i,j,k} - B_{i,j,k-1})$$

$$\Delta_{1x} C = C_{i-\frac{1}{2},j,k}\Delta x_{i-\frac{1}{2},j,k} - C_{i+\frac{1}{2},j,k}\Delta x_{i+\frac{1}{2},j,k}$$

$$\Delta_{1y} C = C_{i,j-\frac{1}{2},k}\Delta y_{i,j-\frac{1}{2},k} - C_{i,j+\frac{1}{2},k}\Delta y_{i,j+\frac{1}{2},k}$$

$$\Delta_{1z} C = C_{i,j,k-\frac{1}{2}}\Delta z_{i,j,k-\frac{1}{2}} - C_{i,j,k+\frac{1}{2}}\Delta z_{i,j,k+\frac{1}{2}}$$

Rearranging **Equation (2.25)**, there is:

$$\Delta T_g \Delta\left(p_{fg} - \gamma_g H\right) + \Delta T_D \Delta(\frac{s_g}{B_g}) + \lambda_{bg}\Delta_1 T_g + \left(q_{mfg}V\right)_{i,j,k} - \left(q_{vg}V\right)_{i,j,k} = \frac{V_{i,j,k}}{\Delta t}\left[(\frac{\phi_f S_g}{B_g})^{n+1}_{i,j,k} - (\frac{\phi_f S_g}{B_g})^{n}_{i,j,k}\right] \tag{2.26}$$

Similarly, differential equation for the water phase can be derived as follows:

$$\Delta T_g \Delta(p_{fw} - \gamma_w H) + \lambda_{bw}\Delta_1 T_w - V_{i,j,k} q_{vwi,j,k} = \frac{V_{i,j,k}}{\Delta t}\left[(\frac{\phi_f s_w}{B_w})^{n+1}_{i,j,k} - (\frac{\phi_f s_w}{B_w})^{n}_{i,j,k}\right] \tag{2.27}$$

Define $\Phi = p_f - \gamma H$, the fully implicit non linear partial differential equations for gas and water phase are as follows:

$$\begin{aligned}
&\Delta T_g{}^{n+1}\Delta\left(\Phi_g\right)^{n+1} + \Delta T_D{}^{n+1}\Delta(\frac{s_g}{B_g})^{n+1} + \lambda_{bg}\Delta_1 T_g{}^{n+1} + \left(q_{mfg}V\right)_{i,j,k}{}^{n+1} - \left(q_{vg}V\right)_{i,j,k}{}^{n+1} \\
&= \frac{V_{i,j,k}}{\Delta t}\left[(\frac{\phi_f s_g}{B_g})^{n+1}_{i,j,k} - (\frac{\phi_f s_g}{B_g})^{n}_{i,j,k}\right]\Delta T_w{}^{n+1}\Delta(\Phi_w)^{n+1} + \lambda_{bw}\Delta_1 T_w{}^{n+1} - V_{i,j,k} q_{vwi,j,k}{}^{n+1} \\
&= \frac{V_{i,j,k}}{\Delta t}\left[(\frac{\phi_f s_w}{B_w})^{n+1}_{i,j,k} - (\frac{\phi_f s_w}{B_w})^{n}_{i,j,k}\right]
\end{aligned} \tag{2.28}$$

2.4.2 Basic theory of fully implicit method

This method that is used for solving non-linear equation is based on the Newton method. The specific procedure for it is as follows:

Suppose the difference equation of any X within time Δt (from t^n to t^{n+1}) is:

$$\delta X = X^{n+1} - X^n$$

In the meantime, define the difference equation of X from k to $k+1$:

$$\bar{\delta} X = X^{k+1} - X^k$$

$$X^{k+1} = X^k + \bar{\delta} X$$

Here, then $X^0 = X$ when $k = 0$, and $X^{k+1} = X^{n+1}$ if $\left| X^{k+1} - X^k \right| < \varepsilon$ during the iteration process. Moreover, δX can be expressed as follows during the iteration process:

$$\delta X \approx X^{k+1} - X^n = X^k + \bar{\delta} X - X^n$$

Thus, **Equation (2.28)** becomes the following form during the iterative process from time t^n to t^{n+1}:

$$\begin{aligned}
&\Delta T_g^{\,k+1} \Delta\left(\Phi_g\right)^{k+1} + \Delta T_D^{\,k+1} \Delta\left(\frac{S_g}{B_g}\right)^{k+1} + \lambda_{bg} \Delta_1 T_g^{\,k+1} + \left(q_{mfg} V\right)_{i,j,k}^{\,k+1} - \left(q_{vg} V\right)_{i,j,k}^{\,k+1} \\
&= \frac{V_{i,j,k}}{\Delta t}\left[\left(\frac{\phi_f S_g}{B_g}\right)_{i,j,k}^{k} + \bar{\delta}\frac{\phi_f S_g}{B_g} - \left(\frac{\phi_f S_g}{B_g}\right)_{i,j,k}^{n} \right] \\
&\Delta T_w^{\,k+1} \Delta(\Phi_w)^{k+1} + \lambda_{bw} \Delta_1 T_w^{\,k+1} - V_{i,j,k} q_{vwi,j,k}^{\,k+1} = \frac{V_{i,j,k}}{\Delta t}\left[\left(\frac{\phi_f S_w}{B_w}\right)_{i,j,k}^{k} + \bar{\delta}\frac{\phi_f S_w}{B_w} - \left(\frac{\phi_f S_w}{B_w}\right)_{i,j,k}^{n} \right]
\end{aligned} \tag{2.29}$$

2.4.3 Linearization for the fully implicit equation

Then linearly expand both the left and right hand of equations. The solving variables are p_{fg} and s_w, while the variable increments $\bar{\delta} p_{fg}$ and $\bar{\delta} s_w$ are calculated for convenience.

2.4.3.1 Darcy item in the left side of the equations

Through introducing the variables: $\Delta x_g^{\,k+1} = \Delta(x_g^{\,k} + \bar{\delta} x_g)$, $\bar{\delta}\Phi_g = \bar{\delta}(p_{fg} - \lambda_g H) = \bar{\delta} p_{fg}$,

$\overline{\delta}T_g = \frac{\partial T_g}{\partial p_{fg}}\overline{\delta}p_{fg} + \frac{\partial T_g}{\partial s_w}\overline{\delta}s_w$, and assuming that $\Delta(\frac{\partial T_g}{\partial p_{fg}}\overline{\delta}p_{fg} + \frac{\partial T_g}{\partial s_w}\overline{\delta}s_w)\Delta\overline{\delta}p_{fg}$ is so small that it can be ignored. Finally, the $\Delta T_g^{k+1}\Delta\left(\Phi_g\right)^{k+1}$ on the left side of the gas phase can be expressed as:

$$\Delta T_g^{k+1}\Delta\left(\Phi_g\right)^{k+1} = \Delta T_g^k\Delta\Phi_g^k + \Delta T_g^k\Delta\overline{\delta}p_{fg} + \Delta(\frac{\partial T_g}{\partial p_{fg}}\overline{\delta}p_{fg} + \frac{\partial T_g}{\partial s_w}\overline{\delta}s_w)\Delta\Phi_g^k \tag{2.30}$$

In case that the diffusion coefficient itself is very small, so is within each iteration step. Thus it is reasonable to define $T_D^{k+1} = T_D^k$ and $\overline{\delta}T_D = T_D^{k+1} - T_D^k = 0$. In addition, define $c_g = -\frac{1}{B_g}\frac{\partial B_g}{\partial p_{fg}}$, and the diffusion item for gas and water phase can be arranged as:

$$\begin{aligned}
&\Delta T_D^{k+1}\Delta(\frac{S_g}{B_g})^{k+1} = \Delta T_D{}^k\Delta(\frac{S_g}{B_g})^k - \Delta T_D{}^k\Delta\left[(\frac{1}{B_g})^k\overline{\delta}s_w\right] + \Delta T_D{}^k\Delta\left[(\frac{S_g c_g}{B_g})^l\overline{\delta}p_{fg}\right]\\
&\Delta_1 T_g^{k+1} = \Delta_1 T_g^k + \Delta_1\frac{\partial T_g}{\partial p_{fg}}\overline{\delta}p_{fg} + \Delta_1\frac{\partial T_g}{\partial s_w}\overline{\delta}s_w\\
&\Delta T_w^{k+1}\Delta\left(\Phi_w\right)^{k+1} = \Delta T_w^k\Delta\Phi_w^k + \Delta T_w^k\Delta\overline{\delta}p_{fg}\\
&-\Delta T_w^k\frac{\partial p_{cgw}}{\partial s_w}\overline{\delta}s_w + \Delta\frac{\partial T_w}{\partial p_{fg}}\overline{\delta}p_{fg}\Delta\Phi_w^k + \Delta\frac{\partial T_w}{\partial s_w}\overline{\delta}s_w\Delta\Phi_w^k\\
&\Delta_1 T_w^{k+1} = \Delta_1 T_w^k + \Delta_1\frac{\partial T_w}{\partial p_{fg}}\overline{\delta}p_{fg} + \Delta_1\frac{\partial T_w}{\partial s_w}\overline{\delta}s_w
\end{aligned} \tag{2.31}$$

2.4.3.2 Linearization of the diffusion adsorption term

Separate the variables of **Equation (2.15)**, and integrating both side of the equation from time n to n+1, there is:

$$\int_{V_{mi,j,k}^n}^{V_{mi,j,k}^{n+1}}\frac{dV_m i,j,k}{\left(V_{mi,j,k} - V_{Ei,j,k}\right)} = -\int_n^{n+1}\frac{1}{\tau}dt \tag{2.32}$$

Suppose that the adsorbed gas content is constant within the iteration step, note it as $V_E^{n+1/2}$, and define $V_{Ei,j,k}^{n+1/2} = \frac{V_{Ei,j,k}^{n+1} + V_{Ei,j,k}^n}{2}$, then rearranging **Equation (2.32)**:

$$V_{mi,j,k}^{n+1} = V_{mi,j,k}^n e^{-\frac{\Delta t}{\tau}} + (1 - e^{-\frac{\Delta t}{\tau}})\frac{V_{Ei,j,k}^{n+1} + V_{Ei,j,k}^n}{2} \tag{2.33}$$

2.4.3.3 Average desorption rate

The average desorption rate of gas from coal matrix system to fracture system within iteration step n to $n+1$ is defined as follows:

$$q_{mfgi,j,k}^{n+1} = -\rho_c \frac{V_{mi,j,k}^{n+1} - V_{mi,j,k}^{n}}{B_g^{n+1}\Delta t} \tag{2.34}$$

Substituting **Equation (2.33)** into **Equation (2.34)**, and define $V_{Ei,j,k}^{k+1} = V_{Ei,j,k}^{k} + \bar{\delta}V_{Ei,j,k}$,

$\bar{\delta}V_E = \frac{V_L b}{(1+bp_{fg}^{\ k})^2}\bar{\delta}p_{fg}$, $\frac{1}{B_g^{\ k+1}} = \frac{1}{B_g^{\ k}} + \bar{\delta}\frac{1}{B_g} = \frac{1}{B_g^{\ k}} - \frac{1}{B_g^2}\frac{\partial B_g}{\partial p_{fg}}\bar{\delta}p_{fg}$, **Equation (2.34)** becomes:

$$\begin{aligned} q_{mfgi,j,k}^{k+1} &= \frac{\rho_c}{2B_g^{\ k}\Delta t}[1+c_g^k\bar{\delta}p_{fg}](e^{-\frac{\Delta t}{\tau}}-1)\frac{\partial V_E}{\partial p_{fg}}\bar{\delta}p_{fg} \\ &+ \frac{\rho_c}{2B_g^{\ k}\Delta t}[1+c_g^k\bar{\delta}p_{fg}](e^{-\frac{\Delta t}{\tau}}-1)(V_{Ei,j,k}^{n} + V_{Ei,j,k}^{k} - 2V_{mi,j,k}^{n}) \\ &= \frac{\rho_c}{2B_g^{\ k}\Delta t}(e^{-\frac{\Delta t}{\tau}}-1)\frac{\partial V_E}{\partial p_{fg}}\bar{\delta}p_{fg} + \frac{\rho_c}{2B_g^{\ k}\Delta t}[1+c_g^k\bar{\delta}p_{fg}] \\ &(e^{-\frac{\Delta t}{\tau}}-1)(V_{Ei,j,k}^{n} + V_{Ei,j,k}^{k} - 2V_{mi,j,k}^{n}) \end{aligned} \tag{2.35}$$

2.4.3.4 Linearization of production term on the left side of the equation

Define $WI = \frac{2\pi h}{\ln(r_e/r_w)+s'}$, $\chi_g = \frac{k_f k_{rg\infty}}{B_g\mu_g}(p_{fg} + p_{wf} - \lambda_{bg}r_e - \lambda_{bg}r_w)$, and the production term for gas phase can be expressed as:

$$q_{vg} = WI \times \chi_g(p_{fg} - p_{wf} - \lambda_{bg}r_e + \lambda_{bg}r_w) \tag{2.36}$$

$\bar{\delta}q_{vg}$ has the following form through using the expansion way of $\bar{\delta}ab = a^{n+1}\bar{\delta}b + b^n\bar{\delta}a$:

$$\bar{\delta}q_{vg} = WI\{(\chi_g^k + \bar{\delta}\chi_g)\bar{\delta}p_{fg} + (p_{fg}^k - p_{wf} - \lambda_{bg}r_e + \lambda_{bg}r_w)\bar{\delta}\chi_g\} \tag{2.37}$$

Where : $\bar{\delta}\chi_g = \frac{\partial\chi_g}{\partial p_{fg}}\bar{\delta}p_{fg} + \frac{\partial\chi_g}{\partial k_{rg\infty}}\frac{\partial k_{rg\infty}}{\partial s_w}\bar{\delta}s_w = (c_g\chi_g)^k\bar{\delta}p_{fg} + (\frac{\chi_g}{k_{rg\infty}})^k\frac{\partial k_{rg\infty}}{\partial s_w}\bar{\delta}s_w$

Finally, the production terms for gas and water phase are:

$$q_{vgi,j,k}^{k+1} = q_{vgi,j,k}^{k} + \frac{q_{vg}^{k}}{(p_{fg}^{k} - p_{wf} - \lambda_{bg} r_e + \lambda_{bg} r_w)} \overline{\delta} p_{fg}$$
$$+ (c_g q_{vg})^k \overline{\delta} p_{fg} + \frac{q_{vg}^{k}}{k_{rg\infty}} \frac{\partial k_{rg\infty}}{\partial s_w} \overline{\delta} s_w$$
$$q_{vwi,j,k}^{k+1} = q_{vwi,j,k}^{k} + \left[\begin{array}{l} (\frac{q_{vw}}{k_{rw\infty}})^k \frac{\partial k_{rw\infty}}{\partial s_w} - (c_w q_{vw} \\ + \frac{q_{vw}}{q_{fg} - p_{cgw} - p_{wf} - \lambda_{bw} r_e + \lambda_{bw} r_w})^k \frac{\partial p_{cgw}}{\partial w_w} \end{array} \right] \overline{\delta} s_w \quad (2.38)$$
$$+ \left[c_w q_{vw} + \frac{q_{vw}}{p_{fg} - p_{cgw} - p_{wf} - \lambda_{bw} r_e + \lambda_{bw} r_w} \right]^k \overline{\delta} p_{fg}$$

2.4.3.5 Linearization of accumulation items (right hand-side of the equations)

Through using the differential rule for variable product or function product: $\delta(ab) = (ab)^{k+1} - (ab)^k$, $\overline{\delta}(ab) = a^{k+1}\overline{\delta}b - b^k \overline{\delta}a$, the accumulation items $\overline{\delta}(\frac{\phi_f s_g}{B_g})$ can be expanded as follows:

$$\overline{\delta}(\frac{\phi_f s_g}{B_g}) = -(\frac{\phi_f}{B_g})^k \overline{\delta} s_w + s_g{}^k \left[(\frac{\phi_f c_g}{B_g})^l + (\frac{1}{B_g})^k \frac{\partial \phi_f}{\partial p_{fg}} \right] \overline{\delta} p_{fg} \quad (2.39)$$

$\frac{\partial \phi_f}{\partial p_{fg}}$ can be expressed as according to **Equation (2.6)**:

$$\frac{\partial \phi_f}{\partial p_{fg}} = \frac{1}{M} + (1 - \frac{K}{M}) \frac{\rho_c V_L R T}{V_0 E} \frac{b}{1 + b p_{fg}} \quad (2.40)$$

Substituting **Equation (2.40)** into **Equation (2.39)**, rearranging:

$$\overline{\delta}(\frac{\phi_f s_g}{B_g}) = -(\frac{\phi_f}{B_g})^k \overline{\delta} s_w + s_g{}^k \left[(\frac{\phi_f c_g}{B_g})^k + (\frac{1}{B_g})^k [\frac{1}{M} + (1 - \frac{K}{M}) \frac{\rho_c V_L R T}{V_0 E} \frac{b}{1 + b p_{fg}}] \right] \overline{\delta} p_{fg} \quad (2.41)$$

The items on the right hand of the gas and water phase can be got as:

$$\frac{V_{i,j,k}}{\Delta t} \left[(\frac{\phi_f s_g}{B_g})^k + \overline{\delta}(\frac{\phi_f s_g}{B_g}) - (\frac{\phi_f s_g}{B_g})^n \right] = \frac{V_{i,j,k}}{\Delta t} \left\{ (\frac{\phi_f s_g}{B_g})^k - (\frac{\phi_f s_g}{B_g})^n - (\frac{\phi_f}{B_g})^k \overline{\delta} s_w + s_g{}^k \left[(\frac{\phi_f c_g}{B_g})^k + (\frac{1}{B_g})^k [\frac{1}{M} + (1 - \frac{K}{M}) \frac{\rho_c V_L R T}{V_0 E} \frac{b}{1 + b p_{fg}}] \right] \overline{\delta} p_{fg} \right\} \quad (2.42)$$
$$\frac{V_{i,j,k}}{\Delta t} \left[(\frac{\phi_f s_w}{B_w})^k + \overline{\delta}(\frac{\phi_f s_w}{B_w}) - (\frac{\phi_f s_w}{B_w})^n \right] = \frac{V_{i,j,k}}{\Delta t} \left\{ (\frac{\phi_f s_w}{B_w})^k - (\frac{\phi_f s_w}{B_w})^n + (\frac{\phi_f}{B_w})^k \overline{\delta} s_w + s_w{}^k \left[(\frac{\phi_f c_w}{B_w})^k + (\frac{1}{B_w})^k [\frac{1}{M} + (1 - \frac{K}{M}) \frac{\rho_c V_L R T}{V_0 E} \frac{b}{1 + b p_{fg}}] \right] \overline{\delta} p_{fg} \right\}$$

2.4.4 Development of fully implicit linear equations

For gas phase

$$\Delta T_g^k \Delta\bar{\delta} p_{fg} + \Delta(\frac{\partial T_g}{\partial p_{fg}}\bar{\delta} p_{fg} + \frac{\partial T_g}{\partial s_w}\bar{\delta} s_w)\Delta\Phi_g^k + \Delta T_D{}^k \Delta\left[(\frac{s_g c_g}{B_g})^k \bar{\delta} p_{fg}\right]$$
$$+\lambda_{bg}(\Delta_1 \frac{\partial T_g}{\partial p_{fg}}\bar{\delta} p_{fg} + \Delta_1 \frac{\partial T_g}{\partial s_w}\bar{\delta} s_w) - \Delta T_D{}^k \Delta\left[(\frac{1}{B_g})^k \bar{\delta} s_w\right]$$
$$+\frac{\rho_c}{2B_g{}^k \Delta t}(e^{-\frac{\Delta t}{\tau}} - 1)\left\{\frac{V_L b}{(1+bp_{fg}^k)^2} + c_g^k (V_{Ei,j,k}^{\ n} + V_{Ei,j,k}^{\ k} - 2V_{mi,j,k}^{\ n})\right\}\bar{\delta} p_{fg}$$
$$-[\frac{Q_{vg}^k}{(p_{fg}^k - p_{wf} - \lambda_{bg} r_e + \lambda_{bg} r_w)} + (c_g Q_{vg})^k]\bar{\delta} p_{fg} + [(\frac{\phi_f}{B_g})^k \frac{V_{i,j,k}}{\Delta t} - \frac{Q_{vg}^k}{k_{rg\infty}}\frac{\partial k_{rg\infty}}{\partial s_w}]\bar{\delta} s_w$$
$$-\frac{V_{i,j,k}}{\Delta t}\left[(\frac{\phi_f s_g c_g}{B_g})^k + (\frac{s_g}{B_g})^k[\frac{1}{M} + (1-\frac{K}{M})\frac{\rho_c V_L RT}{V_0 E}\frac{b}{1+bp_{fg}^k}]\right]\bar{\delta} p_{fg}$$
$$= \frac{V_{i,j,k}}{\Delta t}\left\{(\frac{\phi_f s_g}{B_g})^k - (\frac{\phi_f s_g}{B_g})^n\right\} - \Delta T_g^k \Delta\Phi_g^k - \Delta T_D{}^k \Delta(\frac{s_g}{B_g})^k - \lambda_{bg}\Delta_1 T_g^k$$
$$-\frac{\rho_c}{2B_g{}^k \Delta t}(e^{-\frac{\Delta t}{\tau}} - 1)(V_{Ei,j,k}^{\ n} + V_{Ei,j,k}^{\ k} - 2V_{mi,j,k}^{\ n}) + Q_{vgi,j,k}^k \qquad (2.43)$$

For water phase

$$\Delta T_w^k \Delta\bar{\delta} p_{fg} - \Delta T_w^k \frac{\partial p_{cgw}}{\partial s_w}\bar{\delta} s_w + \Delta\frac{\partial T_w}{\partial p_{fg}}\bar{\delta} p_{fg}\Delta\Phi_w^k + \Delta\frac{\partial T_w}{\partial s_w}\bar{\delta} s_w \Delta\Phi_w^k$$
$$+\lambda_{bw}(\Delta_1 \frac{\partial T_w}{\partial p_{fg}}\bar{\delta} p_{fg} + \Delta_1 \frac{\partial T_w}{\partial s_w}\bar{\delta} s_w)$$
$$-\left[c_w Q_{vw} + \frac{Q_{vw}}{p_{fg} - p_{cgw} - p_{wf} - \lambda_{bw} r_e + \lambda_{bw} r_w}\right]^k \bar{\delta} p_{fg}$$
$$-[(\frac{Q_{vw}}{k_{rw\infty}})^k \frac{\partial k_{rw\infty}}{\partial s_w} + (\frac{\phi_f}{B_w})^k \frac{V_{i,j,k}}{\Delta t}]\bar{\delta} s_w$$
$$+[(c_w Q_{vw} + \frac{Q_{vw}}{p_{fg} - p_{cgw} - p_{wf} - \lambda_{bw} r_e + \lambda_{bw} r_w})^k \frac{\partial p_{cgw}}{\partial s_w}]\bar{\delta} s_w$$
$$-\frac{V_{i,j,k}}{\Delta t}\left[(\frac{\phi_f s_w c_w}{B_w})^k + (\frac{s_w}{B_w})^k[\frac{1}{M} + (1-\frac{K}{M})\frac{\rho_c V_L RT}{V_0 E}\frac{b}{1+bp_{fg}^k}]\right]\bar{\delta} p_{fg}$$
$$= \frac{V_{i,j,k}}{\Delta t}\left\{(\frac{\phi_f s_w}{B_w})^k - (\frac{\phi_f s_w}{B_w})^n\right\} - \Delta T_w^k \Delta\Phi_w^k - \lambda_{bw}\Delta_1 T_w^k + Q_{vwi,j,k}^k \qquad (2.44)$$

Where:

$$\Delta\overline{\delta T}_{ph}\Delta\Phi_{ph}^{\ k} = \overline{\delta T}_{ph_{i+\frac{1}{2},j,k}}\left(\Phi_{phi+1,j,k}^{\ k} - \Phi_{phi,j,k}^{\ k}\right) + \overline{\delta T}_{ph_{i-\frac{1}{2},j,k}}\left(\Phi_{phi-1,j,k}^{\ k} - \Phi_{phi,j,k}^{\ k}\right)$$
$$+\overline{\delta T}_{ph_{i,j+\frac{1}{2},k}}\left(\Phi_{phi,j+1,k}^{\ k} - \Phi_{phi,j,k}^{\ k}\right) + \overline{\delta T}_{ph_{i,j-\frac{1}{2},k}}\left(\Phi_{phi,j-1,k}^{\ k} - \Phi_{phi,j,k}^{\ k}\right)$$
$$+\overline{\delta T}_{ph_{i,j,k+\frac{1}{2}}}\left(\Phi_{phi,j,k+1}^{\ k} - \Phi_{phi,j,k}^{\ l}\right) + \overline{\delta T}_{ph_{i,j,k-\frac{1}{2}}}\left(\Phi_{phi,j,k-1}^{\ k} - \Phi_{phi,j,k}^{\ k}\right)$$

$$\Delta_1\overline{\delta T}_{ph} = \overline{\delta T}_{ph_{i-\frac{1}{2},j,k}}\Delta x_{i-\frac{1}{2},j,k} - \overline{\delta T}_{ph_{i+\frac{1}{2},j,k}}\Delta x_{i+\frac{1}{2},j,k}$$
$$+\overline{\delta T}_{ph_{i,j-\frac{1}{2},k}}\Delta y_{i,j-\frac{1}{2},k} - \overline{\delta T}_{ph_{i,j+\frac{1}{2},k}}\Delta y_{i,j+\frac{1}{2},k}$$
$$+\overline{\delta T}_{ph_{i,j,k-\frac{1}{2}}}\Delta z_{i,j,k-\frac{1}{2}} - \overline{\delta T}_{ph_{i,j,k+\frac{1}{2}}}\Delta z_{i,j,k+\frac{1}{2}}$$

$$ph = w, g$$

$$\overline{\delta T}_w = (\frac{T_w}{k_{rw\infty}})^k \frac{\partial k_{rw\infty}}{\partial s_w}\overline{\delta s}_w$$

$$\overline{\delta T}_g = (c_g T_g)^k \overline{\delta} p_{fg} + (\frac{T_g}{k_{rg\infty}})^k \frac{\partial k_{rg\infty}}{\partial s_w}\overline{\delta s}_w$$

2.4.5 Parameter values and boundary conditions

2.4.5.1 Absolute permeability

Absolute permeability is calculated through harmonic average value, that is:

$$k_{fx_{i\pm\frac{1}{2},j,k}} = \frac{\Delta x_{i\pm1} + \Delta x_i}{\frac{\Delta x_{i\pm1}}{k_{fxi\pm1,j,k}} + \frac{\Delta x_i}{k_{fxi,j,k}}} \tag{2.45}$$

$$k_{fy_{i,j\pm\frac{1}{2},k}} = \frac{\Delta y_{j\pm1} + \Delta y_j}{\frac{\Delta y_{j\pm1}}{k_{fxi,j\pm1,k}} + \frac{\Delta y_j}{k_{fxi,j,k}}} \tag{2.46}$$

$$k_{fz_{i,j,k\pm\frac{1}{2}}} = \frac{\Delta z_{k\pm1} + \Delta z_k}{\frac{\Delta z_{k\pm1}}{k_{fzi,j,k\pm1}} + \frac{\Delta z_k}{k_{fzi,j,k}}} \tag{2.47}$$

And the relationship between permeability and porosity is as follows:

$$\frac{k_f}{k_0} = \frac{\phi^3}{\phi_0^{\ 3}} \tag{2.48}$$

2.4.5.2 Mobility coefficient

The expression of the mobility for water phase is: $\lambda_w = \frac{k_f k_{rw\infty}}{\mu_w B_w}$, where the absolute permeability is calculated through harmonic average value and the other parameters are determined by upstream regulation. For example:

$$\left(\frac{k_f k_{rw\infty}}{\mu_w B_w}\right)_{i+\frac{1}{2},j,k} = \begin{cases} \left(\frac{k_{rw\infty}}{\mu_w B_w}\right)_{i,j,k} & \Phi_{w,i,j,k} > \Phi_{w,i+1,j,k} \\ \left(\frac{k_{rw\infty}}{\mu_w B_w}\right)_{i+1,j,k} & \Phi_{w,i,j,k} < \Phi_{w,i+1,j,k} \end{cases} \tag{2.49}$$

2.4.5.3 Derivative terms

Derivative items such as $\frac{\partial k_{rw\infty}}{\partial s_w}$ and $\frac{\partial p_{cgw}}{\partial s_w}$ are supposed to be equal to the slope of the secant line (composed by the latest iteration value and the value in step n) in order to make the calculation process more stable:

$$\frac{\partial k_{rw\infty}}{\partial s_w} = \frac{k_{rw\infty}(s_w^k) - k_{rw\infty}(s_w^n)}{s_w^k - s_w^n} \tag{2.50}$$

$$\frac{\partial p_{cgw\infty}}{\partial s_w} = \frac{p_{cgw\infty}(s_w^k) - p_{cgw\infty}(s_w^n)}{s_w^k - s_w^n} \tag{2.51}$$

2.4.5.4 Relative permeability and capillary pressure

The relative permeability and capillary pressure can be obtained through linear interpolation method:

$$k_{rg\infty}^k = k_{rg0} + \frac{k_{rg1} - k_{rg0}}{s_{w1} - s_{w0}}(s_w^k - s_{w0}) \tag{2.52}$$

$$k_{rw\infty}^k = k_{rw0} + \frac{k_{rw1} - k_{rw0}}{s_{w1} - s_{w0}}(s_w^k - s_{w0}) \tag{2.53}$$

$$p_{cgw}^k = p_{cgw0} + \frac{p_{cgw1} - p_{cgw0}}{s_{w1} - s_{w0}}(s_w^k - s_{w0}) \tag{2.54}$$

2.4.5.5 High velocity and non-Darcy term in gas phase

Define gas slippage effect as:

$$F_{ndg} = 1 + \beta_1 \left(\frac{k_f k_{rg\infty}(s_w)}{\phi_g}\right)^{-\beta_2} / p_m \tag{2.55}$$

It is differenced using the upstream regulation, the expression is as follows:

$$1+\left(\beta_1\left(\frac{k_f k_{rg\infty}(s_w)}{\phi_g}\right)^{-\beta_2} / p_m\right)_{i\pm\frac{1}{2},j,k} = \begin{cases} 1+\left(\beta_1\left(\frac{k_f k_{rg\infty}(s_w)}{\phi_g}\right)^{-\beta_2} / p_m\right)_{i,j,k} & \Phi_{i,j,k} > \Phi_{i\pm1,j,k} \\ 1+\left(\beta_1\left(\frac{k_f k_{rg\infty}(s_w)}{\phi_g}\right)^{-\beta_2} / p_m\right)_{i\pm1,j,k} & \Phi_{i,j,k} < \Phi_{i\pm1,j,k} \end{cases} \tag{2.56}$$

$$1+\left(\beta_1\left(\frac{k_f k_{rg\infty}(s_w)}{\phi_g}\right)^{-\beta_2} / p_m\right)_{i,j\pm\frac{1}{2},k} = \begin{cases} 1+\left(\beta_1\left(\frac{k_f k_{rg\infty}(s_w)}{\phi_g}\right)^{-\beta_2} / p_m\right)_{i,j,k} & \Phi_{i,j,k} > \Phi_{i,j\pm1,k} \\ 1+\left(\beta_1\left(\frac{k_f k_{rg\infty}(s_w)}{\phi_g}\right)^{-\beta_2} / p_m\right)_{i,j\pm1,k} & \Phi_{i,j,k} < \Phi_{i,j\pm1,k} \end{cases} \tag{2.57}$$

$$1+\left(\beta_1\left(\frac{k_f k_{rg\infty}(s_w)}{\phi_g}\right)^{-\beta_2} / p_m\right)_{i,j,k\pm\frac{1}{2}} = \begin{cases} 1+\left(\beta_1\left(\frac{k_f k_{rg\infty}(s_w)}{\phi_g}\right)^{-\beta_2} / p_m\right)_{i,j,k} & \Phi_{i,j,k} > \Phi_{i,j,k\pm1} \\ 1+\left(\beta_1\left(\frac{k_f k_{rg\infty}(s_w)}{\phi_g}\right)^{-\beta_2} / p_m\right)_{i,j,k\pm1} & \Phi_{i,j,k} < \Phi_{i,j,k\pm1} \end{cases} \tag{2.58}$$

The average pressure p_m is differenced by the arithmetic average value of two adjacent points, for example:

$$(p_m)_{i\pm\frac{1}{2},j,k} = \frac{p_{i\pm1,j,k} + p_{i,j,k}}{2} \tag{2.59}$$

2.4.5.6 Threshold pressure gradient

The threshold pressure gradients for gas and water phase are defined as:

$$\begin{aligned} \lambda_{bg} &= (\alpha_1 / (k_f k_{rg\infty}) + \alpha_2 \\ \lambda_{bw} &= (\alpha_3 \mu_w / (k_f k_{rw\infty})^{\alpha_4} \end{aligned} \tag{2.60}$$

They also adopted the upstream regulation rule for the differentiation, for example:

$$(\lambda_{bg})_{i\pm\frac{1}{2},j,k}=\begin{cases}(\dfrac{\alpha_1}{k_f k_{rg\infty}}+\alpha_2)_{i,j,k} & (\Phi_g)_{i,j,k}>(\Phi_g)_{i\pm1,j,k}\\ (\dfrac{\alpha_1}{k_f k_{rg\infty}}+\alpha_2)_{i\pm1,j,k} & (\Phi_g)_{i,j,k}<(\Phi_g)_{i\pm1,j,k}\end{cases}$$

$$(\lambda_{bw})_{i,j,k\pm\frac{1}{2}}=\begin{cases}(\dfrac{\alpha_3\mu_w}{k_f k_{rw\infty}})^{\alpha_4}_{i,j,k} & (\Phi_w)_{i,j,k}>(\Phi_w)_{i,j,k\pm1}\\ (\dfrac{\alpha_3\mu_w}{k_f k_{rw\infty}})^{\alpha_4}_{i,j,k\pm1} & (\Phi_w)_{i,j,k}<(\Phi_w)_{i,j,k\pm1}\end{cases} \tag{2.61}$$

2.4.5.7 Well parameter

The equivalent radius, average permeability, and skin factor are shown as:

$$r_e=0.28\frac{[(\dfrac{k_{fy}}{k_{fx}})^{\frac{1}{2}}\Delta x^2+(\dfrac{k_{fx}}{k_{fy}})^{\frac{1}{2}}\Delta y^2]}{(\dfrac{k_{fy}}{k_{fx}})^{\frac{1}{4}}+(\dfrac{k_{fx}}{k_{fy}})^{\frac{1}{4}}}$$

$$k_f=\sqrt{k_{fx}k_{fy}}$$

$$S=-\ln(\frac{x_f}{2r_w})$$

2.4.6 Solution of the equations

2.4.6.1 Final matrix equation for the CBM reservoir

Make the solving variables and coefficients in the above equations whose subscripts are $(i+\frac{1}{2},j,k)$, $(i-\frac{1}{2},j,k)$ $(i,j+\frac{1}{2},k)$, $(i,j-\frac{1}{2},k)$, $(i,j,k+\frac{1}{2})$, $(i,j,k-\frac{1}{2})$ tie to their corre- sponding nodes. Then the difference equations for gas and water phase are arranged in a sequence of $\overline{\delta}p_{fg}$ and $\overline{\delta}s_w$ as follows:

$$\begin{aligned}&a^1_{gi,j,k}\overline{\delta}p_{fgi-1,j,k}+a^2_{gi,j,k}\overline{\delta}s_{wi-1,j,k}+b^1_{gi,j,k}\overline{\delta}p_{fgi,j-1,k}+b^2_{gi,j,k}\overline{\delta}s_{wi,j-1,k}+c^1_{gi,j,k}\overline{\delta}p_{fgi,j,k-1}+c^2_{gi,j,k}\overline{\delta}s_{wi,j,k-1}\\&+d^1_{gi,j,k}\overline{\delta}p_{fgi,j,k}+d^2_{gi,j,k}\overline{\delta}s_{wi,j,k}+e^1_{gi,j,k}\overline{\delta}p_{fgi+1,j,k}+e^2_{gi,j,k}\overline{\delta}s_{wi+1,j,k}+f^1_{gi,j,k}\overline{\delta}p_{fgi,j+1,k}+f^2_{gi,j,k}\overline{\delta}s_{wi,j+1,k}\\&+g^1_{gi,j,k}\overline{\delta}p_{fgi,j,k+1}+g^2_{gi,j,k}\overline{\delta}s_{wi,j,k+1}=h_{gi,j,k}\end{aligned} \tag{2.62}$$

$$\begin{aligned}&a^1_{wi,j,k}\bar{\delta}p_{fgi-1,j,k}+a^2_{wi,j,k}\bar{\delta}s_{wi-1,j,k}+b^1_{wi,j,k}\bar{\delta}p_{fgi,j-1,k}+b^2_{wi,j,k}\bar{\delta}s_{wi,j-1,k}+c^1_{wi,j,k}\bar{\delta}p_{fgi,j,k-1}+c^2_{wi,j,k}\bar{\delta}s_{wi,j,k-1}\\&+d^1_{wi,j,k}\bar{\delta}p_{fgi,j,k}+d^2_{wi,j,k}\bar{\delta}s_{wi,j,k}+e^1_{wi,j,k}\bar{\delta}p_{fgi+1,j,k}+e^2_{wi,j,k}\bar{\delta}s_{wi+1,j,k}+f^1_{wi,j,k}\bar{\delta}p_{fgi,j+1,k}+f^2_{wi,j,k}\bar{\delta}s_{wi,j+1,k}\\&+g^1_{wi,j,k}\bar{\delta}p_{fgi,j,k+1}+g^2_{wi,j,k}\bar{\delta}s_{wi,j,k+1}=h_{wi,j,k}\end{aligned} \tag{2.63}$$

Where: a,b,c,d,e,f represent solving variable coefficient of left node, forward node, down node, current node, right node, afterward node and up node. Superscript 1 and 2 present the coefficient of $\bar{\delta}p_{fg}$ and $\bar{\delta}s_w$. Then the above equations can be expressed in the matrix form as follows:

$$\begin{aligned}&\begin{bmatrix}a^1_{gi,j,k} & a^2_{gi,j,k}\\ a^1_{wi,j,k} & a^2_{wi,j,k}\end{bmatrix}\begin{bmatrix}\bar{\delta}p_{fgi-1,j,k}\\ \bar{\delta}s_{wi-1,j,k}\end{bmatrix}+\begin{bmatrix}b^1_{gi,j,k} & b^2_{gi,j,k}\\ b^1_{wi,j,k} & b^2_{wi,j,k}\end{bmatrix}\begin{bmatrix}\bar{\delta}p_{fgi,j-1,k}\\ \bar{\delta}s_{wi,j-1,k}\end{bmatrix}+\begin{bmatrix}c^1_{gi,j,k} & c^2_{gi,j,k}\\ c^1_{wi,j,k} & c^2_{wi,j,k}\end{bmatrix}\begin{bmatrix}\bar{\delta}p_{fgi,j,k-1}\\ \bar{\delta}s_{wi,j,k-1}\end{bmatrix}\\&+\begin{bmatrix}d^1_{gi,j,k} & d^2_{gi,j,k}\\ d^1_{wi,j,k} & d^2_{wi,j,k}\end{bmatrix}\begin{bmatrix}\bar{\delta}p_{fgi,j,k}\\ \bar{\delta}s_{wi,j,k}\end{bmatrix}+\begin{bmatrix}e^1_{gi,j,k} & e^2_{gi,j,k}\\ e^1_{wi,j,k} & e^2_{wi,j,k}\end{bmatrix}\begin{bmatrix}\bar{\delta}p_{fgi+1,j,k}\\ \bar{\delta}s_{wi+1,j,k}\end{bmatrix}+\begin{bmatrix}f^1_{gi,j,k} & f^2_{gi,j,k}\\ f^1_{wi,j,k} & f^2_{wi,j,k}\end{bmatrix}\begin{bmatrix}\bar{\delta}p_{fgi,j+1,k}\\ \bar{\delta}s_{wi,j+1,k}\end{bmatrix}\\&+\begin{bmatrix}g^1_{gi,j,k} & g^2_{gi,j,k}\\ g^1_{wi,j,k} & g^2_{wi,j,k}\end{bmatrix}\begin{bmatrix}\bar{\delta}p_{fgi,j,k+1}\\ \bar{\delta}s_{wi,j,k+1}\end{bmatrix}=\begin{bmatrix}h_{gi,j,k}\\ h_{wi,j,k}\end{bmatrix}\end{aligned} \tag{2.64}$$

Obviously, a seven sparse point diagonal, band-structured block coefficient matrix is formed finally, and every node corresponds to a sub-matrix with two orders. Thus $2\times II\times JJ\times KK$ order equations correspond to $II\times JJ\times KK$ mesh system. The matrix can be written as: $AX=b$. Where, A is a seven diagonal block coefficient matrix, and every block is a two order sub-matrix.

2.4.6.2 Procedure of block preconditioned orthogonal minimisation method

Block preconditioned orthogonal minimisation method is used to solve the equations according to the characteristic of the final matrix equation. The minimization processes can be expected to offer the following advantages:

1, Convergence more readily guaranteed

2, No need for iteration parameters

3, Insensitivity to the number of equations

4, Insensitivity to transmissibility ratios

The procedure for it is:

Step1, make incomplete LU decomposition for matrix A and get the preconditioned matrix.

Step2, equivalently transfer the original equations $AX = b$ to $(AM^{-1})Mx = b$.

Step3, Define $y = Mx$, then, the equation $(AM^{-1})y = b$ is solved using orthogonal minimization method instead of solving $AX = b$.

Step4, the value of x is got through $x = M^{-1}y$.

Step5, go to step2 for iteration until the value of x is converged.

The specific *ILU*-orthogonal minimisation method can be described as follows:

$$
\begin{aligned}
R^{(0)} &= b - AX^{(0)} \\
V^{(k)} &= M^{-1}R^{(k)} \\
q^{(k)} &= V^{(k)} + \sum_{i=m,m\le M}^{M} \alpha_i^{(k)} q^{(i)} \\
Aq^{(k)} &= AV^{(k)} + \sum_{i=m,m\le M}^{M} \alpha_i^{(k)} Aq^{(i)}
\end{aligned}
$$

Where, Orthogonal coefficient is: $\alpha_i^{(k)} = -\dfrac{(AV^{(k)}, Aq^{(i)})}{(Aq^{(i)}, Aq^{(i)})}$, with $(Aq^{(k)}, Aq^{(i)}) = 0$.

$$
\begin{aligned}
X^{(k+1)} &= X^{(k)} + \omega^{(k)} q^{(k)} \\
R^{(k+1)} &= R^{(k)} - \omega^{(k)} Aq^{(k)}
\end{aligned}
$$

Minimization parameter is: $\omega^{(k)} = \dfrac{(Aq^{(k)}, R^{(k)})}{(Aq^{(k)}, Aq^{(k)})}$. And $\min \left\| R^{(k+1)} \right\|_2 = \min \left\| R^{(k)} - \omega^{(k)} Aq^{(k)} \right\|_2$.

After getting $\delta p_{fg}, \delta s_w$ in $k+1$ iteration, then calculating p_{fg}^{k+1}, s_w^{k+1} through the following formula:

$$
\begin{aligned}
p_{fg}^{k+1} &= p_{fg}^{k} + \delta p_{fg}^{k+1} \\
s_w^{k+1} &= s_w^{k} + \delta s_w^{k+1}
\end{aligned}
\tag{2.65}
$$

Followed that p_{fw}^{k+1}, s_g^{k+1} can be got through the following expression:

$$
\begin{aligned}
p_{fw}^{k+1} &= p_{fg}^{k+1} - p_{cgw}^{k+1} \\
s_g^{k+1} &= 1 - s_w^{k+1}
\end{aligned}
\tag{2.66}
$$

Then repeat the above calculation process until $\delta p_{fg}, \delta s_w$ is small enough.

2.5 Case studies

Reservoir physical parameters			
Average reservoir depth	4000 ft	Wellbore pressure	4000 psia
Formation thickness	29.527 ft	Diffusion Coefficient	0.02
Effective porosity	0.02	Sorption time constant	231.8 day
Absolute permeability	3.0md	Initial gas content	0.1 Mscf/ft^3
Formation compressibility	0.30E-5 $psia^{-1}$	Skin factor	-2
Formation temperature	113 ^0F	ν	0.39
Initial formation pressure	1109.5 psia	E	1.24E5 psia
Initial water saturation	0.35	M/E	0.76
Well radius	0.088 ft	K/M	2.0

Table 2.1 Simulation parameter of three dimensional CBM model

Water saturation	Relative permeability for gas	Relative permeability for water
0.350	0.0000	1.0000
0.400	0.0088	1.0000
0.450	0.0193	0.9705
0.500	0.0351	0.9168
0.550	0.0598	0.8111
0.600	0.0931	0.6625
0.650	0.1406	0.4974
0.700	0.1951	0.3550
0.750	0.2601	0.2270
0.800	0.3497	0.1283
0.850	0.4499	0.0537
0.900	0.5694	0.0173
0.950	0.7153	0.0000
0.975	0.8140	0.0000
1.000	1.0000	0.0000

Table 2.2 Data for relative permeability curve

The simulator called COAFOR are developed for the model in this chapter, then three consecutive case studies are made by using COAFOR. The purpose for this is to investigate the effect of basic parameter (such as desorption time, Langmuir pressure/volume, permeability anisotropy), gas slippage, threshold pressure gradient effects, and matrix shrinkage effects on the production of the CBM reservoir. The parameters for this two phase (gas and water) CBM reservoir are listed (**Table 2.1**), the relative permeability data used for the simulation is also given (**Table 2.2**). The grid partition of the CBM reservoir fracture system is also illustrated as in **Figure 2.2**.

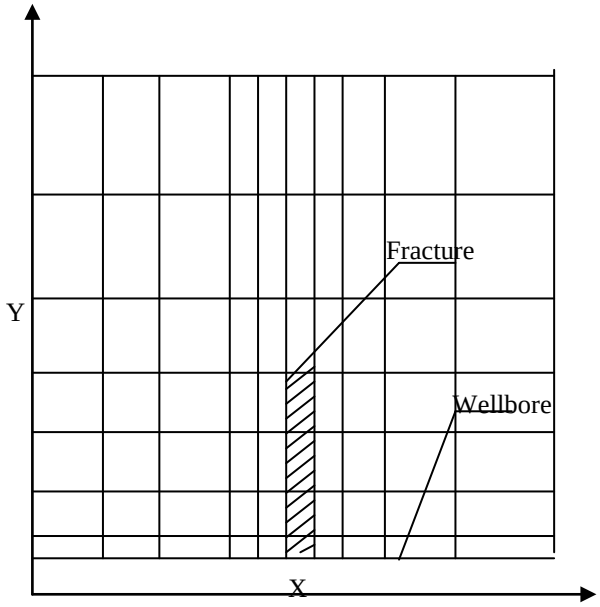

Figure 2.2 Grid partition for CBM reservoir fracture system

2.5.1 Case study 1

The validation of the basic model is made through comparing the result comes from COAFOR and Eclipse, they are running under the same parameters. Secondly, the sensitivity analysis of the Langmuir pressure, Langmuir volume, desorption time and the heterogeneity are made. The daily gas production rate simulated by COAFOR has an excellent agreement with the result from Eclipse software (**Figure 2.3**). The relative error is less than 10%, which indicates the accuracy of the basic model built in this chapter.

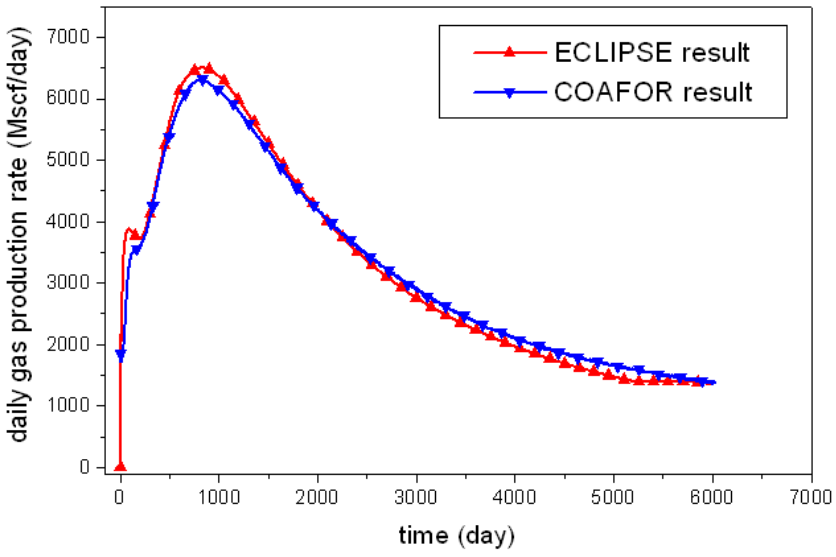

Figure 2.3 Comparison of Eclipse and Numerical simulation result on the daily gas production

The daily gas production rate and total gas production rate is shown in **Figure 2.4**. These data suggest that, typically, there are three stages in coal dewatering process, which just fits the theory study. At stage one, which corresponds to the first 300 days in the figure, a huge amount of water is produced at the initial drainage because water initially occupies the cleat porosity in the reservoir, which controls the flow to the production well, the relative permeability for water is high.

As the water production continues, the hydrostatic pressure decreases, which result in the adsorbed methane desorbing and entering into the cleat porosity. The gas production rate is low and it increases as the water continues to be removed from the cleat system. Thus, the relative permeability to water decreases while the relative permeability to the gas increases. In addition, most of the water is pumped off and the gas production rate reached at its maximum at the end of 1000 days, this is the second stage, which corresponds to 300 days to 1000 days in the figure.

The gas production reaches its maximum while the water production rate is considerably reduced. The reservoir flow condition is almost stabilized until the beginning of the third stage. The gas production rate is to decline at stage three, which corresponding to the 1500 days and thereafter, , and the water production is low or negligible. Also, the relative permeability to both gas and water change very little. What is more, the total gas production rate increases with the time going on.

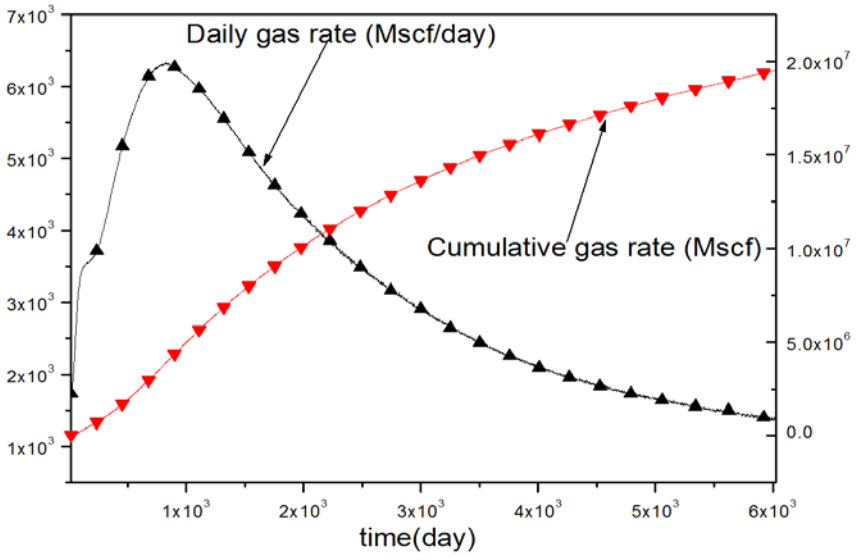

Figure 2.4 Daily gas and total gas production rate

The relationship between gas production rate and pressure is given in this study **(Figure 2.5)**. It is easily to see that the pressure decreases with the increasing of gas production rate. The total gas production rate is the highest when the bottom-hole pressure is specified at its lowest level, while the lowest when the bottom-hole pressure is the highest. This is because gas is produced with the pressure depletion.

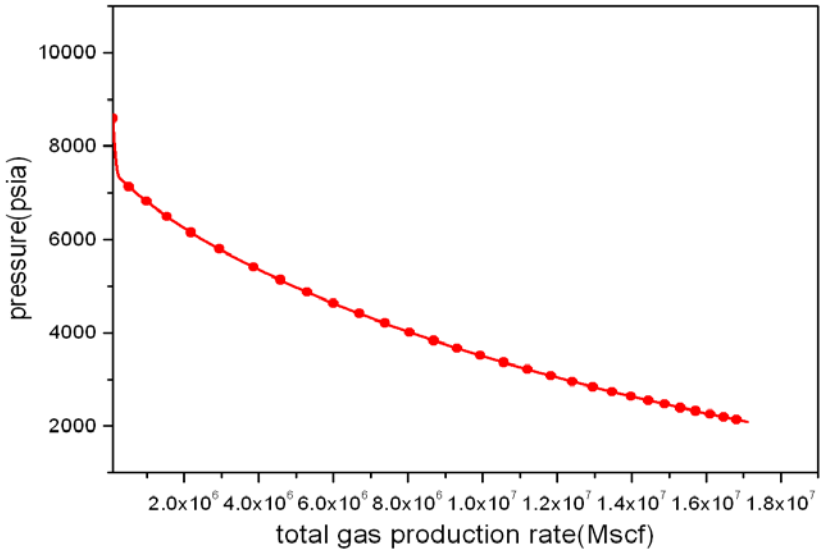

Figure 2.5 Relationship between pressure and gas rate

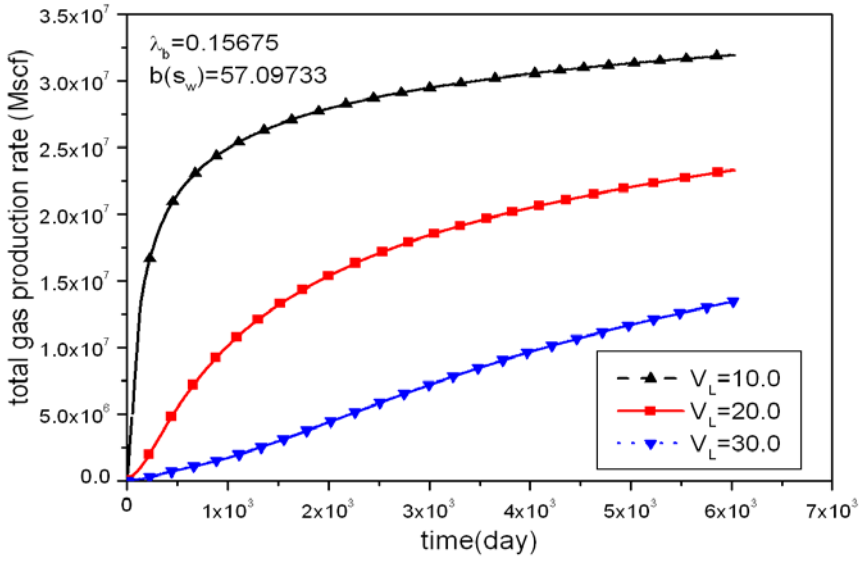

Figure 2.6 The effect of Langmuir volume on total gas rate

The Langmuir volume on the total gas production rate is studied. It can be seen that the increase of Langmuir volume constant results in a corresponding decrease in the amount

of total gas production rate and the shorter breakthrough time (**Figure 2.6**). This is attributed to the lower diffusion rate affected by the Langmuir volume.

The effect of desorption time on the total water production rate is also illustrated (**Figure 2.7**). The total water production rate increases with the decreasing of desorption time, it is the smallest with desorption time 100 day compared to the other two cases. This is caused by the slower diffusion rate when desorption time is longer.

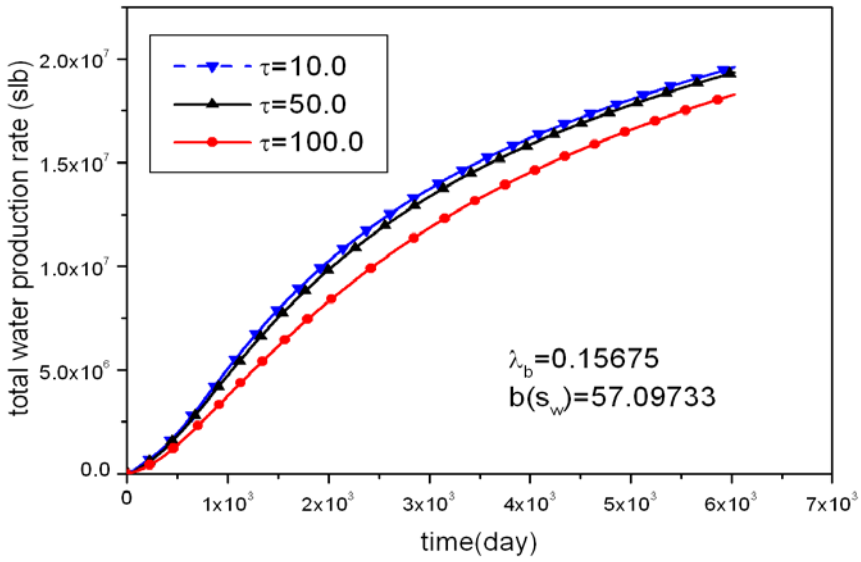

Figure 2.7 The effect of desorption time on total water rate

Heterogeneity in cleat permeability is very important in determining the water and gas flow in the reservoir and therefore has significant influence on the gas production. As shown in the figure, the stronger the heterogeneous of cleat permeability, the earlier for the gas to reach its maximum (**Figure 2.8**).

When $k_x = 30, k_y = 3$, the gas production rate reached at its maximum at the end of about the 500 days, while the time to reach at gas peak is much later for $k_x = 25, k_y = 10$ and $k_x = 10, k_y = 10$.

And after this period, the daily gas production began to drop. However, the heterogeneous of cleat permeability shows the opposite effect on the deccreasing stage of daily gas production rate. For example, the daily production rate drops the fastest when $k_x = 10, k_y = 10$, while decreases the slowest when $k_x = 30, k_y = 3$ during the late simulation stage.

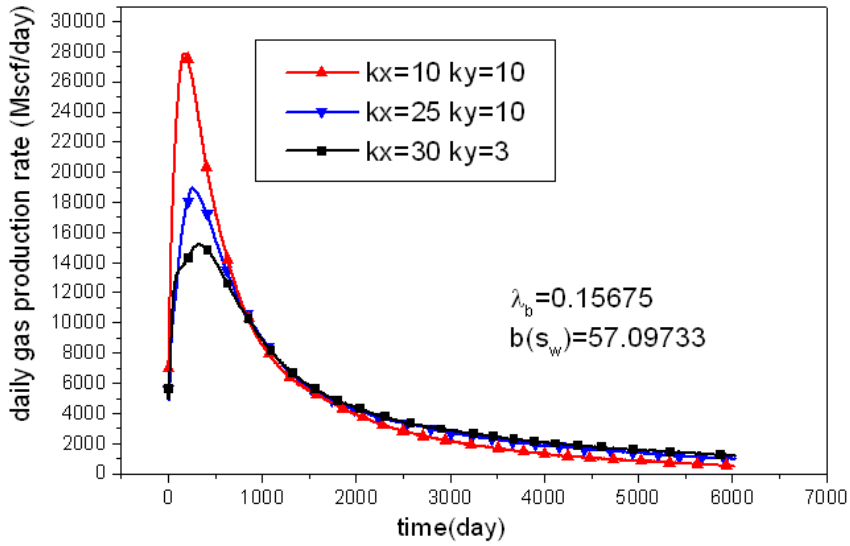

Figure 2.8 The effect of anisotropy in permeability on daily gas rate

The total gas production rate under the effect of Langmuir pressure is shown in **Figure 2.9**. The gas slippage and threshold pressure gradient effects are both considered, their values are shown in the figure. It can be seen that the total gas production rate increases as the Langmuir pressure increases. This is attributed to the increased gas concentration with larger Langmuir pressure. For example, the total gas rate can be only 3.0E6Mscf with Langmuir pressure equal to 1000 psia, while around 7.5E6Mscf with 1600 psia Langmuir pressure, totally increased by 4.5E6Mscf.

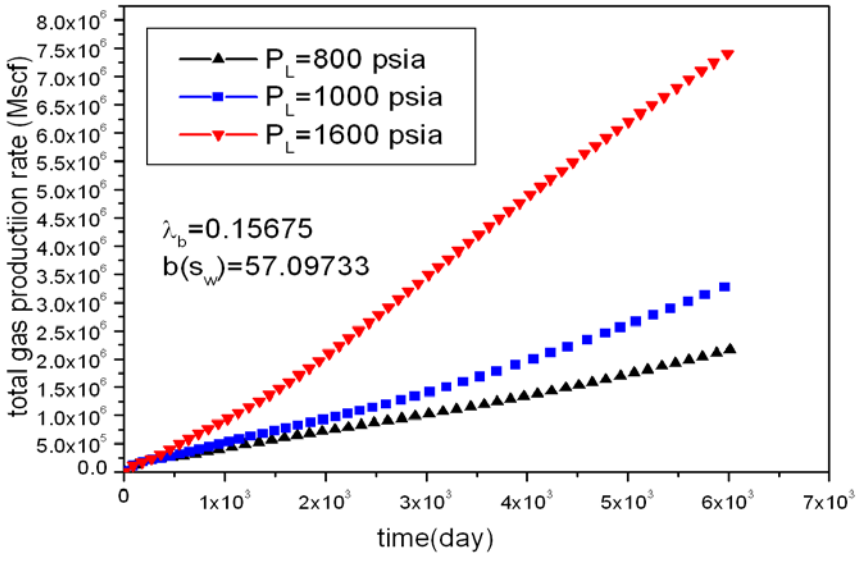

Figure 2.9 The effect of Langmuir pressure on total gas rate

2.5.2 Case study 2

This case study focused on investigating the impact of threshold pressure and gas slippage on the water and gas production rate in a quantitative way.

The daily gas production rate changes with the threshold pressure gradient are presented (**Figure 2.10**). As can be seen from this figure, gas production rate reaches at its maximum of 6500 Mscf/day after around 700 days production without considering the threshold pressure gradient. And the peak gas production rate is 6000 Mscf/day after 600 days production when $\lambda_b = 0.15675$; while gas production rate reaches its maximum of 4500 Mscf/day after around 1000 days production for $\lambda_b = 0.56489$, which is much smaller than the case for not considering the threshold pressure gradient, decreased by nearly 31%. Which indicates that the threshold pressure gradient should not be neglected for the simulation of CBM reservoir, otherwise, the gas production rate will be overestimated.

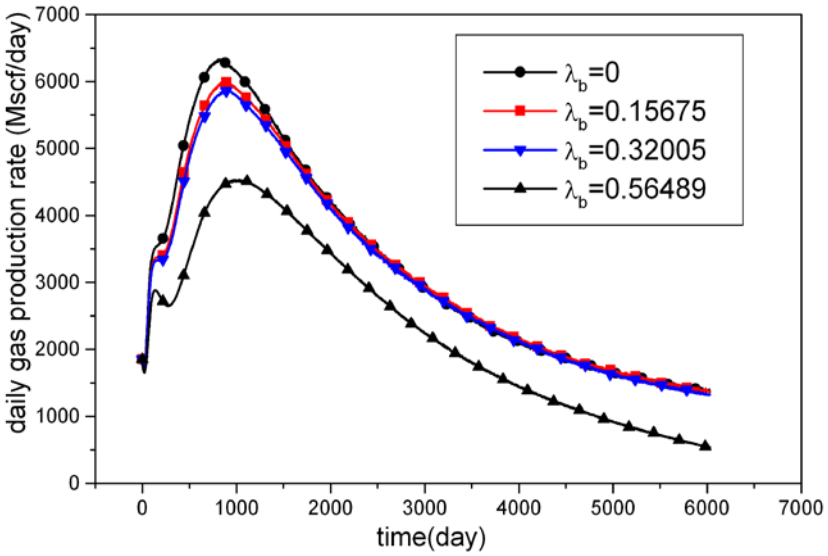

Figure 2.10 The effect of threshold pressure gradient on daily gas rate

The daily water production rate under the impact of threshold pressure gradient is illustrated in this study (**Figure 2.11**). It is easy to conclude that the lowest threshold pressure gradient corresponds to the highest water production rate. For example, the water production rate is higher with λ_b equal to 0.15675 than λ_b equal to 0.56489. This effect is much more obvious after around 400 days' production. Moreover, the water is earlier to be pumped off with smaller threshold pressure gradient.

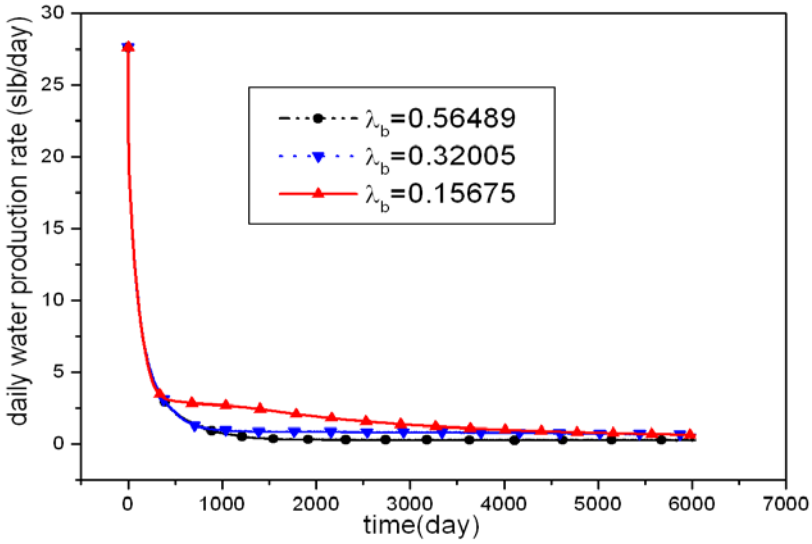

Figure 2.11 The effect of threshold pressure gradient on daily water rate

The total gas production rate under different value of threshold pressure gradient factor is presented (**Figure 2.12**). It decreases with the increasing of threshold pressure gradient. The decreasing scale of the total gas production rate is bigger when λ_b goes from 0.32005 to 0.56489 than the case when λ_b increases from 0.15675 to 0.32005. This again indicates the fact that the gas in the reservoir has to overcome the threshold pressure gradient before it can flow. Similar trend can be found in **Figure 2.14**.

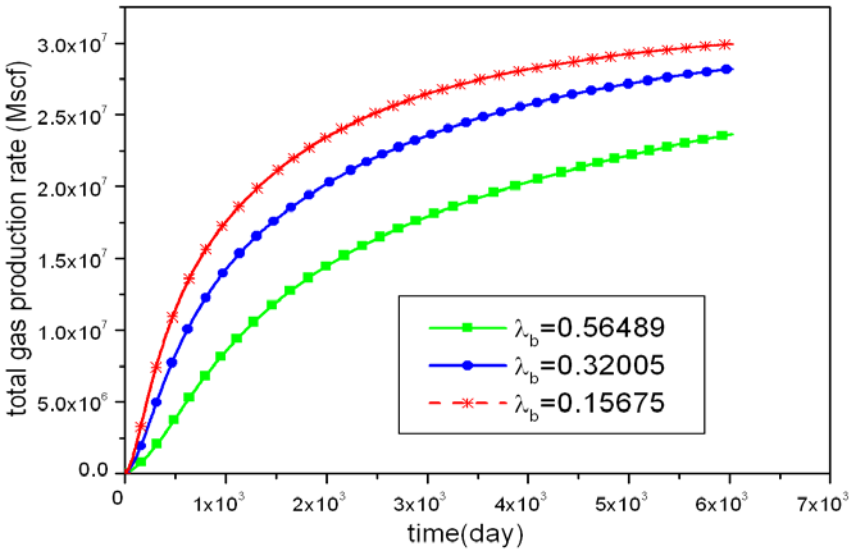

Figure 2.12 The effect of threshold pressure gradient on total gas rate

The pressure changes under the effect of different threshold pressure gradient are investigated (**Figure 2.13**). The threshold pressure gradient effect on the pressure changes is not very clearly around the first 5 days production, and after that, the effect becomes much more obvious. In addition, as shown in the figure, the pressure drops much more sharply with smaller threshold pressure gradient value than the larger value. This is because the gas and water production rate is higher with smaller threshold pressure gradient.

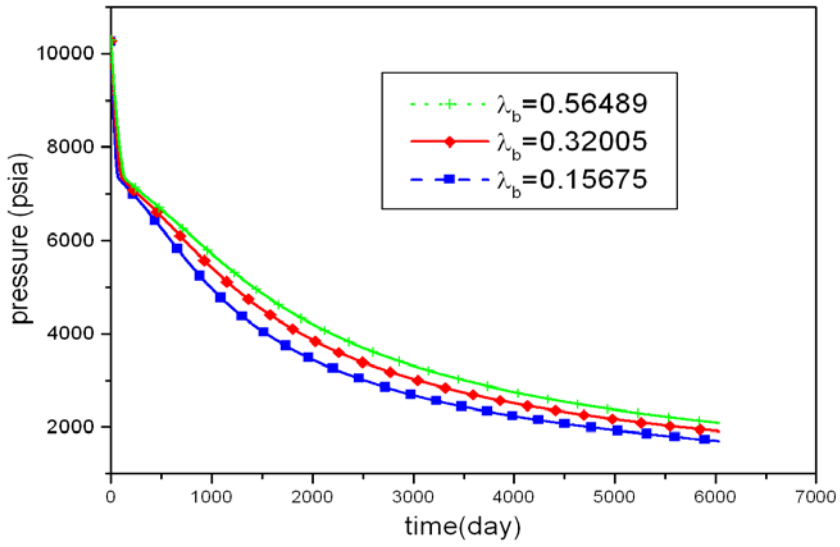

Figure 2.13 The effect of threshold pressure gradient on bottom-hole pressure

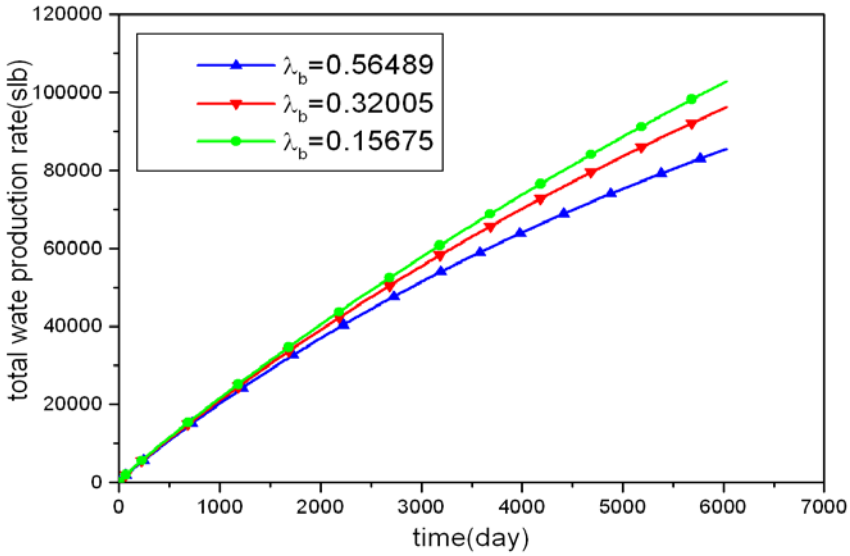

Figure 2.14 The effect of threshold pressure gradient on total water rate

The sensitivity analysis of the daily gas, daily water, total gas, total water production rate and bottom-hole pressure under different gas slippage factors are studied (**Figure 2.15, Figure 2.16, Figure 2.17, Figure 2.18 and Figure 2.19**).

From **Figure 2.15**, one can see that gas production rate reaches at a maximum of 19000 Mscf/day after around 499 days production when $b(s_w) = 437.6083$; while peak gas production rate is 6000 Mscf/day after around 999 days' production, which corresponding to $b(s_w) = 57.09733$. While the later stage shows the opposite trend. This indicates that gas production rate can be largely increased by considering the gas slippage effect during the early stage, however, the larger the gas slippage factor the lower the gas production rate at the later production stage. The increase of the gas production rate at the early stage attributes to the increasing of permeability owing to the effect of gas slippage. And with time going on, the effect of gas slippage becomes weaker due to the decreasing of water saturation. The similar result can be obtained for the daily water production rate, as shown in **Figure 2.16**.

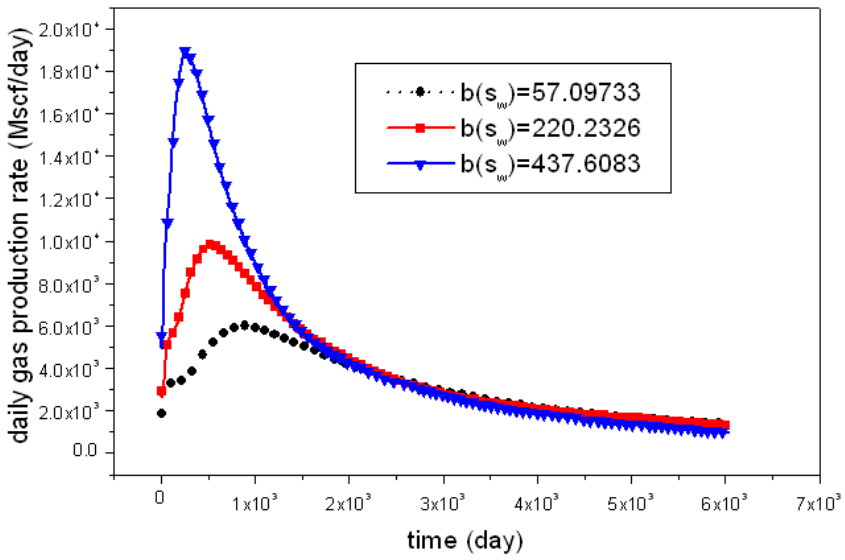

Figure 2.15 The effect of gas slippage factor on daily gas rate

The effect of gas slippage factor on the total gas production rate is illustrated **Figure 2.17**. This effect is a little bit obscure for the first 400 days production, while after that it is clearly seen from this figure that the total gas production rate increases with the rising of gas slippage factor. It can reach at about 1.75E7Mscf with $b(s_w) = 437.6083$, and 1.625E7Mscf with $b(s_w) = 220.2326$, while only about 1.48E7 Mscf with

$b(s_w) = 57.09733$. Similarly effects can also be seen for the changes of total water production rate, while the difference is that obvious gas slippage effect begins after about 2000 days well production, shown in **Figure 2.18**.

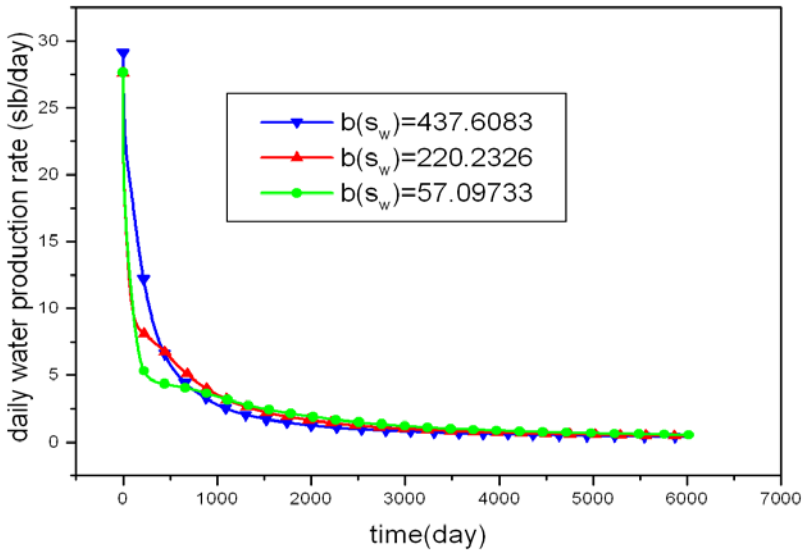

Figure 2.16 The effect of gas slippage factor on daily water rate

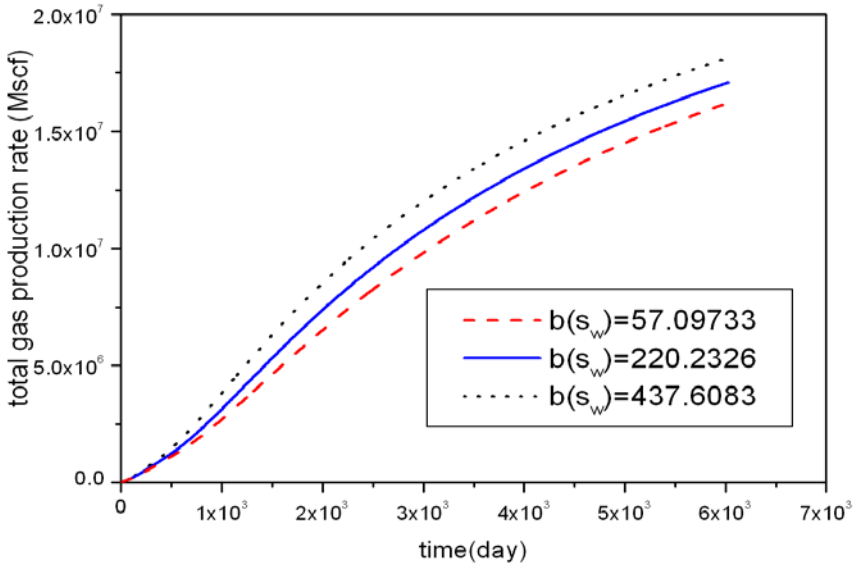

Figure 2.17 The effect of gas slippage factor on total gas rate

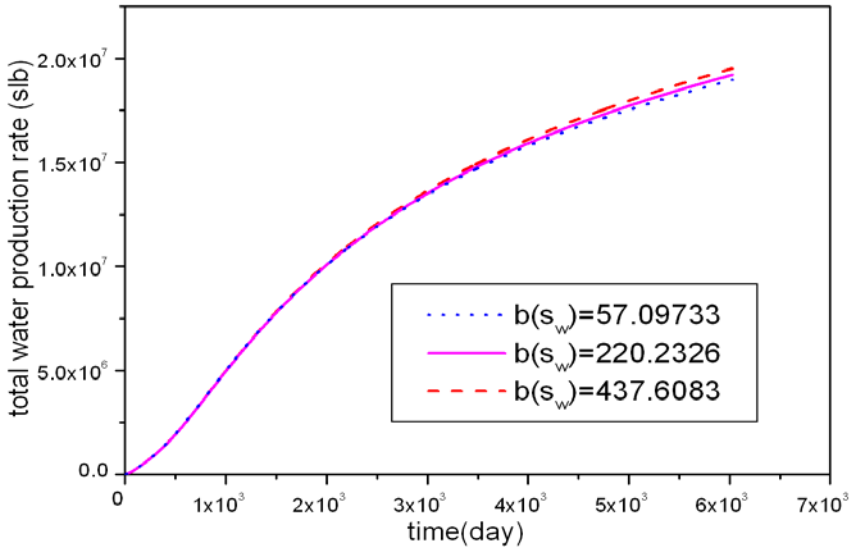

Figure 2.18 The effect of gas slippage factor on total water rate

The pressure changes under different gas slippage factors are presented (**Figure 2.19**). Obviously, the pressure depletion is larger with larger gas slippage factor, which is caused by the enhancement in the gas and water production rate. However, the pressure is still bigger with relatively larger gas slippage factor than with relatively smaller gas slippage factor. For example, the pressure became about 800 psia after 6000 days production when $b(s_w) = 57.09733$, and around 1700 psia with $b(s_w) = 220.2326$, while nearly 2500 psia with $b(s_w) = 437.6083$.

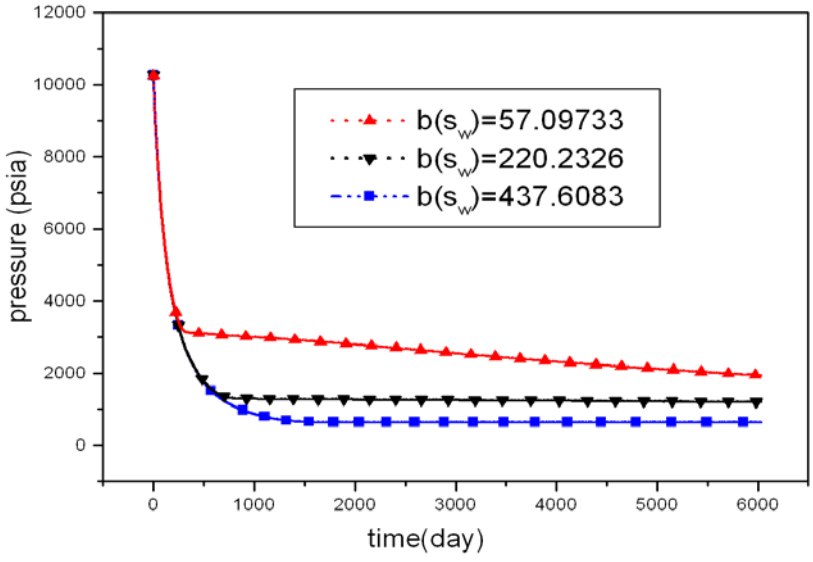

Figure 2.19 The effect of gas slippage factor on bottom-hole pressure

2.5.3 Case study 3

This study is designed to find out the impact of matrix shrinkage on the gas production rate, gas concentration and pressure in an inverted five spot pattern. The Cartesian axis is used for this model.

The gas concentration changes under the impact of matrix shrinkage as a function of time is illustrated (**Figure 2.20**). It is clearly seen from the figure that the coal gas concentration is gradually dropping down owning to the production of gas with time. Moreover, the coal gas concentration drops down much more sharply with matrix shrinkage. This is caused by the enhanced gas production rate due to the enlarged permeability under the effect of matrix shrinkage.

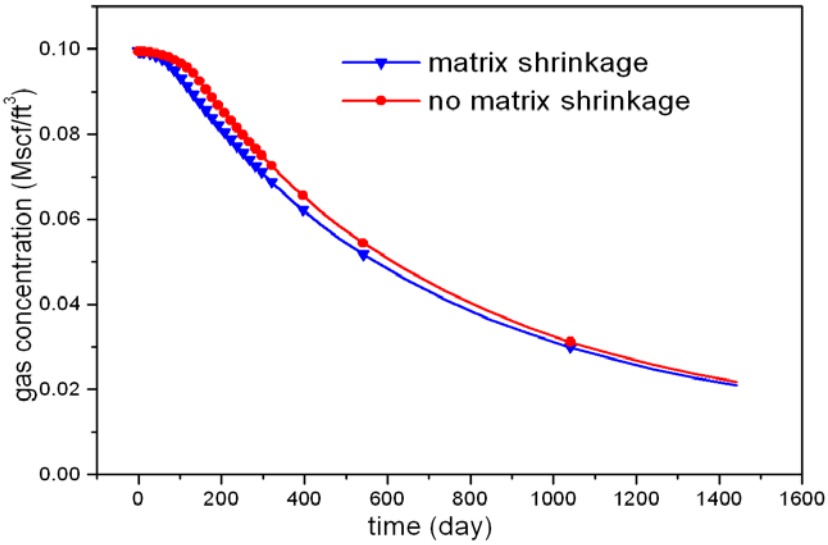

Figure 2.20 Effect of matrix shrinkage on coal gas concentration

The impact of matrix shrinkage on the gas production rate as a function of time is studied in this case study part (**Figure 2.21**). The existence of matrix shrinkage results in the permeability increases during primary methane production, so it can largely increase the gas production rate. The gas production breakthrough after 99 days production when the matrix shrinkage is considered and the maximum production rate is about 7800 Mscf/day. While the gas production breakthrough occurs at the 102 day in the case of neglecting matrix shrinkage with the maximum production rate of less than 2000 Mscf/day. After this period, the gas production rate gradually decreases and keeps at a constant level after about 400 days production for both case. However, the daily gas rate variation trend is reversed compared with the initial and middle stage.

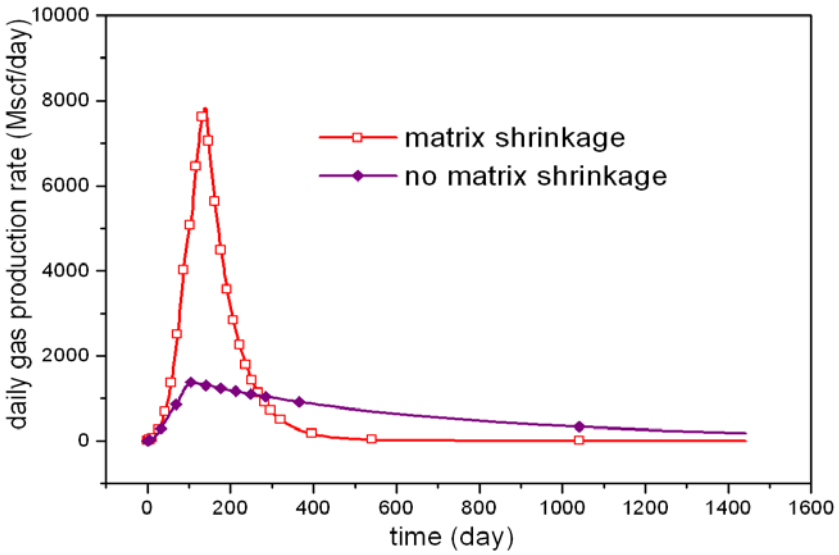

Figure 2.21 Effect of matrix shrinkage on gas production rate

The effect of matrix shrinkage on total gas production rate as a function of time is presented (**Figure 2.22**). Obviously, the total gas production rate increases during the production process, and the matrix shrinkage can only have obvious effect on it at the initial and middle stage. Moreover, the total gas rate is much bigger when the matrix shrinkage is taken into consideration than being ignored. Finally they reach nearly the same maximum rate during the simulation process. Similar trend can also be found in **Figure 2.23**, which shows the total water rate under the impact of matrix shrinkage.

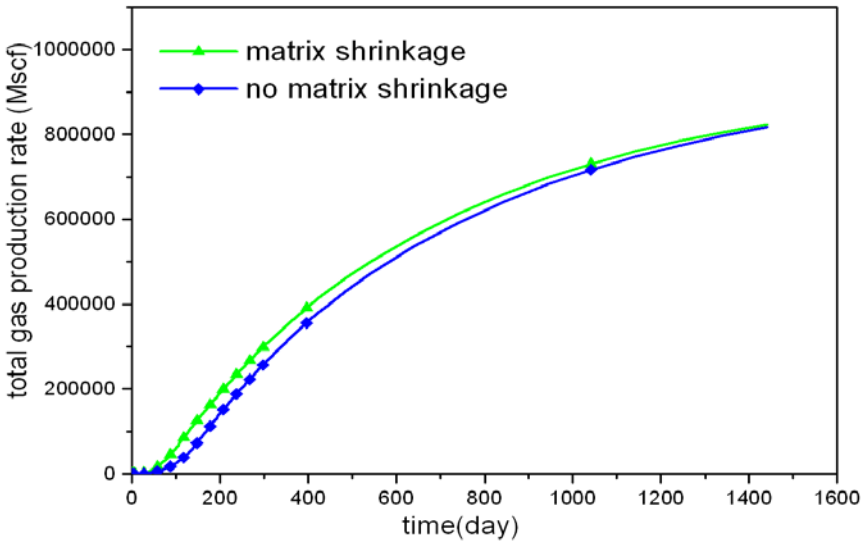

Figure 2.22 Effect of matrix shrinkage on total gas production rate

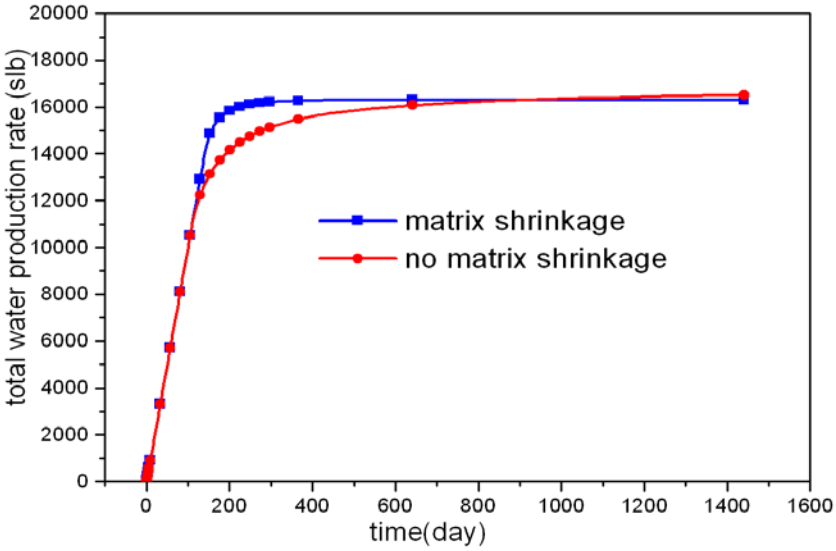

Figure 2.23 Effect of matrix shrinkage on total water production rate

The comparison of average field pressure under the impact of matrix shrinkage as a function of time is made (**Figure 2.24**). The average pressure drops quickly under the impact of matrix shrinkage, it decreases from around 4000 psia to approximately 250 psia during the whole simulation process. In addition, the pressure for the case that considers the matrix shrinkage effect is lower than the case that ignores the matrix shrinkage effect at the same production time. And after about 200 days declining, the pressure keeps at a constant level of 250 psia for both case.

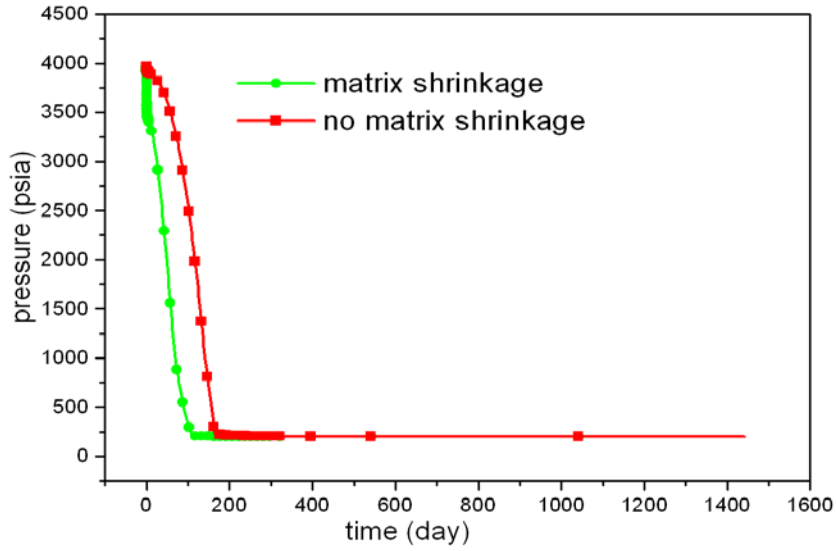

Figure 2.24 Effect of matrix shrinkage on average pressure

Figure 2.25 illustrates the impact of matrix shrinkage on water production rate as a function of time. The water production decreases much more sharply if the matrix shrinkage is taken into consideration than it is being ignored. This is because the matrix shrinkage can enlarge the cleat permeability, and in turn enhance the gas and water rate.

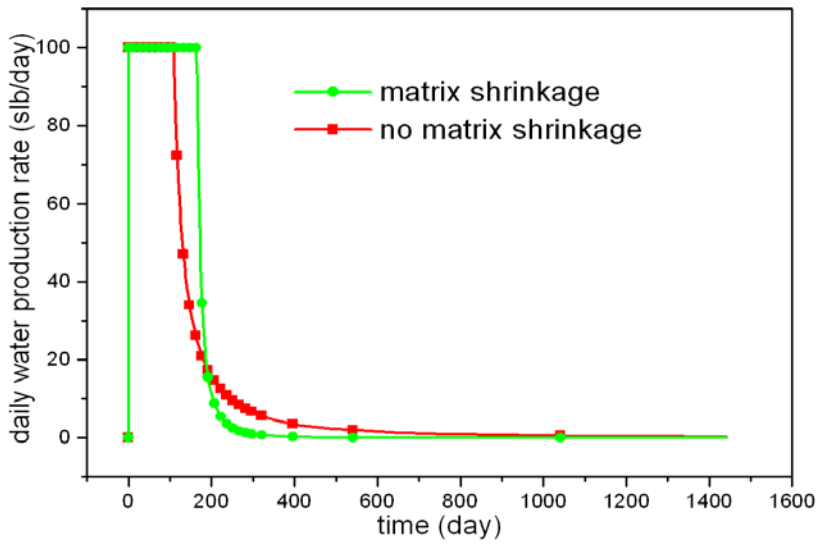

Figure 2.25 Effect of matrix shrinkage on water production rate

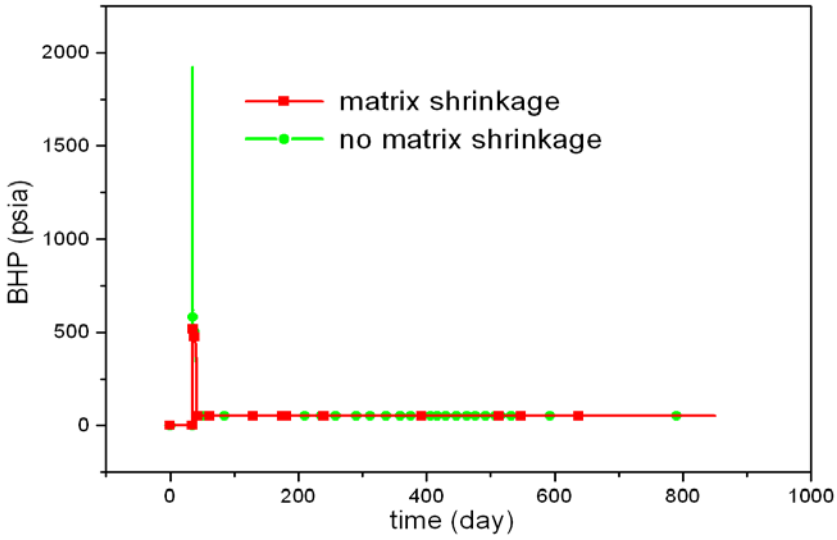

Figure 2.26 Effect of matrix shrinkage on bottom-hole pressure

The changes of well bottom-hole pressure under the impact of matrix shrinkage as a function of time is presented (**Figure 2.26**). It can be seen from the figure that the maximum bottom-hole pressure is only about 510 psia when taking matrix shrinkage

into consideration, however, if the matrix shrinkage is neglected, the maximum bottom-hole pressure can reach about 1950 psia. This means that the matrix shrinkage effect can make the well bottom-hole pressure in a very small value due to the large gas production rate.

2.6 Chapter conclusions

According to the studies in this Chapter, the following conclusions have been made:

(1) A new three dimensional, dual porosity, single permeability, non-equilibrium adsorption, gas water two phase flow, pseudo-steady state mathematical model was developed, which reflects the concrete influence factors in low permeability CBM reservoirs, and it was followed by a new theoretical formulation of permeability and porosity including the effect of matrix shrinkage. The breakthrough of this model is that it is beyond the limitation of researches nowadays that the gas slippage effect model is only applied to single phase permeability study.

(2) A computer programme called COAFOR has been developed for this model. Three synthetic case studies were made, which proved that the developed algorithm works well for solving the problem stated above. The good agreement between the results that come from COAFOR and Eclipse under the same parameters further validates the accurate of the model in this chapter.

(3) The results for this chapter have revealed that gas and water rate increases with Langmuir pressure, while decreases with Langmuir volume, which means the larger the Langmuir volume, the lower the gas rate. Moreover, larger desorption time can lower the desorption rate, thus the gas and water rate drops with the increasing of desorption time. In addition, the stronger the heterogeneous of the reservoir, the earlier for the gas to reach its maximum, and the bigger the gas rate, however, this effect is reversed for the late stage production.

(4) In addition, the results show that there exist three stages in coal de-watering and production processes. The existence of threshold pressure gradient can largely reduce the gas and water production rate, so is the total gas and water production rate. The gas slippage factor can increase the gas and water production rate at the initial and middle stage of production. In addition, the matrix shrinkage effect increases the gas rate owing to the enhanced permeability.

Chapter 3 Advanced coupled models to simulate the fluid flow in the low permeability CBM reservoir and horizontal borehole

3.1 Introduction

Horizontal wells are widely used in many new oil and gas fields as well as in further development of mature CBM fields. Productivity of a horizontal well can usually be greater than that of vertical well for several reasons. Firstly, horizontal wells can be open to a larger portion of the reservoir than vertical wells. A larger contact area allows lower drawdown to recover more oil and gas. Secondly, horizontal wells can be drilled perpendicular to oriented natural fractures and therefore intersect with more fractures. Also it may be possible to induce multiple hydraulic fractures in a horizontal well. Increased productivity is not the only benefit of horizontal wells; improved sweep efficiency, reduced coning of water or gas and increased drainage area are other advantages of horizontal wells over vertical wells. Therefore, horizontal wells are believed to perform better than their vertical counterparts in thin reservoirs.

Recent interest in horizontal wells has been accelerating owning to the improved drilling and completion technology, which has resulted in the increased efficiency and economics in oil and gas recovery. The increases in oil and gas production rate and improvement in ultimate recovery has given horizontal wells the edge over vertical wells in many margin reservoirs. The disadvantages here are that it is relatively much more expensive to drill and complete a horizontal well than a vertical one. Thus, reservoir engineers need to find a balance for the best profit.

In addition, multi-branch horizontal well technology is a fast developed oil and gas exploitation technology, it is based on the orientation well, large displacement well and horizontal well technology. It can largely enhance the oil and gas recovery rate, reduce the oil and gas comprehensive exploitation cost. Thus, it has significant economic benefit and has a bright future in both the oil and gas field. If the multi-branch horizontal well technology is combined with the CBM reservoir characteristic, it can be used for the low permeability CBM reservoir exploitation. The difference of multi-branch horizontal well technology between conventional low permeability and CBM reservoir is that multi-branch horizontal well technology needs longer horizontal displacement and more branches for CBM reservoir than conventional low permeability reservoir.

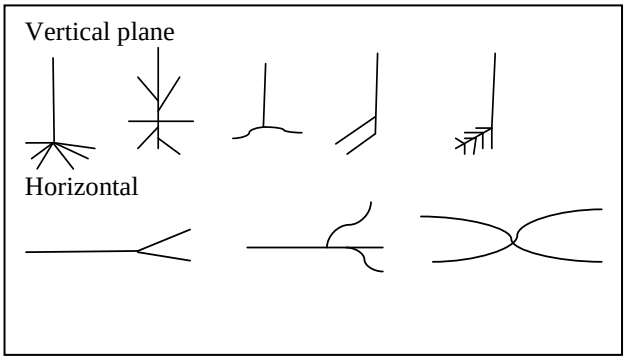

Figure 3.1 Typical horizontal well and multi-branch well profiles

The schematic diagram of different horizontal and multi-branch well configurations is shown in **Figure 3.1**. In vertical well plane, it is typically divided into five types: clustered branch horizontal well; radial branch horizontal well; reverse branch horizontal well; folder branch horizontal well; pinnate horizontal well. In horizontal plane, there are three type of horizontal well as shown in the figure, among them the pinnate horizontal well configuration is the most popular one.

As described in **Chapter 2**, the fluid flow in CBM reservoir can be simulated by using the basic dual porosity, single permeability two phase vertical well model, and the drilling fees for the horizontal well is not very expensive. However, most of the CBM reservoir around the world is low permeability reservoir, while the vertical well model can't accurately predict the gas and water production rate for the low permeability reservoir. For example, the recovery of the gas is very low and needs to be improved from the economic view. Thus this chapter focuses on the finding of much more optimized methods for the simulation of the low permeability CBM reservoir to enhance the gas recovery rate. Finally, the advanced coupled models to simulate the fluid flow in the low permeability CBM Reservoir and Horizontal Borehole is presented in this Chapter.

In order to gain the in-depth understanding of the advanced coupled models, three case studies are conducted for the sensitivity analysis in this Chapter. Firstly, the comparison of the results come from the multi-branch horizontal well model, single branch horizontal well model and vertical well model are made to investigate the recovery rate of different horizontal well patterns. Secondly, the threshold pressure and gas slippage effect on the gas, water rate and pressure changes are studied for single branch horizontal well, to get a good understanding of how the two effects affect on the production rate and pressure changes in the well. Finally, the effect of the Langmuir

pressure and volume as well as the branch number and angle are shown in this Chapter to find the best value of these parameters.

3.2 Wellbore pressure drop model

The horizontal well is divided into several segments (**Babu, D.K., et al., 1989[80]**) in the three dimensional unsteady state steady flow model. The fluid in the reservoir flows into every small segment. Suppose that there is a horizontal well with its radius r_w and length L, and the height, length and width of the reservoir is h, a and b respectively.

The six external boundaries for the reservoir are closed, as shown in **Figure 3.2**, and the well is designed from (x_0, y_1, z_0) to (x_0, y_2, z_0), which is parallel to axis y. The well can be located at anywhere in the reservoir, its length can also be arbitrarily long. However, it must parallel to one axis, that mean it can parallel to x, y or z. The reservoir is heterogeneity, while the anisotropic porosity ϕ can be seen as a constant; the permeability in the x, y, z direction is k_x, k_y, k_z respectively; the fluid flow in the reservoir is compressible gas and water two phase flow; and the initial pressure (corresponding to $t = 0$) in the whole reservoir is p_{ini}.

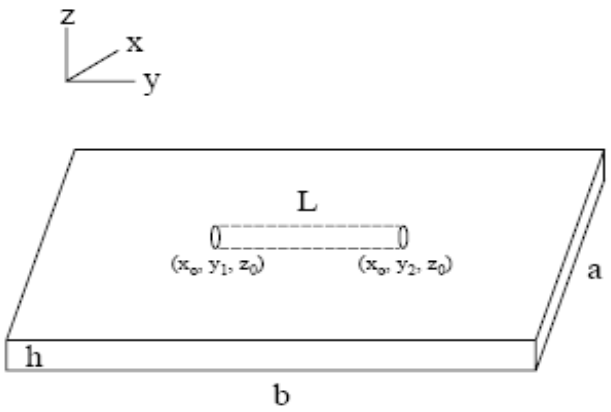

Figure 3.2 Horizontal well in cassette reservoir

The wellbore is assumed as finite conductivity to develop the coupled horizontal wellbore model distributed in various reservoirs. The horizontal well is also divided into several segments in the model of this chapter. Moreover, the effect of friction, acceleration and mixing loss are all considered for the fluid flow of each segment in the wellbore model.

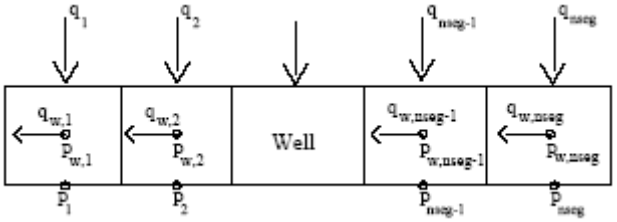

Figure 3.3 Horizontal well divided into segments

The wellbore is divided into n_{seg} parts (**Figure 3.3**). The first section is called the heel section, and the n_{seg} section is called the toe section. The pressure relationship between two adjacent well segments is:

$$p_{wf_{i-1}} = p_{wf_i} + 0.5\left(\Delta p_{wf_{i-1}} + \Delta p_{wf_i}\right) \quad i = 2,3,\cdots,n \tag{3.1}$$

If the well pressure is specified, that means the heel section pressure is known, thus:

$$p_{wf_n} = p_{wfc} + 0.5\Delta p_{wf_n} \tag{3.2}$$

If the gas production rate is specified, another equation has to be added because the well bottom-hole pressure is unknown. The production rate should be equal to the summation of the reservoir mass flowing rate that entered to the wellbore from the toe section (n_{seg}) up to the segment being analyzed (n). The expression for it is shown as follows:

$$q_{sum} = \sum_{i=1}^{n} PI_i \frac{k_{rg}}{\mu_g}\left(p_g - p_{wf_i}\right) \tag{3.3}$$

Where: $\Delta p_{wfi} = \Delta p_{fric_i} + \Delta p_{acc_i}$

3.2.1 Mass conservation equation

According to the mass conservation law, the mass flow rate into a node (segment) is equal to the summation of the reservoir mass flow rate entered into the wellbore from the toe section (n_{seg}) up to the segment being analyzed (n). Suppose that the density of the fluid in the wellbore is constant, then the flow rate in the wellbore can be derived as:

$$q_{w,n} = \sum_{i=n}^{n_{seg}} q_i \tag{3.4}$$

3.2.2 Pressure drop equation

The effect of friction, acceleration and the gas mixture between the main branch stream and branch for multi-branch well is considered in this study. In addition, the momentum loss caused by the gas mixture should be considered, because there is an angle between the main stream and branch.

3.2.2.1 Friction loss

Friction pressure drop can be calculated by the standard equation of pipe flow (**Govier, G.W. and Aziz, K., 1973[147]**):

$$\frac{dp}{dx} = 1.079 \times 10^{-4} \frac{f \rho v^2}{d} \tag{3.5}$$

The pressure drop in the wellbore can be calculated through multiplying the solution of the above equation by the distances of every well node. Friction factor f is related to the velocity v, the value of v is determined by $q_{w,n}$. And $q_{w,n}$ can determine the fluid status (laminar flow, unsteady state flow, turbulence flow) in one location. Finally, f can be calculated through the fluid status in a specified location of one well.

The following method is used in order to explain the dynamic fluid inflow status. Determine the fluid status (laminar flow, unsteady state flow, turbulence flow) by calculating the Reynolds number of each segment. Then calculate the friction coefficient. Some scholars (**Ouyang, et al., 1998[148]**) found that the radial flow friction factor can be written as:

Laminar flow

$$f = \frac{64}{N_{\mathrm{Re}}}[1 + 0.04304 N_{\mathrm{Re}w}^{0.6142}] \tag{3.6}$$

Turbulence flow:

$$f = f_0[1 - 0.0153 N_{\mathrm{Re}w}^{0.3978}] \tag{3.7}$$

It is obviously to see that the effective friction factor can increase the inflow rate for laminar flow and decrease the inflow rate for turbulence flow.

3.2.2.2 Acceleration effect

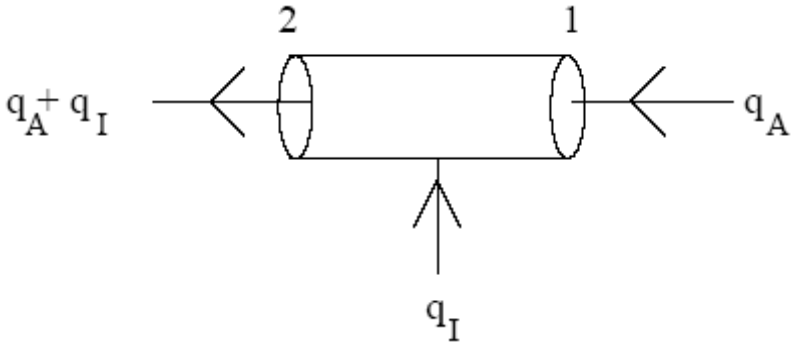

Figure 3.4 Effect of acceleration

The effect of acceleration for well segment n is shown in **Figure 3.4**. The fluid flows in from the right side, and flows out from the left side. Axial flux that flows into pipe is q_A. The flux flows from the reservoir into the well segment is q_l. The variation of momentum F_{acc} in this well is:

$$F_{acc} = \rho A(v_2^2 - v_1^2) \tag{3.8}$$

Where:

$$v_1 = \frac{q_A}{A}, \quad v_2 = \frac{q_A + q_I}{A} \tag{3.9}$$

Substituting **Equation (3.9)** into **Equation (3.8)**, then the acceleration pressure drop in this well segment is:

$$\Delta p_{acc} = \frac{F_{acc}}{A} = \frac{\rho}{A^2}\left[q_I^2 + 2q_A q_I \right] \tag{3.10}$$

3.2.2.3 Mixing loss

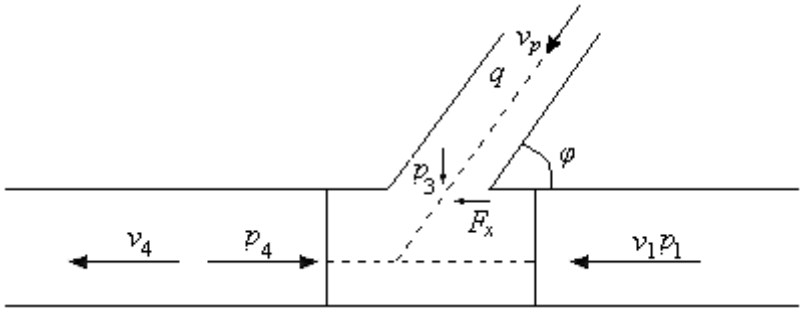

Figure 3.5 Effect of gas mixture in a multi-branch well

Figure 3.5 presents the effect of gas mixture in a multi-branch well model, where exists gas mixing between main stream and branch. Assuming h_{14} is the energy loss of unit weight fluid caused by the mixing loss. And F_x has the following expression according to momentum equations and Newton's third law:

$$F_x = \rho q v_3 \cos\varphi \tag{3.11}$$

Thus the momentum equation before and after gas mixing is:

$$p_1 A - p_4 A + F_x = \rho Q_4 v_4 - \rho Q_1 v_1 \tag{3.12}$$

Continuity equation can be expressed as:

$$v_1 A + q = v_4 A \tag{3.13}$$

Energy equation can be shown as:

$$\frac{p_1}{\rho g} + \frac{v_1^{\,2}}{2g} = \frac{p_4}{\rho g} + \frac{v_4^{\,2}}{2g} + h_{14} \tag{3.14}$$

h_{14} can be derived as the following form through **Equation(3.13)** and **Equation (3.14)**:

$$h_{14} = \frac{q^2 + 2v_1 qA}{2gA^2} - \frac{q v_p \cos\varphi}{gA} \tag{3.15}$$

Thus Δp_{wf_i} can be expressed as：

$$\Delta p_{wf_i} = \Delta p_{fric_i} + \Delta p_{acc_i} + \rho_i g h_{14i} \tag{3.16}$$

3.2.3 Constraint equation

Flux constraint equation:

$$\sum_{i=1}^{n_{seg}} q_i - Q_{\max} = 0 \tag{3.17}$$

Well bottom-hole pressure equation:

$$p_0 - p_{wf,\min} = 0 \tag{3.18}$$

3.3 Advanced coupled CBM reservoir model with horizontal wellbore

The coupled horizontal wellbore model consists two parts: formation model and wellbore pressure drop model.

3.3.1 Formation model

The formation model is the same as shown in **Chapter 2**:

$$
\begin{cases}
\dfrac{\partial}{\partial x}\left(\dfrac{k_f k_{rg\infty}}{\mu_g B_g}(1+\beta_1(\dfrac{k_f k_{rg\infty}(s_g)}{\phi_g})^{-\beta_2}/p_m)(\dfrac{\partial}{\partial x}(p_{fg}-\gamma_g H)-\lambda_{bg})+D_a\dfrac{\partial}{\partial x}(\dfrac{s_g}{B_g})\right) \\
+\dfrac{\partial}{\partial y}\left(\dfrac{k_f k_{rg\infty}}{\mu_g B_g}(1+\beta_1(\dfrac{k_f k_{rg\infty}(s_g)}{\phi_g})^{-\beta_2}/p_m)(\dfrac{\partial}{\partial y}(p_{fg}-\gamma_g H)-\lambda_{bg})+D_a\dfrac{\partial}{\partial y}(\dfrac{s_g}{B_g})\right) \\
+\dfrac{\partial}{\partial z}\left(\dfrac{k_f k_{rg\infty}}{\mu_g B_g}(1+\beta_1(\dfrac{k_f k_{rg\infty}(s_g)}{\phi_g})^{-\beta_2}/p_m)(\dfrac{\partial}{\partial z}(p_{fg}-\gamma_g H)-\lambda_{bg})+D_a\dfrac{\partial}{\partial z}(\dfrac{s_g}{B_g})\right) \\
-q_{vg}+q_{mfg}=\dfrac{\partial}{\partial t}\left(\dfrac{\phi_f s_g}{B_g}\right) \\
\dfrac{\partial}{\partial x}\left(\dfrac{k_f k_{rw\infty}}{\mu_w B_w}(\dfrac{\partial}{\partial x}(p_{fw}-\gamma_w H)-\lambda_{bw})\right)+\dfrac{\partial}{\partial y}\left(\dfrac{k_f k_{rw\infty}}{\mu_w B_w}(\dfrac{\partial}{\partial y}(p_{fw}-\gamma_w H)-\lambda_{bw})\right) \\
+\dfrac{\partial}{\partial z}\left(\dfrac{k_f k_{rw\infty}}{\mu_w B_w}(\dfrac{\partial}{\partial z}(p_{fw}-\gamma_w H)-\lambda_{bw})\right)-q_{vw}=\dfrac{\partial}{\partial t}\left(\dfrac{\phi s_w}{B_w}\right) \\
q_{mfg}=-\dfrac{\rho_c}{B_g}\dfrac{\partial V_m}{\partial t} \qquad \dfrac{\partial V_m}{\partial t}=-\dfrac{1}{\tau}[V_m-V_E(p_{fg})] \\
q_{vg}=\dfrac{2\pi hkk_{rg\infty}}{\mu_g B_g \ln(\dfrac{r_e}{r_w}+s')}[(p_{fg}-\lambda_{bg}r_e)^2-(p_{wf}-\lambda_{bg}r_w)^2] \\
q_{vw}=\dfrac{2\pi hkk_{rw\infty}}{\mu_w B_w \ln(\dfrac{r_e}{r_w}+s)}[(p_{fw}-\lambda_{bw}r_e)-(p_{wf}-\lambda_{bw}r_w)] \\
\phi-\phi_0=\dfrac{1}{M}(p-p_0)-(1-\dfrac{K}{M})\dfrac{\rho_c V_L RT}{V_0 E}[\ln(1+bp_0)-\ln(1+bp_0)] \\
k=k_0(\phi/\phi_0)^3;\ p_{cgw}(s_g)=p_{fg}-p_{fw};\ s_g+s_w=1.0 \\
p_{fg}\big|_{t=0}=p_{fg}^0;\ p_{fw}\big|_{t=0}=p_{fw}^0;\ s_g\big|_{t=0}=s_g^0;\ V_m\big|_{t=0}=V_m^0 \\
p_{fg}\big|_{x=x_w,y=y_w;z=z_w}=p_{wf};\ p_{fg}\big|_{(x,y,z)\in\Gamma}=p_e;\ \partial s_g/\partial n\big|_\Gamma=0
\end{cases}
\tag{3.19}
$$

3.3.2 Single branch wellbore model

In the horizontal wellbore model, the acceleration pressure drop effect that caused by the changes of flowing speed as well as the wellbore friction pressure drop effect are both considered. The horizontal well is divided into *n* segments, and the pressure relationship of two adjacent segments can be presented as follows:

$$p_{wf_{i-1}} = p_{wf_i} + 0.5(\Delta p_{wf_{i-1}} + \Delta p_{wf_i})\ i = 2,3,...,n \tag{3.20}$$

If well pressure is specified, which means the well bottom-hole pressure p_{wfc} is known, thus there is:

$$p_{wf_n} = p_{wfc} + 0.5\, p_{wf_n} \tag{3.21}$$

If the gas production rate is specified, which means the well bottom-hole pressure p_{wfc} is not known, another equation is needed for solving the problem. In addition, the total gas production rate is equal to the sum of gas production rate in each segment. The formula is written as follows:

$$q_{sum} = \sum_{i=1}^{n} PID_i \frac{k_{rg}}{\mu_g}(p_g - p_{wfi}) \tag{3.22}$$

$$\Delta p_{wf_i} = \Delta p_{fric_i} + \Delta p_{acc_i} \tag{3.23}$$

The friction pressure drop can be calculated through the following equation:

$$\Delta p_{fric_i} = \frac{1}{2}\frac{\rho_i f_i}{D}\overline{V}_i^2 \Delta x_i \tag{3.24}$$

Here, f_i is the well friction coefficient, which is related to the wellbore flow velocity $\overline{V}_i$, while $\overline{V}_i$ is determined by flux Q_i. The flux Q_i in turn determines the well section's flowing state: turbulence flow, laminar flow or shun variable flow. f_i can be calculated through the well flowing state in a specified position.

3.3.2.1 Friction effect

The radial friction coefficient factors are shown in **Equation (3.6)** and **Equation (3.7)**, the Reynolds constant is expressed as: $\mathrm{Re}_i = \dfrac{\overline{V}_i \rho_i D}{\mu_i}$.

Where: $\overline{V_i} = \frac{V_i + V_{i-1}}{2}$, $\rho_i = \frac{\rho_{gi} q_{gi} + \rho_{wi} q_{wi}}{q_{gi} + q_{wi}}$, $\mu_i = \mu_{wi}^{f_{wi}} \mu_{gi}^{1-f_{wi}}$, $f_{wi} = \frac{\rho_{wi} q_{wi}}{\rho_{wi} q_{wi} + \rho_{gi} q_{gi}}$.

3.3.2.2 Acceleration effect

In addition, the acceleration pressure drop in the wellbore can be calculated through the following formula:

$$\Delta p_{acci} = \rho_i (V_i + V_{i-1})(V_i - V_{i-1}) \tag{3.25}$$

Then the following equation can be got according to the mass conservation law:

$$\rho_i V_{i-1} \frac{\pi D^2}{4} + \rho_i V_{vi} \pi D \Delta x_i - \rho_i V \frac{\pi D^2}{4} = 0 \tag{3.26}$$

Here: $Q_i = \frac{V_i \pi D^2}{4}$, $q_i = V_{vi} \Delta x_i \pi D$.

Thus the pressure drop can be expressed by the fluid flux as follows:

$$\Delta p_{wfi} = \frac{2 f_i \rho_i}{\pi^2 D^5} (2Q_i + q_i)^2 \Delta x_i + \frac{16 \rho_i q_i}{\pi^2 D^4} (2Q_i + q_i) \tag{3.27}$$

3.3.2.3 Coupled single branch wellbore model

Notice that the fluid flux can be finally derived as the function of well bottom-hole pressure and formation pressure. So formation model **Equation (3.19)** can be coupled with **Equation (3.27)** to form the nonlinear equations, with formation pressure, formation gas, water saturation and well bottom-hole pressure as unknowns. This coupled single branch horizontal wellbore model can be used to simulate the fluid flow in the low permeability CBM reservoir and horizontal wellbore.

3.3.3 Multi-branch horizontal wellbore model

The coupled multi-branch horizontal wellbore model also consist two parts: formation model and wellbore pressure drop model. The formation model is still use **Equation (3.19)**.

3.3.3.1 Wellbore pressure model derivation

Suppose that the multi-branch wells are located in XY plane, the branch well is divided into several segments by the grid in this plane. In addition, the flow flux of the gas

reservoir in the segment is considered to be constant because the segment length is very small. The whole well segment is uncased completion, so the flux flows into the main stream and branch well segment is considered as the sink of the flowing equation.

The big difference between multi-branch horizontal wellbore model and single branch horizontal wellbore model is: the wellbore flux of every segment in the multi-branch horizontal wells not only contains adjacent upstream segment flow flux and formation flow flux, it also contains the flow flux comes from the branch wellbore. What is more, the momentum loss caused by the gas mixture has to be considered except the effect of friction pressure drop and acceleration pressure drop. Thus, the pressure drop for the well segment with branches can be expressed as:

$$\Delta p_{wfi} = \Delta p_{frici} + \Delta p_{acci} + \rho_i g h_{14i} \tag{3.28}$$

The mass conservation equation in the multi-branch horizontal wellbore is as follows:

$$\rho_i V_{i-1} \frac{\pi D^2}{4} + \rho_i V_{vi} \pi D \Delta x_i - \rho_i V \frac{\pi D^2}{4} + \rho_i \frac{\pi D^2}{4} V_{Ri} = 0 \tag{3.29}$$

Define: $Q_i = \frac{V_i \pi D^2}{4}, q_i = V_{vi} \Delta x_i \pi D, Q_{Ri} = \frac{V_{Ri} \pi D^2}{4}$, then the pressure drop equation for the multi-branch horizontal wellbore can be got as follows:

Segment with no branch:

$$\Delta p_{wfi} = \frac{2 f_i \rho_i}{\pi^2 D^5} (2Q_i + q_i + Q_{Ri})^2 \Delta x_i + \frac{16 \rho_i (q_i + Q_{Ri})}{\pi^2 D^4} (2Q_i + q_i + Q_{Ri}) \tag{3.30a}$$

Segment with branch:

$$\begin{aligned} \Delta p_{wfi} &= \frac{2 f_i \rho_i}{\pi^2 D^5} (2Q_i + q_i + Q_{Ri})^2 \Delta x_i + \frac{16 \rho_i (q_i + Q_{Ri})}{\pi^2 D^4} (2Q_i + q_i + Q_{Ri}) \\ &+ \frac{4 Q_i \rho_i}{\pi^2 D^4} (9Q_i - 4Q_{Ri} \cos\varphi) \end{aligned} \tag{3.30b}$$

3.3.3.2 Coupled multi-branch wellbore model

Equation (3.19) can be coupled with **Equation (3.30a)** and **Equation (3.30b)** to form the coupled multi-branch horizontal wellbore model. This coupled model can then be used to simulate the fluid flow of low permeability CBM reservoir and the multi-branch horizontal wellbore simutaneously.

3.4 Numerical solutions

The CBM reservoir formation model in this Chapter is solved using the modified IMPES method originially used for the solution of conventional black oil model.

3.4.1 Formation model difference equation

In order to solve the equation, firstly multiply B_g on both side of gas phase equation in the cleat system, and then manage the right side of the equation for gas and water phase as follows:

$$\begin{aligned} B_g \frac{\partial}{\partial t}\left(\frac{\phi_f s_g}{B_g}\right) &= s_g \phi_f c_f \frac{\partial p_{fg}}{\partial t} + \phi_f \frac{\partial s_g}{\partial t} + \phi_f s_g c_g \frac{\partial p_{fg}}{\partial t} \\ B_w \frac{\partial}{\partial t}\left(\frac{\phi_f s_w}{B_w}\right) &= s_w \phi_f c_f \frac{\partial p_{fg}}{\partial t} + \phi_f \frac{\partial s_w}{\partial t} + \phi_f s_w c_w \frac{\partial p_{fg}}{\partial t} \end{aligned} \tag{3.31}$$

Where: $c_f = \frac{1}{\phi_f}\frac{\partial \phi_f}{\partial p_{fg}}, c_g = -\frac{1}{B_g}\frac{\partial B_g}{\partial p_{fg}}, c_w = -\frac{1}{B_w}\frac{\partial B_w}{\partial p_{fg}}$

Then, add the left side of both gas and water phase equation together, write it in the form of differential operator:

$$\begin{aligned} &B_g\{\nabla\cdot[\frac{k_f k_{rg\infty}}{\mu_g B_g}(1+\alpha_1(\frac{k_f k_{rg\infty}(s_g)}{\phi_g})^{-\alpha_2} / p_m)(\nabla(p_{fg}-\gamma_g H)-\lambda_{bg})]-q_{vg}\} \\ &+B_g\{\nabla\cdot[D_a\nabla(\frac{s_g}{B_g})]+q_{mfg}\}+B_w\{\nabla\cdot[\frac{k_f k_{rw\infty}}{\mu_w B_w} \\ &(\nabla(p_{fg}-p_{acgw}-\gamma_w H)-\lambda_{bw})]-q_{vw}\} = \phi_f c_t \frac{\partial p_{fg}}{\partial t} \end{aligned} \tag{3.32}$$

Where: $c_t = c_f + c_w s_w + c_g s_g$, $p_{fw} = p_{fg} - p_{cgw}$

Suppose that the cell body volume is V_b, and the difference equation can be developed through cell body method:

$$\begin{aligned} &B_w\left[\Delta T_w \cdot \Delta p_{fg} + G_w - Q_{vw}\right] + B_g[\Delta T_g \cdot \Delta p_{fg} + \Delta T_D \cdot \Delta\left(\frac{s_g}{B_g}\right) + G_g \\ &-Q_{vg} + Q_{mfg}] = \left(\frac{V_b \phi_f c_t}{\Delta t}\right)_{ijk}^{n} \left(p_{fgijk}^{n+1} - p_{fgijk}^{n}\right) \end{aligned} \tag{3.33}$$

Where: $G_w = -\Delta T_w \cdot [\Delta(p_{cgw} + \gamma_w H) + \lambda_{bw}]$, $G_g = -\Delta T_g \cdot [\Delta(\gamma_g H) + \lambda_{bg}]$, $Q_{vw} = V_b q_{vw}$

$Q_{vg} = V_b q_{vg}$, $Q_{mfg} = V_b q_{mfg}$, $V_b = \Delta x \Delta y \Delta z$

Followed that, utilize the pressure implicit, saturation, production item and transmissibility explicit method to expand the difference equation:

$$
\begin{aligned}
&B_{gi,j,k}[T_{g_{i+\frac{1}{2},j,k}}^{n}(p_{fgi+1,j,k}^{n+1} - p_{fgi,j,k}^{n+1}) - T_{g_{i-\frac{1}{2},j,k}}^{n}(p_{fgi,j,k}^{n+1} - p_{fgi-1,j,k}^{n+1}) \\
&+T_{g_{i,j+\frac{1}{2},k}}^{n}(p_{fgi,j+1,k}^{n+1} - p_{fgi,j,k}^{n+1}) - T_{g_{i,j-\frac{1}{2},k}}^{n}(p_{fgi,j,k}^{n+1} - p_{fgi,j-1,k}^{n+1}) \\
&+T_{g_{i,j,k+\frac{1}{2}}}^{n}(p_{fgi,j,k+1}^{n+1} - p_{fgi,j,k}^{n+1}) - T_{g_{i,j,k-\frac{1}{2}}}^{n}(p_{fgi,j,k}^{n+1} - p_{fgi,j,k-1}^{n+1}) \\
&+T_{D_{i+\frac{1}{2},j,k}}^{n}((\frac{s_g}{B_g})_{i+1,j,k}^{n} - (\frac{s_g}{B_g})_{i,j,k}^{n}) - T_{D_{i-\frac{1}{2},j,k}}^{n}((\frac{s_g}{B_g})_{i,j,k}^{n} - (\frac{s_g}{B_g})_{i-1,j,k}^{n}) \\
&+T_{D_{i,j+\frac{1}{2},k}}^{n}((\frac{s_g}{B_g})_{i,j+1,k}^{n} - (\frac{s_g}{B_g})_{i,j,k}^{n}) - T_{D_{i,j-\frac{1}{2},k}}^{n}((\frac{s_g}{B_g})_{i,j,k}^{n} - (\frac{s_g}{B_g})_{i,j-1,k}^{n}) \\
&+T_{D_{i,j,k+\frac{1}{2}}}^{n}((\frac{s_g}{B_g})_{i,j,k+1}^{n} - (\frac{s_g}{B_g})_{i,j,k}^{n}) - T_{D_{i,j-\frac{1}{2},k}}^{n}((\frac{s_g}{B_g})_{i,j,k}^{n} - (\frac{s_g}{B_g})_{i,j,k-1}^{n}) \\
&+(G_g + Q_{mfg} - Q_{vg})_{i,j,k}^{n}] \\
&+B_{wi,j,k}[T_{w_{i+\frac{1}{2},j,k}}^{n}(p_{fgi+1,j,k}^{n+1} - p_{fgi,j,k}^{n+1}) - T_{w_{i-\frac{1}{2},j,k}}^{n}(p_{fgi,j,k}^{n+1} - p_{fgi-1,j,k}^{n+1}) \\
&+T_{w_{i,j+\frac{1}{2},k}}^{n}(p_{fgi,j+1,k}^{n+1} - p_{fgi,j,k}^{n+1}) - T_{w_{i,j-\frac{1}{2},k}}^{n}(p_{fgi,j,k}^{n+1} - p_{fgi,j-1,k}^{n+1}) \\
&+T_{w_{i,j,k+\frac{1}{2}}}^{n}(p_{fgi,j,k+1}^{n+1} - p_{fgi,j,k}^{n+1}) - T_{w_{i,j,k-\frac{1}{2}}}^{n}(p_{fgi,j,k}^{n+1} - p_{fgi,j,k-1}^{n+1}) \\
&+(G_w - Q_{vw})_{i,j,k}^{n}] = (\frac{V_b \phi_a c_t}{\Delta t})_{i,j,k}^{n}(p_{fgi,j,k}^{n+1} - p_{fgi,j,k}^{n})
\end{aligned}
\tag{3.34}
$$

Where:

$$
T_{g(i\pm\frac{1}{2}),j,k} = \frac{(Ak_f)_{(i\pm\frac{1}{2}),j,k}}{0.5(\Delta x_i + \Delta x_{i\pm1})}(\frac{k_{rg\infty}}{B_g \mu_g}(1 + \alpha_1(\frac{k_f k_{rg\infty}(s_g)}{\phi_g}))^{-\alpha_2} / p_m)_{(i\pm\frac{1}{2}),j,k}
$$

$$
T_{gi,(j\pm\frac{1}{2}),k} = \frac{(Ak_f)_{i,j\pm\frac{1}{2},k}}{0.5(\Delta y_j + \Delta y_{j\pm1})}(\frac{k_{rg\infty}}{B_g \mu_g}(1 + \alpha_1(\frac{k_f k_{rg\infty}(s_g)}{\phi_g}))^{-\alpha_2} / p_m)_{i,(j\pm\frac{1}{2}),k}
$$

$$
T_{gi,j,(k\pm\frac{1}{2})} = \frac{(Ak_f)_{i,j,k\pm\frac{1}{2}}}{0.5(\Delta z_k + \Delta z_{k\pm1})}(\frac{k_{rg\infty}}{B_g \mu_g}(1 + \alpha_1(\frac{k_f k_{rg\infty}(s_g)}{\phi_g}))^{-\alpha_2} / p_m)_{i,j,k\pm\frac{1}{2}}
$$

$$T_{w(i\pm\frac{1}{2}),j,k)}=\frac{(Ak_f)_{(i\pm\frac{1}{2}),j,k}}{0.5(\Delta x_i+\Delta x_{i\pm1})}(\frac{k_{rw}}{B_w\mu_w})_{(i\pm\frac{1}{2}),j,k}$$

$$T_{wi,(j\pm\frac{1}{2}),k}=\frac{(Ak_f)_{i,j\pm\frac{1}{2},k}}{0.5(\Delta y_j+\Delta y_{j\pm1})}(\frac{k_{rw}}{B_w\mu_w})_{i,(j\pm\frac{1}{2}),k}$$

$$T_{wi,j,(k\pm\frac{1}{2})}=\frac{(Ak_f)_{i,j,k\pm\frac{1}{2}}}{0.5(\Delta z_k+\Delta z_{k\pm1})}(\frac{k_{rw}}{B_w\mu_w})_{i,j,k\pm\frac{1}{2}}$$

$$T_{D(i\pm\frac{1}{2}),j,k}=\frac{(AD_f)_{i\pm\frac{1}{2},j,k}}{0.5(\Delta x_i+\Delta x_{i\pm1})}$$

$$T_{Di,(j\pm\frac{1}{2}),k}=\frac{(AD_f)_{i,j\pm\frac{1}{2},k}}{0.5(\Delta y_j+\Delta y_{j\pm1})}$$

$$T_{Di,j,k\pm\frac{1}{2}}=\frac{(AD_f)_{i,j,k\pm\frac{1}{2}}}{0.5(\Delta z_k+\Delta z_{k\pm1})}$$

3.4.2 Diffusion difference equation

Difference diffusion equation:

$$\frac{V_{mijk}^{n+1}-V_{mijk}^{n}}{\Delta t}=\frac{1}{\tau}\left[V_E\left(p_{fgijk}^{n}\right)-V_{mijk}^{n}\right] \tag{3.35}$$

$$V_E\left(p_{fgijk}^{n}\right)=\frac{V_L p_{fgijk}^{n}}{p_L+p_{fgijk}^{n}} \tag{3.36}$$

Let $V_{Ei,j,k}^{n+1/2}=\frac{V_{Ei,j,k}^{n}+V_{Ei,j,k}^{n+1}}{2}$, one can get:

$$V_{mijk}^{n+1}=V_{mijk}^{n}e^{-\frac{\Delta t}{\tau}}+\frac{1-e^{-\frac{\Delta t}{\tau}}}{2}(V_{Ei,j,k}^{n}+V_{Ei,j,k}^{n+1}) \tag{3.37}$$

Then define:

$$V_{Ei,j,k}^{n+1}=V_{Ei,j,k}^{n}+(\frac{\partial V_E}{\partial p})_{i,j,k}\delta p_{i,j,k}=V_{Ei,j,k}^{n}+\frac{V_L p_L}{(p_L+p_{fgi,j,k}^{n})^2}(p_{fgi,j,k}^{n+1}-p_{fgi,j,k}^{n}) \tag{3.38}$$

The cross flow flux can be arranged as:

$$(q_{mfg})_{i,j,k}^{n+1} = -\frac{\rho_c}{2B_g\Delta t}(1-e^{-\frac{\Delta t}{\tau}})[V_{Ei,j,k}^{\ n} + \frac{V_L p_L}{(p_L + p_{fgi,j,k}^n)^2}(p_{fgi,j,k}^{\ n+1} - p_{fgi,j,k}^{\ n})$$
$$+(V_{Ei,j,k}^{\ n} - 2V_{mi,j,k}^{\ n})] = -\frac{\rho_c}{2B_g\Delta t}(1-e^{-\frac{\Delta t}{\tau}})[\frac{V_L p_L}{(p_L + p_{fgi,j,k}^n)^2} p_{fgi,j,k}^{\ n+1} + \quad (3.39)$$
$$2(V_{Ei,j,k}^{\ n} - 2V_{mi,j,k}^{\ n}) - \frac{V_L p_L}{(p_L + p_{fgi,j,k}^n)^2} p_{fgi,j,k}^{\ n}]$$

3.4.3 Initial and boundary condition

The difference equation for initial and boundary condition can be found in **Chapter 2**.

3.4.4 Difference equation for the single branch horizontal wellbore

Difference equation for **Equation (3.27)** can be derived as:

$$0.5\Delta p_{wfi} = \frac{\rho_i}{\pi^2 D^4}[\frac{f_i}{D}(2Q_i + q_i)^2\Delta x_i + 8q_i(2Q_i + q_i)] \quad (3.40)$$

Here, $q_i = q_{gi} + q_{wi} = PID_i\frac{K_{rgi}}{\mu_{gi}}(p_{gi} - p_{wfi}) + PID_i\frac{K_{rwi}}{\mu_{wi}}(p_{wi} - p_{wfi})$, $Q_i = \sum_{j=1}^{i-1} q_j$

Then the wellbore pressure equation for each segment is shown as follows:

$$p_{wf_{i-1}} = p_{wf_i} + \frac{\rho_i}{\pi^2 D^4}[\frac{4f_i\Delta x_i}{D}Q_i^{\ 2} + (\frac{f_i\Delta x_i}{D} + 8)q_i^{\ 2} + 4(\frac{f_i\Delta x_i}{D} + 4)Q_i q_i]$$
$$+\frac{\rho_{i-1}}{\pi^2 D^4}[\frac{4f_{i-1}\Delta x_{i-1}}{D}Q_{i-1}^{\ 2} + (\frac{f_{i-1}\Delta x_{i-1}}{D} + 8)q_{i-1}^{\ 2} + 4(\frac{f_{i-1}\Delta x_{i-1}}{D} + 4)Q_{i-1}q_{i-1}] \quad (3.41)$$
$$i = 2,3,...,n$$

$$p_{wf_n} = p_{wfc} + \frac{\rho_n}{\pi^2 D^4}[\frac{4f_n\Delta x_n}{D}Q_n^{\ 2} + (\frac{f_n\Delta x_n}{D} + 8)q_n^{\ 2} + 4(\frac{f_n\Delta x_n}{D} + 4)Q_n q_n] \quad (3.42)$$

The difference equation of coupled single branch horizontal wellbore model can be got through coupling formation difference equation **Equation (3.34)** with **Equation (3.41)** and **Equation (3.42)**.

3.4.5 Difference equation for the multi-branch horizontal wellbore

Difference **Equation (3.30)**, then there is:

$$0.5\Delta p_{wfi} = \frac{\rho_i}{\pi^2 D^4}[\frac{f_i \Delta x_i}{D}(2Q_i + q_i + Q_{Ri})^2 + 8(q_i + Q_{Ri})(2Q_i + q_i + Q_{Ri})] \tag{3.43a}$$

Or

$$\begin{aligned} 0.5\Delta p_{wfi} &= \frac{\rho_i}{\pi^2 D^4}[\frac{f_i \Delta x_i}{D}(2Q_i + q_i + Q_{Ri})^2 + 8(q_i + Q_{Ri})(2Q_i + q_i + Q_{Ri}) \\ &+2Q_i(9Q_i - 4Q_{Ri}\cos\varphi)] \end{aligned} \tag{3.43b}$$

Considering that $q_i = q_{gi} + q_{wi} = PID_i \frac{K_{rgi}}{\mu_{gi}}(p_{gi} - p_{wfi}) + PID_i \frac{K_{rwi}}{\mu_{wi}}(p_{wi} - p_{wfi})$, $Q_i = \sum_{j=1}^{i-1} q_j$,

then the wellbore pressure equation of each segment can be expressed as:

$$\begin{aligned} p_{wf_{i-1}} &= p_{wf_i} + \frac{\rho_i}{\pi^2 D^4}[\frac{f_i \Delta x_i}{D}(2Q_i + q_i + Q_{Ri})^2 + 8(q_i + Q_{Ri})(2Q_i + q_i + Q_{Ri})] \\ &+ \frac{\rho_{i-1}}{\pi^2 D^4}[\frac{f_{i-1} \Delta x_{i-1}}{D}(2Q_{i-1} + q_{i-1} + Q_{Ri-1})^2 + 8(q_{i-1} + Q_{Ri-1})(2Q_{i-1} + q_{i-1} + Q_{Ri-1})] \\ &i = 2,3,...,n \end{aligned} \tag{3.44a}$$

$$\begin{aligned} p_{wf_{i-1}} &= p_{wf_i} + \frac{\rho_i}{\pi^2 D^4}[\frac{f_i \Delta x_i}{D}(2Q_i + q_i + Q_{Ri})^2 + 8(q_i + Q_{Ri})(2Q_i + q_i + Q_{Ri}) \\ &+2Q_i(9Q_i - 4Q_{Ri}\cos\varphi)] + \frac{\rho_{i-1}}{\pi^2 D^4}[\frac{f_{i-1} \Delta x_{i-1}}{D}(2Q_{i-1} + q_{i-1} + Q_{Ri-1})^2 \\ &+8(q_{i-1} + Q_{Ri-1})(2Q_{i-1} + q_{i-1} + Q_{Ri-1}) + 2Q_{i-1}(9Q_{i-1} - 4Q_{Ri-1}\cos\varphi)] \\ &i = 2,3,...,n \end{aligned} \tag{3.44b}$$

$$p_{wf_n} = p_{wfc} + \frac{\rho_n}{\pi^2 D^4}[\frac{f_n \Delta x_n}{D}(2Q_n + q_n + Q_{Rn})^2 + 8(q_n + Q_{Rn})(2Q_n + q_n + Q_{Rn})] \tag{3.45}$$

The difference equation of coupled multi-branch horizontal wellbore model consists of formation difference equation **Equation (3.34)**, **Equation (3.44)** and **Equation (3.45)**.

The two difference equations are coupled through the wellbore pressure. For the constant bottom hole pressure production external boundary condition, the wellbore pressure is known as the bottom-hole pressure; for the constant rate production condition, the wellbore pressure can be set to any arbitrarily reasonable value. By this way, the formation model can be solved using the conjugate gradient method. Firstly, the corresponding formation pressure can be got, then if take the solved formation pressure into the wellbore pressure equation, the wellbore pressure can be calculated. The newly wellbore pressure can be used in the formation pressure equation again for iteration. When the pressure difference of two adjacent nodes becomes very small, the

formation pressure and wellbore segment pressure can both be got. Finally, the saturations of gas and water can be solved using saturation equations.

3.4.6 IMPES method for the numerical model

3.4.6.1 IMPES mehod

Substituting **Equation (3.39)** into **Equation (3.34)**, rearranging there is:

$$A_{Ti,j,k}p_{fgi,j,k-1}^{n+1}+A_{Si,j,k}p_{fgi,j-1,k}^{n+1}+A_{Wi,j,k}p_{fgi-1,j,k}^{n+1}+E_{i,j,k}p_{fgi,j,k}^{n+1}+A_{Ei,j,k}p_{i+1,j,k}^{n+1}+A_{Ni,j,k}p_{fgi,j+1,k}^{n+1}+A_{Bi,j,k}p_{fgi,j,k}^{n+1}=B_{i,j,k} \tag{3.46}$$

Where:

$$A_{Ti,j,k}=B_{wi,j,k}T_{Wi,j,k-1/2}^{n}+B_{gi,j,k}T_{gi,j,k-1/2}^{n},\ A_{Bi,j,k}=B_{wi,j,k}T_{Wi,j,k+1/2}^{n}+B_{gi,j,k}T_{gi,j,k+1/2}^{n},$$

$$A_{Si,j,k}=B_{wi,j,k}T_{Wi,j-1/2,k}^{n}+B_{gi,j,k}T_{gi,j-1/2,k}^{n},\ A_{Ni,j,k}=B_{wi,j,k}T_{Wi,j+1/2,k}^{n}+B_{gi,j,k}T_{gi,j+1/2,k}^{n},$$

$$A_{Wi,j,k}=B_{wi,j,k}T_{Wi-1/2,j,k}^{n}+B_{gi,j,k}T_{gi-1/2,j,k}^{n},\ A_{Ei,j,k}=B_{wi,j,k}T_{Wi+1/2,j,k}^{n}+B_{gi,j,k}T_{gi+1/2,j,k}^{n},$$

$$E_{i,j,k}=-[A_{Ti,j,k}+A_{Bi,j,k}+A_{Si,j,k}+A_{Ni,j,k}+A_{Wi,j,k}+A_{Ei,j,k}+AQ_{mfg}^{n+1}+\frac{(\phi_f V_b C_t)^n}{\Delta t}]$$

$$B_{i,j,k}=-\frac{(\phi_f V_b C_t)^n}{\Delta t}p_{i,j,k}^{n}-W_{i,j,k}$$

$$W_{i,j,k}=B_{wi,j,k}(G_w+Q_{vw})_{i,j,k}+B_{gi,j,k}(G_g+Q_{vg}+AQ_{mfg}^{n})_{i,j,k}$$

Write the above equation in the form of matrix, there is:

$$A=\left\{\begin{array}{l} A_{T1,1,1}\ A_{S1,1,1}\ A_{W1,1,1}\ E_{1,1,1}\ A_{E1,1,1}\ A_{N1,1,1}\ \cdots\cdots\cdots\cdots \\ \quad A_{T2,2,2}\ A_{S2,2,2}\ A_{W2,2,2}\ E_{2,2,2}\ A_{E2,2,2}\ A_{N2,2,2}\ A_{B2,2,2}\cdots\cdots\cdots\cdots \\ \qquad\qquad \cdots\cdots \\ \qquad\qquad A_{Ti,j,k}\ A_{Si,j,k}\ A_{Wi,j,k}\ E_{i,j,k}\ A_{Ei,j,k}\ A_{Ni,j,k}\ A_{Bi,j,k}\cdots\cdots\cdots \\ \qquad\qquad \cdots\cdots \\ \qquad\qquad\qquad A_{Sn,n,n}\ A_{Wn,n,n}\ E_{n,n,n}\ A_{En,n,n}\ A_{Nn,n,n}\ A_{Bn,n,n} \end{array}\right\}$$

This formation difference model coupled with **Equation (3.41)** and **Equation (3.42)**, or **Equation (3.44)** and **Equation (3.45)** can form the coupled single branch or multi-bran -ch horizontal wellbore difference model. The threshold pressure gradient and the gas

slippage effects are both considered in the models, and the permeability model that indicates the matrix shrinkage effect is also integrated into the coupled models.

3.4.6.2 Preconditioning conjugate method

Obviously, a seven point diagonal, sparse band-structured block coefficient matrix is finally formed for each model. Iteration method is usually used for such big sparse equations. Here, the preconditioning conjugate method is used to solve the problem. The reason for choosing this method is: (1) no need to choose the iterative factor; (2) fast convergence; (3) high precision; (4) good adaptability. So it is very good for the complex numerical reservoir simulation. The process of this method is as follows:

(1) Do LDU decomposition for matrix A, that is: $A = LDU - R$.

Where: L, D, U is the lower triangular matrix, diagonal matrix, upper triangular matrix, R is the error matrix.

(2) Define $M = LDU$, take the matrix M as preconditioning matrix for matrix A, using the preconditioning conjugate gradient method (PCG method) to solve the problem:

Get any $x^0 \in R^n$, define $r^{(0)} = b - Ax^{(0)}, z^{(0)} = M^{-1}r^{(0)}, p^{(0)} = z^{(0)}$. For k=0, 1, 2…

$$\alpha_k = \frac{(z^{(k)}, r^{(k)})}{(p^{(k)}, Ap^{(k)})};$$
$$x^{(k+1)} = x^{(k)} + \alpha_k p^{(k)};$$
$$r^{(k+1)} = r^{(k)} - \alpha_k Ap^{(k)};$$
$$z^{(k+1)} = M^{-1}r^{(k+1)};$$
$$\beta_k = \frac{(z^{(k+1)}, r^{(k+1)})}{(z^{(k)}, r^{(k)})};$$
$$p^{(k+1)} = z^{(k+1)} + \beta_k p^{(k)}.$$

3.4.6.3 Saturation solution

The gas and water saturation in the cleat system have to be solved. In this chapter, water saturation is solved through the explicit method, its difference equation can be shown as:

$$\Delta T_w^n \Delta p_w^{n+1} + G_w + Q_{vw} = \frac{1}{\Delta t}[(\frac{\phi_f V_b S_w}{B_w})_{i,j,k}^{n+1} - (\frac{\phi_f V_b S_w}{B_w})_{i,j,k}^{n+1}] \quad (3.47)$$

Thus, the following formula for solving gas and water saturation can be derived:

$$s_{wi,j,k}^{n+1} = (\frac{B_w}{\phi_f V_b})_{i,j,k}^{n+1}[\Delta t(\Delta T_w^n \Delta p_{fg}^{n+1} + G_w + Q_{vw}) + (\frac{\phi_f V_b s_w}{B_w})_{i,j,k}^{n}] \tag{3.48}$$

$$s_{gi,j,k}^{n+1} = 1 - s_{wi,j,k}^{n+1} \tag{3.49}$$

3.5 Grid Partitions and parameter processing

3.5.1 Grid partitions

The fact that there exists big difference between the multi-branch horizontal wellbore and single branch horizontal wellbore: the multi-branch horizontal well exist an angle among different branches. And it involves calculation the length of horizontal branch in the grid. Here, in order to facilitate the calculation, the following method is adopted: adjusting the length of the grid to make the branch with angle just across the grid intersection in the grid partition, and the heel of the branch is in the centre of the grid. The schematic diagram of grid partition for the single branch (the branches are deleted) and multi-branch horizontal well is described as follows (**Figure 3.6**):

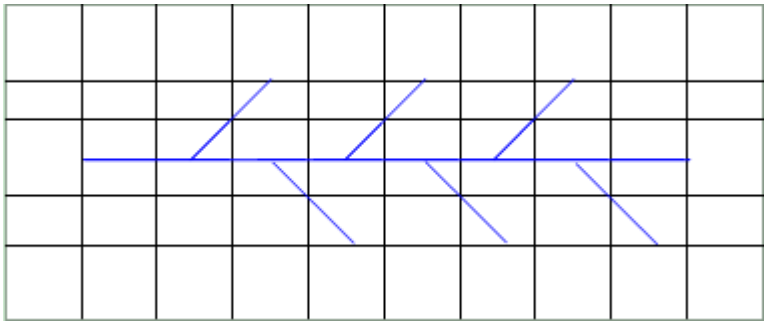

Figure 3.6 The sketch map of grid generation with horizontal well

3.5.2 Gas compression factor

Using compression factor to calculate the natural gas compression is proposed in 1990 (**Abou-Kassem, J.H., et al., 1990[149]**). The detailed method is as follows:

ρ_r and $\left(\frac{p_r}{\partial \rho_r}\right)_{T_r}$ are solved using the Newton iterative method in the process of solving natural compression factor Z. Where p_r and t_r are the gas relatively pressure and gas relatively temperature respectively: $p_r = p / p_c$, $t_r = t / t_c$. p_c and t_c are the critical pressure and critical temperature for the gas.

$$\left(\frac{\partial p_r}{\partial \rho_r}\right)_{T_r} = \{T_r + 2\left(C_0\rho_r\right) + 3\left(C_2\rho_r^2\right) + 6\left(C_3\rho_r^5\right) + \left(C_4\rho_r^2\right) \left[3 + 3\left(C_5\rho_r^2\right) - 2\left(C_5\rho_r^2\right)^2\right]\exp\left[-\left(C_5\rho_r^2\right)\right]\}\Big/ Z_c \tag{3.50}$$

According to the definition of c_r, c_r can be expressed mathematically as:

$$c_r = \frac{1}{\rho_r}\left(\frac{\partial \rho_r}{\partial p_r}\right)_{t_r} \tag{3.51}$$

In addition, $c_r = cp_c$, thus the gas compression factor c can be solved. What is more, $C_0 - C_5$ are the experimental coefficients.

3.5.3 Production index for multi-branch wellbore model

The multi-branch horizontal wellbore structure is different from the vertical well and the basic horizontal well, for there is an angle between the main stream and branch segment. Thus the exploitation of multi-branch horizontal well is much more different from others. The production index for each segment can be calculated as follows:

$$PI = 2\pi\frac{K_i L_i}{\ln\frac{r_b}{r_w} + S} \tag{3.52}$$

Where:

$K_i = \left(K_x K_y K_z\right)^{1/3}$; $L_i = \sqrt{L_x^2 + L_y^2}$, $L_x = L\sqrt{K_i / K_x}\cos\omega$, $L_y = L\sqrt{K_i / K_y}\sin\omega$,

$r_b = \sqrt{r_{bx}^2 + r_{by}^2}$, $r_{bx} = R_{bx}\cos\omega$, $r_{by} = R_{by}\sin\omega$,

$R_{bx} = 0.14\sqrt{\left(K_i / K_y\right)\Delta y^2 + \left(K_i / K_z\right)\Delta z^2}$, $R_{by} = 0.14\sqrt{\left(K_i / K_x\right)\Delta x^2 + \left(K_i / K_z\right)\Delta z^2}$;

$r_w = \sqrt{r_{wx}^2 + r_{wy}^2}$, $r_{wx} = R_{wx}\cos\omega$, $r_{wy} = R_{wy}\sin\omega$; $R_{wx} = \frac{R_w}{2}\left(\sqrt{K_i / K_y} + \sqrt{K_i / K_z}\right)$,

$R_{wy} = \frac{R_w}{2}\left(\sqrt{K_i / K_x} + \sqrt{K_i / K_z}\right)$.

3.5.4 Threshold pressure gradient and gas slippage effects

Threshold pressure gradient and gas slippage effects equations are differenced using the upstream regulations, the details can be found in **Chapter 2**.

3.6 Synthetic data analysis

Three case studies are designed in order to study the effect of the parameters on the production rate and pressure changes. The simulation parameters for the coupled CBM reservoir are shown in **Table 3.1**, and the PVT parameters used for the simulation are shown in **Table 3.2**. The layouts of the single branch horizontal wellbore and multi-branch horizontal wellbore that are used for simulation are presented in this study (**Figure 3.7** and **Figure 3.8**).

Coal depth ft	457.2	Coal thickness ft	7.0
Initial reservoir pressure psia	10342	Initial water saturation fraction	0.92
Fracture porosity fraction	0.02	Fracture permeability md	3.0
Water phase viscosity cp	0.58	Initial gas content Mscf/ft^3	10.0
Langmuir volume ft^3	20.0	Langmuir pressure psia	4.0
Adsorption time day	35.0	Coal density lb/ ft^3	1.3
Gas density lb / ft^3	0.5768	Water density lb / ft^3	1006.0
Well BHP psia	5000	Coal temperature K	328
ν	0.39	E	1.24E5
K/M	0.76	M/E	2.0
Main stream wellbore radius ft	0.26	Branch wellbore radius ft	0.16

Table 3.1 Simulation parameters of CBM reservoirs

Pressure (psia)	Viscosity (cp)	Volume coefficient
100	0.00858	1.01932
200	0.00860	0.50806
400	0.00862	0.25273
600	0.00864	0.16776
800	0.00867	0.12528
1000	0.00886	0.09979
2500	0.00965	0.03862
4000	0.01010	0.02335
6500	0.01020	0.01361
8000	0.01024	0.01072
9000	0.01030	0.00935
20000	0.01058	0.00401

Table 3.2 PVT Character parameters for the models

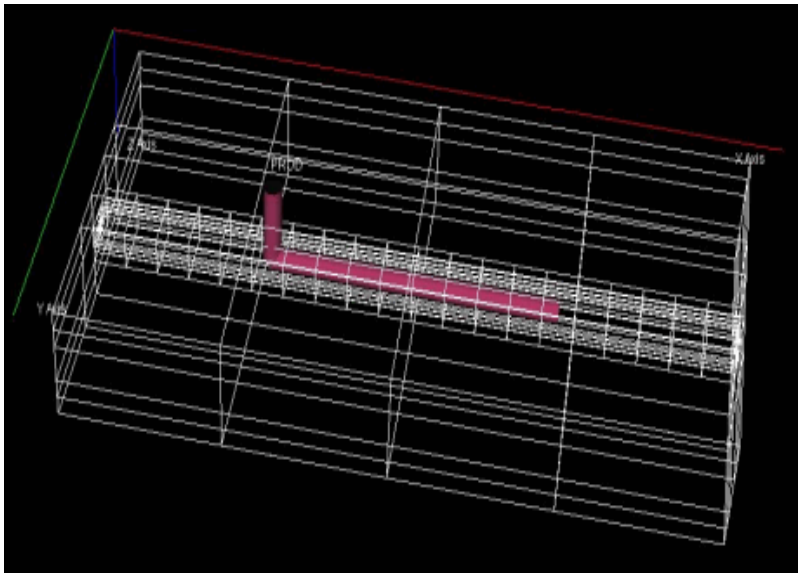

Figure 3.7 Layout of horizontal well model

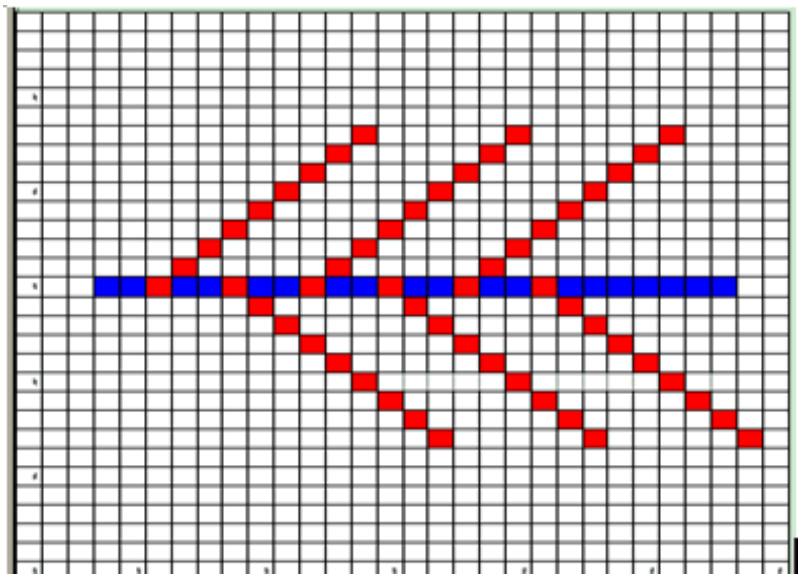

Figure 3.8 Layout of multi-branch horizontal wellbore model

3.6.1 Case study 1: Comparison

In order to study the advantage of the new models, the comparison of the results comes from the multi-branch horizontal well model, single branch horizontal well model and vertical well model is made. Results showed that the multi-branch horizontal model can largely enhance the gas and water production rate.

The average pressure changes with time under multi-branch horizontal well production, horizontal well production and vertical well production is illustrated (**Figure 3.9**). There obviously exists two parts of the pressure changes, the first part pressure decrease

and second part pressure drops. In addition, it is also easy to see that the first part pressure decrease is much sharply than the second part, owning to the fact that much of the water is pumped out initially and combined with gas production. Then after finishing this period, the speed of the gas production rate becomes much slower, so this is why the pressure drop becomes more gently. What is more, one can see from this figure that the sharper pressure decreasing time of multi-branch well model is longer than both horizontal well and vertical well model, which is attributed to its enhanced gas and water production rate.

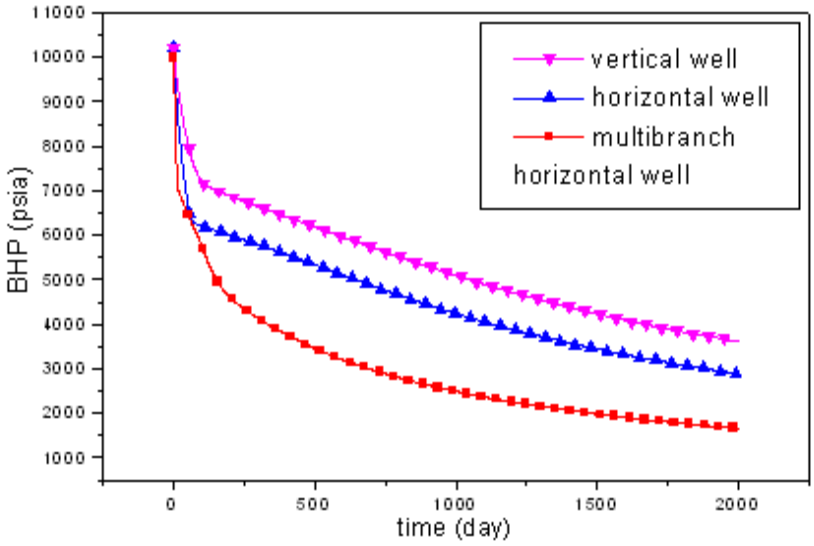

Figure 3.9 Comparison of bottom-hole pressure

The comparison of daily gas production rate among the results of multi-branch horizontal well model, horizontal well model and vertical well model is studied (**Figure 3.10**). The break through time is the earliest from multi-branch horizontal well model result, and also the daily gas production rate is the largest compared with the other cases. From the figure one can also notice that breakthrough of the vertical well model happens after approximately 800 days production; while, the daily gas rate for horizontal well begins to break through after only about 200 days production; however, the daily gas production only takes about 20 days to reach at the break through for multi-branch horizontal well model case. Additionally, the maximal daily gas rate of multi-branch horizontal well model is nearly 90000 Mscf/day, approximately 77% higher than the result from horizontal well model, and over 88% than the result from vertical well model.

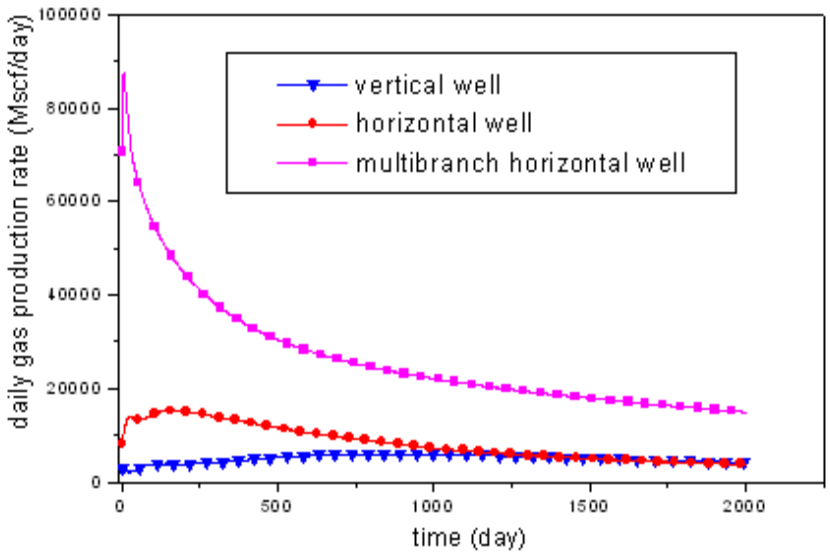

Figure 3.10 Comparison of daily gas production rate

The daily water production rate comes from the three models is shown in **Figure 3.11**. From this figure it is easily to make the conclusion that the daily water rate is the largest for the multi-branch well model compared to the others. Moreover, the water production time for multi-branch horizontal well model is around 500 days before the water tends to constant, while it only takes about 250 days and 20 days for the horizontal well model and vertical well model respectively. The final constant water rate for vertical well and horizontal well model is nearly the same, is about 5 Mscf/day.

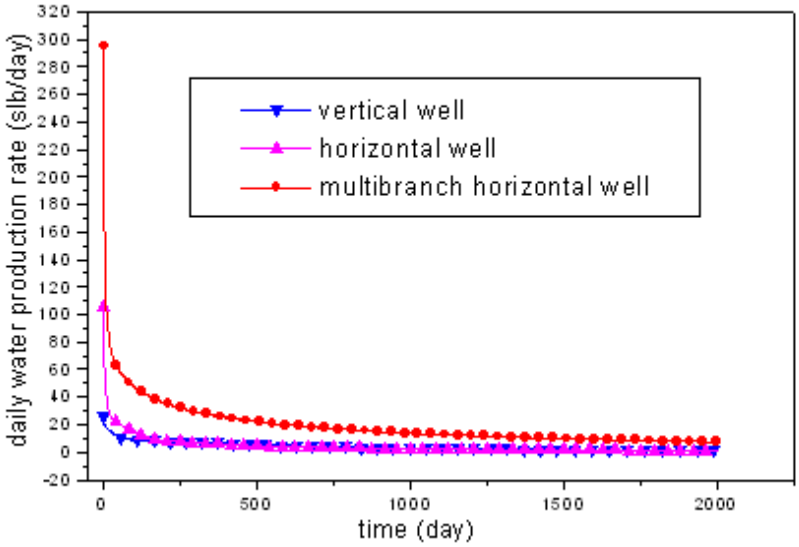

Figure 3.11 Comparison of daily water production rate

However, it is around 20 Mscf/day for the multi-branch horizontal well model, which is much higher than the other two models.

The total gas rate for the vertical well model can reach nearly 0.8×10^7 Mscf after 2000 days production (**Figure 3.12**), and it reaches at 1.5×10^7 Mscf at the end of 2000 days production time for the horizontal well model, while, it can be largely enhanced for the multi-branch horizontal well model, which is approximately 5.4×10^7 Mscf, nearly 72% enhancement than horizontal well model, 85% production rate improvement than vertical well model. So it can be easily concluded that although drilling the multi-branch horizontal well is much more expensive than the vertical wells, the profit comes from the production enhancement can offset the extra drilling fees. Thus, drilling multi-branch horizontal well has great importance in the CBM production industry.

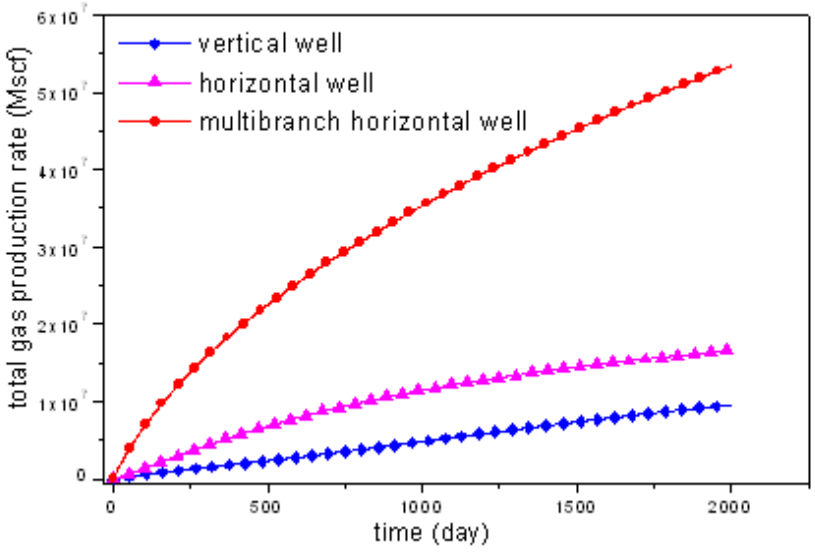

Figure 3.12 Comparison of total gas production rate

The trend of total water production rate is a little different from the total gas production rate (**Figure 3.13**). The total water production rate of vertical well and horizontal well converges into one point after 2000 days production, the corresponding rate is about 0.75×10^4 Mscf. While the water production rate for the multi-branch model can be nearly 3.8×10^4 Mscf after 2000 days production, 80% percent higher than the vertical well and horizontal well model. This is because the branches in the multi-branch model give the gas and water path to flow into the cleat system.

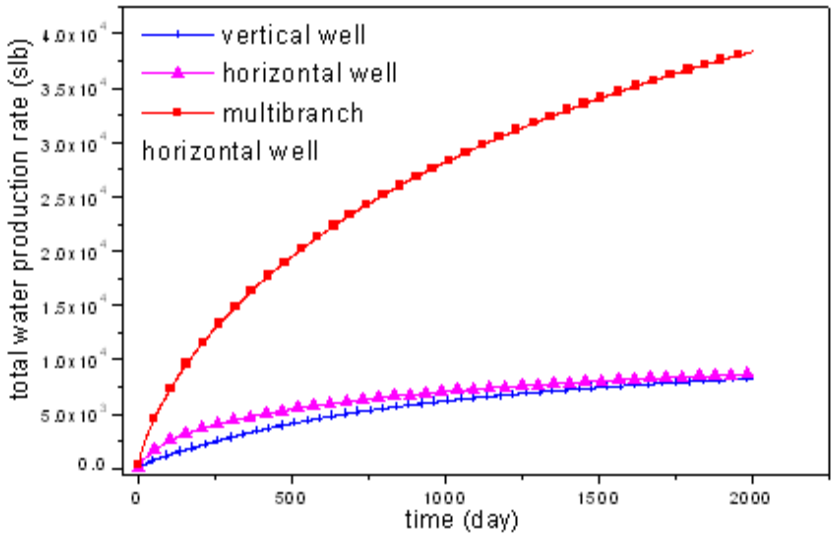

Figure 3.13 Comparison of total water production rate

In conclusion, the changes of water, gas production rate as well as the bottom-hole pressure indicate that the coupled multi-branch horizontal wellbore model can largely enhance the gas and water production rate, which validates the significance of developing the comprehensive coupled multi-branch horizontal well model.

3.6.2 Case study 2: Single branch model

3.6.2.1 Gas slippage effect

Gas slippage effect is studied in this case study, and the threshold pressure gradient is ignored here. The results show that the gas slippage effect can have great influence on the gas and water production: when the gas slippage factor is taken into consideration, the reservoir development degree is better than the case if the gas slippage factor is ignored, which implies that there will be great error in the forecasting of gas and water production rate if it is ignored.

The gas slippage factor $b(s_w)$ is determined by β_1 and β_2 as can be seen in **Chapter 2**, so two cases are chosen for the sensitive analysis.

(1) Choose different β_2, and keep the other parameter invariant (where $\beta_1 = 81$, lower critical Reynolds number $R_{ecd} = 0.0001$). The corresponding gas slippage factor $b(s_w)$ for different β_2 in the CBM reservoir is as follows:

$$\begin{cases} b(s_w) = 86.84786 & \beta_2 = 0.94 \\ b(s_w) = 220.2326 & \beta_2 = 0.47 \\ b(s_w) = 437.6087 & \beta_2 = 0.123 \end{cases}$$

(2) Choose different β_1, and keep the other parameter as constant (where $\beta_2 = 0.47$, lower critical Reynolds number, $R_{ecd} = 0.0001$). The gas slippage factor $b(s_w)$ with different β_1 in the CBM reservoir is as follows:

$$\begin{cases} b(s_w) = 57.09733 & \beta_1 = 21 \\ b(s_w) = 220.2326 & \beta_1 = 81 \\ b(s_w) = 437.6083 & \beta_1 = 161 \end{cases}$$

The daily gas production rate is the lowest when the gas slippage factor is not taken into consideration (**Figure 3.14**). As known, the gas slippage factor increases with the decreasing of β_2. So it is not strange to see that the daily gas production rate is much higher when $\beta_2 = 0.156$ than that when $\beta_2 = 0.32$, but still higher than the case that the gas slippage effect is ignored. It is also obvious from the figure that it is not always the lower the gas slippage factor β_2 the better the well production status. For example, the gas production rate maximum is 1.05E5 Mscf/day when $\beta_2 = 0.289$, and it gradually reaches its maximum and then slowly decreases which is the more analogous to the act-

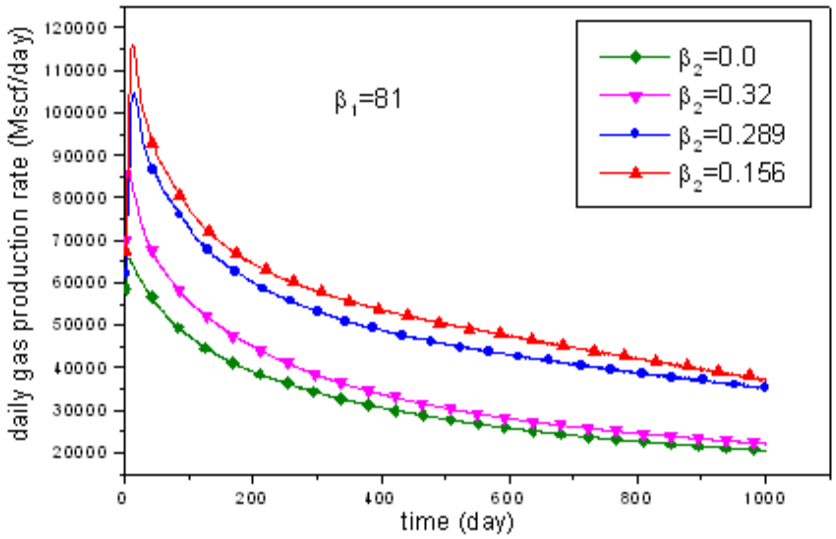

Figure 3.14 Daily gas production rate changes with β_2

ual field data production than the case when $\beta_2 = 0.32$ and $\beta_2 = 0.156$. Thus $\beta_2 = 0.289$ is the best parameter for the field data application.

The daily gas production under the impact of β_1 is studied (**Figure 3.15**). The gas production rate maximum is about 85000 Mscf/day when the gas slippage factor parameter $\beta_1 = 0.0$. And the gas production maximum can reach 1.05E5 Mscf/day when $\beta_1 = 81.0$, nearly 19% higher than the case when the gas slippage factor is ignored. And it can be nearly 1.15E5 Mscf/day when $\beta_1 = 121.0$, approximately 10% enhancement than the case of $\beta_1 = 81.0$, about 35% higher than the fact that gas slippage is not considered. While If β_1 is equal to 161.0, the daily gas production maximum is the highest, a little less than 1.25E5 Mscf/day, and the breakthrough time is the latest to get compared to the other cases. From this result, it is clearly to get the conclusion that $\beta_1 = 161.0$ should be chosen for further study.

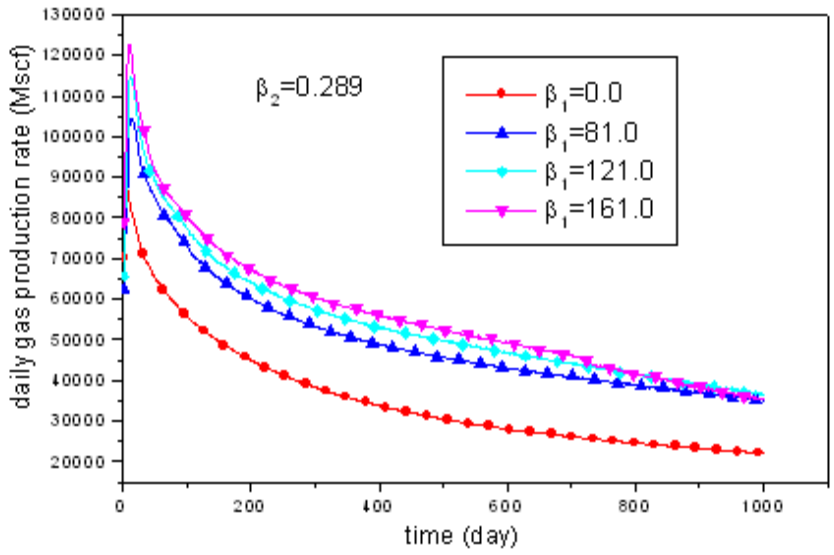

Figure 3.15 Daily gas production rate changes with β_1

Figure 3.16 illustrates the daily water production rate changes with the gas slippage factor β_2. It is easily to see that the gas slippage effect on the water production rate mainly happens at the initial stage and middle stage. Thus the daily water rate shows great improvement variation during these stages. When the gas slippage factor β_2 is equal to 0.156, the daily water production rate is nearly 400 Mscf/day before

production, while if $\beta_2 = 0.0$, it can only be a little more than 130 Mscf/day. The daily water production rate drops sharply then for $\beta_2 = 0.0$, but it decreases slowly with the production time going on for $\beta_2 = 0.156$, and keeps at the highest constant level compared to the other cases with different β_2 values. In addition, they all nearly converge into one point after 1000 days' production. The similar trend can be found in

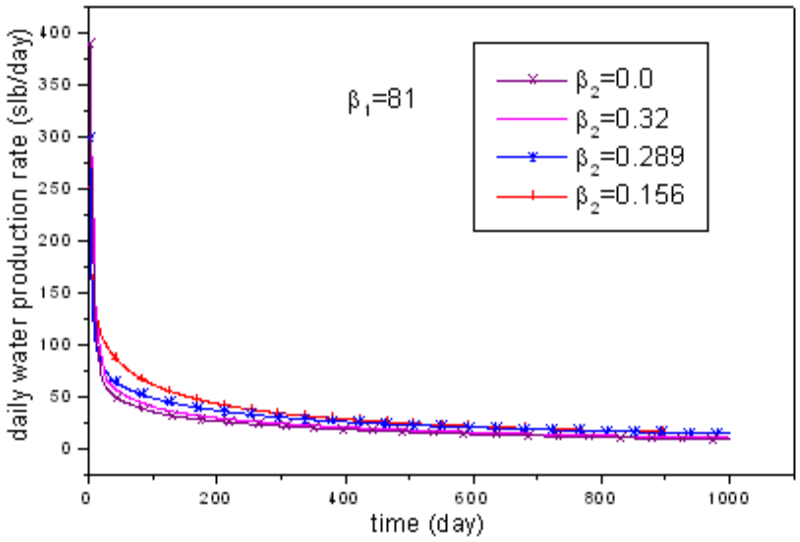

Figure 3.16 Daily water production rate changes with β_2

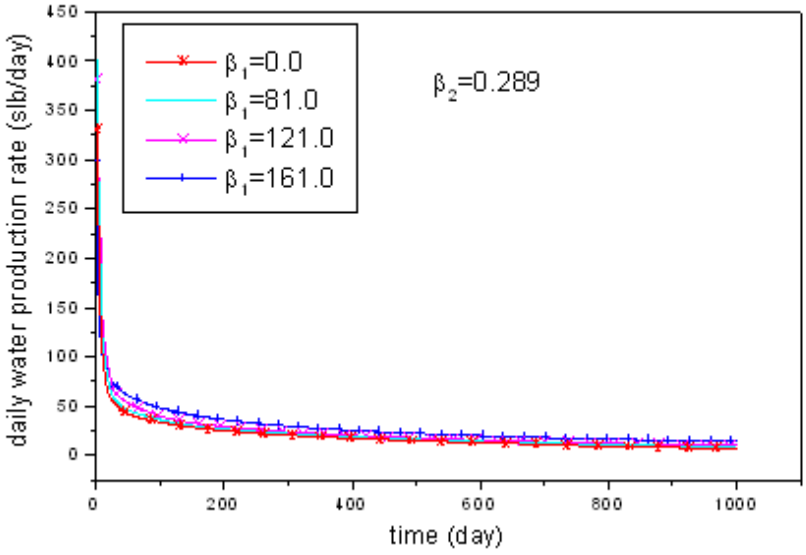

Figure 3.17 Daily water production rate changes with β_1

Figure 3.17 which shows the daily water production rate changes with β_1. The only difference lies in that the water production rate increases with β_1 and drops with β_2. The reason is that the gas slippage factor rises with the increasing of β_1 and decreases with the rising of β_2.

The total gas production rate changes under the impact of gas slippage factor β_1 are also presented (**Figure 3.18**). Obviously, the total gas rate is much lower when the gas slippage effect is ignored in the model than the case when the gas slippage effect is taken into consideration. The total gas production rate can reach around 3.75E7 Mscf after 1000 days production if $\beta_1 = 0$, however, the total gas production rate is about 5.0E7 Mscf, 5.5E7 Mscf and 5.70E7 Mscf if the $\beta_1 = 81,121,161$ respectively after 1000 days production, can be 52% improvement than the case when if $\beta_1 = 0$.

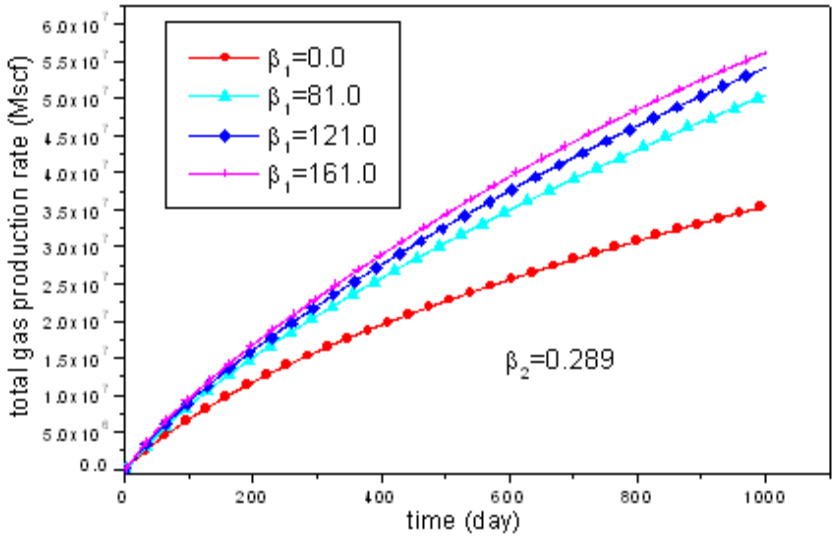

Figure 3.18 Total gas production rate changes with β_1

While the total gas production rate changes a little bit different under the impact of β_2, as shown in **Figure 3.19**, which is caused by the value of the β_2. The total gas rate variation are similar when β_2 set at zero (no gas slippage effect considered) and 0.32 or $\beta_2 = 0.289$ and $\beta_2 = 0.156$. In addition, the total gas rate increases with the decreases of β_2, and it has the highest value when $\beta_2 = 0.156$. This indicates that the value of β_2 should be better controlled between 0.156 and 0.289, because the total gas

production rate can be obviously distinguished between considering the gas slippage effect and ignoring the gas slippage effect. This figure also indicates the importance of considering the gas slippage effect. Otherwise, the total gas rate will be underestimated.

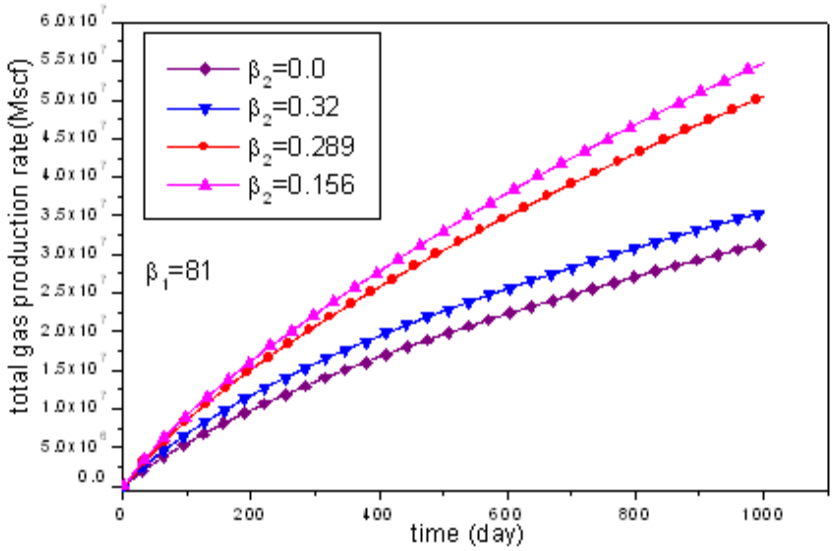

Figure 3.19 Total gas production rate changes with β_2

Obviously, the total water rate begins to be the highest after about 200 days' production with β_1 set at 161.0 among the other cases (**Figure 3.20**). Moreover, the total water production rate can be approximately 2.8E4 Mscf after 1000 days' production with β_1

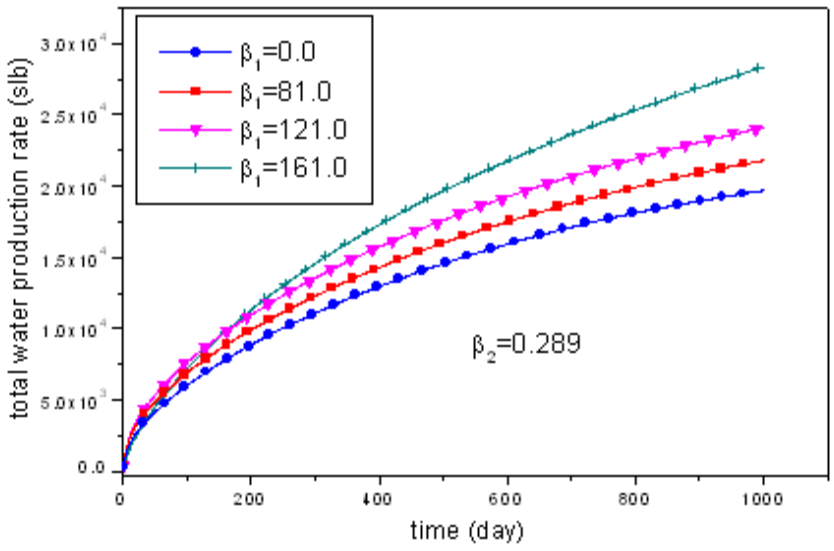

Figure 3.20 Total water production rate changes with β_1

$=161.0$, while it can only be 1.8E4 Mscf for $\beta_1 = 0.0$, decreases totally 8000 Mscf. This means that it increases with the rising of β_1, which means the total water rate rises with increasing of the gas slippage factor. The effect of gas slippage factor β_2 on the total water production rate is similar with β_1 (**Figure 3.21**), the only difference is that the total water production rate begins to be highest with $\beta_1 = 0.156$ among the other curves in the figure after only about 140 days' production. In a word, the total water production rate increases with rising of the gas slippage effect, which is attributed to the enhanced cleat permeability due to this effect.

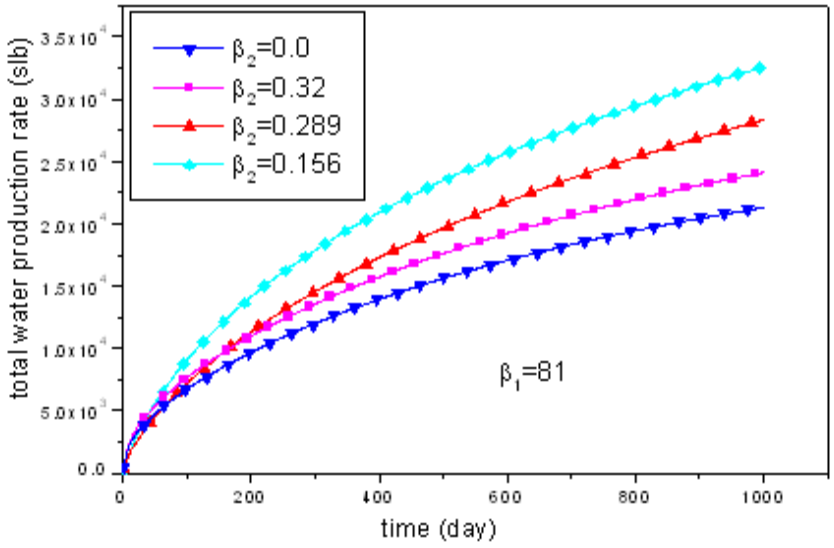

Figure 3.21 Total water production rate changes with β_2

3.6.2.2 Gas threshold pressure gradient

The variation of bottom-hole pressure under the impact of gas threshold pressure gradient parameter α_2 is presented in **Figure 3.22**. As can be seen from the figure, the initial pressure is about 3550 psia for $\alpha_2 = 0.8$, then the bottom-hole pressure decreases gradually as the gas and water produced out, and the pressure is about 1000 psia after about 2000 days simulation. If the gas threshold pressure gradient is ignored, the bottom-hole pressure drops quickly from 1900 psia tp 800 psia, this is because the threshold pressure gradient can hinder the gas and water production rate. Comparatively speaking, the pressure changes slowly if the threshold pressure gradient is considered. In addition, the higher the threshold pressure gradient, the more difficult

for the gas and water to overcome, thus this is the reason why the bottom-hole pressure changes the slowest with the highest threshold pressure gradient parameter α_2.

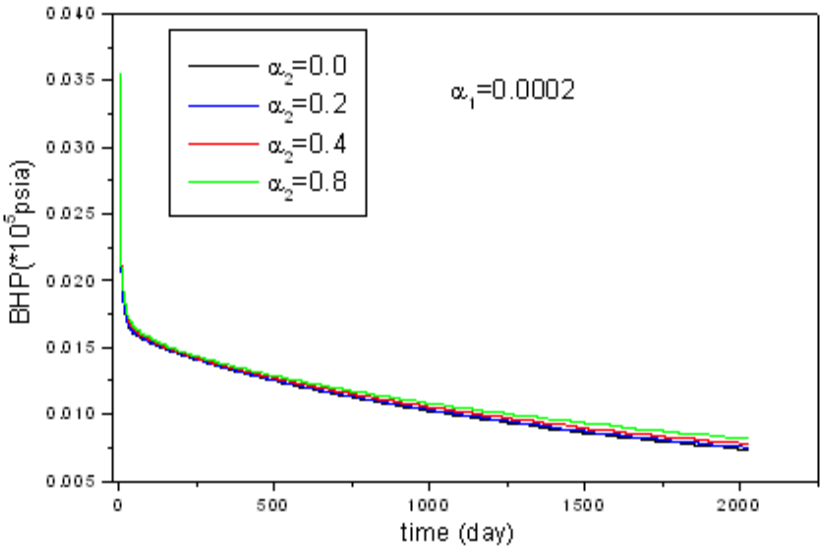

Figure 3.22 Bottom-hole pressure changes with α_2

The effect of gas threshold pressure gradient parameter α_2 on the daily gas production rate is given in **Figure 3.23**. The gas threshold pressure gradient has little effect on the initial and middle stage for the daily gas production rate according to the parameter cho

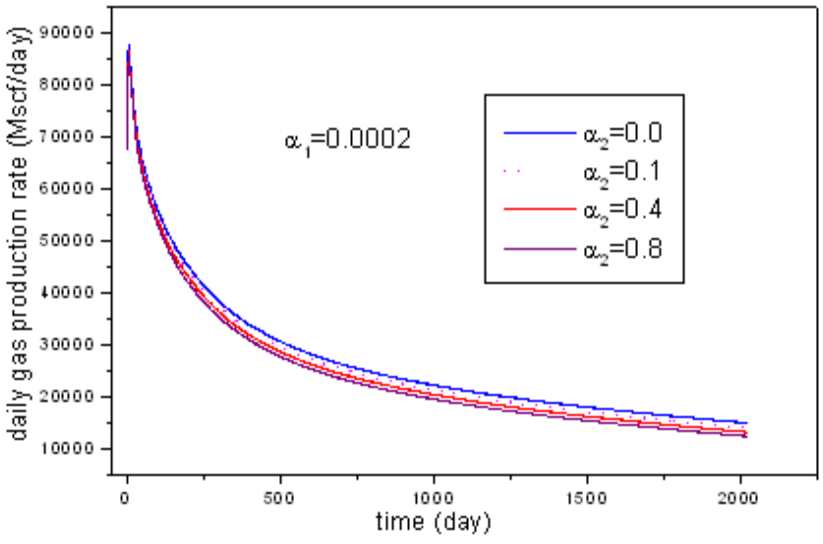

Figure 3.23 Daily gas production rate changes with α_2

-sen in this work. And the daily gas production rate with α_2 equal to 0.8 is smaller than $\alpha_2 = 0.4, \alpha_2 = 0.1$ and $\alpha_2 = 0.0$ (gas threshold pressure gradient is not taken into consideration) during the late stage. This means that the daily gas production rate decreases with increasing of the α_2. The similar pattern can be seen in **Figure 3.24**, which shows the total gas production rate changes under the effect of gas threshold pressure gradient.

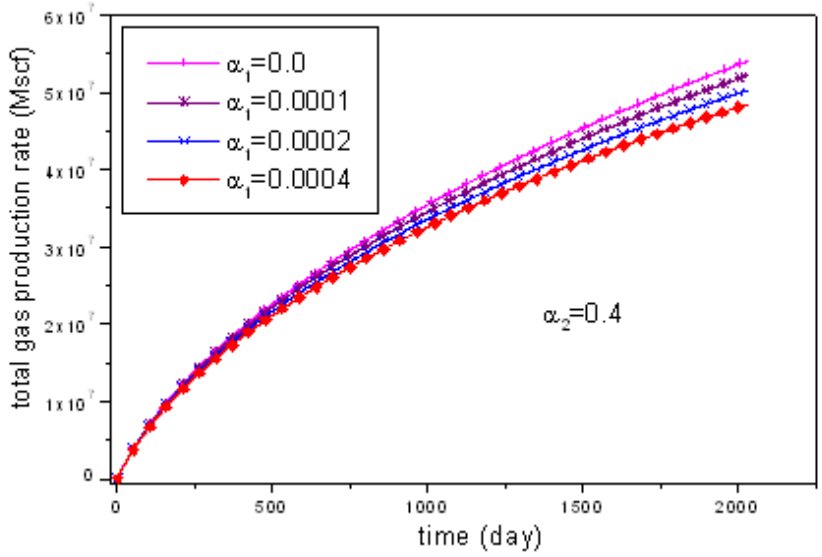

Figure 3.24 Total gas production rate changes with α_1

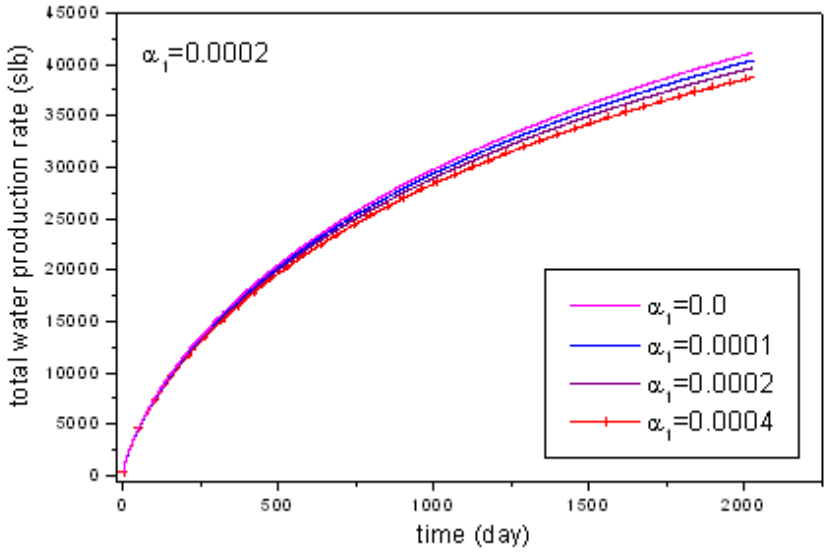

Figure 3.25 Total water production rate changes with α_1

Moreover, according to the simulation results, the total water production rate also increases with the rising of gas threshold pressure gradient, as shown in **Figure 3.25**, which means that the gas threshold pressure gradient has the same effect on the water production rate.

Because that the water production rate gradually decreases with the simulation time, nearly no production during the late stage, and the gas production dominates the late stage, thus it can explain the bottom-hole pressure changes in **Figure 3.22**.

3.6.2.3 Water threshold pressure gradient

The effect of water threshold pressure gradient on the gas, water production rate and average pressure is studied in this period. The water threshold pressure gradient is determined by α_3 and α_4, and it increases with α_3 and α_4.

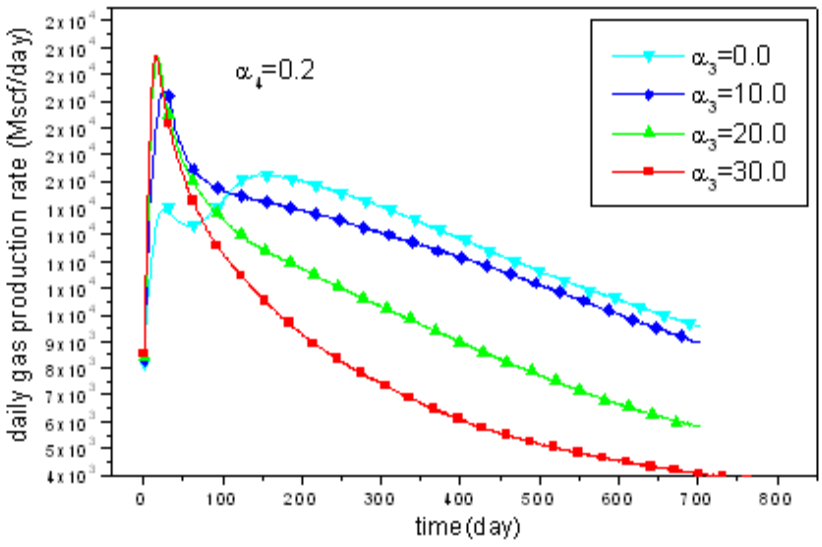

Figure 3.26 The effect of α_3 on the daily gas production rate

Two cases are considered for this purpose, firstly, set α_4 as constant, α_3=10.0, 20.0, 30.0 respectively; secondly, set α_3=10.0 as constant, α_4=0.2, 0.6, 0.8, 1.0 respectively. In addition, when α_3=0, α_4 is also equal to zero (means no threshold pressure gradient is considered).

As can be seen from **Figure 3.26**, if the threshold pressure gradient is ignored, gas production rate is the lowest before the daily gas production rate reaches its maximum, and it is the latest to get its gas production maximum. In addition, it rises with the

increasing of α_3. However, the gas production rate began to decrease with the rising of α_3 after reaching at the maximal daily gas production rate.

As known from **Figure 3.27**, the total gas production rate can reach at a maximal value of 9.0E6 Mscf after 700 days production, while it can only reach a little more than 5.0E6 when α_3=30.0. This indicates that the total gas production rate decreases with the increasing of α_3.

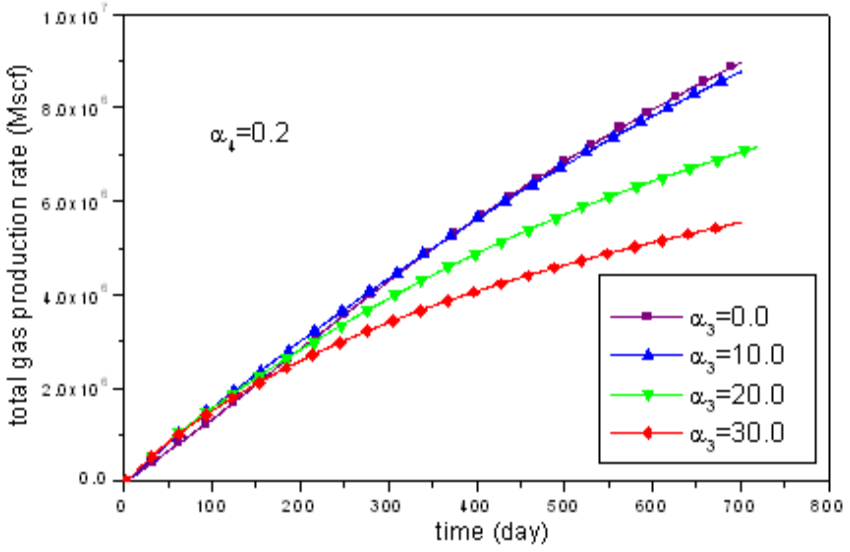

Figure 3.27 The effect of α_3 on the total gas production rate

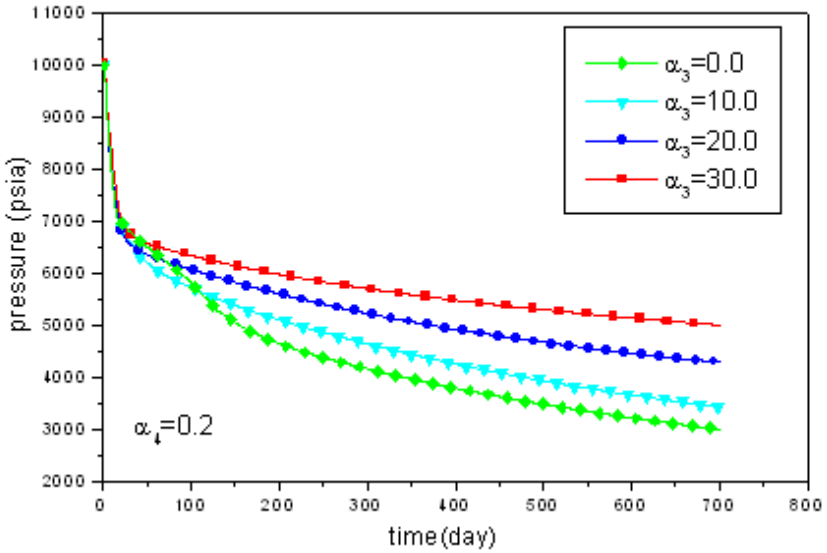

Figure 3.28 The effect of α_3 on the average pressure

The average pressure nearly converges into one point in the initial stage, and after that, average pressure becomes the lowest when the threshold pressure gradient is ignored, which is caused by the large gas production rate (**Figure 3.28**). Thus it can conclude that the average pressure increases with the rising value of α_3 (water threshold pressure increases with α_3).

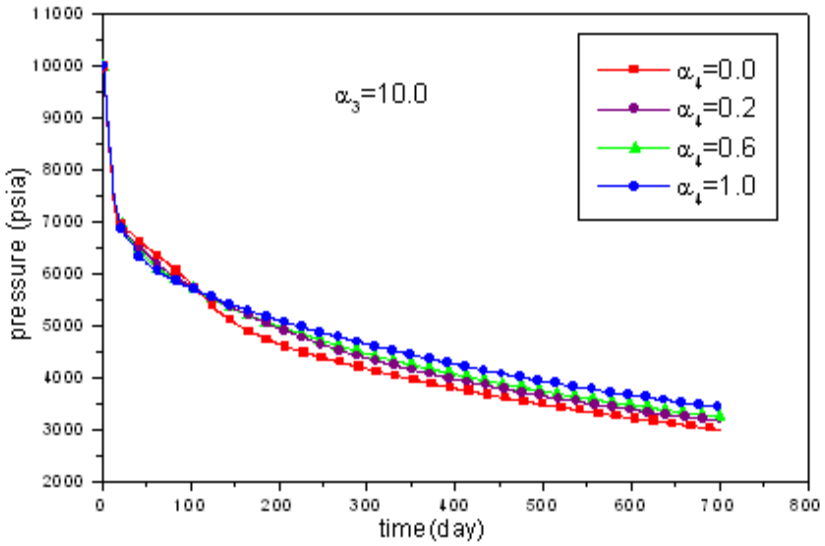

Figure 3.29 The effect of α_4 on the average pressure

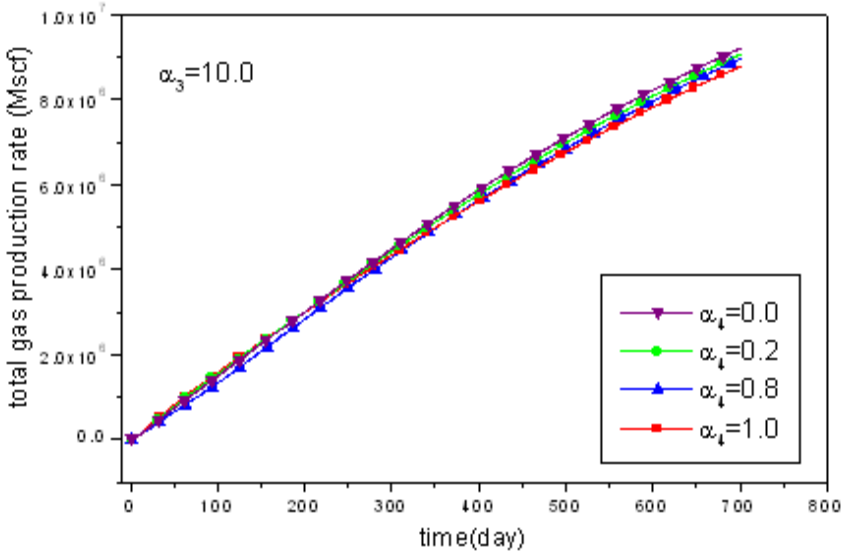

Figure 3.30 The effect of α_4 on the total gas production rate

The average pressure converges into one point initially, and it gradually decreases with time going on (**Figure 3.29**). What is more, it decreases with the increasing of α_4 for the first 100 days production, while this trend is reversed then, which is caused by the decreased gas and water production rate due to the water threshold pressure gradient.

Similar principle, it can be seen that the total gas production rate is the highest when $\alpha_4 = 0.0$ compared with the case when $\alpha_4 = 0.2, 0.8, 1.0$. In addition, it decreases with the increasing of α_4 (**Figure 3.30**).

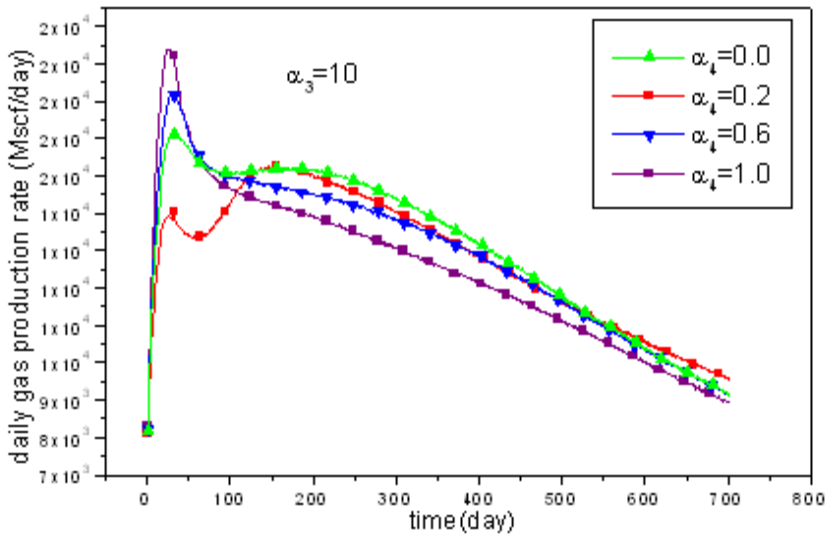

Figure 3.31 The effect of α_4 on the daily gas production rate

Figure 3.31 gives the daily gas production rate changes with water threshold pressure gradient α_4. When the water threshold pressure is ignored, daily gas production rate is the highest initially, and it is the latest to get its gas production maximum. Also, it is easy to see that it decreases with the increasing of α_4 during the late and middle stage, the higher of α_4, the lower of the daily gas production. This is because the water threshold pressure gradient can hinder the production of gas.

3.6.3 Case study 3: Multi-branch model

3.6.3.1 The Langmuir pressure and Langmuir volume effect

The effect of Langmuir pressure and Langmuir volume on the gas, water production rate is studied here.

The effect of Langmuir pressure on the daily gas production rate is presented (**Figure 3.32**). The daily gas production rate increases with the Langmuir pressure, this is caused by the higher desorption rate with bigger Langmuir pressure. But it has small impact on the daily gas production breakthrough time.

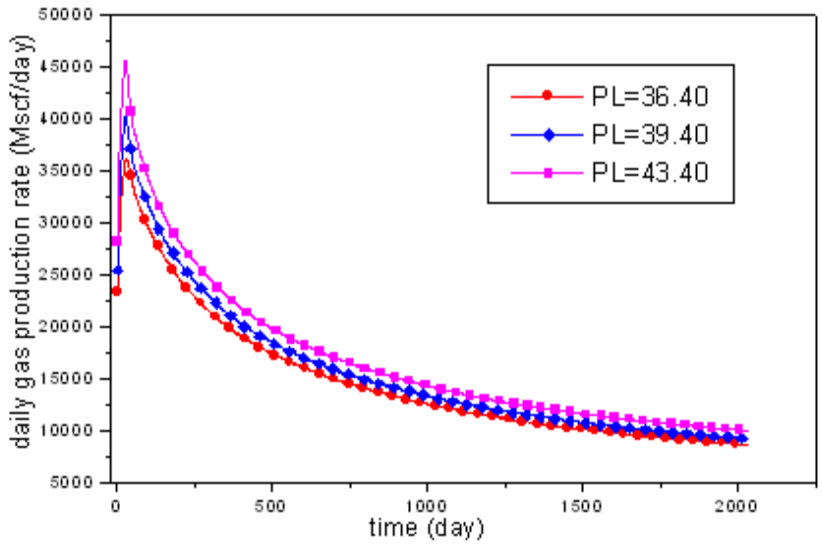

Figure 3.32 Daily gas production rate changes with Langmuir pressure

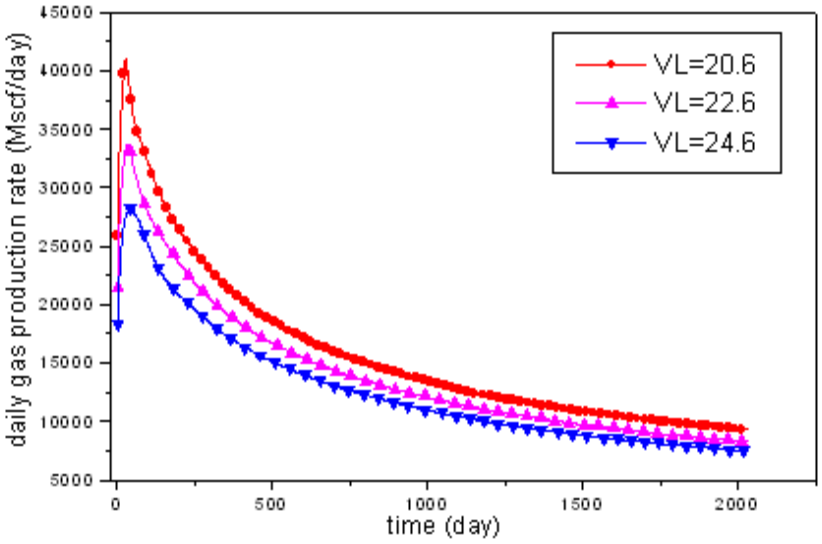

Figure 3.33 Daily gas production rate changes with Langmuir volume

The impact of Langmuir volume on the daily gas production rate is much bigger than Langmuir pressure, as shown in **Figure 3.33**. However, the daily gas production rate decreases with Langmuir volume, this is attributed to the lower desorption rate with

bigger Langmuir volume. Langmuir pressure and Langmuir volume have the similar effect on the total gas production rate, as shown in **Figure 3.34** and **Figure 3.35**.

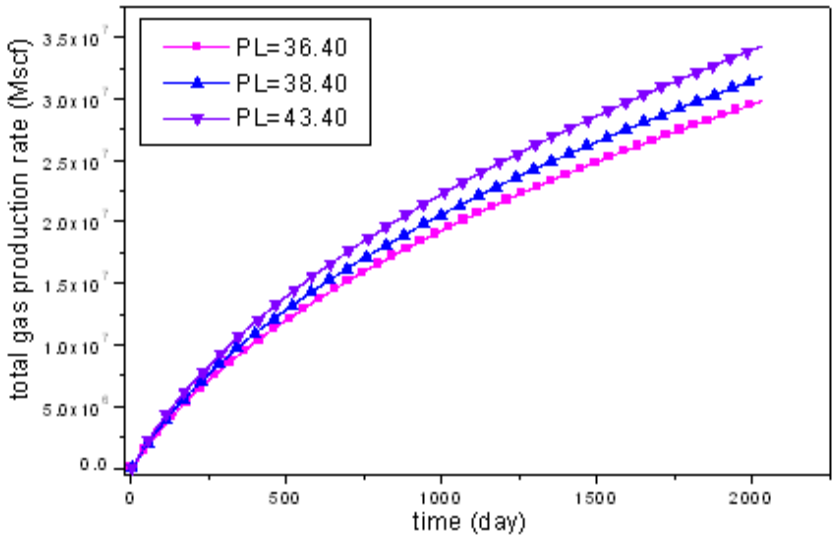

Figure 3.34 Total gas production rate changes with Langmuir pressure

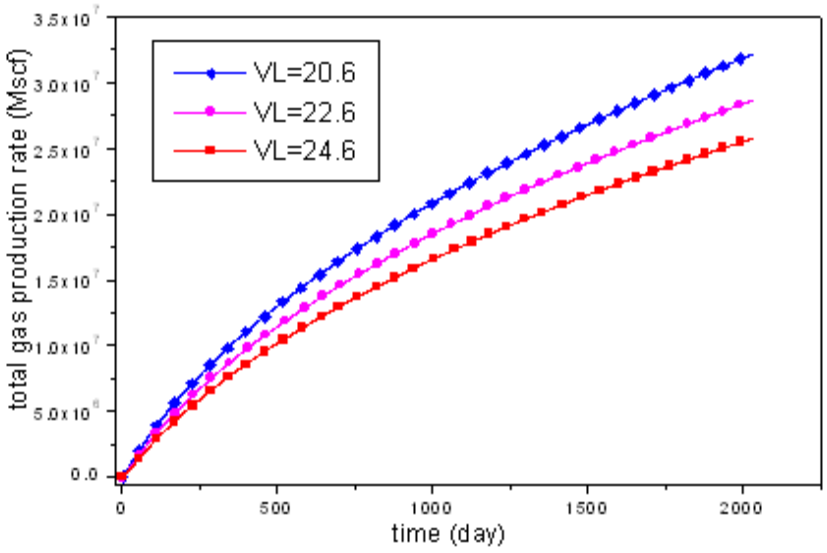

Figure 3.35 Total gas production rate changes with Langmuir volume

3.6.3.2 Branch number and angle effect

The total gas production rate increases with the branch number, and the incremental of total gas production rate is the biggest when the branch number is 8 (**Figure 3.36**).

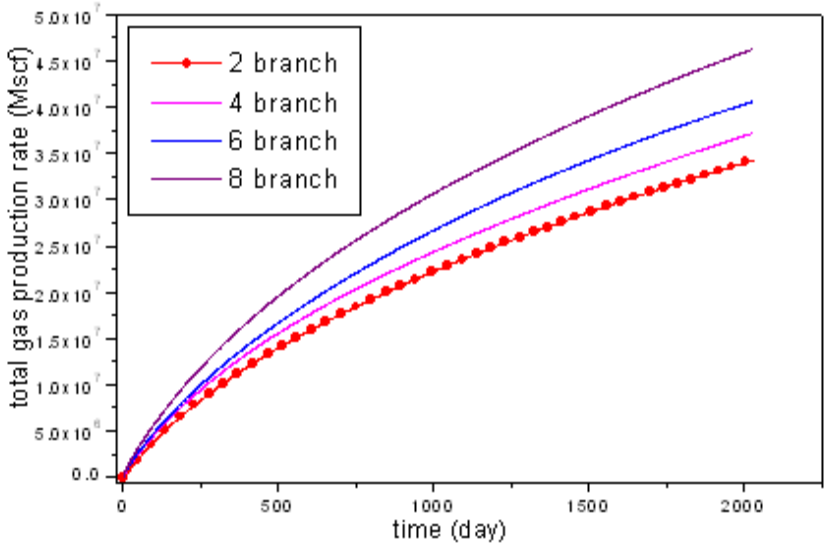

Figure 3.36 Total gas production rate changes with branch number

In addition, the daily water production rate also rises with the increasing of branch number. The difference exists in the fact that the water production rate increases much slower when branch number goes from 6 to 8 compared to the branch number goes from 4 to 6. So this indicates that it is not the case that the more the branch numbers, the better for the water production (**Figure 3.37**).

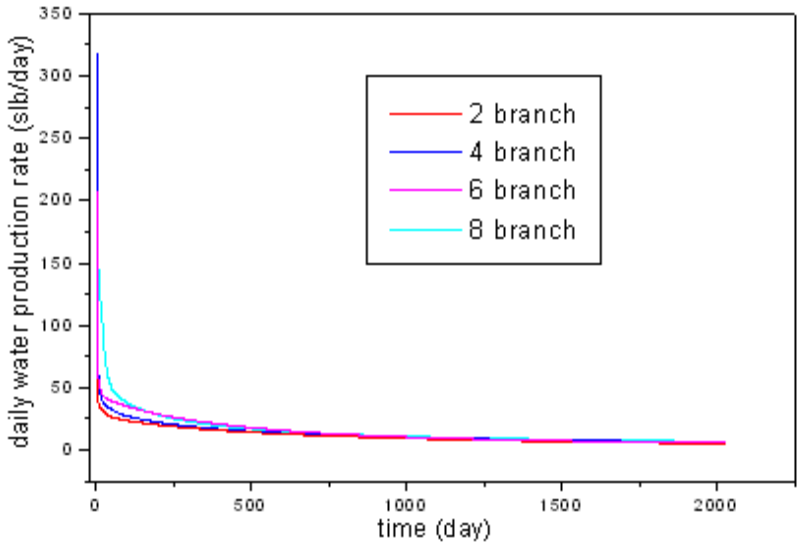

Figure 3.37 Daily water production rate changes with branch number

Obviously, the pressure drops the fastest when the branch number is 8 and drops the slowest when the branch number is 2 (**Figure 3.38**). This phenomenon is consistent

with the changes of gas production rate: the gas production rate is the maximum with branch number 8 and the smallest with branch number 2.

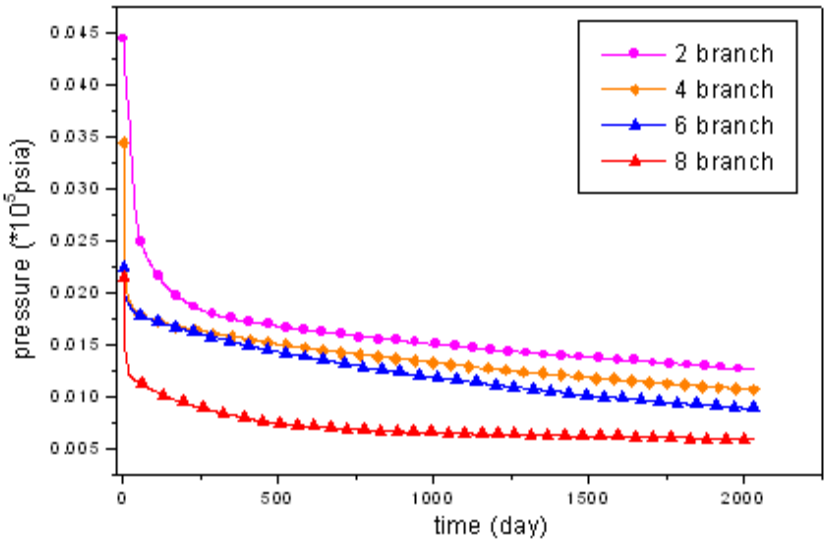

Figure 3.38 Average pressure changes with branch number

The daily gas production rate is the biggest when the angle between main stream and branch is 45^0 , second is angle 60^0 , the smallest is angle 30^0 (**Figure 3.39**). The reason for the fact lies in that the branch well control area with angle 45^0 is bigger than that with other angles. The branch angle has the similar effect on the total gas production rate, as shown in **Figure 3.40**.

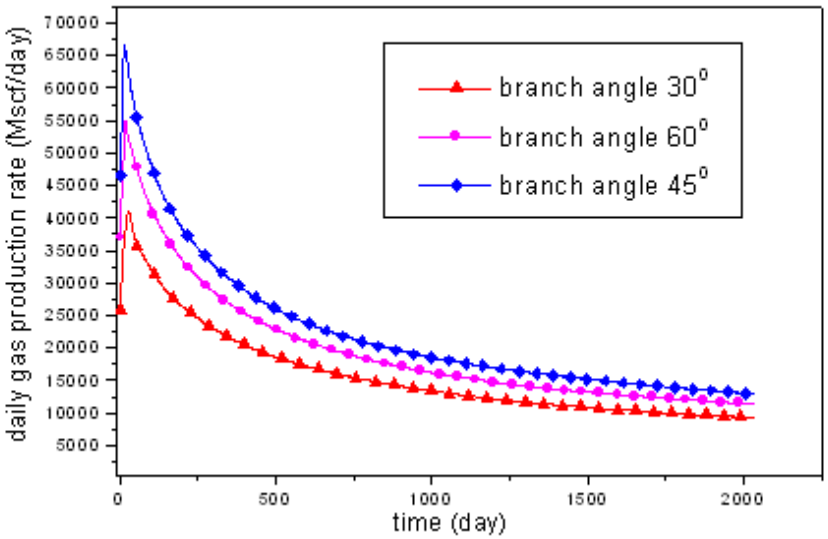

Figure 3.39 Daily gas production rate changes with branch angle

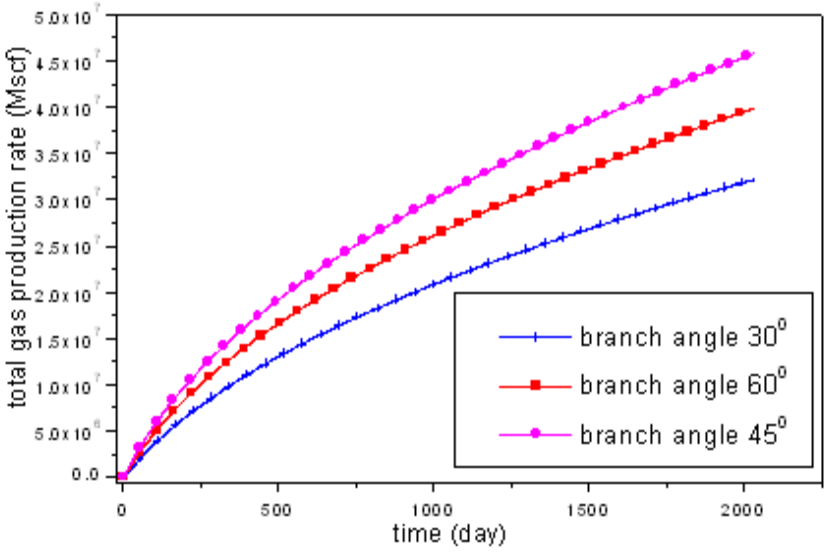

Figure 3.40 Total gas production rate changes with branch angle

The daily water production rate and total water production rate under the impact of branch angle is illustrated (**Figure 3.41 and Figure 3.42**). The daily water production rate (**Figure 3.41**) is the highest during the whole simulation period with branch angle 45 degree, and lowest with branch angle 30 degree. This is also caused by the larger control area when the branch angle is 45 degree. Similar trend can be found for total water rate (**Figure 3.42**). It can reach 3.75E4 Mscf if the branch angle is 45 degree, while it is only about 3.5E4 Mscf with 30 degree branch angle.

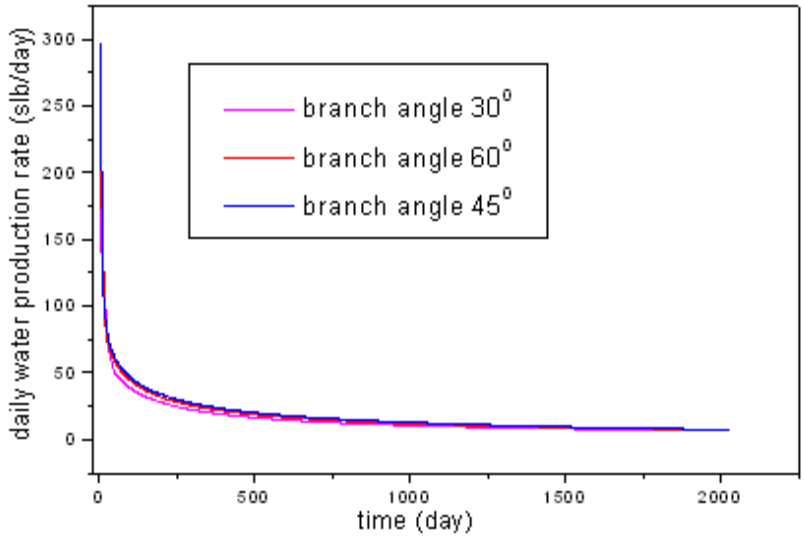

Figure 3.41 Daily water production rate changes with branch angle

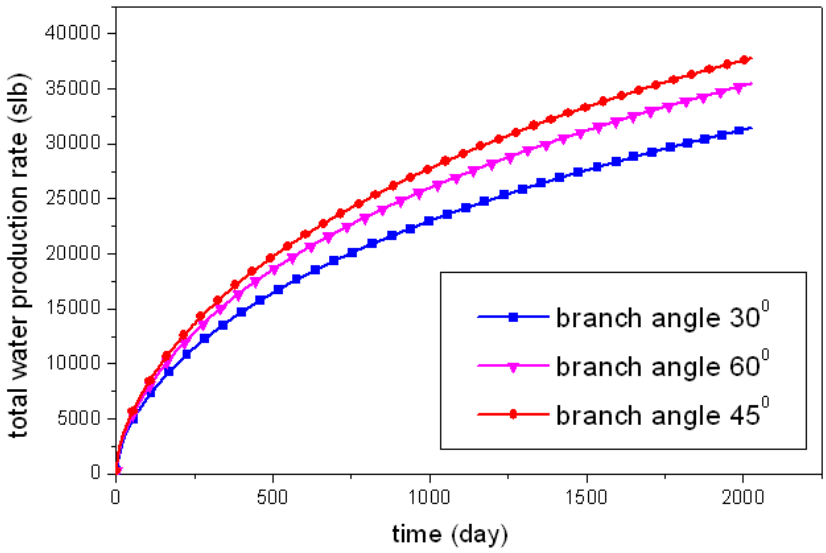

Figure 3.42 Total water production rate changes with branch angle

3.7 Chapter Conclusions

(1) The advanced coupled horizontal wellbore models of single and multi-branch well considering the effects of threshold pressure gradient and gas slippage are developed. The matrix shrinkage effect is modelled using a new developed permeability model as shown in **Chapter 2**. The models are solved using the IMPES method, and a program is coded using Fortran.

(2) The comparisons of the results come from the multi-branch horizontal wellbore model, single branch horizontal wellbore model and vertical wellbore model are made. Results showed that the coupled multi-branch horizontal wellbore model can largely enhance the gas and water production rate, this result has great significance in guiding the industry development.

(3) The gas slippage factor is determined by β_1 and β_2, two cases are studied based on this: set β_1 and β_2 as constant respectively. Results showed that the gas production rate and water production rate increase with the increasing of gas slippage factor, while the average pressure decreases with the rising of gas slippage factor.

(4) Gas threshold pressure is determined by α_1 and α_2, when α_1 is set at a given value, the water and gas production rate nearly converge to one point at the initial stage, and decrease with the increasing of α_2 at the late stage. While α_2 has an opposite effect on

the pressure changes: the average reservoir increases with the rising value of α_2. This is because of the lower gas and water production rate. Similar trend can be found when α_2 is set as constant.

(5) Water threshold pressure gradient is determined by α_3 and α_4. The daily gas production rate increases with the water threshold pressure gradient before gas production rate reaches its maximum, while this effect is reversed after this period. And the total water production rate decreases with the increasing of water threshold pressure gradient during the whole simulation process. What is more, the average pressure increases with the rising of water threshold pressure gradient.

(6) The daily gas production rate increases with the Langmuir pressure and decreases with Langmuir volume, which are attributed to the higher desorption rate with higher Langmuir pressure and lower Langmuir volume.

(7) The gas production rate increases with the branch number, while the increasing speed of water production rate becomes slower once the branch number goes from 6 to 8 than from 4 to 6. So it is not always the bigger the branch number the better for the well production. In addition, branch angle 45 degree is the best choice for the well production pattern.

Chapter 4 Application of ECBM technology into the advanced coupled triple porosity model

4.1 Introduction

Unlike conventional gas reservoirs, methane in coalbeds is stored primarily as a sorbed gas, at near-liquid densities, on the internal surface area of the microporous coal. The surface area of the coal on which the methane is adsorbed is very large (20 to 200 m^2 /kg) (**Patching, T.H., 1970[130]**). And, if saturated, CBM can have five times the volume of gas contained in a conventional sandstone gas reservoir of comparable size. Thus the exploitation of CBM reservoir has great significance, especially the implementation of enhanced technology on it for the recovery of the gas rate. In addition, the coal also becomes the key fuel for the power generation, shown in **Figure 4.1**.

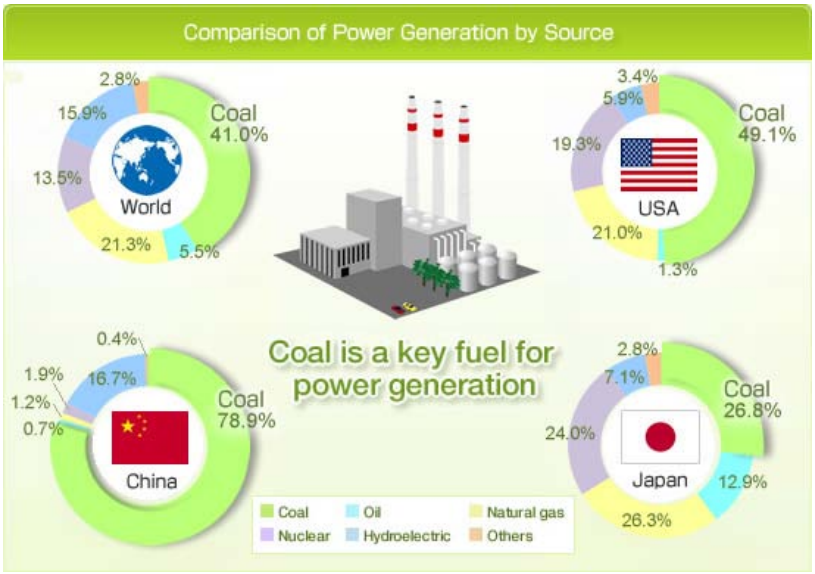

Figure 4.1 Comparison of fuel for power generation

The basic simulation models utilized for the CBM reservoir is characterized as dual porosity (**King, G.R., et al., 1986[43]**) and triple porosity models (**Scott, R. and Larry, P., et al., 2001[51]**), and study had found that the triple porosity model can get better history matching result than the traditional dual porosity model. Later, an advanced Coalbed Methane transport model is proposed by considering both the effects of stress and matrix shrinkage on the permeability (**Zhang, X.M. and Tong, D.K., 2008[48]**). Then the compositional dual porosity CBM reservoir model is also developed for the purpose of CO_2 sequestration (**Ozdemir, E., 2009[50]**). The problem is that they didn't extend the novel idea into the coupled triple porosity CBM reservoir model.

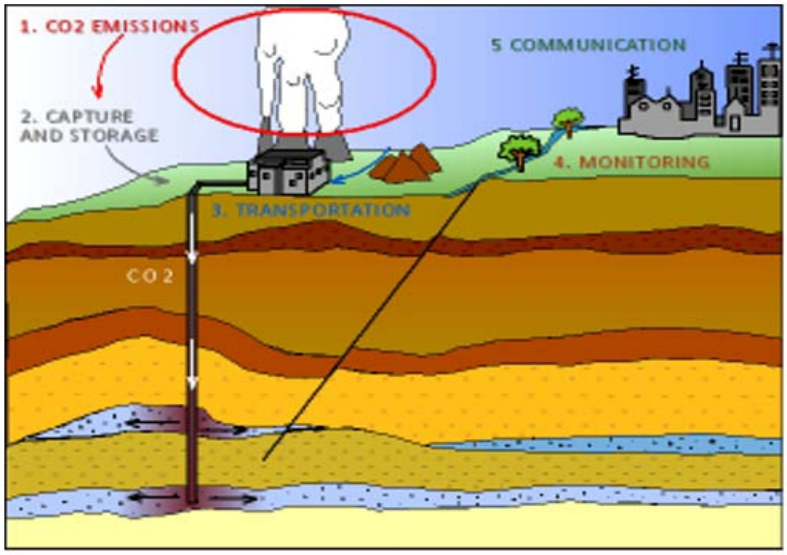

Figure 4.2 Schematic representation of the coal seam CO_2 storage

Moreover, the most popular ECBM recovery technology is injecting gas (CO_2 /N_2). **Figure 4.2** illustrates the CO_2 injection and storage process in the CBM reservoir. In addition, the main reason for the injecting of CO_2 is to diminish the increasing rate of CO_2, which will become a serious problem in the future, as illustrated in **Figure 4.3** and **Figure 4.4**. There are mainly two types of ECBM recovery methods according to the current study: one is the numerical simulation method, and the other one is the experimental method.

Figure 4.3 The global warming in Alberta

The ECBM models are proposed to investigate the parameters that affect the recovery of CBM reservoir (**Smith, H.D., et al., 2005[131]; Balan, H.O. and Gumrah, F., 2009[132]**). They investigate the effects of permeability anisotropies, diffusion time constant, physical properties and operational parameters of coal on the ECBM process.

The multi-scale model (**Wang, G.X., et al., 2009[133]**) and one dimensional mathematical model (**Ronny, P., et al., 2011[134]**) is also developed for the ECBM production and CO_2 sequestration. Although they consider the effect of matrix shrinkage/swelling on the recovery of CBM, the problem is that the permeability model comes from the extended Palmer/Mansoori (**Palmer, I. and Mansoori, J., 1998[61]**) model hasn't already novel.

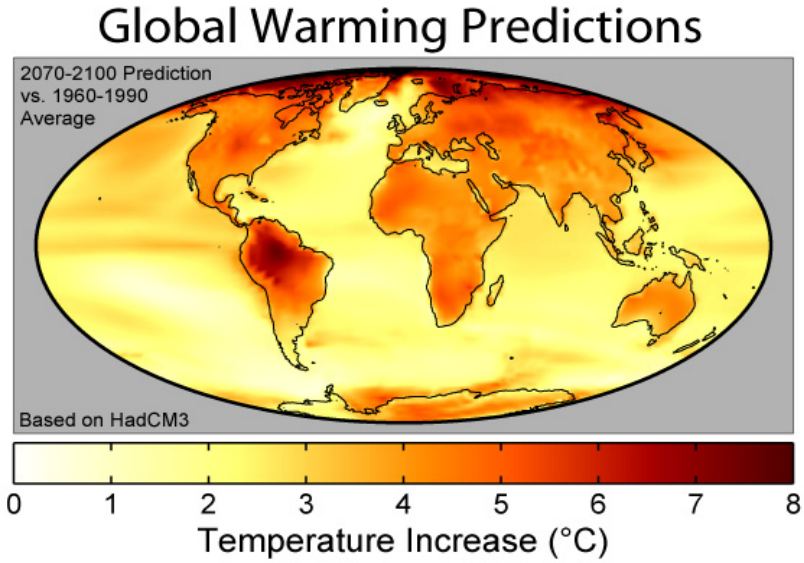

Figure 4.4 The global warming predictions for the future

On the other hand, the laboratory experiments for the ECBM recovery by gas injection have been successfully done (**Shimada, S., et al., 2005[135]**), they studied the effects of pressure on the sorption ability of CO_2, CH_4, N_2 and the injecting pressure on the desorption behavior of CH_4. Some people even combined experiments with numerical simulation to study the injecting process and how the injection of mixture affects the recovery of gas (**Jessen, K., et al., 2008[137]; Shi, J.Q., et al., 2008[54]**).

Although there are so many studies on the primary (as studied in **Chapter 2** and **Chapter 3**) and ECBM recovery, however, the primary CBM production model can't make the best recovery of the gas in the CBM reservoir, in addition, the published ECBM technologies are only confined to very limited conditions.

The current ECBM technology didn't extend the simulation model into the comprehensive compositional triple porosity model that considers the gas slippage and threshold pressure gradient effects for CBM reservoir, which is supposed to have superiority over the conventional dual porosity model as studied in **Chapter 2** and **Chapter 3**. What is more, the horizontal technique study used for ECBM production process is still not strong enough.

In this Chapter, a novel permeability model is developed based on the surface energy theories, to focus on the impact of matrix shrinkage and swelling on ECBM production, followed that a coupled compositional triple porosity horizontal wellbore model for CBM reservoir, considering the gas slippage and threshold pressure gradient effect is proposed. The sensitivity analysis is made through 6 different case studies. Finally, this model is applied to the producing well yan 1-22-10 and injection well #10 of Yanchuan Southern block for history matching.

4.2 Dynamic permeability model

The extended Langmuir equation is used to express the adsorption capacity of every gas component for multi-component phenomena (**Arri, L.E., et al., 1992[150]**):

$$V_i = \frac{V_{Li} b_i y_i p}{1 + \sum_{i=1}^{n} b_i y_i p} \tag{4.1}$$

Where: $b_i = 1/\ p_{Li}$

The coal matrix dilates when its surface energy changes, resulting in the gas molecules adsorption or desorption (**Scherer, G.W., 1986[151]**). Suppose that the change of elastic energy is equal to the surface energy caused by the adsorption/desorption, and the high pressure will result in the gas compression. Then the overall strain induced by both the adsorption/desorption and pressure compression effect is derived as (**Pan, Z.J. and Connell, D.L., 2007[63]**):

$$\varepsilon(p) = -\frac{\gamma A \rho_s}{E_s} f(x, \nu_s) - \frac{p}{E_s}(1 - 2\nu_s) \tag{4.2}$$

Assume that $\nu_s = \nu$, $E_s = E$ in order to make it much more simp, then there is:

$$\varepsilon(p) = -\frac{\gamma A \rho_s}{E} f(x, \nu) - \frac{p}{E}(1 - 2\nu) \tag{4.3}$$

Where:

$$f(x,\nu) = \frac{[2(1-\nu) - (1+\nu)cx][3 - 5\nu - 4(1-2\nu)cx]}{(3-5\nu)(2-cx)},\ c = 1.2,\ x = a/l$$

The surface energy variation of the condensed phase in the coal matrix caused by the gas adsorption is given as (**Zhang, X.M. and Tong, D.K., 2008[48]**):

$$\gamma = -\int_0^p \Gamma RTd \ln p \tag{4.4}$$

Substituting **Equation (4.4)** into **Equation (4.3)**, there is:

$$\varepsilon(p) = \frac{RT\rho_s}{V_0 E} f(x,\nu)\int_0^p Vd \ln p - \frac{p}{E}(1-2\nu) \tag{4.5}$$

On the other side, the matrix shrinkage is caused by the gas desorption. If the reservoir pressure decreases from the critical desorption pressure p_c to p, then the matrix shrinkage effect under multiphase effect can be described as:

$$\Delta\varepsilon = \sum_{i=1}^{n} \frac{V_{Li} b_i y_i \rho_s RT}{E V_0 \sum_{j=1}^{n} b_j y_j} [\ln(1 + p_c \sum_{k=1}^{n} b_k y_k) - \ln(1 + p \sum_{k=1}^{n} b_k y_k)] + \frac{(1-2\nu)}{E}(p - p_c) \tag{4.6}$$

Here, suppose that the CBM reservoir model can be treated as a matchstick geometry, the relationship between porosity and strain (**Seidle, J.P. and Huitt, L.G., 1995[60]**) is:

$$\frac{\Delta\phi_f}{\phi_{fr}} = (1 + \frac{2}{\phi_{fr}})\Delta\varepsilon \tag{4.7}$$

In addition, the reservoir pressure depletion will result in the increase of the effective stress, and the stress related porosity and permeability variation is expressed as (**Palmer, I. and Mansoori, J., 1998[61]**):

$$\frac{\phi_f}{\phi_0} = 1 + \frac{c_f}{\phi_0}(p - p_0) \tag{4.8}$$

$$\frac{k_f}{k_0} = (\frac{\phi_f}{\phi_0})^3 \tag{4.9}$$

Combining the effects of pore compressibility and matrix shrinkage/swelling with permeability and porosity, the final overall relationship between porosity and permeability expression is:

$$\phi_f = \phi_0 + c_f(p - p_0) + \phi_{fr}(1 + 2/\phi_{fr})\Delta\varepsilon \tag{4.10}$$

$$\frac{k_f}{k_0} = (\frac{\phi_f}{\phi_0})^3 \tag{4.11}$$

4.3 Fluid flow simulation in the CBM reservoir

For the presence of CO_2 injection, considering the effects of gas slippage and threshold pressure gradient, the transport equation of CO_2 and CH_4 in the macro-pore and cleat system are presented with the following assumptions:

(1) The coal seams are characterized as a triple porosity nature composes of macro-pore system, micro-pore system and cleat system.
(2) The reservoir is horizontal and its thickness is constant.
(3) The system is isothermal.
(4) The flow in coal seam is two phase flow including gas and water phase.
(5) The free gas is real gas.
(6) The fluid in the macro-pore and cleat system obeys Darcy's law, and the free gas is governed by Fick's first law.
(7) The effects of gravity and capillary pressure are considered.

4.3.1 Transport equation in the macro-pore system

For CO_2 in the gas phase:

$$\begin{aligned}&\nabla\cdot\left(\frac{y_1 k_a k_{arg\infty}}{\mu_{ag}B_{ag}}(1+\beta_1(\frac{k_a k_{arg\infty}(s_{ag})}{\phi_g})^{-\beta_2}/p_{am})(\nabla(p_{ag}-\rho_{ag}gH)-\lambda_{bag})\right.\\&\left.+y_1 D_a\nabla(\frac{s_{ag}}{B_{ag}})+r_{sw1}\frac{k_a k_{arw}}{\mu_{aw}B_{aw}}\nabla p_{aw}\right)-(q_{afg})_1+(q_{mag})_1=\frac{\partial}{\partial t}\left(\frac{y_1\phi_a s_{ag}}{B_{ag}}+r_{sw1}\frac{\phi_a s_{aw}}{B_{aw}}\right)\end{aligned} \tag{4.12}$$

For CH_4 in the gas phase:

$$\begin{aligned}&\nabla\cdot\left(\frac{(1-y_1)k_a k_{arg\infty}}{\mu_{ag}B_{ag}}(1+\beta_1(\frac{k_a k_{arg\infty}(s_{ag})}{\phi_g})^{-\beta_2}/p_{am})(\nabla(p_{ag}-\rho_{ag}gH)-\lambda_{bag})\right.\\&\left.+(1-y_1)D_a\nabla(\frac{s_{ag}}{B_{ag}})+r_{sw2}\frac{k_a k_{arw}}{\mu_{aw}B_{aw}}\nabla p_{aw}\right)-(q_{afg})_2+(q_{mag})_2\\&=\frac{\partial}{\partial t}\left(\frac{(1-y_1)\phi_a s_{ag}}{B_{ag}}+r_{sw2}\frac{\phi_a s_{aw}}{B_{aw}}\right)\end{aligned} \tag{4.13}$$

For the water phase:

$$\nabla\cdot\left(\frac{k_a k_{arw}}{\mu_{aw}B_{aw}}(\nabla(p_{aw}-\rho_{aw}gH)-\lambda_{baw})\right)-q_{afw}=\frac{\partial}{\partial t}\left(\frac{\phi_a s_{aw}}{B_{aw}}\right) \tag{4.14}$$

4.3.2 Transport equation in the cleat system

For component i in the gas phase:

$$\begin{aligned}&\nabla\cdot\left(\frac{y_i k_f k_{frg\infty}}{\mu_{fg}B_{fg}}(1+\beta_1(\frac{k_f k_{frg\infty}(s_{fg})}{\phi_f})^{-\beta_2}/p_{fm})(\nabla(p_{fg}-\rho_{fg}gH)-\lambda_{bfg})\right.\\&\left.+y_i D_f\nabla(\frac{s_{fg}}{B_{fg}})+r_{sw(i+1)}\frac{k_f k_{frw}}{\mu_{fw}B_{fw}}\nabla p_{fw}\right)+(q_{afg})_i-(q_{fvg})_i=\frac{\partial}{\partial t}\left(\frac{y_i\phi_f s_{fg}}{B_{fg}}+r_{sw(i+1)}\frac{\phi_f s_{fw}}{B_{fw}}\right)\end{aligned} \tag{4.15}$$

Where: $i=2,3$, $y_2(CO_2)+y_3(CH_4)=1$

For the water phase:

$$\nabla\cdot\left(\frac{k_f k_{frw}}{\mu_{fw}B_{fw}}(\nabla(p_{fw}-\rho_{fw}gH)-\lambda_{bfw})\right)-q_{fvw}+q_{afw}=\frac{\partial}{\partial t}\left(\frac{\phi_f s_{fw}}{B_{fw}}\right) \tag{4.16}$$

Threshold pressure gradient: $\lambda_{bag}=(\alpha_1/k_a k_{arg\infty})+\alpha_2$; $\lambda_{baw}=(\alpha_3\mu_{aw}/(k_a k_{arw\infty}))^{\alpha_4}$

$\lambda_{bfg}=(\alpha_1/k_f k_{frg\infty})+\alpha_2$; $\lambda_{bfw}=(\alpha_3\mu_{fw}/(k_f k_{frw\infty}))^{\alpha_4}$

Gas slippage effect: $F_{andg}=1+\beta_1(\frac{k_a k_{arg\infty}(s_g)}{\phi_g})^{-\beta_2}/p_{am}$; $F_{fndg}=1+\beta_1(\frac{k_f k_{frg\infty}(s_g)}{\phi_g})^{-\beta_2}/p_{fm}$

4.3.3 Auxiliary equation

Equation (4.12)-Equation (4.16) are the second order partial differential equations which contain eight unknowns: $p_{ag}, p_{fg}, s_{ag}, s_{fg}, p_{aw}, p_{fg}, s_{ag}, s_{fw}$. The other four auxiliary equations are given below:

$$p_{acgw}(s_{ag})=p_{ag}-p_{aw} \tag{4.17}$$

$$p_{fcgw}(s_{fg})=p_{fg}-p_{fw} \tag{4.18}$$

$$s_{ag}+s_{aw}=1.0 \tag{4.19}$$

$$s_{fg}+s_{fw}=1.0 \tag{4.20}$$

The $p_{acgw}(s_{ag})$, $p_{fcgw}(s_{ag})$ in the **Equation (4.17)** and **Equation (4.18)** is called capillary pressure function in macro-pore system and cleat system respectively, which is a given function.

4.3.4 Transport equation in the micro-pore system

The desorbed gas diffusion through the coal matrix system to the cleat system can be described mathematically by Fick's first law, so the migration velocity of desorbed gas is assumed as a result of concentration gradients in the matrix (**Wu, J., 1994[146]**):

$$\frac{\partial V_{im}}{\partial t} = -\frac{1}{\tau}[V_{im} - V_{iE}(p_{ag})] \tag{4.21}$$

$$V_{iE}(p_{ag}) = \frac{V_{Li} y_i p_{ag}}{p_L + \sum_{i=1}^{n} b_i y_i p_L p} \tag{4.22}$$

In addition, the desorption rate of gas from coal micro-pore system to matrix system is:

$$(q_{mag})_i = -\frac{\rho_c}{B_g}\frac{\partial V_{im}}{\partial t} \tag{4.23}$$

4.3.5 Cross flow from macro-pore system to cleat system

The average mass transfer rate (per unit volume of coalbed) between the macro-pore and the cleat system is:

$$q_{afg} = \frac{k_{rg}}{\mu_{ag} B_{ag}}(p_{ag} - p_{fg}) \tag{4.24}$$

Suppose that water can be stored both within the matrix blocks and in the cleat system. And there exist water cross flow from macro-pore system to cleat system owning to the fact that the pressure between the macro-pore system and the cleat system is unequal. Thus, the water cross flow can be expressed as:

$$q_{afw} = \frac{k_{rw}}{\mu_{aw} B_{aw}}(p_{fw} - p_{aw}) \tag{4.25}$$

4.3.6 Single branch horizontal Wellbore model

Considering the effect of friction loss, acceleration loss and mixing loss, the pressure drop in the single branch horizontal wellbore are:

$$\Delta p_{wfj} = \frac{2 f_j \rho_j}{\pi^2 D^5}(2Q_j + q_j)^2 \Delta x_j + \frac{16 \rho_j q_j}{\pi^2 D^4}(2Q_j + q_j) \tag{4.26}$$

The derivation details can be found in **Chapter 3**. $j = 2,3,...,n$ represents the wellbore segments.

4.3.7 Multi-branch horizontal wellbore model

The momentum loss caused by the gas mixture between main stream and branch has to be considered except for the friction pressure and acceleration pressure drop effect in the pressure drop wellbore model. The following pressure drop equation can be got through conducting the mass conservative equation around the horizontal wellbore. The details derivation can also be found in **Chapter 3**.

Segment with no branch:

$$\Delta p_{wfj} = \frac{2 f_j \rho_j}{\pi^2 D^5}(2Q_j + q_j + Q_{Rj})^2 \Delta x_j + \frac{16 \rho_j (q_j + Q_{Rj})}{\pi^2 D^4}(2Q_j + q_j + Q_{Rj}) \tag{4.27a}$$

Segment with branch:

$$\begin{aligned} \Delta p_{wfj} &= \frac{2 f_j \rho_j}{\pi^2 D^5}(2Q_j + q_j + Q_{Rj})^2 \Delta x_j + \frac{16 \rho_j (q_j + Q_{Rj})}{\pi^2 D^4}(2Q_j + q_j + Q_{Rj}) \\ &+ \frac{4 Q_j \rho_j}{\pi^2 D^4}(9Q_j - 4Q_{Rj}\cos\varphi) \end{aligned} \tag{4.27b}$$

Where: $j = 2,3,...,n$ represents the wellbore segments

4.3.8 Advanced coupled horizontal wellbore models

Note that the flux in **Equation (4.26)** and **Equation (4.27)** can be expressed as a function of well bottom hole pressure and formation pressure, which makes the horizontal wellbore model can be coupled with the coal seam reservoir model (**Equation (4.12)-Equation (4.25)**) to simulate the fluid in the CBM reservoir and wellbore simultaneously, and they are called the coupled single branch and multi-branch triple porosity horizontal wellbore model respectively. The injection of CO_2, matrix shrinkage effect, gas slippage effect and threshold pressure gradient effect are all considered in the coupled horizontal wellbore model.

4.3.9 Boundary conditions

4.3.9.1 Initial condition

The initial condition for the governing equations **Equation (4.12)**-**Equation (4.25)** is:

$$p_{ag}(x,y,z,0) = p_{ag}^{0}(x,y,z) \tag{4.28}$$

$$p_{fg}(x,y,z,0) = p_{fg}^{0}(x,y,z) \tag{4.29}$$

$$s_{ag}(x,y,z,0) = s_{ag}^{0}(x,y,z) \tag{4.30}$$

$$s_{fg}(x,y,z,0) = s_{fg}^{0}(x,y,z) \tag{4.31}$$

4.3.9.2 Calculation of the Flow Rates at the Wells

The infinite conductivity boundary condition implying that the well-bore pressure is uniform and the integral of the flux over the perforated interval is equal to the constant specified rate is used in this Chapter. This can be written:

$$q = \int_0^{h_w} \frac{2\pi k_r}{\mu} r \frac{\partial p}{\partial r}\Big|_{r=r_w} dz \tag{4.32}$$

The derivation of the flow rate at the well is straight forward for the incompressible water phase. Assuming a steady-state flow at the well, and the superficial velocity for the water phase according to the Darcy's law can be written as:

$$\bar{v}_{fw} = \frac{q_{fvw} B_{fw}}{2\pi r h} = -\frac{k_f k_{frw}}{\mu_{fw}} \frac{\partial p}{\partial r} \tag{4.33}$$

Then separating the variables and integrating both side of the equation:

$$\frac{q_{fvw}}{2\pi h} \int_{r_w}^{r_e} \frac{dr}{r} = -\int_{p_{fw}}^{p_{wf}} \frac{k_f k_{frw}}{\mu_{fw} B_{fw}} dp \tag{4.34}$$

Since the physical constants nearly can't be affected by pressure for the incompressible fluids, **Equation (4.34)** can be easily integrated. Thus, the water flow rate that considers threshold pressure gradient can be expressed as:

$$q_{fvw} = \frac{2\pi h k_f k_{frw}}{\mu_{fw} B_{fw} \ln(\frac{r_e}{r_w} + s)} [(p_{fw} - \lambda_{bfw} r_e) - (p_{wf} - \lambda_{bfw} r_e)] \tag{4.35}$$

Similarly, the gas flow rate can be shown as:

$$q_{fvg} = \frac{2\pi h k_f k_{frg}}{\mu_{fg} B_{fg} \ln(\frac{r_e}{r_w} + s)} [p_{fg} - \lambda_{bfg} r_e)^2 - (p_{wf} - \lambda_{bfg} r_e)^2] \tag{4.36}$$

4.3.9.3 External boundary condition

The external boundary condition is assumed to be constant pressure outer boundary:

$$p_{ag}(x, y, z, t)\Big|_{(x,y,z)\in\Gamma} = p_{fe}(x, y, z, t) \tag{4.37}$$

$$p_{fg}(x, y, z, t)\Big|_{(x,y,z)\in\Gamma} = p_{fe}(x, y, z, t) \tag{4.38}$$

$$\left.\frac{\partial s_{ag}}{\partial n}\right|_{\Gamma} = 0 \tag{4.39}$$

$$\left.\frac{\partial s_{fg}}{\partial n}\right|_{\Gamma} = 0 \tag{4.40}$$

4.4 Numerical Solution

The IMPES method is used to get the solution for the triple porosity model in CBM reservoir in this Chapter. It has already been utilized for the coupled dual porosity CBM reservoir model in **Chapter 3**, thus the details of how it can be applied to the model for the solution can be found in **Chapter 3**. The difference equations for the mathematical models are shown as follows in this Chapter.

4.4.1 Difference equation in the macro-pore system

$$\begin{aligned} &A_{aEi,j,k} p_{agi+1,j,k}^{n+1} + A_{aNi,j,k} p_{agi,j+1,k}^{n+1} + A_{aBi,j,k} p_{agi,j,k+1}^{n+1} + E_{ai,j,k} p_{agi,j,k}^{n+1} + A_{aWi,j,k} p_{agi-1,j,k}^{n+1} \\ &+ A_{aSi,j,k} p_{agi,j-1,k}^{n+1} + A_{aTi,j,k} p_{agi,j,k-1}^{n+1} = B_{ai,j,k} \end{aligned} \tag{4.41}$$

Here:

$$A_{aE} = B_{agi,j,k} T_{ag}{}^{n}_{i+\frac{1}{2},j,k} + B_{awi,j,k} T_{aw}{}^{n}_{i+\frac{1}{2},j,k}$$

$$A_{aN} = B_{agi,j,k} T_{ag}{}^{n}_{i,j+\frac{1}{2},k} + B_{awi,j,k} T_{aw}{}^{n}_{i,j+\frac{1}{2},k}$$

$$A_{aB} = B_{agi,j,k} T_{ag}{}^{n}_{i,j,k+\frac{1}{2}} + B_{awi,j,k} T_{aw}{}^{n}_{i,j,k+\frac{1}{2}}$$

$$A_{aW} = B_{agi,j,k} T_{ag}{}^{n}_{i-\frac{1}{2},j,k} + B_{awi,j,k} T_{aw}{}^{n}_{i-\frac{1}{2},j,k}$$

$$A_{aS} = B_{agi,j,k} T_{ag}{}^{n}_{i,j-\frac{1}{2},k} + B_{awi,j,k} T_{aw}{}^{n}_{i,j-\frac{1}{2},k}$$

$$A_{aT} = B_{agi,j,k} T_{ag}{}^{n}_{i,j,k-\frac{1}{2}} + B_{awi,j,k} T_{aw}{}^{n}_{i,j,k-\frac{1}{2}}$$

$$E_{ai,j,k} = -[A_{aE} + A_{aN} + A_{aB} + A_{aW} + A_{aS} + A_{aT} + (\frac{V_b \phi_i C_t}{\Delta t})^{n}_{i,j,k}]$$

$$B_{ai,j,k} = -(\frac{V_b \phi_i c_t}{\Delta t})^{n}_{i,j,k} \, p^{n}_{agi,j,k} - W_{ai,j,k} - \sum ai,j,k$$

$$W_{i,j,k} = B_{agi,j,k} (G_{ag} + Q_{mag} - Q_{afg})^{n}_{i,j,k} + B_{awi,j,k} (G_{aw} - Q_{afw})^{n}_{i,j,k}$$

$$G_{ag} = -\Delta T_{ag} . [\Delta(\rho_g g H) + \lambda_{bag}]$$

$$G_{aw} = -\Delta T_{aw} . [\Delta(p_{cgw} + \rho_w g H) + \lambda_{baw}]$$

$$\sum ai,j,k = T_{aDi+\frac{1}{2},j,k} [(\frac{s_{ag}}{B_{ag}})^{n}_{i+1,j,k} - (\frac{s_{ag}}{B_{ag}})^{n}_{i,j,k}] - T_{aDi-\frac{1}{2},j,k} [(\frac{s_{ag}}{B_{ag}})^{n}_{i,j,k} - (\frac{s_{ag}}{B_{ag}})^{n}_{i-1,j,k}]$$

$$+ T_{aDi,j+\frac{1}{2},k} [(\frac{s_{ag}}{B_{ag}})^{n}_{i,j+1,k} - (\frac{s_{ag}}{B_{ag}})^{n}_{i,j,k}] - T_{aDi,j-\frac{1}{2},k} [(\frac{s_{ag}}{B_{ag}})^{n}_{i,j,k} - (\frac{s_{ag}}{B_{ag}})^{n}_{i,j-1,k}]$$

$$+ T_{aDi,j,k+\frac{1}{2}} [(\frac{s_{ag}}{B_{ag}})^{n}_{i,j,k+1} - (\frac{s_{ag}}{B_{ag}})^{n}_{i,j,k}] - T_{aDi,j,k-\frac{1}{2}} [(\frac{s_{ag}}{B_{ag}})^{n}_{i,j,k} - (\frac{s_{ag}}{B_{ag}})^{n}_{i,j,k-1}]$$

$$T_{ag(i\pm\frac{1}{2}),j,k} = \frac{(Ak_a)_{(i\pm\frac{1}{2}),j,k}}{0.5(\Delta x_i + \Delta x_{i\pm1})} (\frac{k_{arg\infty}}{B_{ag}\mu_{ag}} (1 + \alpha_1 (\frac{k_a k_{arg\infty}(s_{ag})}{\phi_{ag}}))^{-\alpha_2} / p_{am})_{(i\pm\frac{1}{2}),j,k}$$

$$T_{agi,(j\pm\frac{1}{2}),k} = \frac{(Ak_f)_{i,j\pm\frac{1}{2},k}}{0.5(\Delta y_j + \Delta y_{j\pm1})} (\frac{k_{rg\infty}}{B_g \mu_g} (1 + \alpha_1 (\frac{k_f k_{rg\infty}(s_g)}{\phi_g}))^{-\alpha_2} / p_m)_{i,(j\pm\frac{1}{2}),k}$$

$$T_{agi,j,(k\pm\frac{1}{2})} = \frac{(Ak_a)_{i,j,k\pm\frac{1}{2}}}{0.5(\Delta z_k + \Delta z_{k\pm1})} (\frac{k_{arg\infty}}{B_{ag}\mu_{ag}} (1 + \alpha_1 (\frac{k_a k_{arg\infty}(s_{ag})}{\phi_{ag}}))^{-\alpha_2} / p_{am})_{i,j,k\pm\frac{1}{2}}$$

$$T_{aw(i\pm\frac{1}{2}),j,k}=\frac{(Ak_a)_{(i\pm\frac{1}{2}),j,k}}{0.5(\Delta x_i+\Delta x_{i\pm1})}(\frac{k_{arw}}{B_{aw}\mu_{aw}})_{(i\pm\frac{1}{2}),j,k}$$

$$T_{awi,(j\pm\frac{1}{2}),k}=\frac{(Ak_a)_{i,j\pm\frac{1}{2},k}}{0.5(\Delta y_j+\Delta y_{j\pm1})}(\frac{k_{arw}}{B_{aw}\mu_{aw}})_{i,(j\pm\frac{1}{2}),k}$$

$$T_{awi,j,(k\pm\frac{1}{2})}=\frac{(Ak_a)_{i,j,k\pm\frac{1}{2}}}{0.5(\Delta z_k+\Delta z_{k\pm1})}(\frac{k_{arw}}{B_{aw}\mu_{aw}})_{i,j,k\pm\frac{1}{2}}$$

$$T_{aD(i\pm\frac{1}{2}),j,k}=\frac{(AD_a)_{i\pm\frac{1}{2},j,k}}{0.5(\Delta x_i+\Delta x_{i\pm1})}$$

$$T_{aDi,(j\pm\frac{1}{2}),k}=\frac{(AD_a)_{i,j\pm\frac{1}{2},k}}{0.5(\Delta y_j+\Delta y_{j\pm1})}$$

$$T_{aDi,j,k\pm\frac{1}{2}}=\frac{(AD_a)_{i,j,k\pm\frac{1}{2}}}{0.5(\Delta z_k+\Delta z_{k\pm1})}$$

4.4.2 Difference equation in the cleat system

Through arranging the difference equation for the cleat system, the following formula can be got:

$$A_{fEi,j,k}p_{fgi+1,j,k}^{n+1}+A_{fNi,j,k}p_{fgi,j+1,k}^{n+1}+A_{fBi,j,k}p_{fgi,j,k+1}^{n+1}+E_{fi,j,k}p_{fgi,j,k}^{n+1}+A_{fWi,j,k}p_{fgi,j-1,k}^{n+1}+A_{fTi,j,k}p_{fgi,j,k-1}^{n+1}=B_{fi,j,k} \quad (4.42)$$

Here:

$$A_{fEi,j,k}=B_{fgi,j,k}T_{fg}{}^{n}_{i+\frac{1}{2},j,k}+B_{fwi,j,k}T_{fw}{}^{n}_{i+\frac{1}{2},j,k}$$

$$A_{fNi,j,k}=B_{fgi,j,k}T_{fg}{}^{n}_{i,j+\frac{1}{2},k}+B_{fwi,j,k}T_{fw}{}^{n}_{i,j+\frac{1}{2},k}$$

$$A_{fBi,j,k}=B_{fgi,j,k}T_{fg}{}^{n}_{i,j,k+\frac{1}{2}}+B_{fwi,j,k}T_{fw}{}^{n}_{i,j,k+\frac{1}{2}}$$

$$A_{fWi,j,k}=B_{fgi,j,k}T_{fg}{}^{n}_{i-\frac{1}{2},j,k}+B_{fwi,j,k}T_{fw}{}^{n}_{i-\frac{1}{2},j,k}$$

$$A_{fSi,j,k} = B_{fgi,j,k} T_{fg}{}^{n}_{i,j-\frac{1}{2},k} + B_{fwi,j,k} T_{fw}{}^{n}_{i,j-\frac{1}{2},k}$$

$$A_{fTi,j,k} = B_{fgi,j,k} T_{fg}{}^{n}_{i,j,k-\frac{1}{2}} + B_{fwi,j,k} T_{fw}{}^{n}_{i,j,k-\frac{1}{2}}$$

$$E_{fi,j,k} = -[A_{fEi,j,k} + A_{fNi,j,k} + A_{fBi,j,k} + A_{fWi,j,k} + A_{fSi,j,k} + A_{fTi,j,k} + (\frac{\phi_f c_{ft} V_b}{\Delta t})^n_{i,j,k}]$$

$$B_{fi,j,k} = -(\frac{\phi_f c_{ft} V_b}{\Delta t})^n_{i,j,k} p_{fg}{}^{n}_{i,j,k} - W_{fi,j,k} - \sum_{fi,j,k}$$

$$W_{fi,j,k} = B_{fgi,j,k}(G_{fg} + Q_{afg} - Q_{fvg})^n_{i,j,k} + B_{fwi,j,k}(G_{fw} + Q_{afw} - Q_{fvw}))^n_{i,j,k}$$

$$\sum_{fi,j,k} = T_{fDi+\frac{1}{2},j,k}[(\frac{s_{fg}}{B_{fg}})^n_{i+1,j,k} - (\frac{s_{fg}}{B_{fg}})^n_{i,j,k}] - T_{fDi-\frac{1}{2},j,k}[(\frac{s_{fg}}{B_{fg}})^n_{i,j,k} - (\frac{s_{fg}}{B_{fg}})^n_{i-1,j,k}]$$
$$+T_{fDi,j+\frac{1}{2},k}[(\frac{s_{fg}}{B_{fg}})^n_{i,j+1,k} - (\frac{s_{fg}}{B_{fg}})^n_{i,j,k}] - T_{fDi,j-\frac{1}{2},k}[(\frac{s_{fg}}{B_{fg}})^n_{i,j,k} - (\frac{s_{fg}}{B_{fg}})^n_{i,j-1,k}]$$
$$+T_{fDi,j,k+\frac{1}{2}}[(\frac{s_{fg}}{B_{fg}})^n_{i,j,k+1} - (\frac{s_{fg}}{B_{fg}})^n_{i,j,k}] - T_{fDi,j,k-\frac{1}{2}}[(\frac{s_{fg}}{B_{fg}})^n_{i,j,k} - (\frac{s_{fg}}{B_{fg}})^n_{i,j,k-1}]$$

$$G_{fg} = -\Delta T_{fg}.[\Delta(\rho_g g H) + \lambda_{bfg}]$$

$$G_{fw} = -\Delta T_{fw}.[\Delta(p_{cgw} + \rho_w g H) + \lambda_{bfw}]$$

$$T_{fg(i\pm\frac{1}{2}),j,k} = \frac{(Ak_f)_{(i\pm\frac{1}{2}),j,k}}{0.5(\Delta x_i + \Delta x_{i\pm1})}(\frac{k_{frg\infty}}{B_{fg}\mu_{fg}}(1+\alpha_1(\frac{k_f k_{frg\infty}(s_{fg})}{\phi_{fg}}))^{-\alpha_2} / p_{fm})_{(i\pm\frac{1}{2}),j,k}$$

$$T_{fgi,(j\pm\frac{1}{2}),k} = \frac{(Ak_f)_{i,j\pm\frac{1}{2},k}}{0.5(\Delta y_j + \Delta y_{j\pm1})}(\frac{k_{frg\infty}}{B_{fg}\mu_{fg}}(1+\alpha_1(\frac{k_f k_{frg\infty}(s_{fg})}{\phi_{fg}}))^{-\alpha_2} / p_{fm})_{i,(j\pm\frac{1}{2}),k}$$

$$T_{fgi,j,(k\pm\frac{1}{2})} = \frac{(Ak_f)_{i,j,k\pm\frac{1}{2}}}{0.5(\Delta z_k + \Delta z_{k\pm1})}(\frac{k_{frg\infty}}{B_{fg}\mu_{fg}}(1+\alpha_1(\frac{k_f k_{frg\infty}(s_{fg})}{\phi_{fg}}))^{-\alpha_2} / p_{fm})_{i,j,k\pm\frac{1}{2}}$$

$$T_{fw(i\pm\frac{1}{2}),j,k} = \frac{(Ak_f)_{(i\pm\frac{1}{2}),j,k}}{0.5(\Delta x_i + \Delta x_{i\pm1})}(\frac{k_{frw}}{B_{fw}\mu_{fw}})_{(i\pm\frac{1}{2}),j,k}$$

$$T_{fwi,(j\pm\frac{1}{2}),k} = \frac{(Ak_f)_{i,j\pm\frac{1}{2},k}}{0.5(\Delta y_j + \Delta y_{j\pm1})}(\frac{k_{frw}}{B_{fw}\mu_{fw}})_{i,(j\pm\frac{1}{2}),k}$$

$$T_{fwi,j,(k\pm\frac{1}{2})}=\frac{(Ak_f)_{i,j,k\pm\frac{1}{2}}}{0.5(\Delta z_k+\Delta z_{k\pm1})}(\frac{k_{frw}}{B_{fw}\mu_{fw}})_{i,j,k\pm\frac{1}{2}}$$

$$T_{fD(i\pm\frac{1}{2}),j,k}=\frac{(AD_f)_{i\pm\frac{1}{2},j,k}}{0.5(\Delta x_i+\Delta x_{i\pm1})}$$

$$T_{fDi,(j\pm\frac{1}{2}),k}=\frac{(AD_f)_{i,j\pm\frac{1}{2},k}}{0.5(\Delta y_j+\Delta y_{j\pm1})}$$

$$T_{fDi,j,k\pm\frac{1}{2}}=\frac{(AD_f)_{i,j,k\pm\frac{1}{2}}}{0.5(\Delta z_k+\Delta z_{k\pm1})}$$

4.4.3 Difference equation for the single branch horizontal wellbore

Difference equation for **Equation (4.26)** can be derived as:

$$0.5\Delta p_{wfi}=\frac{\rho_i}{\pi^2D^4}[\frac{f_i}{D}(2Q_i+q_i)^2\Delta x_i+8q_i(2Q_i+q_i)] \tag{4.43}$$

In addition, $q_i=q_{gi}+q_{wi}=PID_i\frac{K_{rgi}}{\mu_{gi}}(p_{gi}-p_{wfi})+PID_i\frac{K_{rwi}}{\mu_{wi}}(p_{wi}-p_{wfi})$, $Q_i=\sum_{j=1}^{i-1}q_j$, then the wellbore pressure equation of each segment is shown as follows:

$$\begin{aligned}&p_{wf_{i-1}}=p_{wf_i}+\frac{\rho_i}{\pi^2D^4}[\frac{4f_i\Delta x_i}{D}Q_i^2+(\frac{f_i\Delta x_i}{D}+8)q_i^2+4(\frac{f_i\Delta x_i}{D}+4)Q_iq_i]\\&+\frac{\rho_{i-1}}{\pi^2D^4}[\frac{4f_{i-1}\Delta x_{i-1}}{D}Q_{i-1}^2+(\frac{f_{i-1}\Delta x_{i-1}}{D}+8)q_{i-1}^2+4(\frac{f_{i-1}\Delta x_{i-1}}{D}+4)Q_{i-1}q_{i-1}]\\&i=2,3,...,n\end{aligned} \tag{4.44}$$

$$p_{wf_n}=p_{wfc}+\frac{\rho_n}{\pi^2D^4}[\frac{4f_n\Delta x_n}{D}Q_n^2+(\frac{f_n\Delta x_n}{D}+8)q_n^2+4(\frac{f_n\Delta x_n}{D}+4)Q_nq_n] \tag{4.45}$$

4.4.4 Difference equation for the multi-branch horizontal wellbore

Difference **Equation (4.27)**, then there is:

$$0.5\Delta p_{wfi}=\frac{\rho_i}{\pi^2D^4}[\frac{f_i\Delta x_i}{D}(2Q_i+q_i+Q_{Ri})^2+8(q_i+Q_{Ri})(2Q_i+q_i+Q_{Ri})] \tag{4.46a}$$

Or

$$0.5\Delta p_{wfi} = \frac{\rho_i}{\pi^2 D^4}[\frac{f_i \Delta x_i}{D}(2Q_i + q_i + Q_{Ri})^2 + 8(q_i + Q_{Ri})(2Q_i + q_i + Q_{Ri}) + 2Q_i(9Q_i - 4Q_{Ri}\cos\varphi)] \quad (4.46b)$$

Considering that $q_i = q_{gi} + q_{wi} = PID_i \frac{K_{rgi}}{\mu_{gi}}(p_{gi} - p_{wfi}) + PID_i \frac{K_{rwi}}{\mu_{wi}}(p_{wi} - p_{wfi})$, $Q_i = \sum_{j=1}^{i-1} q_j$,

then the wellbore pressure equation of each segment can be expressed as:

$$p_{wf_{i-1}} = p_{wf_i} + \frac{\rho_i}{\pi^2 D^4}[\frac{f_i \Delta x_i}{D}(2Q_i + q_i + Q_{Ri})^2 + 8(q_i + Q_{Ri})(2Q_i + q_i + Q_{Ri})] + \frac{\rho_{i-1}}{\pi^2 D^4}[\frac{f_{i-1}\Delta x_{i-1}}{D}(2Q_{i-1} + q_{i-1} + Q_{Ri-1})^2 + 8(q_{i-1} + Q_{Ri-1})(2Q_{i-1} + q_{i-1} + Q_{Ri-1})] \quad (4.47a)$$
$$i = 2, 3, ..., n$$

$$p_{wf_{i-1}} = p_{wf_i} + \frac{\rho_i}{\pi^2 D^4}[\frac{f_i \Delta x_i}{D}(2Q_i + q_i + Q_{Ri})^2 + 8(q_i + Q_{Ri})(2Q_i + q_i + Q_{Ri}) + 2Q_i(9Q_i - 4Q_{Ri}\cos\varphi)] + \frac{\rho_{i-1}}{\pi^2 D^4}[\frac{f_{i-1}\Delta x_{i-1}}{D}(2Q_{i-1} + q_{i-1} + Q_{Ri-1})^2 + 8(q_{i-1} + Q_{Ri-1})(2Q_{i-1} + q_{i-1} + Q_{Ri-1}) + 2Q_{i-1}(9Q_{i-1} - 4Q_{Ri-1}\cos\varphi)] \quad (4.47b)$$
$$i = 2, 3, ..., n$$

$$p_{wf_n} = p_{wfc} + \frac{\rho_n}{\pi^2 D^4}[\frac{f_n \Delta x_n}{D}(2Q_n + q_n + Q_{Rn})^2 + 8(q_n + Q_{Rn})(2Q_n + q_n + Q_{Rn})] \quad (4.48)$$

4.4.5 Coupled triple porosity model

The difference equation of the coupled single branch horizontal wellbore model can be got through coupling **Equation (4.44)** and **Equation (4.45)** with the formation difference equation **Equation (4.41)** and **Equation (4.42)**. And the coupled muli-branch horizontal wellbore model difference equation can be got through coupling **Equation (4.47)** and **Equation (4.48)** with **Equation (4.41)** and **Equation (4.42)**. The connection for them is the wellbore pressure. Once the pressure got its value, then the corresponding saturation needs to be calculated.

4.4.6 Solution for the saturation equation

4.4.6.1 Gas and water saturation in the macro-pore system

The difference equation of the water phase transport equation for the macro-pore system is derived as follows:

$$\Delta T_{aw}{}^{n}\Delta p_{ag}{}^{n+1} + G_{aw} - Q_{afw} = \frac{1}{\Delta t}[(\frac{\phi_a V_b s_{aw}}{B_{aw}})_{i,j,k}^{n+1} - (\frac{\phi_a V_b s_{aw}}{B_{aw}})_{i,j,k}^{n}] \tag{4.49}$$

The saturation expression is got through using the implicit method as follows:

$$s_{awi,j,k}^{n+1} = (\frac{B_{aw}}{\phi_a V_b})_{i,j,k}^{n+1}[\Delta t(\Delta T_{aw}{}^{n}\Delta p_{ag}{}^{n+1} + G_{aw} - Q_{afw}) + (\frac{\phi_a V_b s_{aw}}{B_{aw}})_{i,j,k}^{n}] \tag{4.50}$$

$$s_{agi,j,k}^{n+1} = 1 - s_{awi,j,k}^{n+1} \tag{4.51}$$

4.4.6.2 Gas and water saturation solution in the cleat system

The difference equation of the water phase transport equation for the cleat system is:

$$\Delta T_{fw}{}^{n}\Delta p_{fg}{}^{n+1} + G_{fw} + Q_{ifw} - Q_{fvw} = \frac{1}{\Delta t}[(\frac{\phi_f V_b s_{fw}}{B_{fw}})_{i,j,k}^{n+1} - (\frac{\phi_f V_b s_{fw}}{B_{fw}})_{i,j,k}^{n}] \tag{4.52}$$

Similarly, using the implicit method to calculate saturation:

$$s_{fwi,j,k}^{n+1} = (\frac{B_{fw}}{\phi_f V_b})_{i,j,k}^{n+1}[\Delta t(\Delta T_{fw}{}^{n}\Delta p_{fg}{}^{n+1} + G_{fw} + Q_{ifw} - Q_{fvw}) + (\frac{\phi_f V_b s_{fw}}{B_{fw}})_{i,j,k}^{n}] \tag{4.53}$$

$$s_{fgi,j,k}^{n+1} = 1 - s_{fwi,j,k}^{n+1} \tag{4.54}$$

4.5 Result discussion

In this Chapter, the advanced coupled horizontal wellbore models are solved through modified IMPES method originally used for the black oil model, then the simulator called TRIPLE-COAL is developed using Fortran program. The whole workflow for the simulator is shown as **Figure 4.5**, **Figure 4.6**, **Figure 4.7** and **Figure 4.8** respectively.

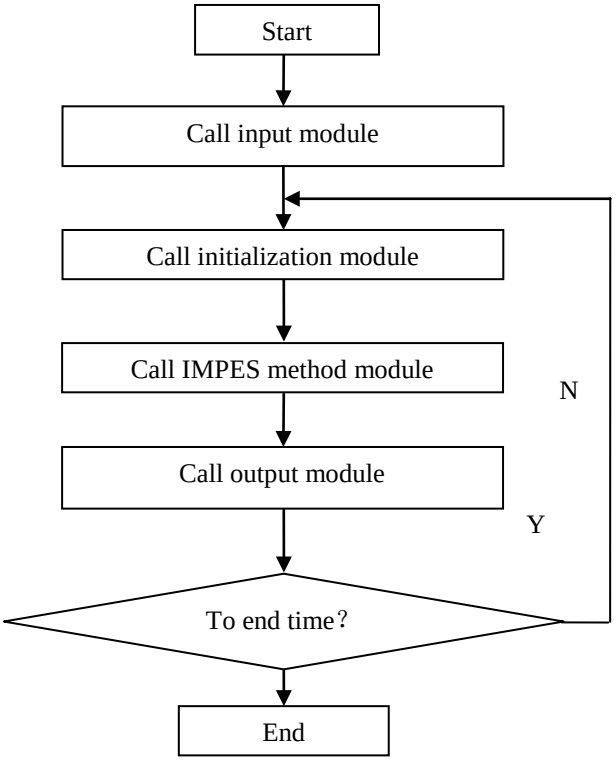

Figure 4.5 Workflow for the main program

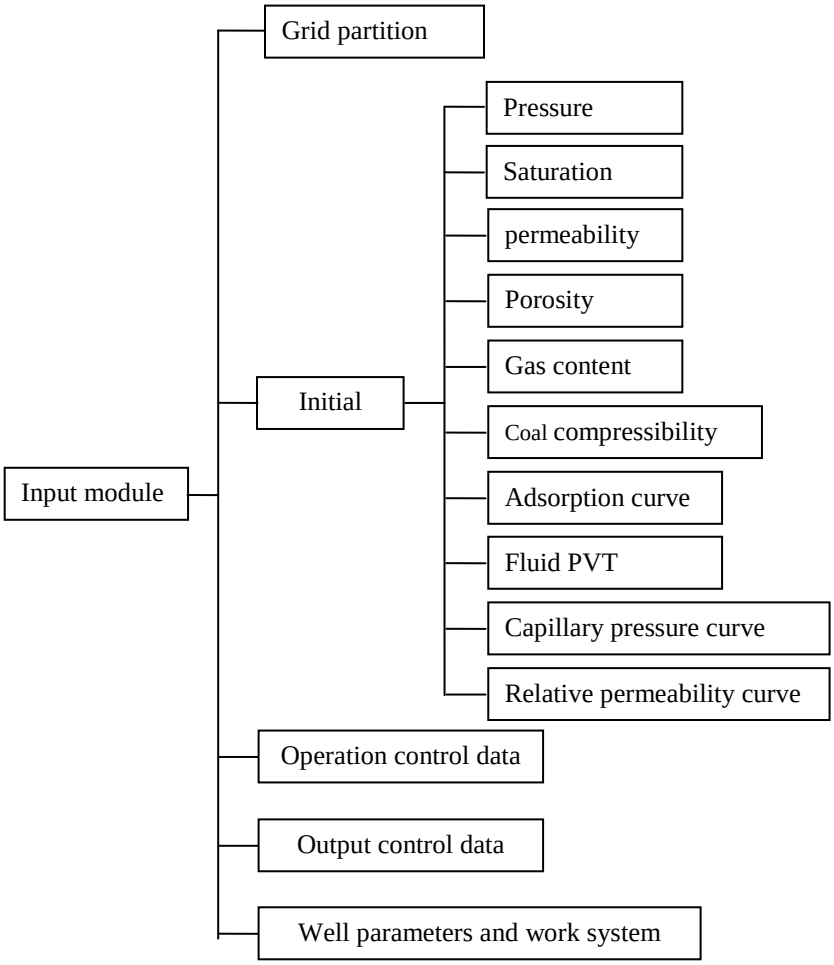

Figure 4.6 Workflow for the input module

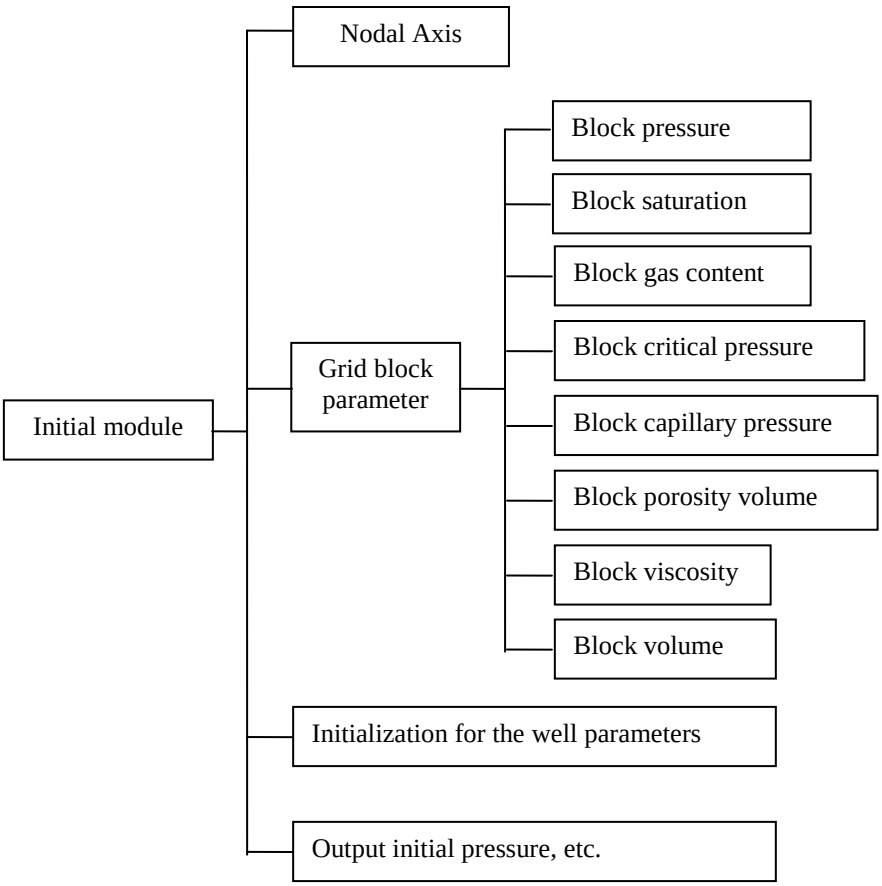

Figure 4.7 Workflow for the Initial module

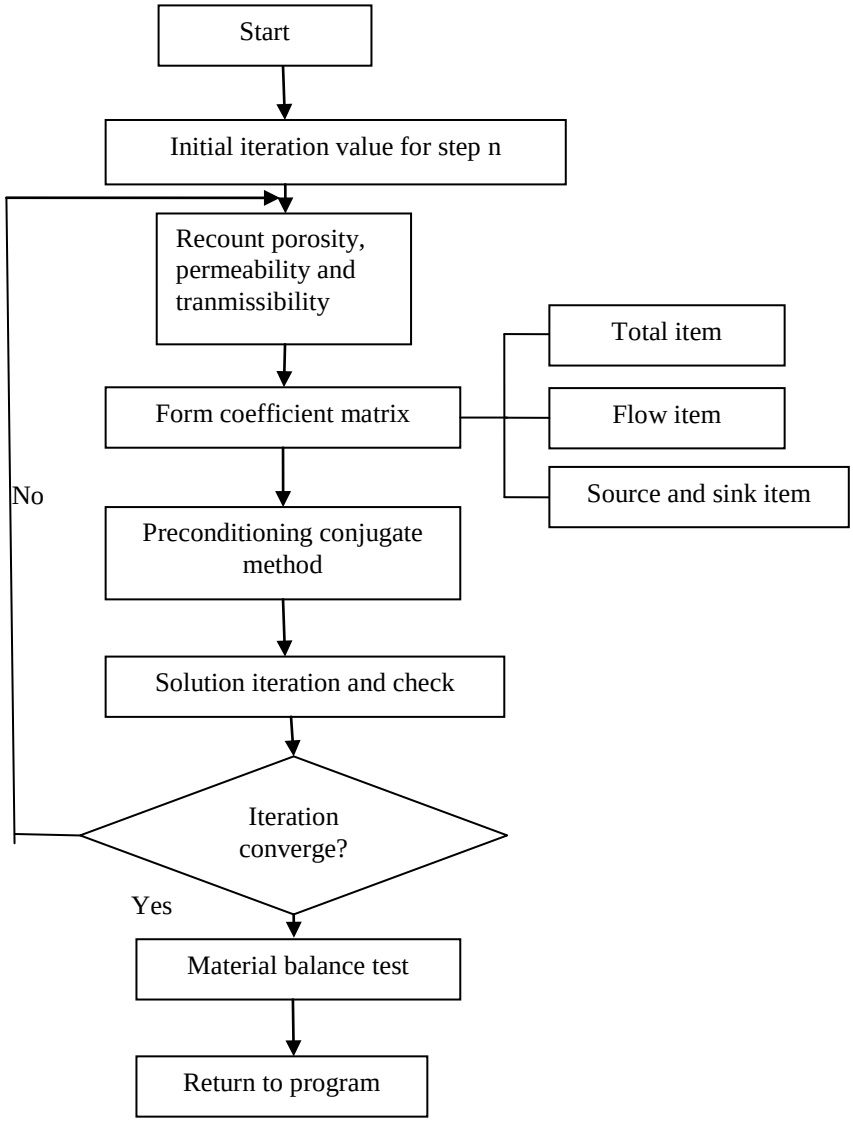

Figure 4.8 Workflow for the IMPES method

The relative permeability curve in this paper is shown in **Figure 4.9**. The geological reservoir model for single branch horizontal wellbore model and multi-branch horizontal wellbore model are presented in **Figure 4.10** and **Figure 4.11** respectively, which are got through connecting the TRIPLE-COAL to Eclipse. **Table 4.1** shows the main parameters come from the Yan Chuan southern block for this study.

The advanced coupled compositional triple porosity models proposed in this study are firstly tested against the basic triple porosity model developed by Reeves (**Scott, R. and Larry, P., et al., 2001[51]**). Both models were run using the same parameters as shown in **Figure 4.9** and **Table 4.1.** The agreement between the two models are better than expected, the relative error is only around 2.3%, which indicates the accurate and reasonable of the coupled horizontal wellbore model. Therefore, this model is considered to study the fluid flow in coal seams and the CO_2 displacement process.

	CBM production	CO_2 production
Coal depth m	857.2	457.2
Coal thickness m	5.85	3.85
Initial reservoir pressure Mpa	20.03	4.25
Initial water saturation fraction	0.92	0.52
Wellbore pressure Mpa	0.1	16.89
Matrix porosity fraction	0.24	0.24
Matrix permeability md	0.5	0.5
Fracture porosity fraction	1.0	1.0
Fracture permeability md	1.2	1.2
Water phase viscosity cp	0.58	0.58
Initial gas content m^3/t	10.0	10.0
Adsorption time day	35.0	35.0
Coal density t / m^3	1.3	1.3
Coal temperature K	328	328
Horizontal wellbore radius m	0.05	0.05
Horizontal wellbore skin factor	-1.5	-1.5
Horizontal wellbore branch radius m	0.035	0.035
Horizontal wellbore branch skin	-1.2	-1.2
Langmuir volume of CH_4 m^3/t	20.0	20.0
Langmuir pressure of CH_4 Mpa	3.68	3.68
Langmuir volume of CO_2 m^3/t	28.4	28.4
Langmuir pressure of CO_2 Mpa	1.8	1.8
Critical desorption pressure Mpa	5.63	-
Young's modulus E Mpa	2400	2400
Poisson's ratio ν fraction	0.34	0.34
Cleat volume compressibility 1/Mpa	7.05	7.05
Critical fracture porosity fraction	0.65	0.65

Table 4.1 Main parameters used in the study

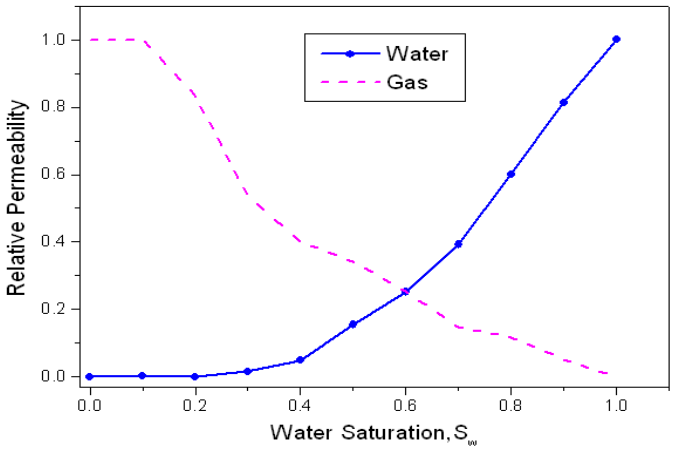

Figure 4.9 Relative-permeability curve for the study

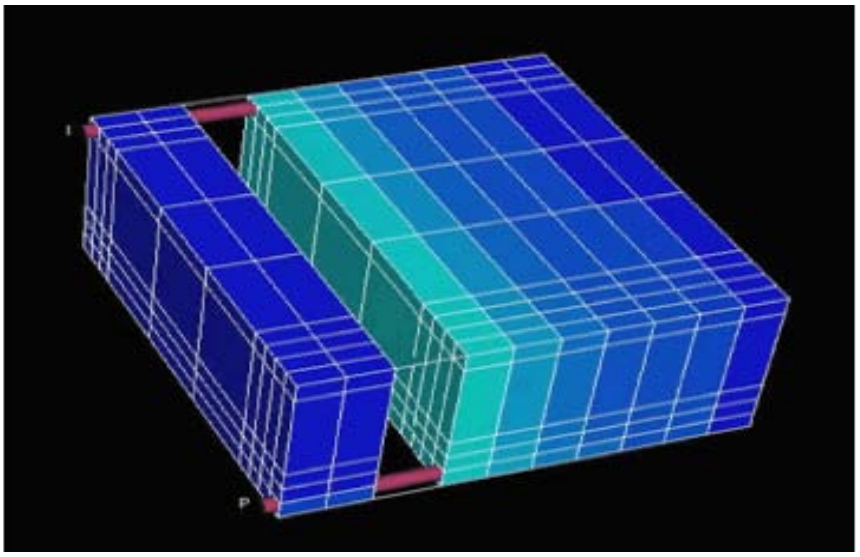

Figure 4.10 Model layout for the single branch horizontal wellbore model

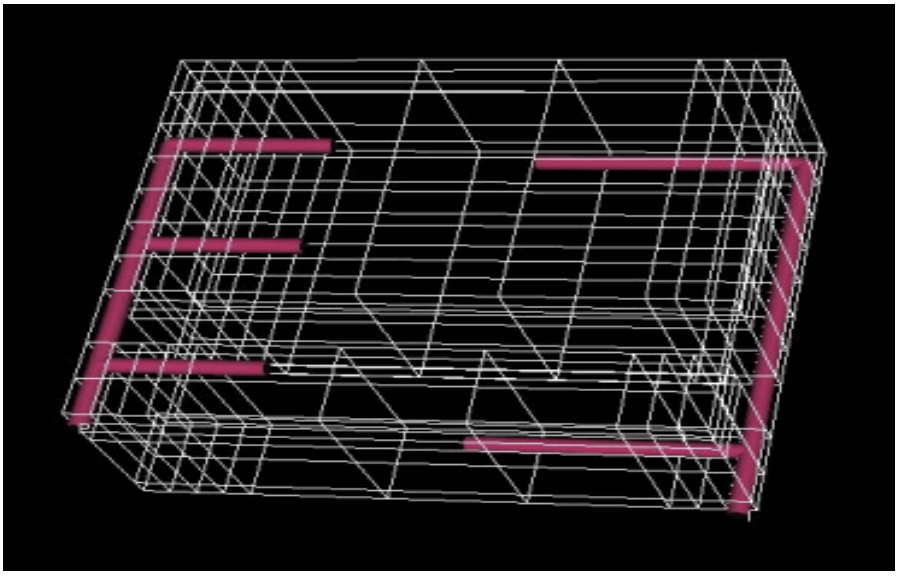

Figure 4.11 Geological model for the multi-branch horizontal wellbore model

4.5.1 Sensitivity analysis

4.5.1.1 Case study 1: comparison of dual and triple model

In order to make sure that the advanced triple porosity CBM reservoir model proposed in this study is superior to the conventional dual porosity, the comparison of the gas and water rate as well as the gas molar fraction changes is made between the dual porosity model and triple porosity model. The gas slippage effect and threshold pressure gradient effect as well the matrix shrinkage effect are all considered in both models.

Figure 4.12 presents the changes of the CO_2 production rate under the conventional dual porosity model and advanced triple porosity model. It is not hard to see that the simulation result of CO_2 production rate is much lower by triple porosity model than the conventional dual porosity model, which has a good agreement with the higher field gas

prediction rate using the dual porosity model. This indicates the field matching superiority of triple porosity model than the dual porosity model.

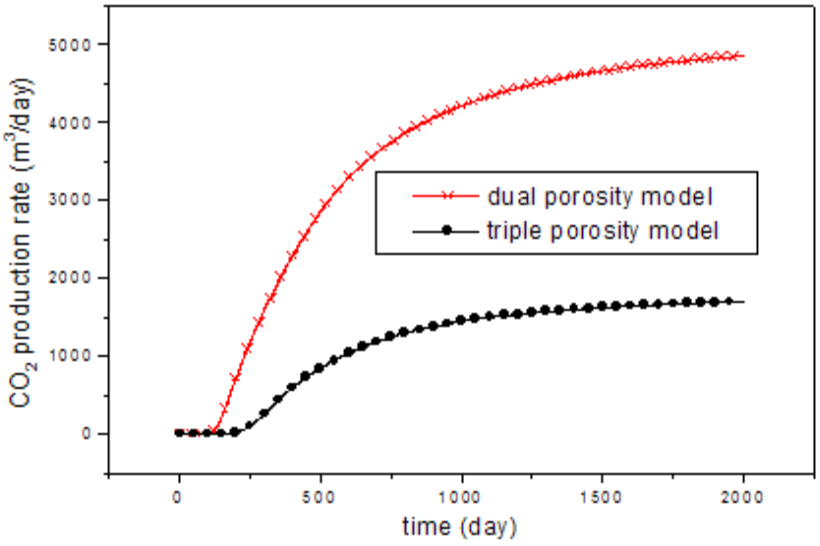

Figure 4.12 CO_2 rate from dual and triple porosity model

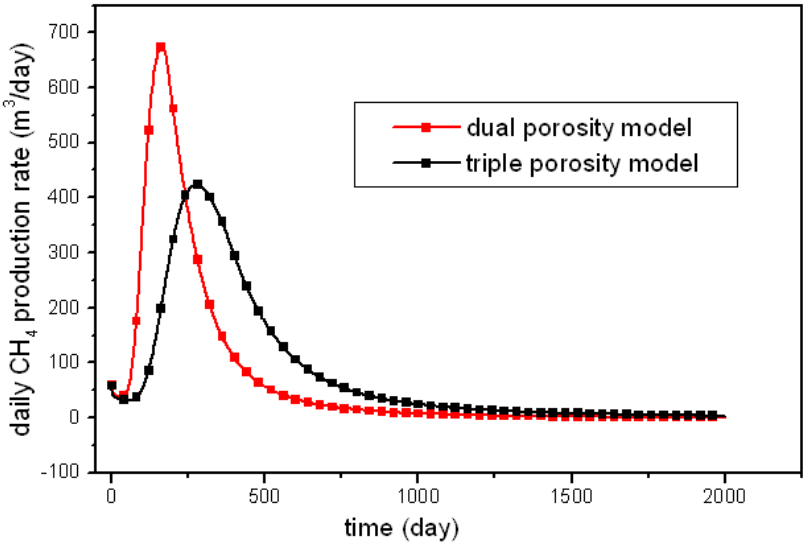

Figure 4.13 Daily gas rate of dual and triple porosity model

Figure 4.13 gives the simulation result of daily gas rate comes from the dual porosity model and triple porosity model respectively. The maximum daily gas production rate simulated from the dual porosity model is a little bit less than 700m^3/day, while it is only a little more than 400 m^3/day from the triple porosity model simulation result. In addition, it takes relatively longer time for the triple porosity model to get its gas maximum than the dual porosity model. However, the gas production rate for triple

porosity model is higher than the conventional dual porosity model after the daily gas production rate of triple porosity model reaches at its maximum, which can better explain the field prediction data (**Scott, R. and Larry, P., et al., 2001[51]**). Thus, triple porosity model can be accurately used for the prediction of the gas rate in the field.

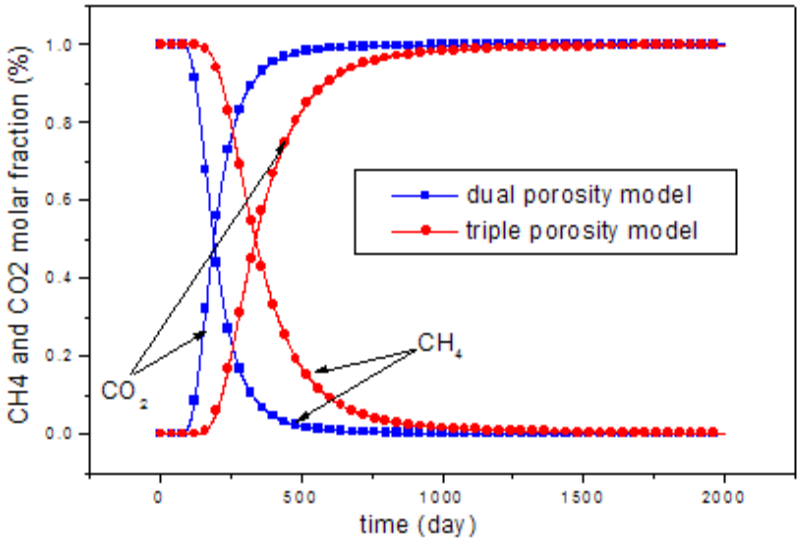

Figure 4.14 Gas molar fraction of dual and triple porosity

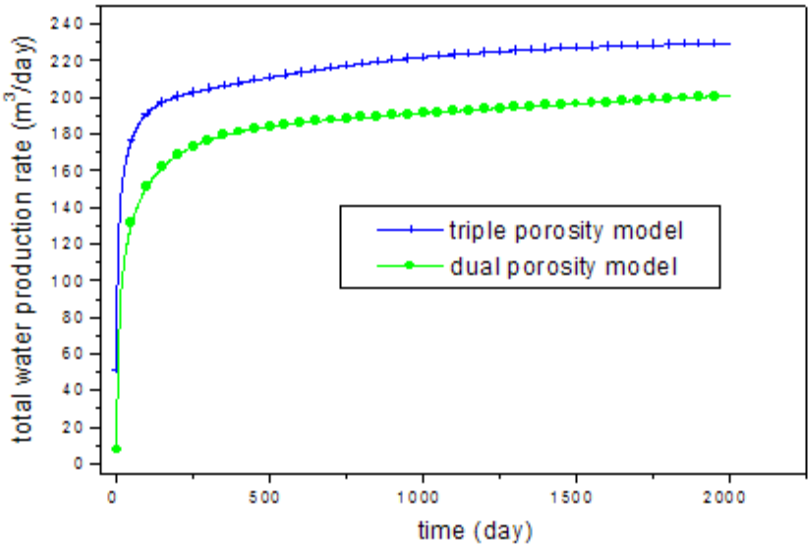

Figure 4.15 Total water rate of dual and triple porosity model

According to simulation result for the gas production rate of triple porosity and dual porosity model, it is easy to conclude that the drop speed of CH_4 molar fraction for the triple porosity model is slower than the dual porosity model initilally, and finally they

converge into one point. In addition, the CO_2 molar fraction rising speed of triple porosity model is also slower than the dual porosity model. As shown in **Figure 4.14**.

Figure 4.15 gives the total water production rate comes from the dual porosity model and triple porosity model respectively. The water production rate simulated by the triple porosity model is higher than dual porosity model, which is contrary to gas production rate trend. This results can again explain the lower water production rate and higher gas production rate from the field observation (**Scott, R. and Larry, P., et al., 2001[51]**). In a word, triple porosity model is much more robust and reasonable for the simulation of CBM reservoir.

4.5.1.2 Case study 2: Comparison of three well types

The comparison of the result comes from basic vertical well triple porosity model, coupled single branch horizontal wellbore triple porosity model and coupled multi-branch horizontal wellbore triple porosity model is made, in order to study the effect of different well types on the gas and water production rate for triple porosity model.

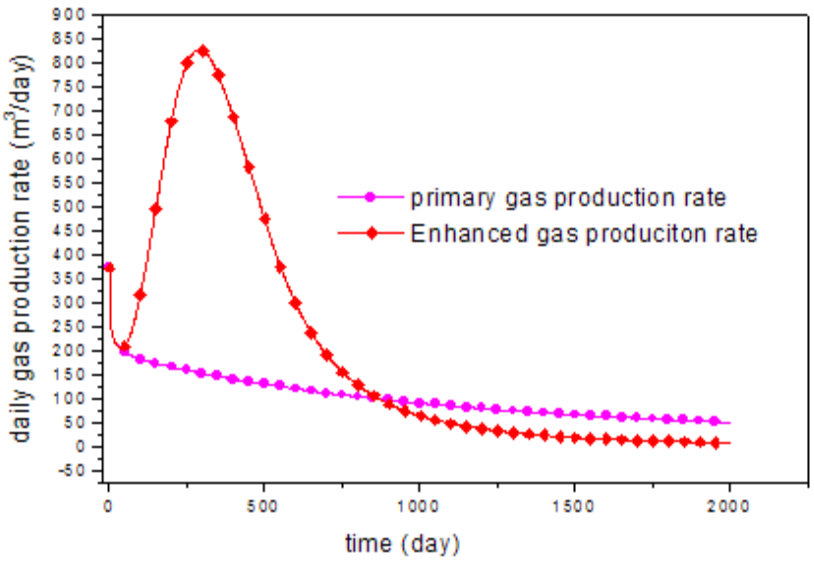

Figure 4.16 Primary and Enhanced gas rate

Firstly, the primary daily gas production rate and the enhanced daily gas production rate are simulated by the basic compositional triple porosity model in horizontal well type, as illustrated in **Figure 4.16**. It is easy to see that the primary daily gas rate is much lower compared with the enhanced daily gas rate. The maximum daily gas rate for the primary production stage is only about 200m^3/day, while it can be around 825m^3/day for enhanced stage. What is more, the primary daily gas rate gradually decreases during

the whole production time, it is about 50 m^3/day after 2000 days production; while the enhanced daily gas rate initially gradually decreases from 375 m^3/day to about 200 m^3/day, and then it increases little by little for the next 300 days until it reaches its maximum, since then it begins to decreases until there is nearly no gas in the reservoir. Thus it can be concluded that the triple porosity model proposed in this study can pump most of the gas in the reservoir, which is very important for the field exploration.

The daily water production rate simulated by the multi-branch horizontal well model is the highest compared to the other two well types as shown in **Figure 4.17**. It drops from around 75 m^3/day to only about 48 m^3/day in the first few days production, then it gradually increases to 55 m^3/day for the next 10 days, since then it begins to decrease until its rate is 5 m^3/day after 4000 days production. The simulation results for the other two well types model have the similar trend, but with lower water production rate. In addition, the daily water production rate is nearly the same for the three well types after 4000 days production.

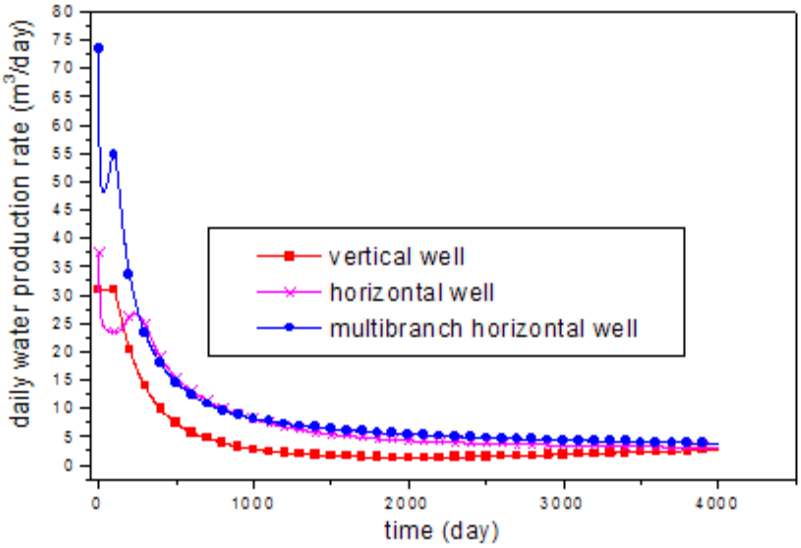

Figure 4.17 Daily water rate under three different models

Figure 4.18 shows the total CH_4 production rate of three different well type models. The difference of total CH_4 production is not very obvious for the initial 300 days, while after that the multi-branch horizontal well type shows distinguished enhanced gas rate. For example, the total CH_4 produciton rate is about 8.0E5m^3 for vertical well type after 4000 days production, while nearly 1.1E6m^3 for single branch horizontal well type and 1.9E6m^3 for multi-branch horizontal well type. The gas rate result from the multi-branch well model is 42% enhancement than single branch horizontal well type, and

58% improvement than vertical well type. This can perfectly explain the changes of the molar fraction under different well models: the drop speed of CH_4 is faster for multi-branch horizontal well type than others, the corresponding increasing speed of CO_2 is also larger than others, as shown in **Figure 4.19**.

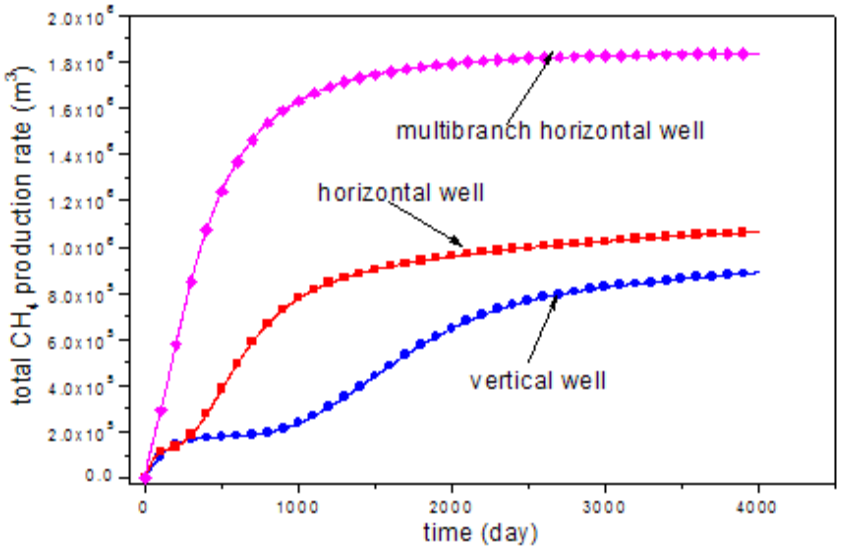

Figure 4.18 Total CH_4 production rate under three different models

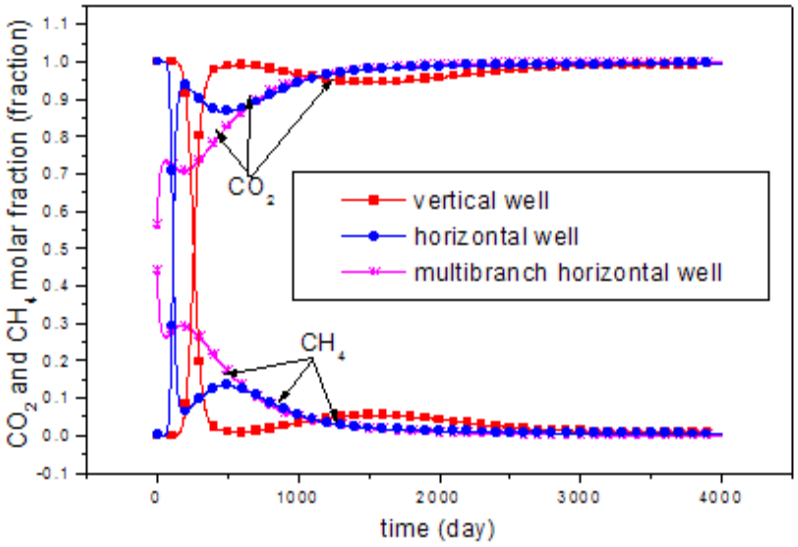

Figure 4.19 Gas molar fraction under three different models

4.5.1.3 Case study 3: branch angle and branch number

As illustrated above, the multi-branch well type model is considered as the most productive one for the gas and water production in the simulation, thus followed that the best branch angle and branch number need to be found out for better field application.

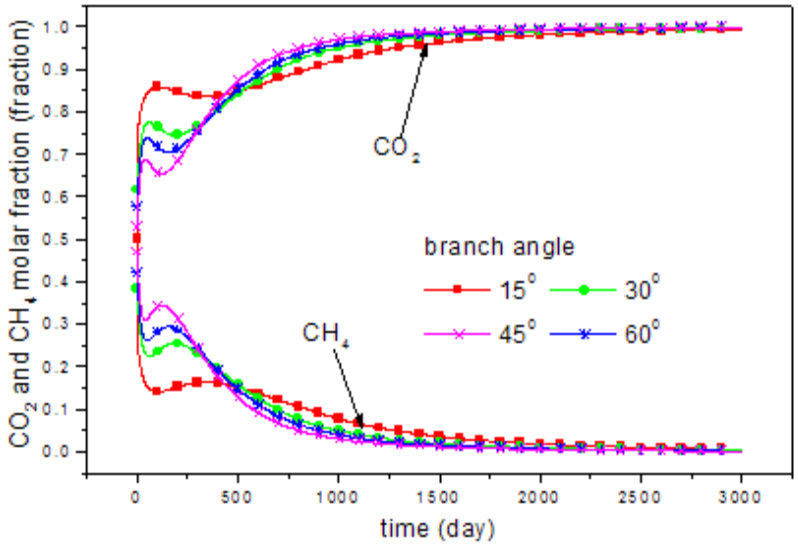

Figure 4.20 Molar fraction under different branch angles

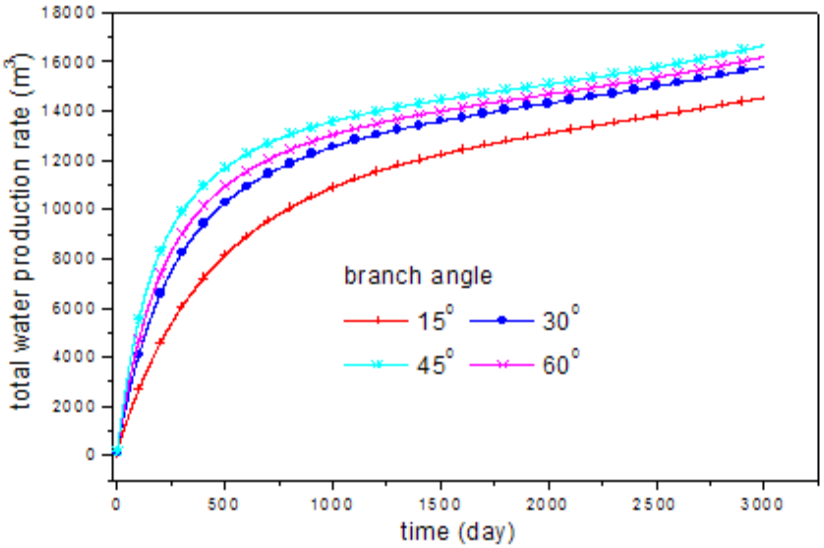

Figure 4.21 Total water rate under different branch angles

Figure 4.20 presents the effect of branch angle on the CO_2 and CH_4 molar fraction. The decreasing scale of CH_4 molar fraction is the smallest with angle 45 degree initially (around the first 100 days), while since then its drop speed is much faster than the other

cases as shown in the figure. This is attributed to the relatively higher gas and water rate with angle 45 degree (as shown in **Figure 4.21**, which illustrates the effect of different branch angle on the total water production rate). For angle 45 degree can open larger control area than the other angles.

The changes of CO_2 has the similar phenomena, however, the molar fraction of CO_2 increase with the simulation time. Because it has stonger adsorption rate than the CH_4, and the production of CO_2 happens after most of the CH_4 is pumped out. From this point, it can be concluded that angle 45 degree for the multi-branch model is the best choice for the field application.

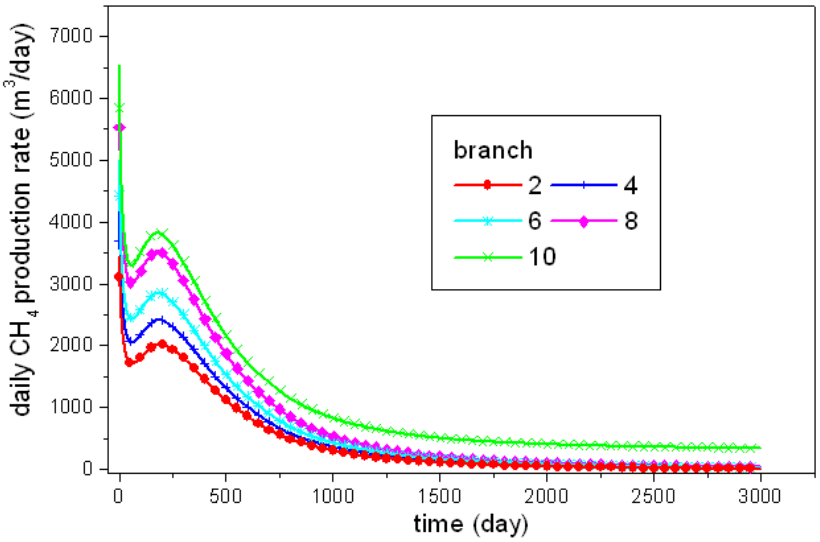

Figure 4.22 Daily gas rate under different branches

Figure 4.22 depicts the variation of daily gas rate with different branches. As shown in the figure, the daily gas rate increases with the branch number, while the rising scale from branch 8 to 10 is lower than that from branch 6 to 8. Additionally, the daily CH_4 production rate is still around 500 m^3/day with branch number 10 after 3000 days' production, while it is nearly zero with branch number 2,4,6,8, which means that most of the water in the reservoir is produced. From this result it is easy to see that branch number 8 gives the best simulation result.

The similar conclusion can also be got from **Figure 4.23**, which gives the water and gas ratio changes under the effect of branch number. The water and gas ratio also increases with the branch number, however, there exists no difference in the water gas ratio

between branch number 8 and branch number 10. Thus branch number 8 is again the best choice for simulation from the economic point.

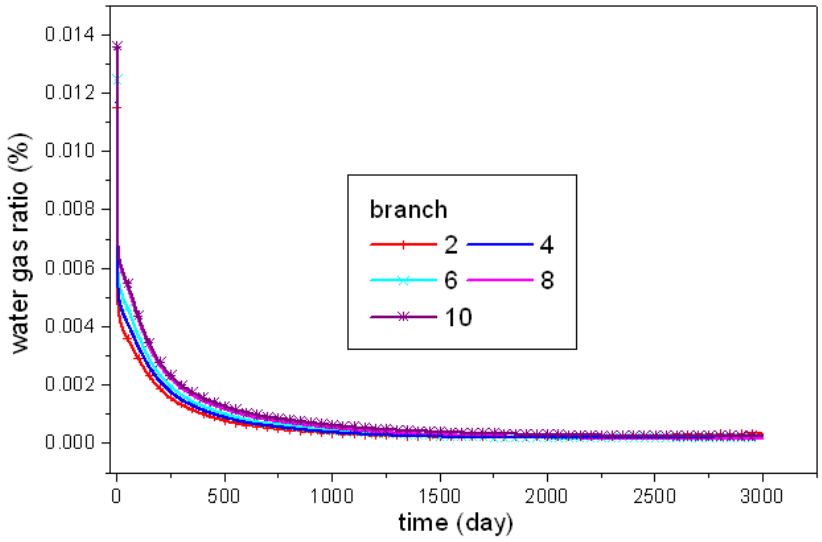

Figure 4.23 Water gas ratio under different branches

4.5.1.4 Case study 4: Effect of fluid parameters

According to the above investigation, it is found that branch number 8 and branch angle 45 degree is the best during the simulation for the multi-branch horizontal wellbore model. Thus the effect of fluid parameters on the gas and water production rate with branch number 8 and branch angle 45 degree is conducted in this part for this model.

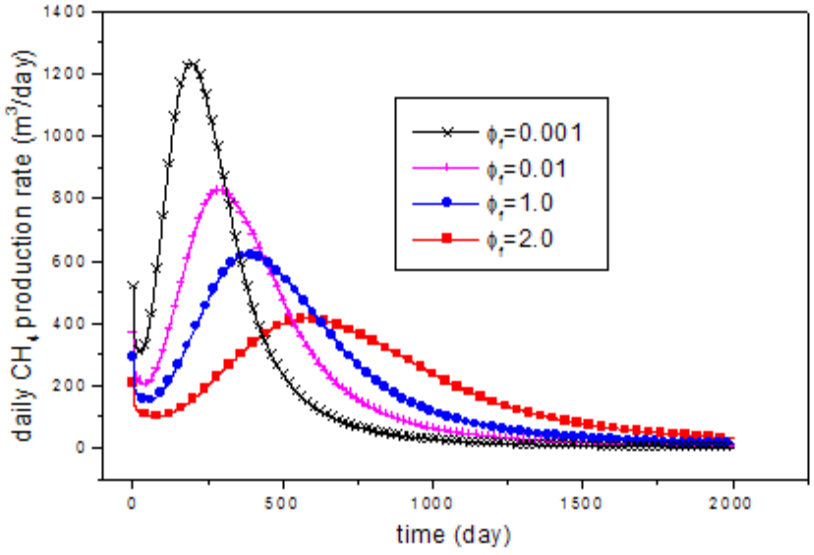

Figure 4.24 Effect of fracture porosity on the daily CH_4 rate

Figure 4.24 shows the daily CH_4 production rate changes under different fracture porosities. Its maximum production rate is the highest when the fracture porosity is 0.001, while is the lowest with fracture porosity 2.0. What is more, the maximum production rate is earlier to be reached with smaller fracture porosity than the relatively larger fracture porosity. This is because the water content is lower with smaller cleat porosity, which makes the pumping water time shorter and enhances the pressure depletion in the reservoir. However, this trend is reversed after the daily CH_4 rate gets its maximum, which is caused by the larger residue gas content with bigger porosity.

Figure 4.25 shows the variation of total water production rate under different cleat permeability. As shown in the figure, it increases with the cleat permeability, and, its value is nearly the same when the cleat permeability is equal to 0.8 with the case when the cleat permeability is 1.0 during the late stage simulation, but it is still a little bit higher with cleat permeability equal to1.0 than with cleat permeability equal to 0.8. This is because the larger cleat permeability can give wider path for the gas and water phase to flow.

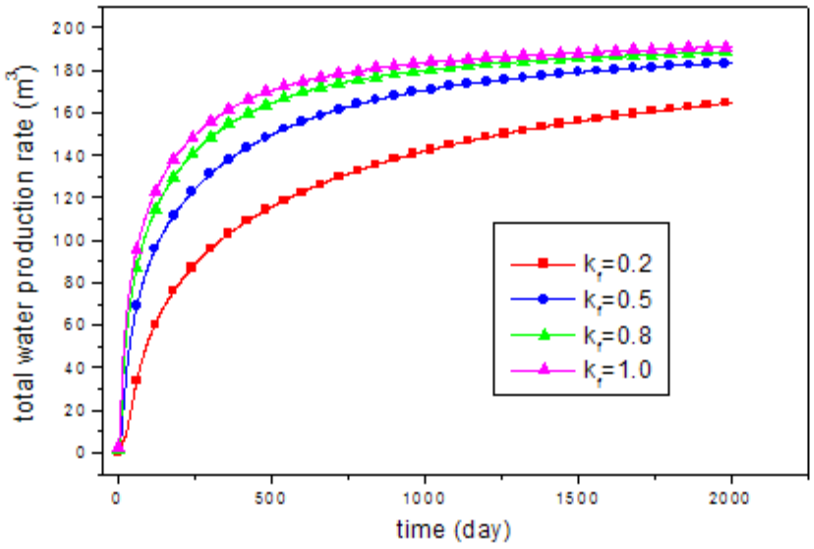

Figure 4.25 Effect of cleat permeability on total water rate

Figure 4.26 and **Figure 4.27** give the CH_4 production rate variation trend under the impact of the Langmuir pressure and Langmuir volume. It can be that the Langmuir pressure and volume show noticeable effect on the gas production in the middle production stage. And the gas rate increases with the Langmuir pressure, while decreases with Langmuir volume. This is caused by the larger desorption rate with larger Langmuir pressure and smaller Langmuir volume.

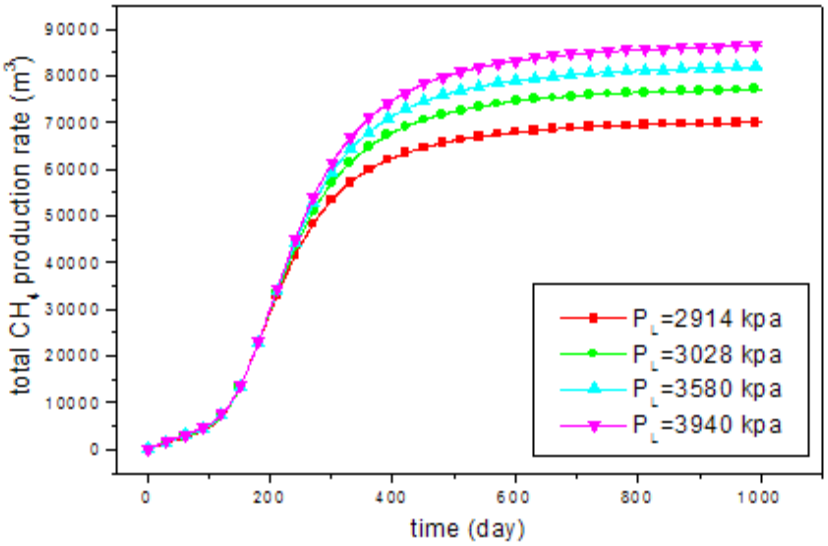

Figure 4.26 Effect of Langmuir pressure on total CH_4 rate

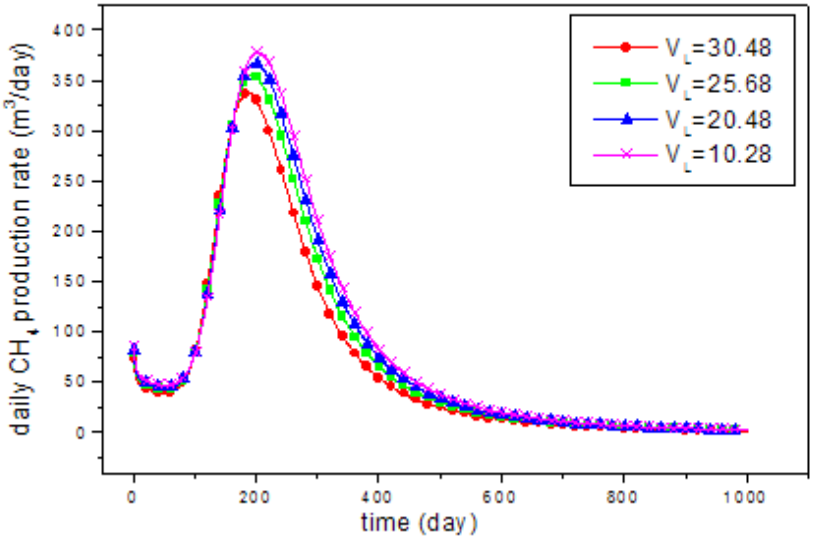

Figure 4.27 Effect of Langmuir volume on the daily CH_4 rate

4.5.1.5 Case study 5: Threshold pressure gradient and gas slippage effect

The impact of threshold pressure gradient, gas slippage and matrix shrinkage/swelling on the gas and water rate is particularly interest here.

Figure 4.28 shows the daily CH_4 production rate changes with the gas slippage factor. Here, $\beta_1 = 0$ means the gas slippage factor is ignored. As shown in the figure, the gas rate increases with the value of β_1 during the initial and middle stage. And the larger the β_1, the later for the gas to reach its maximum rate. Furthermore, the rising scale of

the daily gas rate is strongly influenced by β_1: rising from around 1750 m^3 /day to nearly 2500 m^3 /day as the gas slippage factor β_1 increased from 85 to 165. While β_1 has nearly no effect on the gas rate in the late stage, for he gas production rate curve converges to one point since around 3000 days. This simulated result is consistent with the fact that the reservoir permeability can be enlarged by considering the gas slippage effect.

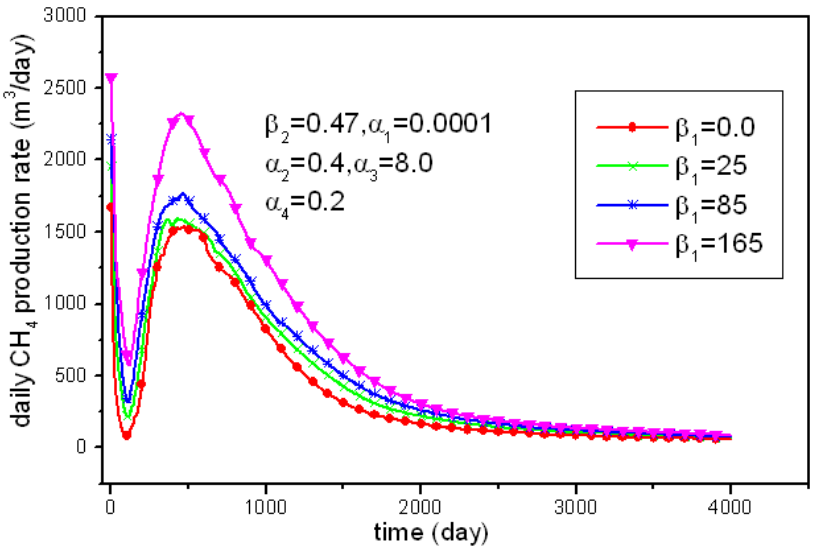

Figure 4.28 The impact of β_1 on daily gas rate

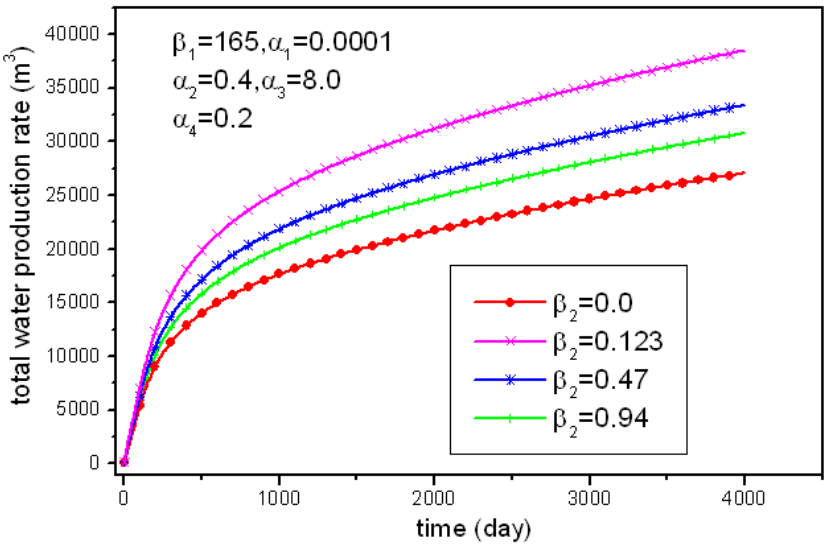

Figure 4.29 The impact of β_2 on total water production rate

The impact of gas slippage factor β_2 on the total water production rate has the opposite trend, as shown in **Figure 4.29**, because the gas slippage increases with the decreasing of β_2. Obviously, the total water production rate is the smallest if the gas slippage effect is ignored. In addition, the rising scale of it is the smallest when β_2 drops from 0.94 to 0.47, while the largest when β_2 decreases from 0.47 to 0.123.

Figure 4.30 shows the pressure changes under the gas threshold pressure gradient factor α_1. Again, here $\alpha_1 = 0.0$ implies that the gas threshold pressure gradient is not considered. As can be seen from the figure, there is a drastic fall in the pressure when $\alpha_1 = 0.0$, and the pressure increases with α_1. What is more, the rising scale of permeability is the biggest as α_1 increased from 0.0004 to 0.0006, and smallest when α_1 went from 0.0004 to 0.0006. The result is just in line with the fact that water and gas have to overcome the threshold pressure gradient before it can flow, which leads to the lower water and gas rate and results in the much slower pressure drop.

The daily CH_4 production rate decreases with the increasing parameter α_2 (the gas threshold pressure gradient parameter) initially, as shown in **Figure 4.31**. While this effect is not obvious after the daily gas production rate reaches it maximum, thus it can be concluded that α_2 have small effect on the daily gas production in the late stage.

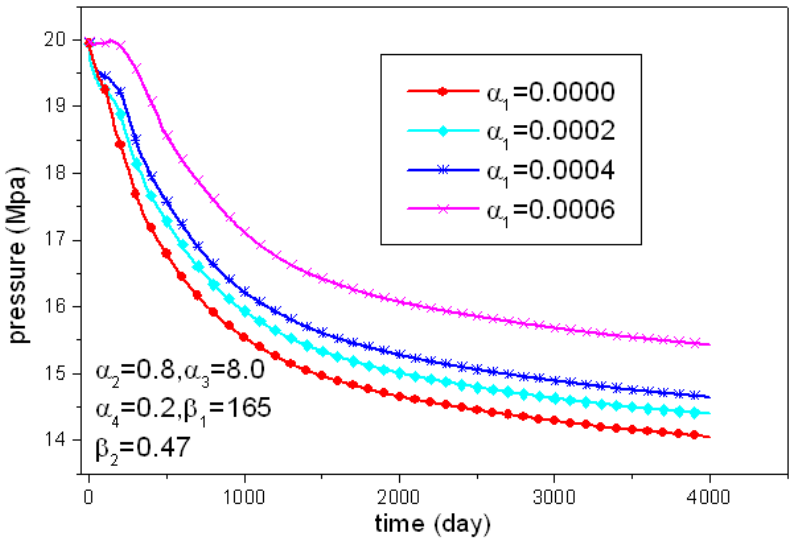

Figure 4.30 The impact of α_1 on the pressure changes

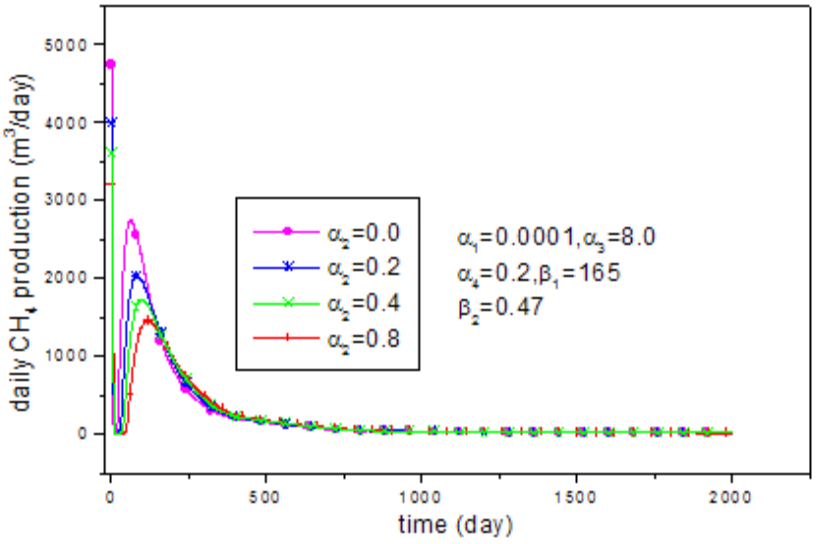

Figure 4.31 The impact of α_2 on daily CH_4 rate

4.5.1.6 Case study 6: Matrix shrinkage /swelling effect

The permeability model proposed in this study requires four parameters except for the Langmuir constant: E, ν, c_f, ϕ_{fr} as input for the CBM reservoir. The initial value for the parameters is shown in **Table 4.1**. Permeability behavior of the CBM reservoir around the producing well and injecting well under different CO_2 molar fraction and critical fracture porosity are studied. Results are shown in **Figure 4.32**, **Figure 4.33** and **Figure 4.34** respectively.

Figure 4.32 shows the molar fraction variation under the model considering the permeability changes and ignoring the permeability changes respectively. The noticeable CO_2 break through is observed around after 500 days production for both cases. It is obviously to see that the methane molar fraction decreases faster (after around 100 days production) with permeability calibrated model than the common advanced horizontal wellbore model, and the corresponding carbon dioxide molar fraction increases quicker. This is because the matrix shrinkage effect is stronger than the stress effect during the simulation process.

Figure 4.33 indicates that the permeability performs an obvious rebound after its initial decline, and will reach its initial value (around 0.98md) when the pressure decreases to 5.6Mpa, then increases to nearly 10md when the pressure is very low, nearly 10 times of its initial value. While for the injection well, shown in **Figure 4.34**, the permeability drops obviously around the well with the CO_2 injection. Moreover, it is strongly

affected by the critical fracture porosity ϕ_{fr}. For example, when the pressure is equal to 20.0 Mpa, it drops from 2.0md to 0.02md with the critical fracture porosity decreases from 0.45 to 0.2(**Figure 4.34**).

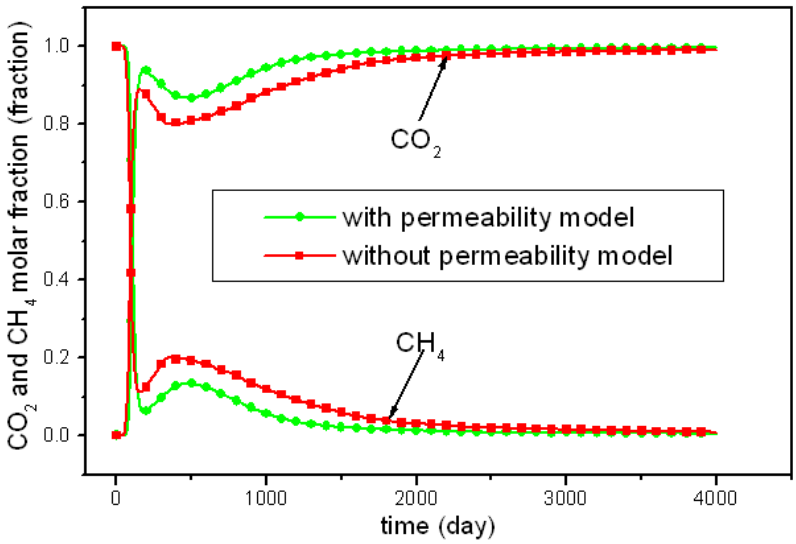

Figure 4.32 The effect of permeability model on the gas composition

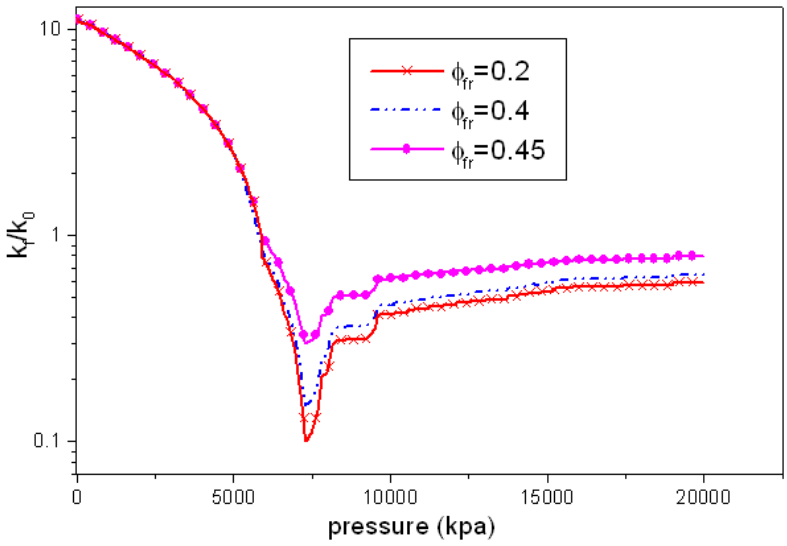

Figure 4.33 Permeability behaviour for the producing well (YCO_2=0.01)

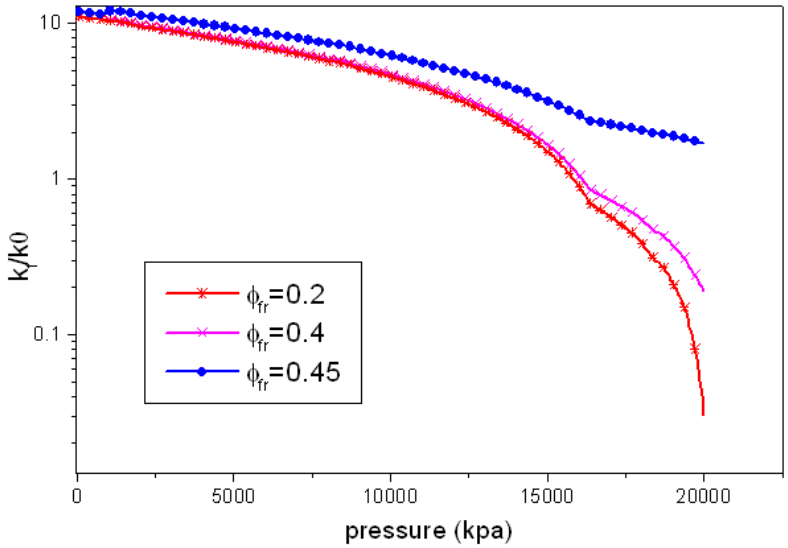

Figure 4.34 Permeability behaviour for the injecting well (YCO_2=0.98)

4.6 Field application

The well yan1-22-10 is a production well located in Yanchuan Southern, and it drills through ZhongTong majiagou group (O_{2s}), FengFeng group (O_{2f}), Carboniferous ZhongTong existing group (C_{2b}),Stockings on Taiyuan formation (C_{3t}), Permian next tasseled Shanxi groups(P_1s), Xiashihezi group (P_1x), Permian stockings on stone box group (P_2s), Shiqianfeng group (P_2sh), Triassic next tasseled Liujiagou group(T_{11}), Cainozoic neogene on new stockings group (N_2) and Quaternary system next update tasseled (Q_1).

The 2# coal seam in Stockings on Taiyuan formation (C_{3t}) is the main coal bearing sequences, the thickness and the burial depths of it is listed in **Table 4.1**. As can be seen from the table, the thickness of 2# coal seam can be nearly around 6.0m, which results in the existing of 1 to 3 layers waste rock inside the coal seam. The development of the studied coal layer is stable, and it has produced some commercial gas flow, which indicates its potential prospects for exploration. Moreover, it is low rank anthracite coal, the coal body has a simple structure and mainly contains the bright coal.

The roof and floor of 2# coal seam are composed of mudstone and sandstone with low permeability. The sandstone is very tight and then can provide a good conservation conditions for Coalbed Methane. There also exists a big set of developing mudstone under the 2# coal seam, which makes it independent from other coal layers during the

production process. Thus rainfall becomes the main supplier for the ground water and coal seam.

Well #10 is the injection well located in the opposite angles of production well yan1-22-10, the injection rate and well bottom-hole pressure are shown in **Figure 4.35**.

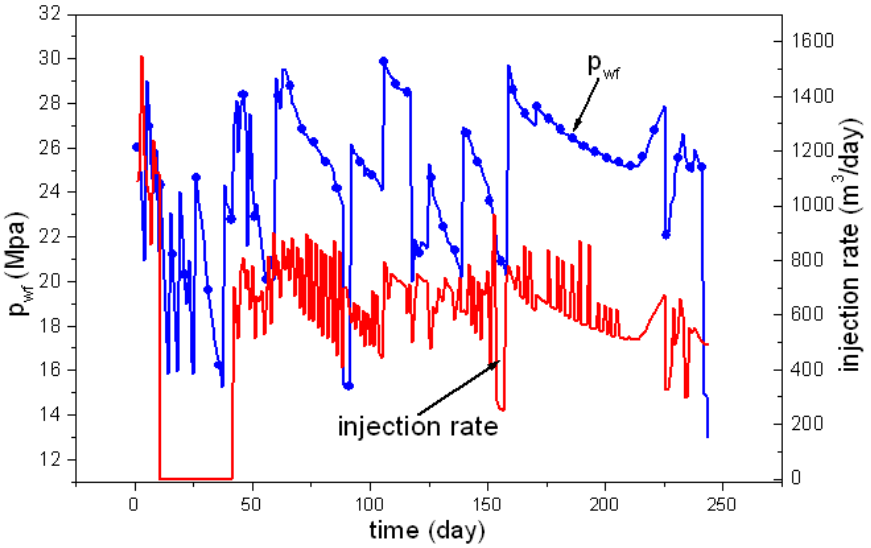

Figure 4.35 Injection rate and bottom-hole pressure of well #10

The related reservoir parameters are initially captured through build up/down well test and the coal sample adsorption/desorption experiment, following that the completed production data are observed after implementing fracture and injection technology on this well.

The observed data for well yan1-22-10 and well #10 from 18th, November, 2010 to 18th, August, 2011 is utilized for the history matching, which are totally 244 days. The TRIPLE-COAL simulator is used for the history matching.

The producer yan1-22-10 is shut in during the first 40 days of CO_2 production, the injectors were then shut in for the other 40 days. The well #10 experiences substantial CO_2 injection rate drops following shut in. It drops from the initial high value of around1400 m^3/day to less than 600-800 m^3/day, as shown in **Figure 4.35**, a total reduction of around 46%.

The availability of the gas, water rate and well block pressure enables the determination of critical fracture porosity ϕ_{fr} , gas slippage factor and threshold pressure gradient factor in a direct manner through history matching. It was found that critical fracture porosity

0.2, gas slippage factor $\beta_1 = 165, \beta_2 = 0.123$, and threshold pressure gradient factor $\alpha_1 = 0.002, \alpha_2 = 0.4, \alpha_2 = 0.65, \alpha_2 = 0.16$, branch number 8 and branch angle 45 degree give the best overall match for well bottom-hole pressure. This has good agreement with the simulation result shown above in sensitivity analysis part.

The history matching result for well #10 is shown in **Figure 4.36**. It is easy to see that the matching result between simulated result and observed data is better than expected. And the well block pressure is also plotted in this figure for comparison, it obviously experiences continuous downward trend throughout the injection period. This implies that the relatively higher well bottom-hole injection pressure is needed for the maintaining of injection rate.

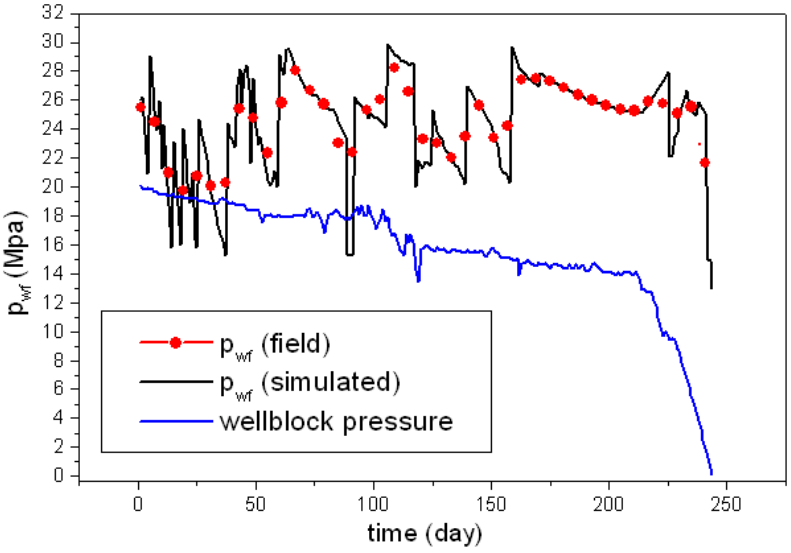

Figure 4.36 History matching of well bottom-hole pressure for well #10

The success in history matching the injection bottom hole pressure at well #10 shows the accuracy and reasonable of the permeability model proposed in this study. It is also worth to point out that the permeability is more sensitive to the critical fracture porosity after the CO_2 reaches the breakthrough time, where the gas composition of CO_2 is relatively higher.

Figure 4.37 and **Figure 4.38** show the history matching result of gas and water rate for production well yan1-22-10. They show an excellent agreement with the field data, the relative overall error is less than 2.8%. In addition, the gas and water production rate is still showing increasing trend after the simulation process, and imply that the well is still in the recovering process.

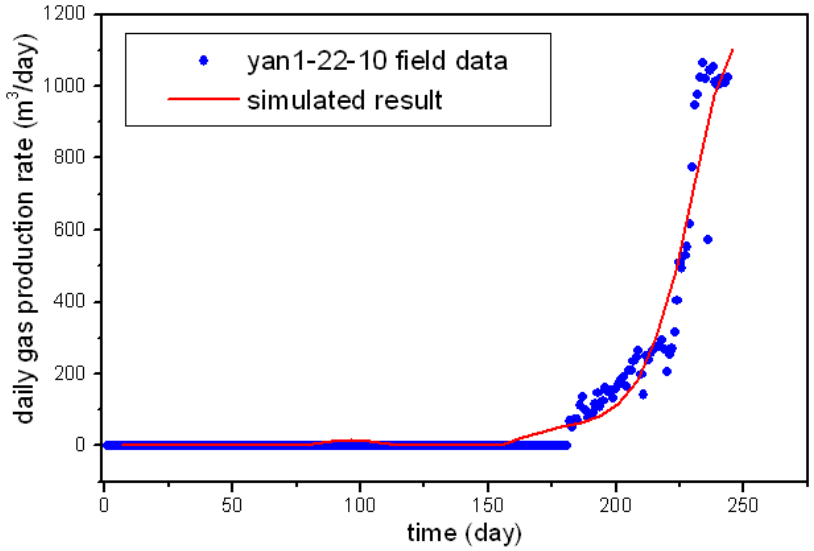

Figure 4.37 History matching of daily gas rate for yan1-22-10 well

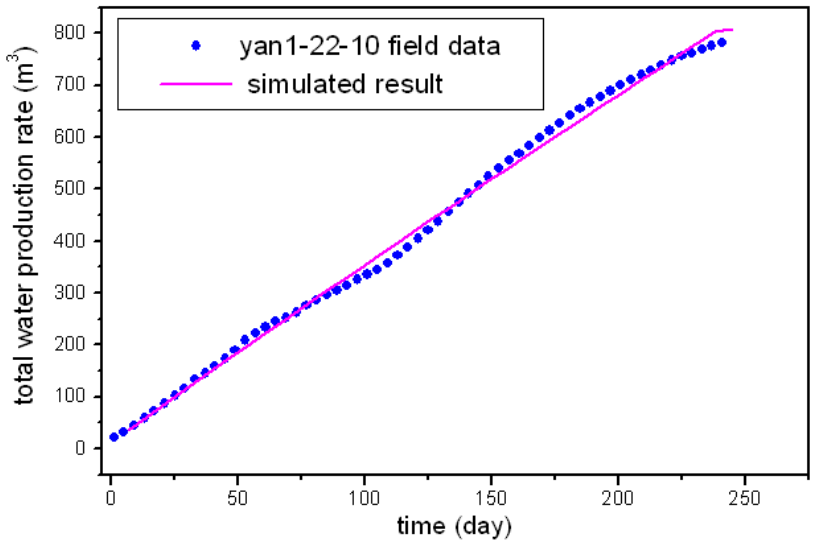

Figure 4.38 History matching of total water rate for yan1-22-10 well

Figure 4.39 shows the variation of well block permeability during the production time of well yan1-22-10. The permeability gradually decreases for the first 98 days, goes from 2.0md to around 0.25md, then it performs as the upward trend, gradually goes from 0.25md to 0.5md. This indicates that the stress effect is the leading role for permeability changes initially, and following that the matrix shrinkage effect is stronger than the stress effect. In addition, this simulation results is just in line with the result from theory study, which again validates the accuracy and reasonability of the permeability model for this particular field application.

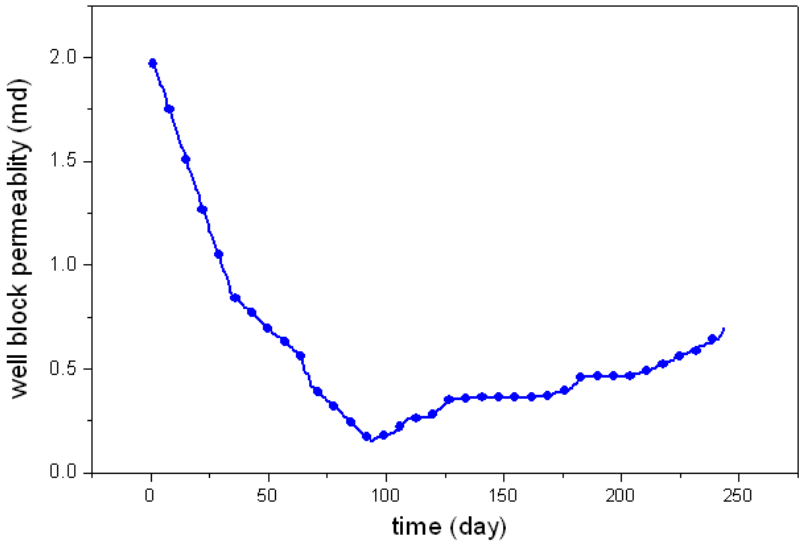

Figure 4.39 Wellblock permeability behaviour for yan1-22-10 well

4.7 Chapter Conclusions

(1) This paper has developed a novel permeability model based on the surface energy theories, to focus on the impact of matrix shrinkage/swelling on ECBM production. Follow that a coupled compositional triple porosity horizontal wellbore model for CBM reservoir, considering the gas slippage and threshold pressure gradient effects is proposed. And it is solved through modified IMPES method originally used for block oil model, then the simulator called TRIPLE-COAL is developed using Fortran program.

(2) The simulation results show that the triple porosity model has great superiority than the dual porosity model, which can much more accurately simulate the field data. In addition, the multi-branch well type model can largely enhance the gas and water rate, especial when the branch number is chosen as 8 and branch angle is 45 degree.

(3) The gas production rate decreases with the cleat porosity before it reaches its maximum rate, while the trend is reversed after this period. Because the initial water content is lower with smaller cleat porosity than with larger cleat porosity, and the residual gas content is bigger with larger cleat porosity. Additionally, the gas production rate increases with the cleat permeability owing to the larger flowing path for the gas provided by bigger cleat permeability. Bigger desorption rate can enhance the gas rate, and it increases with Langmuir pressure, decreases with Langmuir volume.

Thus the gas rate rises with the increasing of Langmuir pressure and drops with the increasing of Langmuir volume.

(4) The gas slippage effect can only improve the gas and water rate in the early and middle stage, while the threshold pressure gradient effect can influence the pressure during the whole production process. The larger the threshold pressure gradient, the slower the pressure drop. Moreover, the gas molar fraction rising speed is faster when the permeability model is applied to the advance coupled triple porosity model after around 100 days' production, which means the matrix shrinkage effect is stronger than the stress effect during this process. The critical fracture porosity ranging from 0.2 to 0.45 has dramatic effect on the permeability for injection well, while relative marginal effect for production well.

(5) It was found that the critical fracture porosity 0.2, the gas slippage factor $\beta_1 = 165, \beta_2 = 0.123$ and the threshold pressure gradient factor $\alpha_1 = 0.002, \alpha_2 = 0.4,$ $\alpha_2 = 0.65, \alpha_2 = 0.16$, branch number 8, branch angle 45 degree give the best overall match through history matching of injection well bottom hole pressure, which further validate the accuracy of the model proposed in this Chapter. What is more, the history matching results for gas and water rate in the production well show excellent agreement between simulated result and observed data. Additionally, the well block permeability behavior for production well further validates the accuracy of the permeability model proposed in this Chapter.

Chapter 5 Well testing method for the triple porosity CBM reservoir model

5.1 Background

The accuracy and reasonability of the triple porosity model has been validated in **Chapter 4**, and the sensitivity analysis of the fluid parameters as well as the field application had also been done based on that model. Transient testing is especially a useful tool in managing CBM reservoirs, however, we don't have enough information from actual field data to determine if the permeability will increase or decrease with decreasing pressure and to what extent. Therefore, the study for its well testing method needs to be done in order to investigate the pressure changes or logarithm pressure changes and determine the cleat permeability, which is a very important parameter in forecasting the production rate of CBM wells. This chapter provides a systematic study of the well testing method for the triple porosity CBM reservoir model.

As studied earlier, there are mainly three types of well testing methods for interpreting the multi-phase flow: total mobility method (P-M method), pseudo pressure approach and pressure square method. Some people had applied the total mobility method into the interpretation of multi-phase well testing for CBM reservoir, however, only the total mobility λ_t can be got through the well testing interpretation method, this is because the relative permeability data is difficult to get through well testing for CBM wells. Also, some scholars (**Kamal, M.M. and Six, J.L., 1989[23]**) try to use the pseudo pressure method to interpret the parameters in CBM reservoir, and their pseudo pressure solution for the two phase CBM wells is based on the two phase model of Raghavan (**Raghavan, R., 1989[29]**), its definition is:

$$p_{pod} = 2\int_{p_{ref}}^{p}\left(\frac{k_{rg}}{\mu_g z_g}+\frac{k_{rw}}{\mu_w z_w}\right)pdp \tag{5.1}$$

Kamal and Six assumes a fast diffusion of gas upon desorption from the coal micro-pores and neglects gravity and capillary effects. The desorption compression coefficient is calculated through the isothermal adsorption line. The final diffusivity equation for the system is written as:

$$\frac{1}{r}\frac{\partial}{\partial r}\left(r\lambda_t\frac{\partial p_{pod}}{\partial r}\right)=\phi C_t\frac{\partial p_{pod}}{\partial t} \tag{5.2}$$

In addition, another assumption in Kamal and Six's model is: the gas saturation in any portion of the reservoir below desorption pressure will continue to increase until the gas flow rate from that portion is equal to the gas flow rate into it (**Ayan, C. and Lee, W.J., 1986[27]**):

$$\frac{k_{rw}}{k_{rg}} = \frac{v_w}{v_g}\frac{\mu_w}{\mu_g} \tag{5.3}$$

This condition is only limited to the case when the gas desorption rate in the CBM reservoir is very fast.

What is more, the isothermal adsorption line data and the relative permeability data are required for the pseudo pressure method, but they are really difficult to get in CBM reservoir. For example, the cleat system relative permeability data can only get through history matching, no way by experiment, only the matrix system relative permeability data can be got through experiment test.

The pressure square method for the three phase (oil, gas and water) reservoir was proposed (**AI-Khalifah, A-J.A., et al., 1987[22]**), the final equation used for well testing is as follows, which is derived based on the oil dominated method:

$$\nabla^2 p + \nabla p.\nabla[\ln[\frac{k_o}{\mu_o B_o}]] = \frac{\phi C_t}{\lambda_t}\frac{\partial p}{\partial t} \tag{5.4}$$

There is no oil in the CBM reservoir, so the derivation for the well testing method shouldn't be oil dominated. In addition, the relationship between $\frac{k_o}{\mu_o B_o}$ and pressure can't be directly applied to the gas and water phase in the CBM reservoir. Thus the conventional pressure squared well testing method should be modified before it can apply to the CBM wells. Some people (**Hu, X.H., et al., 2011[152]**) had modified the pressure squared to CBM reservoir based on the dual porosity single permeability model. However, the well testing method for triple porosity CBM reservoir model has not been studied jet. This Chapter gives the well testing model and interpretation method for triple porosity CBM wells.

5.2 Pressure square well testing model

5.2.1 Assumption

(1) Methane is adsorbed on the surface of micro-pore system of CBM reservoir;

(2) The water and gas exist in the matrix and cleat system;

(3) The fluid flow in the well obeys Darcy law, and gas flow obeys Fick's first law;

(4) The water gas ratio is very low before well test;

(5) Well testing time is short enough to ignore the variation of the absolute permeability;

(6) Formation pressure is low, <15Mpa;

(7) Gravity and capillary effect is ignored.

5.2.2 Well testing model

5.2.2.1 Well testing model in matrix system

The gas and water material balance transport equation in the matrix system can be written as:

$$\nabla(\frac{k_a k_{\arg}}{B_{ag}\mu_{ag}}\nabla p_{ag}) = \frac{\partial}{\partial t}(\frac{s_{ag}\phi_a}{B_{ag}}) + \frac{q_{ag}}{B_{ag}} \tag{5.5}$$

$$\nabla(\frac{k_a k_{arw}}{B_{aw}\mu_{aw}}\nabla p_{aw}) = \frac{\partial}{\partial t}(\frac{s_{aw}\phi_a}{B_{aw}}) \tag{5.6}$$

The diffusion flux in **Equation (5.5)** can be calculated by the isothermal adsorption line:

$$q_{ag} = \frac{p_{sc}ZT}{p_{ag}Z_{sc}T_{sc}}\frac{V_m b\rho_b}{(1+bp_{ag})^2}\frac{\partial p_{ag}}{\partial t} \tag{5.7}$$

Define desorption compression coefficient for CBM reservoir as:

$$C_d = \frac{B_{ag}\rho_b V_m b}{\phi_{ag}(1+bp_{ag})^2} \tag{5.8}$$

In addition:

$$B_{ag} = \frac{p_{sc}ZT}{p_{ag}Z_{sc}T_{sc}} \tag{5.9}$$

Substituting **Equation (5.8)** and **Equation (5.9)** into **Equation (5.7)**, there is:

$$q_{ag} = C_d \phi_{ag} \frac{\partial p_{ag}}{\partial t} \tag{5.10}$$

The right hand of **Equation (5.5)** can be arranged as:

$$\frac{\partial}{\partial t}(\frac{\phi_a s_{ag}}{B_{ag}}) = \frac{s_{ag}}{B_{ag}}[-\phi_a C_g + \phi_a C_f]\frac{\partial p_{ag}}{\partial t} + \frac{\phi_a}{B_{ag}}\frac{\partial s_{ag}}{\partial t} \tag{5.11}$$

Similarly, the right hand of **Equation (5.6)** can be derived as:

$$\frac{\partial}{\partial t}(\frac{\phi_a s_{aw}}{B_{aw}}) = \frac{s_{aw}}{B_{aw}}[-\phi_{aw} C_w + \phi_{aw} C_f]\frac{\partial p_{aw}}{\partial t} + \frac{\phi_a}{B_{aw}}\frac{\partial s_{aw}}{\partial t} \tag{5.12}$$

Multiply B_{ag} for **Equation (5.5)** and B_{aw} for **Equation (5.6)**, then add them together:

$$\begin{aligned} &B_{ag}\nabla\left(\frac{k_{ag}}{B_{ag}\mu_{ag}}\nabla p_{ag}\right) + B_{aw}\nabla\left(\frac{k_{aw}}{B_{aw}\mu_{aw}}\nabla p_{ag}\right) = \\ &\left(s_{ag}\left[-\phi_a C_g + \phi_a C_f\right] + s_{aw}\left[-\phi_a C_w + \phi_a C_f\right]\right)\frac{\partial p_{ag}}{\partial t} + C_d \phi_{ag}\frac{\partial p_{ag}}{\partial t} \end{aligned} \tag{5.13}$$

Define the coal total compressibility coefficient as:

$$C_t = C_d + C_f - C_g S_g - C_w S_w \tag{5.14}$$

Thus **Equation (5.13)** can be arranged as:

$$B_{ag}\nabla\left(\frac{k_{ag}}{B_{ag}\mu_{ag}}\nabla p_{ag}\right) + B_{aw}\nabla\left(\frac{k_{aw}}{B_{aw}\mu_{aw}}\nabla p_{ag}\right) = C_t \phi_a \frac{\partial p_{ag}}{\partial t} \tag{5.15}$$

Expansion the first term on the left hand of **Equation (5.15)**:

$$B_{ag}\nabla\left(\frac{k_{ag}}{B_{ag}\mu_{ag}}\nabla p_{ag}\right) = \frac{k_{ag}}{\mu_{ag}}\nabla^2 p_{ag} + B_{ag}\nabla\left(\frac{k_{ag}}{B_{ag}\mu_{ag}}\right)\nabla p_{ag} \tag{5.16}$$

Similarly the second term can be shown as：

$$B_{aw}\nabla\left(\frac{k_{aw}}{B_{aw}\mu_{aw}}\nabla p_{ag}\right) = \frac{k_{aw}}{\mu_{aw}}\nabla^2 p_{ag} + B_{aw}\nabla\left(\frac{k_{aw}}{B_{aw}\mu_{aw}}\right)\nabla p_{ag} \tag{5.17}$$

Define the mobility for gas and water phase in the matrix system as follows:

$$\lambda_{ag} = \frac{k_{ag}}{\mu_{ag}} \tag{5.18}$$

$$\lambda_{aw} = \frac{k_{aw}}{\mu_{aw}} \tag{5.19}$$

$$\lambda_{at} = \frac{k_{ag}}{\mu_{ag}} + \frac{k_{aw}}{\mu_{aw}} \tag{5.20}$$

Define the water gas ratio in the matrix system as:

$$WGR = \frac{k_{aw}}{\mu_{aw} B_{aw}} \frac{\mu_{ag} B_{ag}}{k_{ag}} \tag{5.21}$$

Then there is:

$$\begin{aligned} & B_{aw} \nabla \left(\frac{k_{aw}}{B_{aw} \mu_{aw}} \right) \nabla p_{ag} = B_{aw} \nabla \left(WGR \frac{k_{ag}}{\mu_{ag} B_{ag}} \right) \nabla p_{ag} \\ & = B_{aw} WGR \nabla \left(\frac{k_{ag}}{\mu_{ag} B_{ag}} \right) \nabla p_{ag} + B_{aw} \frac{k_{ag}}{\mu_{ag} B_{ag}} \nabla WGR \nabla p_{ag} \end{aligned} \tag{5.22}$$

It is true that the water production is very low during the two phase stage in the CBM reservoir, thus water gas ratio is very low, from this point, $\nabla WGR \nabla p_{ag}$ can be ignored. Substituting **Equation (5.16)-Equation (5.22)** into **Equation (5.15)**, there is:

$$\nabla^2 p_{ag} + \nabla \ln \left(\frac{k_{ag}}{\mu_{ag} B_{ag}} \right) \nabla p_{ag} = \frac{C_t \phi_a}{\lambda_{at}} \frac{\partial p_{ag}}{\partial t} \tag{5.23}$$

The most important thing is to determine the second term in **Equation (5.23)**. The water production rate drops dramatically once the gas begins to produce, and generally there exists fluctuations before the gas reaches its maximum, so the two phase flow in the CBM reservoir is different from the three phase flow of the common oil reservoir. Overall speaking, the corresponding gas water ratio is relatively low at this time (for example, the water production rate for the CBM reservoir is only a few cubic, while the gas production rate can be thousands or even tens of thousands cubic per day). In this stage, the pressure relief radius of CBM wells gradually increases, while the gas/water saturation is relatively stable behind the dehydration front. Once the well is shut in, the gas water mobility ratio will be varied, which will cause the variation of the near wellbore saturation. However, because the well testing time is much shorter compared

with the whole simulation time, thus, the phase saturation and phase permeability can be seen as constant for both draw down test and build up test.

Regard the saturation as constant, the second term in **Equation (5.23)** can be simplified:

$$B_{ag} = \frac{p_{sc} ZT}{p_{ag} T_{sc}}$$

Thus, there is:

$$\frac{k_{ag}}{\mu_{ag} B_{ag}} = \frac{k_{ag}}{\mu_{ag}} \frac{p_{ag} T_{sc}}{p_{sc} ZT} = \alpha p_{ag} \tag{5.24}$$

Where, the product of gas viscosity and compressibility coefficient is constant under the low pressure (lower than 15Mpa). So there is:

$$\alpha = \frac{k_{ag}}{\left(\overline{\mu_{ag}} \overline{Z}\right)} \frac{T_{sc}}{p_{sc} T} \tag{5.25}$$

Equation (5.23) can be arranged as:

$$\nabla^2 p_{ag} + \frac{1}{p_{ag}} \left(\nabla p_{ag}\right)^2 = \frac{C_t \phi_a}{\lambda_{at}} \frac{\partial p_{ag}}{\partial t} \tag{5.26}$$

Multiply 2p on both side of **Equation (5.26)**:

$$\nabla^2 p_{ag}{}^2 = \frac{C_t \phi_a}{\lambda_{at}} \frac{\partial p_{ag}{}^2}{\partial t} \tag{5.27}$$

5.2.2.2 Well testing model in cleat system

The gas and water phase material balance transportation model in cleat system can be shown as follows:

For gas phase:

$$\nabla \left(\frac{k_f k_{frg}}{B_{fg} \mu_{fg}} \nabla p_{fg} \right) = \frac{\partial}{\partial t} \left(\frac{s_{fg} \phi_f}{B_{fg}} \right) \tag{5.28}$$

For water phase:

$$\nabla\left(\frac{k_f k_{frw}}{B_{fw}\mu_{fw}}\nabla p_{fw}\right)=\frac{\partial}{\partial t}\left(\frac{s_{fw}\phi_f}{B_{fw}}\right) \tag{5.29}$$

Define the total compressibility coefficient for cleat system in coal seams as:

$$C_{tf}=C_f-C_g s_g-C_w s_w \tag{5.30}$$

Equation (5.28) and **Equation (5.29)** can be derived similarly as the equation in matrix system:

$$B_{fg}\nabla\left(\frac{k_{fg}}{B_{fg}\mu_{fg}}\nabla p_{fg}\right)+B_{fw}\nabla\left(\frac{k_{fw}}{B_{fw}\mu_{fw}}\nabla p_{fg}\right)=C_{tf}\phi_f\frac{\partial p_{fg}}{\partial t} \tag{5.31}$$

Define the gas and water mobility in the cleat system as follows:

$$\lambda_{fg}=\frac{k_{fg}}{\mu_{fg}} \tag{5.32}$$

$$\lambda_{fw}=\frac{k_{fw}}{\mu_{fw}} \tag{5.33}$$

$$\lambda_{ft}=\frac{k_{fg}}{\mu_{fg}}+\frac{k_{fw}}{\mu_{fw}} \tag{5.34}$$

And the water gas ratio can be defined as:

$$WGRf=\frac{k_{fw}}{\mu_{fw}B_{fw}}\frac{\mu_{fg}B_{fg}}{k_{fg}} \tag{5.35}$$

The second term in **Equation (5.31)** can be derived as:

$$\begin{aligned}&B_{fw}\nabla\left(\frac{k_{fw}}{B_{fw}\mu_{fw}}\right)\nabla p_{fg}=B_{fw}\nabla\left(WGR\frac{k_{fg}}{\mu_{fg}B_{fg}}\right)\nabla p_{fg}\\&=B_{fw}WGRf\nabla\left(\frac{k_{fg}}{\mu_{fg}B_{fg}}\right)\nabla p_{fg}+B_{fw}\frac{k_{fg}}{\mu_{fg}B_{fg}}\nabla WGRf\nabla p_{fg}\end{aligned} \tag{5.36}$$

Similarly manage the term $\frac{k_{fg}}{\mu_{fg}B_{fg}}$ as the term in matrix system, then the final equation can be simplified as:

$$\nabla^2 p_{fg}{}^2 = \frac{C_{tf}\phi_f}{\lambda_{ft}} \frac{\partial p_{fg}{}^2}{\partial t} \tag{5.37}$$

Finally, the pressure square equation for both the matrix system and cleat system can be shown as:

$$\nabla^2 p^2 = \frac{C_t \phi}{\lambda_t} \frac{\partial p^2}{\partial t} \tag{5.38}$$

5.2.2.3 Boundary condition

Initial boundary:

$$p^2(r,0) = p_i^2 \tag{5.39}$$

Outer boundary:

$$p^2(\infty,t) = p_i^2 \tag{5.40}$$

5.2.2.4 Inner boundary

Suppose that the well production rate is constant during build up stage, the inner boundary condition can be written as:

$$\lim_{r\to 0}\left[r\left[\frac{k_g}{\mu_g B_g} \right] \frac{\partial p}{\partial r} \right] = \lim_{r\to 0}\left[r\alpha p \frac{\partial p}{\partial r} \right] = \frac{q_g}{2\pi h} \tag{5.42}$$

5.2.2.5 Analytical solution

The solution for **Equation (5.38)** is:

$$p_i^2 - p^2(r,t) = \frac{q_g}{2\pi\alpha h}\left[-E_i\left[-\frac{\phi r^2}{4t}\frac{C_t}{\lambda_t} \right] \right] \tag{5.43}$$

Suppose that $m = 4.242\times 10^{-3}\frac{q_g}{\alpha h}$, thus when $\frac{\phi r^2}{4t}\frac{C_t}{\lambda_t}$ <0.01, **Equation (5.43)** can be approximated as:

$$p_i^2(\Delta t) - p_{wf}^2(t) = m\left(\lg t + \lg(\frac{\lambda_t}{\phi C_t r_w{}^2}) + 0.9077 + 0.8686S \right) \tag{5.44}$$

5.2.3 Pressure square well testing interpretation method

Assume the well test length is 1h for pressure draw down, then the skin factor S can be got according to **Equation (5.44)**:

$$S = 1.1513 \times [\frac{p_i^{\ 2} - p^2(\Delta t = 1)}{|m|} - \lg(\frac{\lambda_t}{\phi C_t r_w^{\ 2}}) - 0.9077] \tag{5.45}$$

And the well test length is 1h for pressure build up, the following formula can be derived through **Equation (5.44)**:

$$p_{ws}^2(\Delta t) = p_i^2(t) + m \lg \frac{\Delta t}{t + \Delta t} \tag{5.46}$$

Then the skin factor can be derived as:

$$S = 1.1513 \times [\frac{p_{1h}^{\ 2} - p_{wf}^{\ 2}(\Delta t = 0)}{|m|} - \lg(\frac{\lambda_t}{\phi C_t r_w^{\ 2}}) - 0.9077] \tag{5.47}$$

The slope can be interpreted through **Equation (5.46)**, and the gas permeability k_g and the slope m can be derived through **Equation (5.25)**:

$$k_g = 4.242 \times 10^{-3} \times \frac{q_g \mu_{g0} Z_0 T p_{sc}}{m h T_{sc} q_{sc}} \tag{5.48}$$

Then the water phase permeability k_w can be derived according to the surface water gas ratio:

$$k_w = R_{wg} \times \frac{\mu_w B_w}{\mu_g B_g} k_g \tag{5.49}$$

It is important to mention that the parameters in the cleat system is the ones needed for the study, thus the permeability and skin factor in cleat system are interpreted in the following part.

5.3 Validation of the model

In order to validate the accuracy of this model, Eclipse is initially used to achieve the well testing process of two phase CBM reservoir, then the pressure squared method proposed in this Chapter is utilized for the interpretation. The main parameters for well

testing are shown in **Figure 5.1**. And the corresponding relative permeability data is illustrated in **Figure 5.2**.

parameters	value
Outer boundary radius (m)	4.00
Inner boundary radius (m)	2.53
Langmuir pressure coefficient (b/Mpa^{-1})	0.231
Langmuir volume(m^3/t^{-1})	20.6
Porosity (fraction)	0.02
Absolute permeability ($10^{-3}\mu m^2$)	0.25
Pore compression coefficient (MPa^{-1})	0.045
Skin factor	-3.2
Coal density (t/m^3)	1.35
Wellbore radius (m)	0.108
Wellbore volume(m^3)	4.5
Reservoir temperature (℃)	34
Diffusion coefficient (D/m^2.h^{-1})	0.02
Coal thickness (m)	9
Initial pressure (Mpa)	5.867
Initial water saturation (fraction)	1.0

Table 5.1 Main parameters for well testing

Water saturation	Water permeability	Gas permeability
0.1	0.0193	1.0
0.2	0.0351	0.858
0.345	0.4	0.53
0.567	0.679	0.456
0.876	0.765	0.234
0.956	0.897	0.134
1.0	1.0	0.0000

Table 5.2 Relative permeability parameters

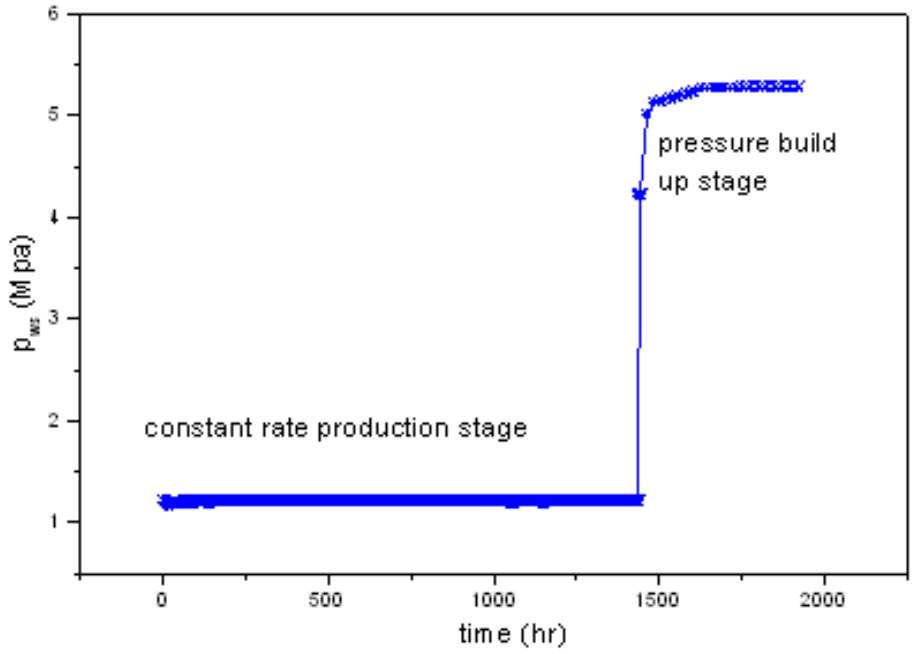

Figure 5.1 Pressure changes of the well

The CBM wells produces 45 days under the specified pressure 0.5869 Mpa, then produces another 15 days under the specified water rate of 25.6 m^3/day, followed that the well is shut in for another 20 days to make the pressure build up again. The pressure changes before and after well shut in is shown in **Figure 5.1**.

5.4 Well testing interpretation

The pressure data of build up stage is used for the interpretation. The semi log plot about the relationship of $p_{ws}^{\ 2}(\Delta t)$ and $\lg(\Delta t/(t+\Delta t))$ is initially made, then the code for the corresponding program is programmed by using Matlab to fit the log plot. As shown in **Figure 5.2**, the fit is a linear fit, means the fitting equation is a linear equation like $y = kx + b$ (here, y represents $p_{ws}^{\ 2}(\Delta t)$, and x represents $\lg(\Delta t/(t+\Delta t))$).

From the linear fit one can get that: the slope m is 12.99, and the intercept b is 52.75. Then one can get the initial value of viscosity, volume factor, gas deviation factor from the gas PVT table, they are: μ_{g0} is 0.0139mpa.s, B_{g0} is 0.0136, Z_0 is 0.3465.

Followed that the gas absolute permeability for the cleat system can be calculated through **Equation (5.48)**, it is $0.53\times10^{-3}um^2$ ($k_{fg} = 4.242\times10^{-3}\times800\times\frac{(275+35)}{(275+20)}\times\frac{0.0139\times0.0865}{9\times12.99}\times14.7$). The water saturation that corresponding to this k_{fg} can be captured using the relative permeability table, that s_{fw} is 0.345.

In addition, the near wellbore value of k_{fg} is between $0.45\mu m^2$ - $0.6\mu m^2$, and s_{fw} is between 0.3-0.4 for simulation. From this one can see that the interpretation value of k_{fg} and s_{fw} using the pressure square method have good agreement with the simulation result, which surely indicates the accuracy of the method.

The absolute permeability k_{fw} for water phase can be got through **Equation (5.49)** by using the already calculated value of k_{fg}. The calculated k_{fw} is $0.4\times10^{-3}um^2$, total compressibility is $0.035Mpa^{-1}$. Thus the total mobility can be calculated through **Equation (5.32)**, and its value is $1.18\times10^{-2}\mu m^2/mpa.s$. Finally, the skin factor in the CBM reservoir can be got through the above calculated value, it is 0.08. The error between the calculated value and input value is 8%, which is in the reasonable error range, indicate the accuracy of the method.

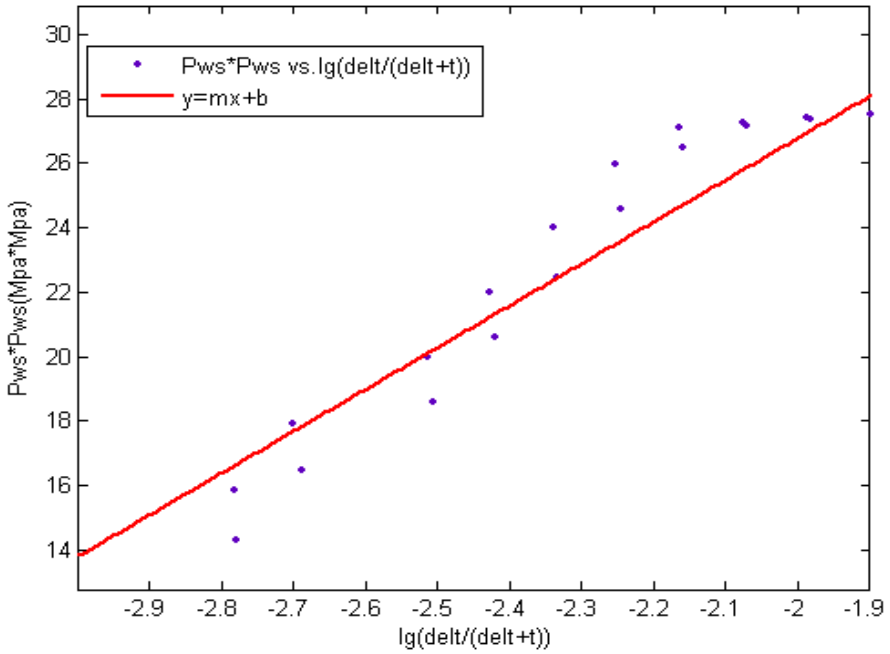

Figure 5.2 Well testing interpretation

5.5 Chapter conclusions

(1) A pressure square method for the triple porosity model of CBM reservoir is proposed. Neither the relative permeability curve nor the variation of the pressure gradient is needed for the well test interpretation in this method, only the gas saturation gradient for the two phase flow needs to be considered. Thus this method has its great superiority over the other well testing methods.

(2) The well testing data for the case study comes from the Eclipse simulation result, and the interpreted result shows better agreement than expected. Thus this method can be applied to the field for well testing interpretation.

Chapter 6 Field Application

6.1 Introduction

Evaluating mature fields is absolutely more challenging than studying the synthetic models. As known to all, the aim of the reservoir engineer is to accurately predict the performance of the real reservoir, while sometimes it is really difficult to reduce the uncertainty of the prediction for the real model, which is caused by the inelasticity of the ideal reservoir mathematical model used for history matching. In this Chapter, three real field blocks have been chosen to test the applicability of the mathematical models for CBM reservoirs.

The insights of **Chapters 2-5** are brought together to carry out the analysis of the field data through the advanced models developed in this work. The first study block is the Heshun block, it is characterized as the single gas components, and its major component is CH_4. For example, the components of the desorbed gas for 3# coal seam in Shanxi group are: CH_4 varied between 72.36% and 98.92%, the average content is 85.64%; N_2 varied between 1.08% and 24.82%, the average percentage is 12.95; CO_2 changes between 0.0% and 2.82%, the average value is 1.41%.

While for the 15# coal seam in Taiyuan group, its component is distributed as: CH_4 varied between 96.87% and 98.42%, the average content is 97.73%; N_2 varied between 1.09% and 2.94%, the average percentage is 1.86; CO_2 changes between 0.0% and 0.64%, the average value is 0.32%.

In addition, the exploration or parameter wells in this block are drilled in a vertical type, and they are completed through the open-hole method. From such kinds of information one can conclude that the advanced vertical well model studied in **Chapter 2** should be used for the history matching or production evaluation/forecast of this block. The investigation of it gives the detailed understanding of the accuracy and reasonability of the advanced vertical well model proposed in this work. Moreover, the interpreted well or fluid parameters are presented in order to adapt to the well testing purpose.

The second study block is the Yanchuan southern block. The exploration for it begins in 2009, and the observed result shows that it has great potential for the exploration. The wells in this block are drilled in the horizontal or multi-branch types, and the desorbed gas for this block is mainly CH_4, which means that the advanced coupled horizontal wellbore models proposed in **Chapter 3** can be used for the history matching

in this block. The history mathing results in this thesis show the reliability and accuracy of the model in **Chapter 3**.

The third study area is the Zhijin block, the desorbed gas of it is complicated, contains about 65% CH_4 , nearly 25% CO_2 and 20% of other gases such as N_2, H_2. What is more, the wells in this area are drilled as multi-branch horizontal well type. The compositional horizontal triple porosity model is used for this block, in addition, the matched results shows perfect consistency between the simulated data and field data.

This chapter provides three successful cases through history matching and production evaluation/forecast using the models developed in **Chapter 2-5**, which indicates the work in **Chapter 2-5** has great significance in the field application.

6.2 Field application cases

6.2.1 Heshun block

In this part, the history matching of He2, He2-3 and He2-5-1 which are drilled as vertical well type in Heshun block are made. The history matched cleat permeability, porosity, skin factor and coal seam thickness are compared with input value for the better future field production. The simulator developed in **Chapter 2** called COAFOR is used for the history matching, the gas slippage and threshold pressure gradient effects are all considered for this study. In addition, he2-2 well is used for the productivity forecast to further verify the model proposed in **Chapter 2** can accurately being applied for the field.

6.2.1.1 Geological characteristic

Heshun block for the CBM reservoir exploration is located in the middle of Shanxi province, and North of Qinshui Basin. It is about 70Km from the provincial capitial Taiyuan City. It belongs to the jurisdiction of Heshun county in Jinzhong City and Xiyang County area according to the administrative divisions. The topography in this region is very complex, most of them are hills and mountains.

Generally, the altitude is more than 1300 meters, and the highest altitude is 2058 meters. The investigation degree regarding the area coalfield geology and area geology is very low. In addition, the basic geological materials are very rare compared to the other region in this basin. This is the reason why it has some difficulties for the geological study of CBM reservoir.

The same as the large area of North China, the crustal in this area has stably subsided from Cambrian to middle Ordovician, thus, the sedimentation there is mainly the shallow sea phase carbonate formed on the ancient crystalline basement. The North China platform is overall uplifted owning to the Gary crustal movement after middle Ordovician ages, which resulted in the missing of sedimentation in the study area from late Ordovician to the early Carboniferous.

During the period of Carboniferous, the earth crust subsided again owning to Haixi movement. Correspondingly, the Carboniferous and Permian strata paralic coal-bearing strata are formed, which is the basement for the formation of Coalbed Methane. The crust in this area is becoming much more stable after three tectonic movements and transformations. And the coal seam in this area becomes exploitable and commercially liable. **Figure 6.1** shows the lateral seismic parabolic map in the East-South part of the Heshun block.

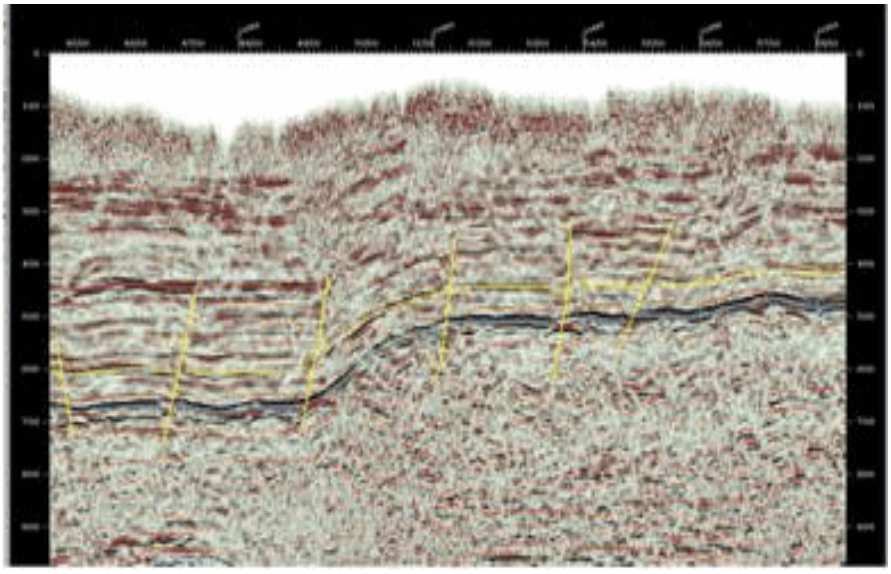

Figure 6.1 Lateral seismic parabolic map in the East-South part of heshun block

3# and 15# coal seams are both the developed structural coal with different degrees and thickness, only the coal in the middle part belongs to the complete structured coal block, which is studied through the cores that come from five CBM wells in Heshun Basin. Moreover, the structure of axial lobe and fault zone in Heshun block resulted in the serious local coal deformation, coal faults and fracture, thus, some of the primary coal seam structure was destroyed in this area.

The structure of 3# and 15# coal seam in Heshun block as well as its neighboring region is the primary structure according to the observation of the underground coal seam wells. 3# coal seam developed a soft coal seam layer structure with the thickness of 1

meter in the northern study area of Yangquan mine 1 and mine 3 well, a field near Shouyang region. While 15# coal seam developed different tectonic coals with different degree and thickenss in the margin coal mine, Zhengbang coal mine, Qiannanyu coal mine and Tianchi coal mine of the Southern studied area.

The occurrence strata in Heshun block contains coal bearing build basal Ordovician ZhongTong fengfeng group (O_{2f}), carboniferous ZhongTong existing group (C_{2t}), Stockings on Taiyuan formation (C_{3t}), Permian next tasseled Shanxi groups(P_1s), Xiashihezi group (P_1x), Permian stockings on stone box group (P_2s), Shiqianfeng group (P_2sh), Triassic next tasseled Liujiagou group(T_1l), Zhongtong Ermaying group (T2er), Cainozoic group tertiary (N) and Quaternary system (Q). The schematic geology of natural gas resources are shown in **Figure 6.2**.

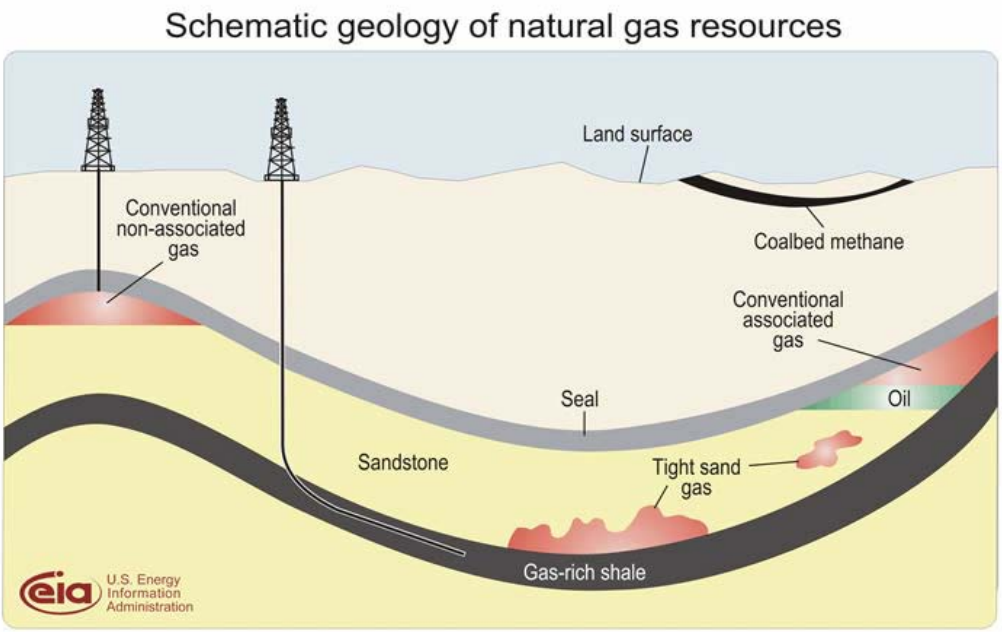

Figure 6.2 Schematic geology of natural gas resources

The study area in this block mainly contains Carboniferous stockings on Taiyuan group and Permian next tasseled Shanxi groups. The average formation thickness of the two groups is 207.34 meter, and the average coal seam thickness is around 10.25 meter. Shanxi group usually contains 3-6 layers coal seam, with average thickness for coal layer is 2.82 meter. While Taiyuan group contains 4-9 floors coal seam, and the average thickness for coal layer is about 7.43 meter. 15# and 3# coal seams are the target coal seams in the study region, the coal types are mainly divided into two types: lean and anthraxcite coal.

6.2.1.2 History matching

Parameters		3# coal seam	15# coal seam
Buried depth (m)		433.86-772.40	452.45-888.00
Gas saturation (%)		9.45	9.89
Gas content (m^3/t)		8.62	6.51
Reservoir pressure (MPa)		3.55	4.0
Critical pressure (MPa)		2.53	1.61
Langmuir pressure(MPa)		2.31	2.23
Langmuir volume (m^3/t)		32.6	34.96
Porosity (fraction)		0.02	0.02
Absolute permeability ($10^{-3}\mu m^2$)	k_x	0.05	0.045
	k_y	0.03	0.03
	k_z	0	0.01
Compressibility coefficient (MPa^{-1})		0.045	0.045
Skin factor		-3.2	-4.55
Coal density(t/m^3)		1.4	1.4
Wellbore radius (m)		0.108	0.108
Reservoir temperature (℃)		34	29.4

Table 6.1 Parameters used for simulation and history matching in heshun block

Pressure (10^{-1}Mpa)	Viscosity (mpa.s)	Volume coefficients
100	0.00858	1.01932
200	0.00860	0.50806
400	0.00862	0.25273
600	0.00864	0.16776
800	0.00867	0.12528
1000	0.00886	0.09979
2500	0.00965	0.03862
4000	0.01010	0.02335
6500	0.01020	0.01361
8000	0.01024	0.01072
9000	0.01030	0.00935
20000	0.01058	0.00401

Table 6.2 PVT characteristic parameters for CBM reservoir

(1) He2 well

The thickness of 3# and 15# coal seam in He2 well are 7.2 meter and 6.8 meter respectively in the study region, and the two coal seams are vertical well type. **Table 6.1** shows the parameters for Heshun block CBM reservoirs, and **Table 6.2** presents the PVT parameters of CBM reservoir used in this Chapter.

The numerical simulation was made according to the formation parameters listed above, the purpose for this is to predict the gas production rate, water production rate and the pressure changes of 3# coal seam and 15# coal seam in he2 well. In addition, the

effects of gas slippage and threshold pressure gradient on the gas, water production rate and the pressure were also investigated.

1) Case study 1

The purpose for this study is mainly to investigate the gas and water production rate of 3# and 15# coal seam. The initial pressure for 3# coal seam is much lower than 15# coal seam, so this can result in the different gas and water production rate in 3# coal seam and 15# coal seam.

Figure 6.3 shows the daily gas production rate according to the field parameters of 3# and 15# coal seam. It is clear from the figure that there exist three stages in coal production process. The first stage is dewatering stage, most water is pumped out from the coal seam because the cleat system is occupied by water initially, after that the adsorbed gas begins to desorb and the gas production rate is gradually increased until it gets its maximum, then the gas production rate is slowly decreasing. This indicates that the gas production rate of 3# and 15# coal seam is consistence with theory proposed in **Chapter 2**. Moreover, the maximum daily gas production of 3# coal seam is higher than 15# coal seam, this is because the critical pressure of 3# coal seam is much lower than 15# coal seam, which makes it easier for gas to desorb from 3# coal seam.

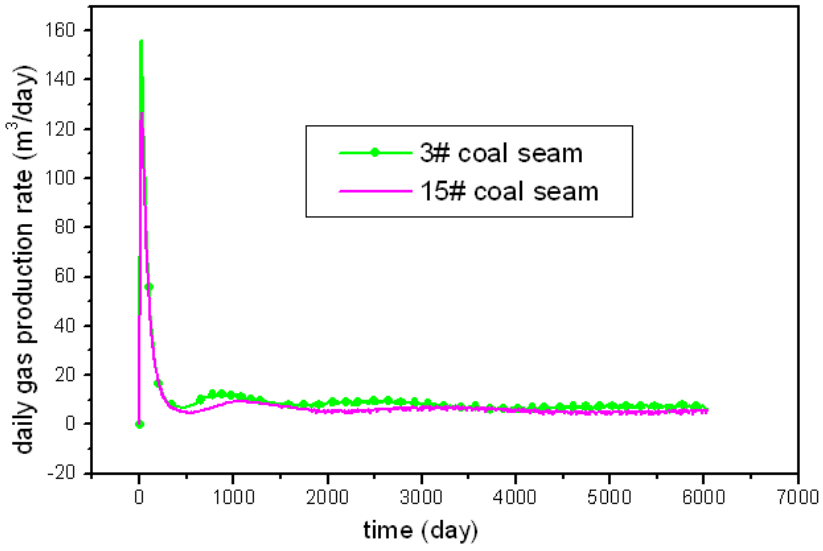

Figure 6.3 Daily gas production rate of 3# and 15# coal seam

Figure 6.4 gives the daily water production rate related to the 3# and 15# field parameters. It can be seen that the water production rate is decreasing with time. At first, the maximum water in 3# coal seam is about 3.72 m^3 compared to the

approximately 2.8 m^3 in 15# coal seam. While the water production rate for 15# coal seam reaches at its minimum after producing about 20 days, however, it took much longer time for 3# coal seam, about 200 days, as shown in the figure.

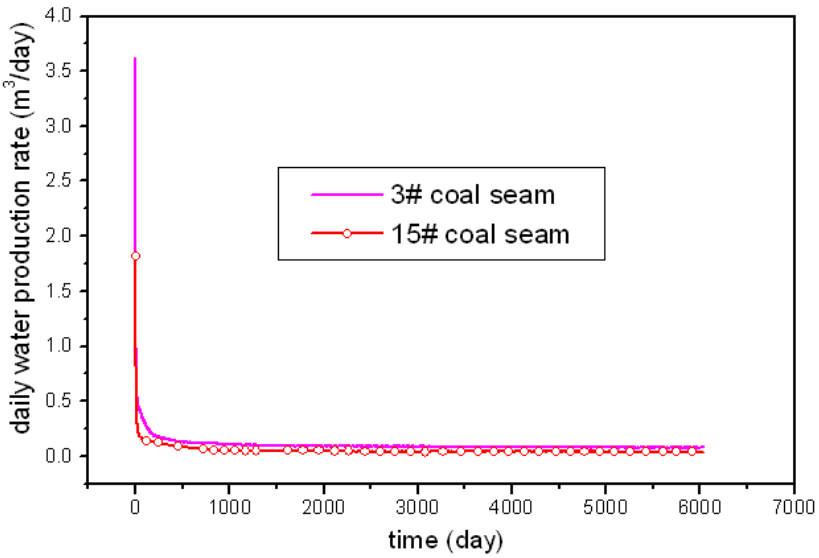

Figure 6.4 Daily water production rate of 3# and 15# coal seam

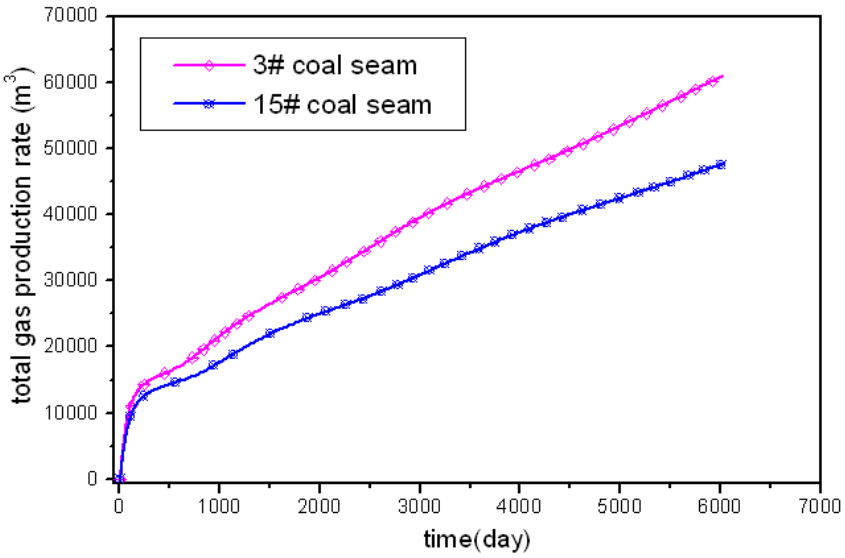

Figure 6.5 Total gas production rate of 3# and 15# coal seam

Figure 6.5 illustrates the changes of total gas production rate with time. It is clearly seen from the figure that the total gas production rate of 3# coal seam is much higher than 15# coal seam. And the total gas production rate increases with time going on for both 3# and 15# coal seam, as can be seen, it increasing slowly for the first 300 days,

and rises rapidly since then. What is more, the total gas production rate of 15# coal seam reaches at about 45000 m^3 after producing 6000 days and around 60000 m^3 for 3# coal seam.

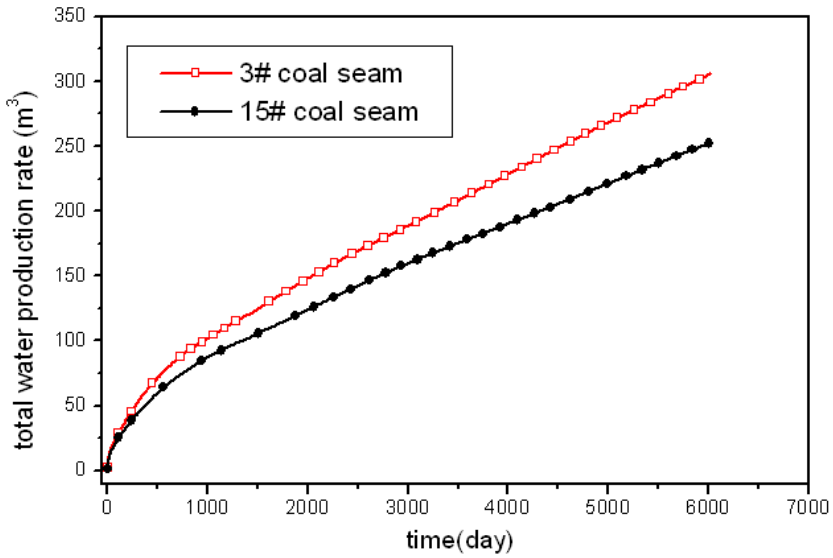

Figure 6.6 Total water production rate of 3# and 15# coal seam

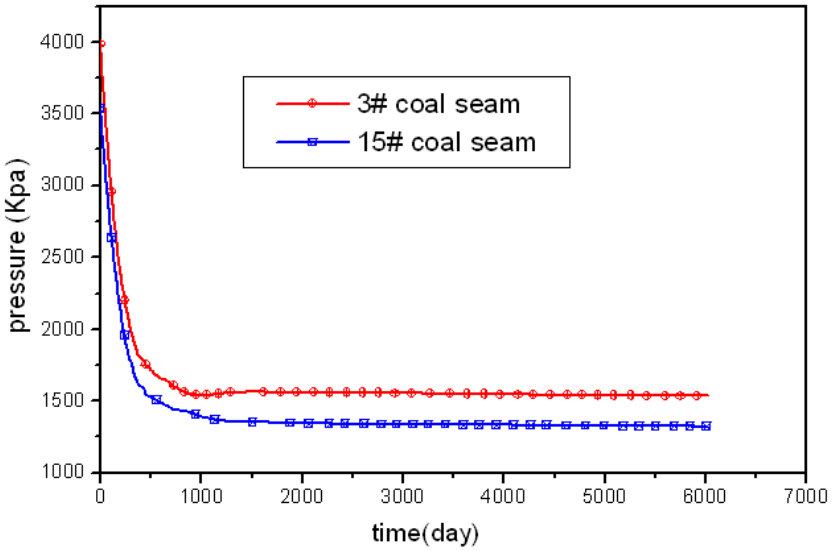

Figure 6.7 Pressure changes of 3# and 15# coal seam

Figure 6.6 presents the total water production rate variation using the parameters came from 3# and 15# coal seam field data. As shown in the figure, the total water production rate increases within the simulation time both for 3# and 15# coal seam, which has the same trend as the total gas production rate changes. And the water production rate merges into one point at the first 200 days production for both 3# and

15# coal seam, while since then 3# coal seam can produce much higher water rate than 15# coal seam owning to different pressure and critical pressure for the two layer coal seams.

Figure 6.7 indicates the pressure changes with time by using the field parameters of 3# and 15# coal seam. From this figure one can get the initial pressure for 3# coal seam is 4000 Kpa, and 3500 Kpa for 15# coal seam. The pressure is slowly decreasing with time going on, the lowest pressure for 3# coal seam is a little more than1500 Kpa after producing 1000 days, and it is less than 1500 Kpa for 15# coal seam after producing about 800 days. Then the pressure keeps a constant level during the simulation time for both 3# coal seam and 15# coal seam.

2) Case study 2

This case study is mainly to investigate the gas slippage and threshold pressure gradient effects on the gas and water production rates as well as the changes of pressure. The two effects were studied at the same time. The parameters for the gas slippage factor and threshold pressure gradient factor are: $\beta_1 = 161, \beta_2 = 0.47, \alpha_1 = 0.002, \alpha_2 = 0.4$.

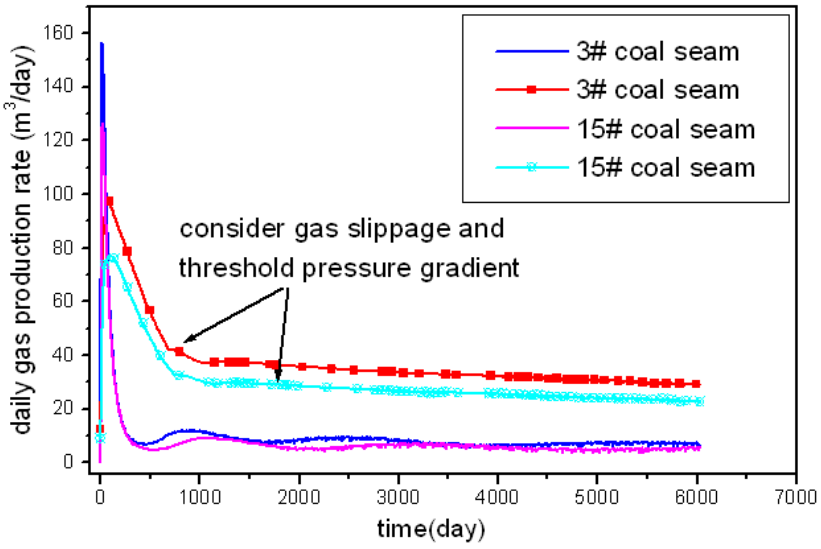

Figure 6.8 Comparison of daily gas production rate for 3# and 15# coal seam

Figure 6.8 gives the comparisons of the daily gas production rate under the field parameters come from 3# and 15# coal seam. One can see that the daily gas production rates are nearly the same initially for both cases, however, the maximum daily gas production rate is relatively lower when the gas slippage and threshold pressure gradient are ignored during middle stage production. The daily gas production rate is gradually

decreasing once it achieved its maximum, and it is much higher when gas slippage effect and threshold pressure gradient effect are both considered during this time than the case that they are ignored. Finally, the daily gas production rate nearly kept a constant for both two cases: about 40 m^3/day when the gas slippage and threshold pressure gradient were both considered, and only about 10 m^3/day for the case that the two effects were ignored. In a word, if the gas slippage and threshold pressure gradient effect are ignored, the daily gas production for the 3# and 15# coal seam will be under estimated. Also, the gas slippage effect plays a leading role for he2 well compared with the gas threshold pressure gradient effect.

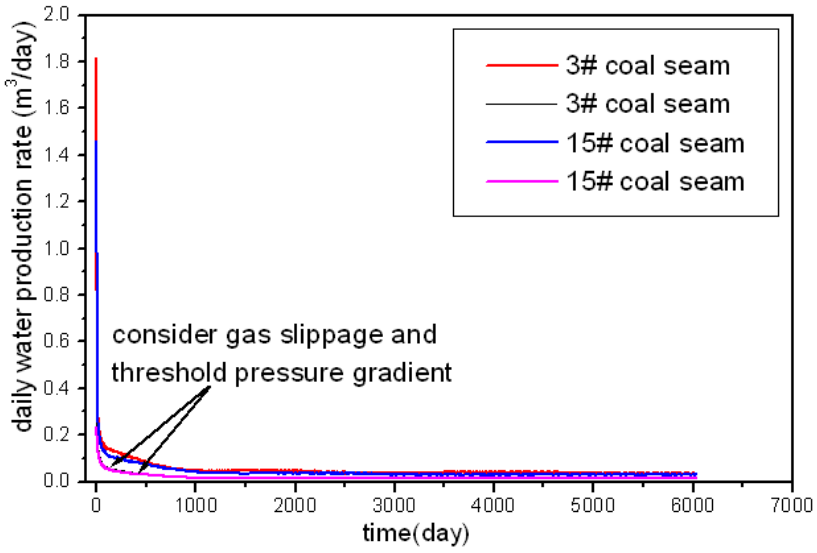

Figure 6.9 Comparison of daily water production rate for 3# and 15# coal seam

Figure 6.9 presents the comparison of daily water production rate under the field parameters come from 3# coal seam and 15# coal seam. It can be concluded from the figure that the daily water production rate is lower if the gas slippage and threshold pressure gradient effects are both ignored than the case that the two effects were considered. As is known to all, the gas slippage effect can increase the cleat permeability, so it can enhance the gas production rate, and it also has the same effect on the water production rate. In addition, the gas and water have to overcome threshold pressure gradient before it can go through the cleat system, so it can decrease the gas and water production rate. Thus, this is the reason why the daily water production rate is relatively lower when the stronger threshold pressure gradient than gas slippage effect

is considered during the initial simulation process. What is more, it also results in the fact that the daily water production rate is earlier to reach its minimum.

Figure 6.10 presents the comparison of the pressure changes with production time, the parameters came from the field data of 3# and 15# coal seam were used here. From the figure it can be seen that the pressure is much higher when the gas slippage effect and threshold pressure gradient were considered at the initial stage compared with the case if the two effects are ignored, while this trend is reversed during the late stage.

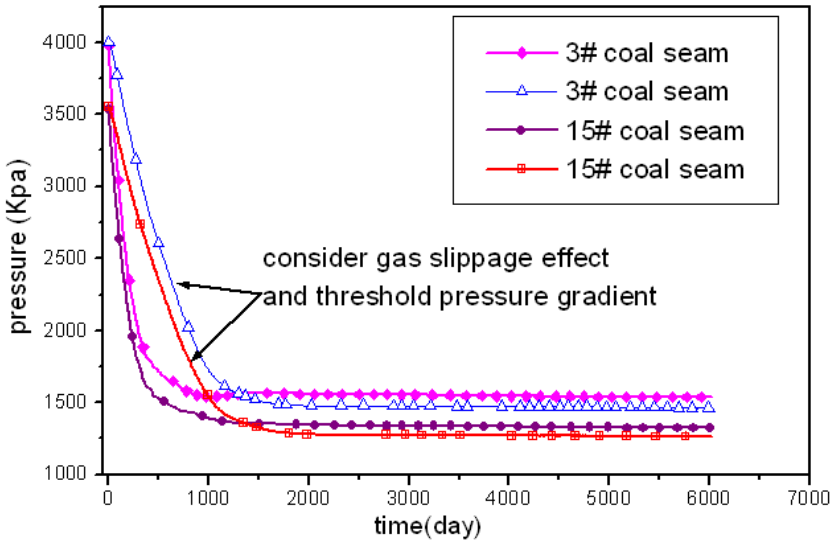

Figure 6.10 Comparison of pressure changes for 3# and 15# coal seam

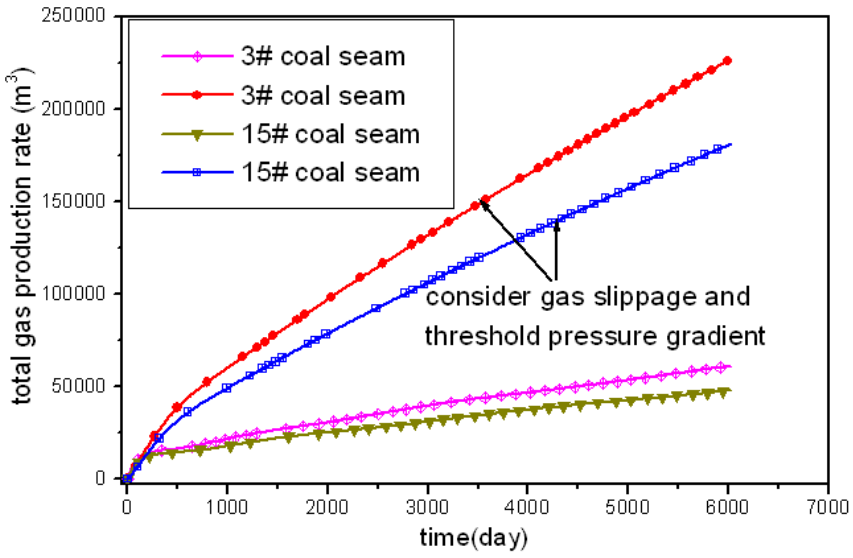

Figure 6.11 Comparison of total gas production rate for 3# and 15# coal seam

Figure 6.11 presents the comparison of the total gas production rate under the field data came from 3# and 15# coal seams. It is obviously to see that the total gas production rate is much higher when both the gas slippage effect and threshold pressure gradient effect were considered, and the gas production rate is nearly the same only at the initial stage. This means that the gas slippage effect was dominant during the simulation time. The total gas production rate can only reach 48000 m^3 after 6000 days simulation in the 15# coal seam, while it can reach 175000 m^3 when the gas slippage effect and threshold pressure gradient were considered as the comprehensive effect. 3# coal seam has the same trend as 15# coal seam.

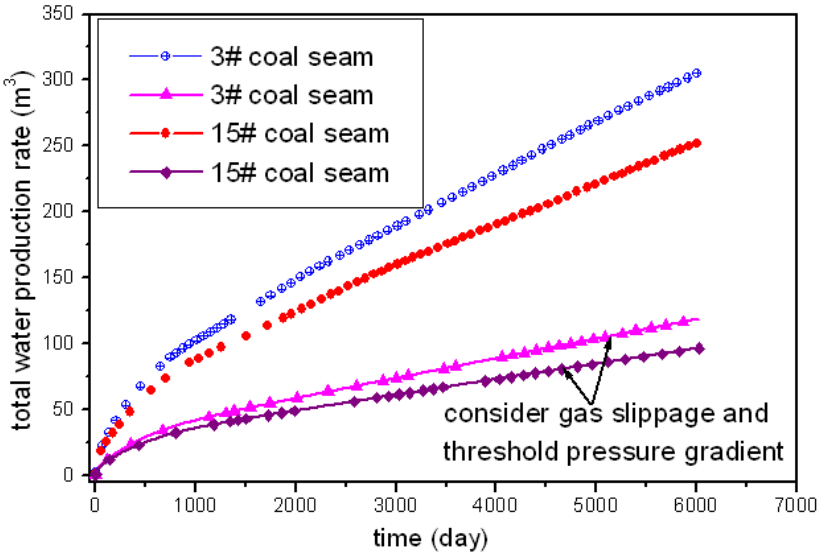

Figure 6.12 Comparison of total water production rate for 3# and 15# coal seam

Figure 6.12 shows the total water production rate of 3# and 15# coal seams. Obviously, the total water production rate is relatively lower when the gas slippage effect and threshold pressure gradient were both considered than the case when the two effects are both ignored. The maximum total water production rate of 3# coal seam is about 125 m^3 after about 6000 days production if the gas slippage effect and threshold pressure gradient were considered in the model, while it can be more than 325 m^3 when the two effects were ignored. It can conclude that the threshold pressure gradient has the leading effect on the water production rate than the gas slippage effect. 15 # coal seam has the similar trend.

3) Case study 3

The main objective is to validate the model developed in this study. The permeability for the coal seam in this region is very small due to the special characteristics of qinshui basin, which makes it hard for the producing the Coalbed Methane. Thus, the artificial fracturing method is used for the development of heshun block for this reason.

He2 well was chosen in heshun block, the production data from January in 2010 to December in 2010 of He2 well in qinshui basin was used for the history matching, totally 365 days. The 3# and 15# coal seams are both infinite on plane and saturated by water in natural situation, thus boundary conditions, consisting of constant pressure and saturation at external boundary, and specified pressure for production well, were used in the simulation. 15# coal seam was chosen as the studied coal layer for He2 well, which is belonging to carboniferous on stocking Taiyuan group.

Figure 6.13 shows the history matching of bottomhole pressure for He2 well. Obviously, the good agreement between the simulated result and observed result is better than expected. Owing to the 10 days stop production of He2 well after a few days production, the pressure initially increases, and then slowly decreases. However, the basic pressure decreasing trend is good enough to be used for the validation of the model.

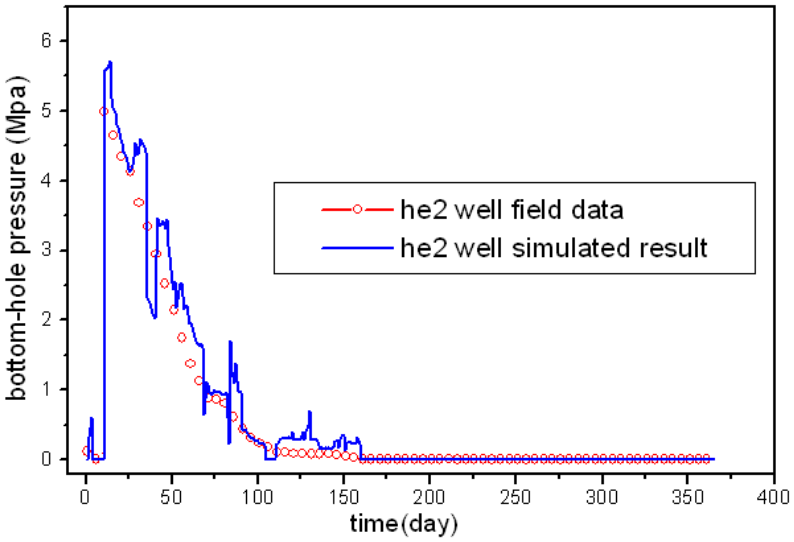

Figure 6.13 History matching curves of BHP for he2 well

The simulated gas production rate, as shown in **Figure 6.14** and **Figure 6.15**, are consistent with the field data observations. The figures have shown better dynamics during primary CBM recovery, which just validated the accuracy and applicability of

the model developed in **Chapter 2**. The initial daily gas production is very high, the highest production rate is about $350\,m^3$. And the well stoped to produce for the next 10 days, so the daily gas production rate is zero during this period. While the well is open to produce again, and the daily gas production rate gradually increases again, but still lower than the largest initial value, as shown in **Figure 6.14**. The total gas production rate increases with the time going on, shown in **Figure 6.15**.

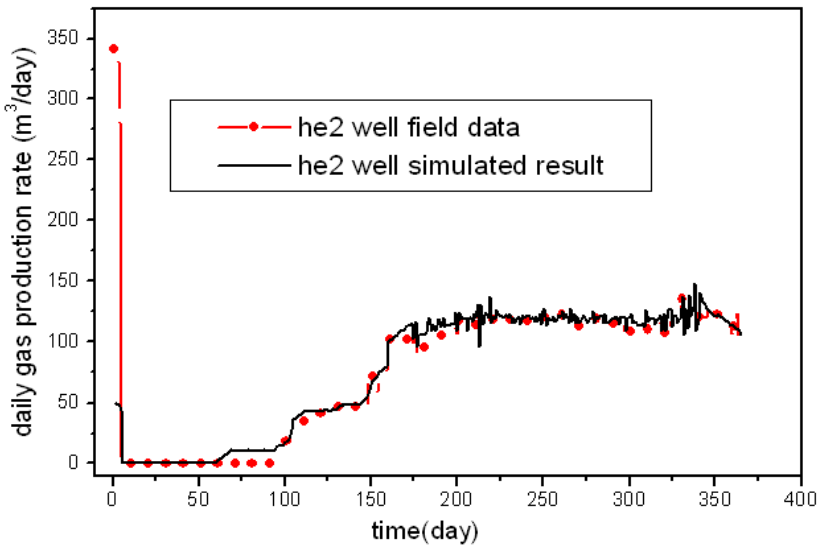

Figure 6.14 History matching curves of daily gas production rate for he2 well

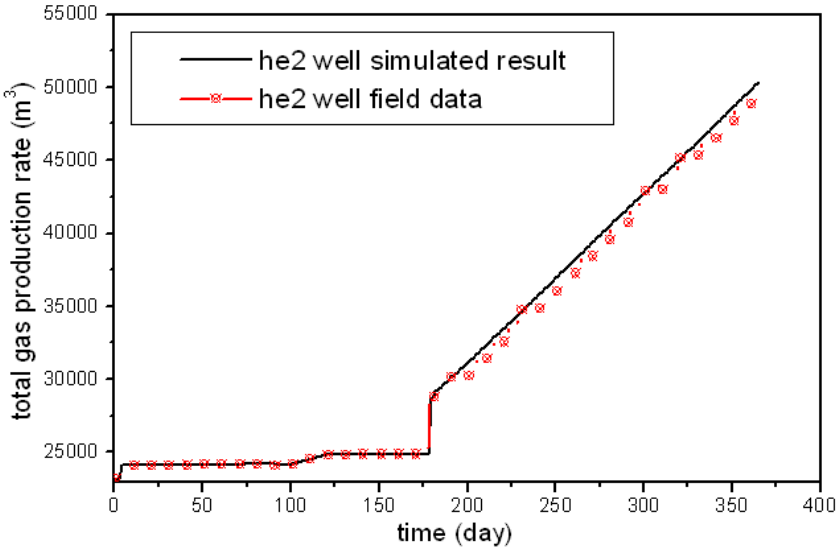

Figure 6.15 History matching curves of total gas production rate for he2 well

Figure 6.16 and **Figure 6.17** present the history matching result for the water production rate of He2 well, which show the good agreement between He2 well field data and simulated data. The reservoir simulation has also indicated that the produced water of He2 well mainly comes from 3# coal seam, which owing to the ground water recharging from the strata, and the reservoir pressure of the 15# coal seam remained at a high level and can not reach the critical pressure at all. Therefore, the 3# coal seam should be plugged in order to exploit the 15# coal seam. A suddenly decline of the water production rate means that the enhancement of the gas production rate.

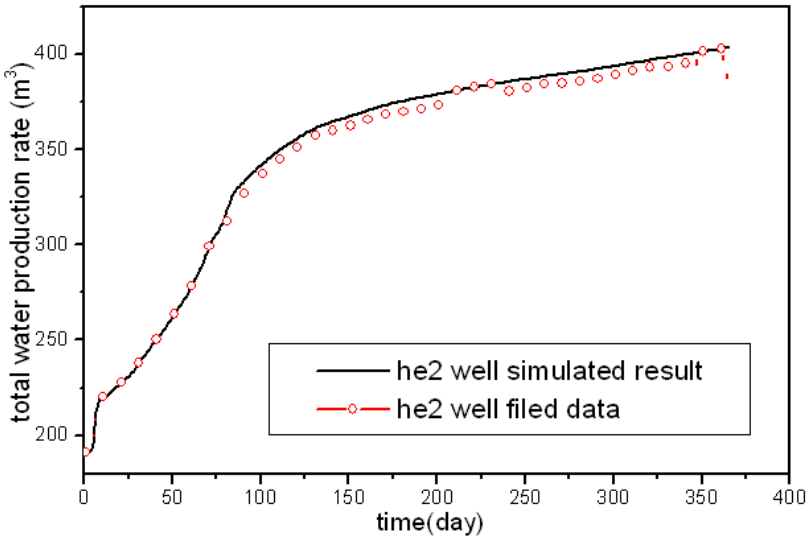

Figure 6.16 History matching curves of total water production rate for he2 well

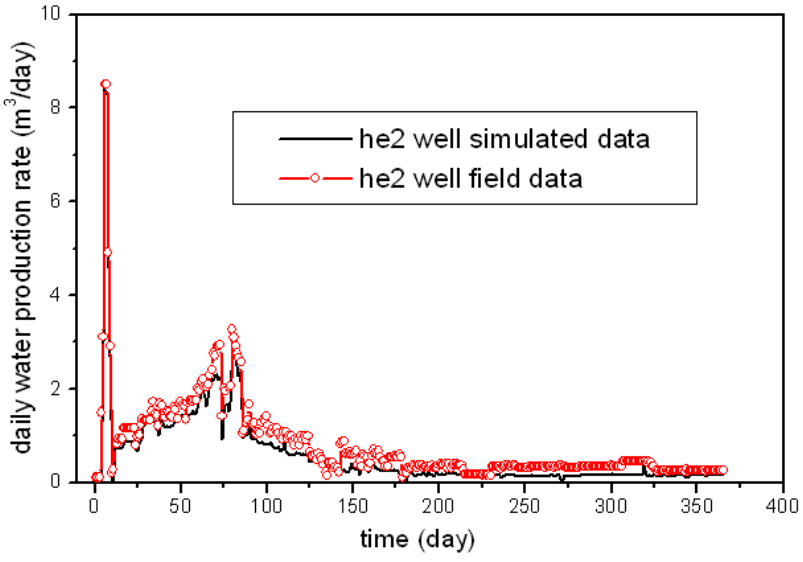

Figure 6.17 History matching curves for daily water production rate of he2 well

The history matching results for He2 well are better than expected if adjusting the proper parameters, as can be seen from the figures. And the best history matching results achieved when the coal seam thickness, porosity, cleat permeability and skin factor take the following values:

Coal seam thickness	Porosity	Cleat permeability	Skin factor
4.562m	0.02	0.4md	0.0148

The input value of the coal seam thickness, porosity, cleat permeability and skin factor are: 4.5, 0.02, 0.017, and 0.015. Thus the relative error between input value and history matched value are as: 0.26%，0%，95.75%，1.35% respectively. It is easily to see that the history matched cleat permeability deviated greatly from the input value, which means the input permeability for the field needs to be adjusted for accurately evaluating the field production. And the interpretated permeability is much more reasonable according to the observed daily gas production.

(2) He2-3 well

He2-3 well is one vertical test well for CBM reservoir, which is drilled by Sinopec Huadong company, located in Heshun town of Shanxi province. The main production layer for this well is 15# coal seam. The basic parameters for 15# coal seam in He2-3 well are got through well test analysis, and they are shown in **Table 6.3**. The history matching work for this well is done in order to test the accuracy of the mathematical model and the well test data. The history data from January in 2010 to December in 2010 are used, totally 365 days.

Coal seam	Depth/m	Structure	Angle/°	Thickness/m	Other
$15^{\#}$	505.30～510.80	5.50	0	5.50	well test

Table 6.3 parameters for 15# coal seam in he2-3 well

Figure 6.18-6.21 shows the history matching of daily gas rate, total gas rate, pressure and total water rate respectively. It can be seen that the simulated results have good agreement with the field data, the corresponding history matched coal thickness, porosity, cleat permeability and skin factor are shown as:

Coal thickness	Porosity	Cleat permeability	Skin factor
5.625m	0.0195	0.46md	-1.698

While the input coal seam thickness, porosity, cleat permeability and skin factor are: 5.5, 0.02, 0.01, and -1.72. So the relative errors between the history matched values and input values are 2%, 2.5%, 97.8%, 1.2% respectively. Again, the relative error for the

cleat permeability is still the biggest among others. However, the history matched permeability value is much more reasonable from the daily gas rate changes curves, shown in **Figure 6.18**.

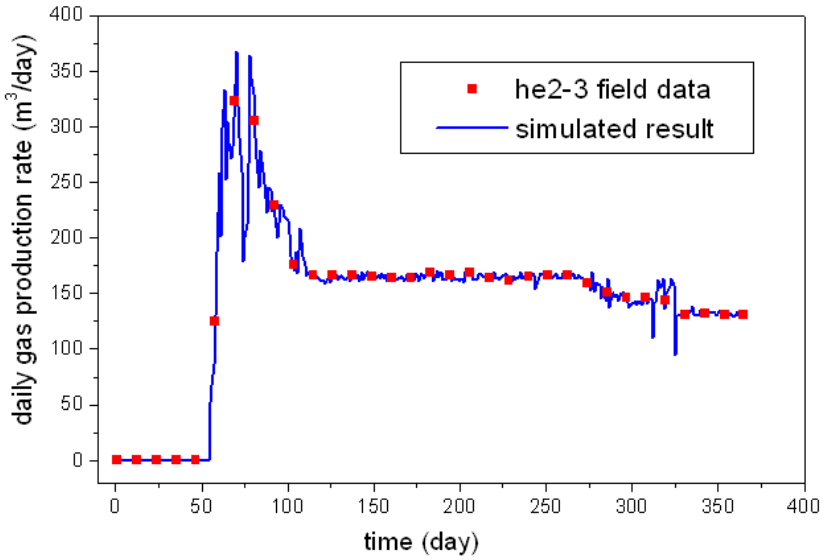

Figure 6.18 History matching of daily gas rate for he2-3 well

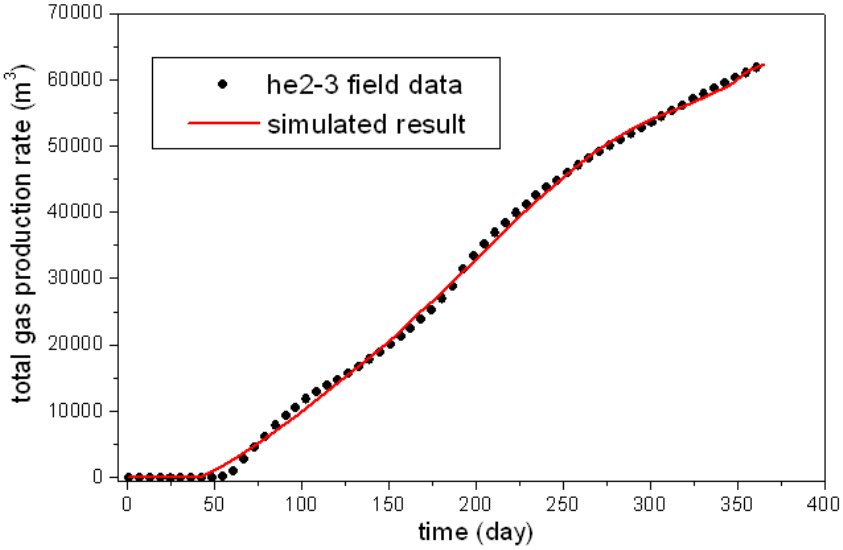

Figure 6.19 History matching of total gas rate for he2-3 well

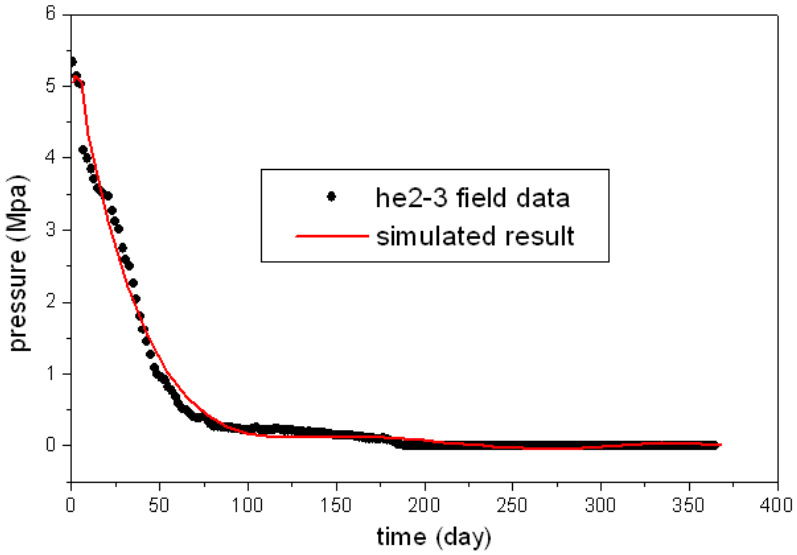

Figure 6.20 History matching of pressure for he2-3 well

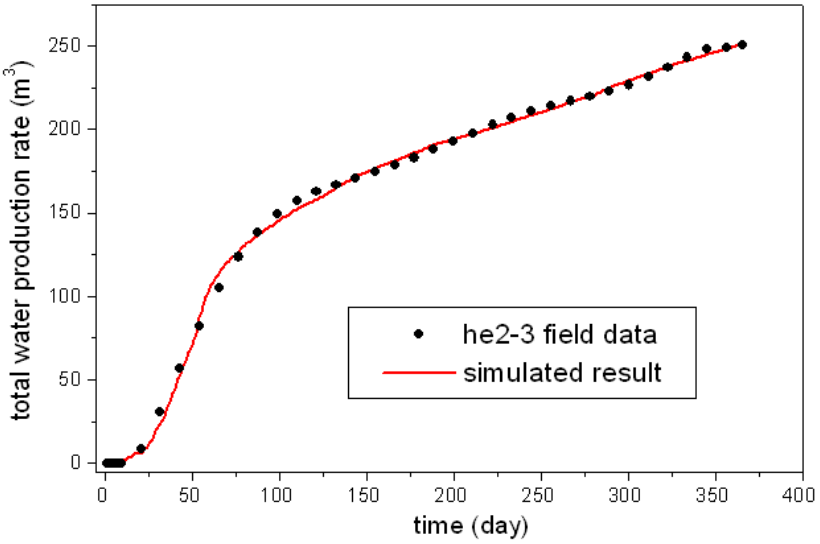

Figure 6.21 History matching of total water rate for he2-3 well

(3) He2-5-1 well

Wellbore track		44.5-589m vertical well						
Formation group section	code	Q	P_{2s}	P_{1x}	P_{1s}	C_{3t}	C_{3b}	C_{3b}
	depth(m)	12	252	366	435	575	581	589
height		2.2m						

Table 6.4 Basic information for he2-5-1 well

He2-5-1 well is one directional vertical production well in heshun block, deployed by Sinopec huadong company. The main production layer for this well is still 15# coal

seam. **Table 6.4** gives the basic information for this well. The history data from 1st March 2010 to 20th Jane 2010 are utilized for the history matching, totally 122 days.

As shown in **Figure 6.22**-**Figure 6.25**, the history matching results for gas, water rate and pressure changes are better than expected with the following parameter value:

Coal seam	Porosity	Cleat permeability	Skin factor
6.23m	0.02	0.23md	-2.53127

These history matched results can be used as the guidance for the future production of He2-5-1 well, this is because the well test data doesn't exist for this well until now.

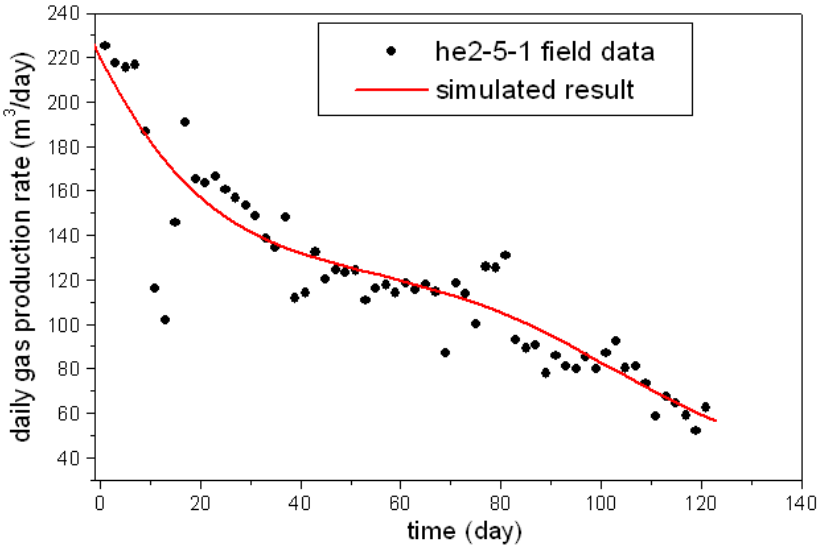

Figure 6.22 History matching of daily gas rate for he2-5-1 well

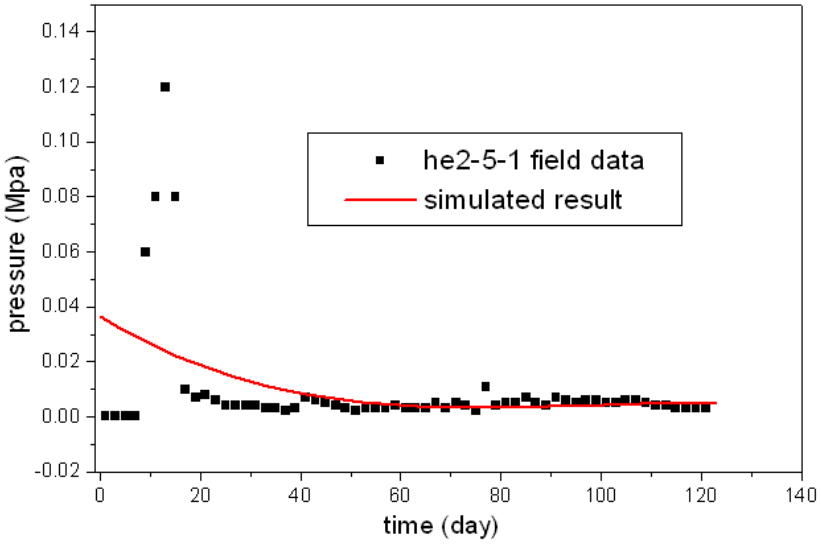

Figure 6.23 History matching of pressure for he2-5-1 well

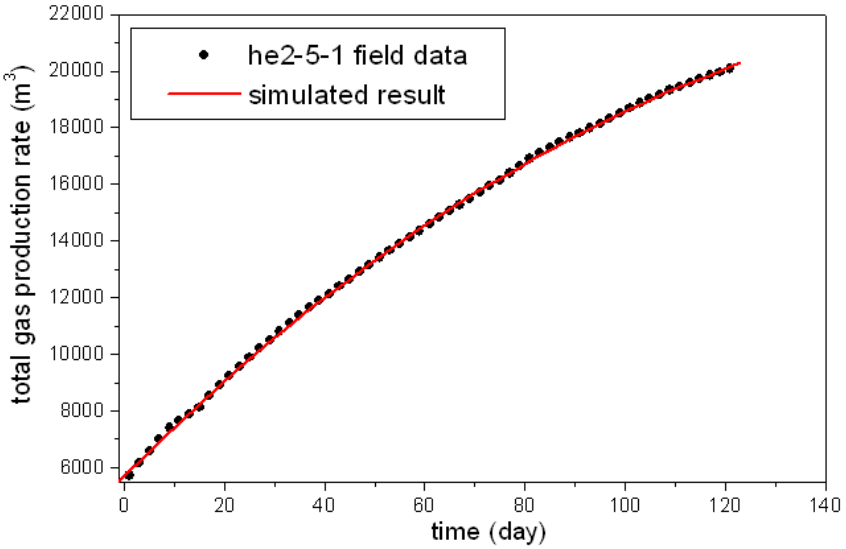

Figure 6.24 History matching of total gas rate for he2-5-1 well

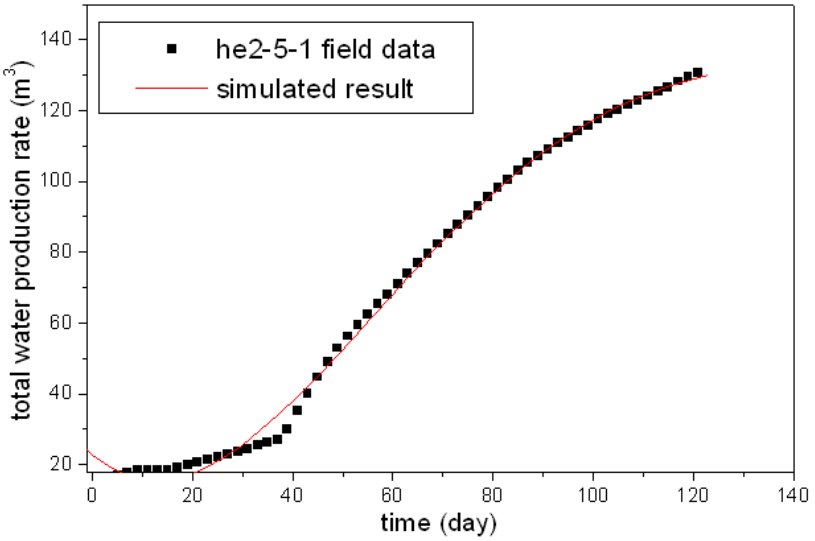

Figure 6.25 History matching of total water rate for he2-5-1 well

6.2.1.3 Productivity forecast

Wellbore track		Vertical well					
Formation group section	code	P_{2s}	P_{1x}	P_{1s}	C_{3t}	C_{2b}	O_{2f}
	depth(m)	318	404	460	582	600	614
height		2.3m					

Table 6.5 Basic information for he2-2 well

He2-2 well is chosen for doing the productivity forecast in Heshun block. It is a vertical

production well and the main production layer is 15# coal seam. This well was drilled in 2009, and the basic information for it is shown in **Table 6.5**.

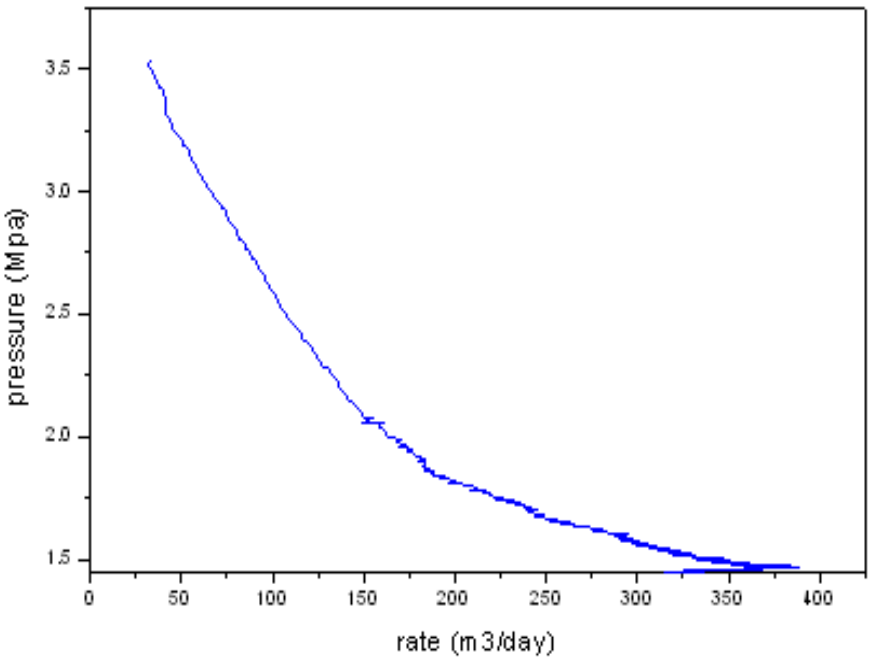

Figure 6.26 Productivity forecast for he2-2 well

The pressure rate changes curve (**Figure 6.26**) is made by the simulator developed for vertical well according to the basic information provided in **Table 6.4**. The production rate of He2-2 well decreases with the pressure depletion. And the productivity forecast value for this well is 375.6 m^3/day, which has good agreement with the reservoir production characteristic of He2-2 well. This again validates the accuracy of the model developed in **Chapter 2**.

6.2.2 Yanchuan Southern block

6.2.2.1 Geological characteristic

Yanchuan Southern block is located in the Southern eastern part of Ordos basin, and it belongs to the interchange of Weibei uplift and Jinxi fold belt. The structure characteristics of Yanchuan South block are not only different from the Shanxi block with strong activities (predated the extrusion drape and late stretch faulted) but also different from the relatively stable internal of Ordos basin (performed as transitional qualitative basin margin structure types).

In the studied zone, the coal seam layer is stabley developed, the placing depth of the main target coal seam layer is between 800-1500 meter, and the area is about 490 km^2. Petro China Daning-Jixian Block and Hanchengheyang block (located in the Northern

and Southern part of the block respectively) have already obtained industrial breakthrough. 2# coal seam of Yan1 well has already produced some commercial gas flow, which indicates the good prospects of CBM exploration.

The Coalbed Methane of the East margin part in Ordos basin is firstly explored in early 1990s. However, they didn't conducted CBM exploration within Yanchuan South block before the east China branch company begin to launch the exploration in this region. Thus this makes the higher exploration potential for this area.

The studied zone has 11 layers coal. Where Shanxi group contains 3 layers coal seam: 1#, 2#, 3# coal; Taiyuan group contains 7 layers coal seam: 4#, 5#, 6#, 7#, 8#, 10#; and the existing group layer 1. In addition, 2# and 10# coal seam are the main recoverable coal seams with good continuity for this block.

The geological structure in Yanchuan Southern block is relatively much simple. The overall strata are single inclined and western-leaned, in addition, the open layer becomes newer from east to west. The occurrence strata in Yanchuan block have Ordovician ZhongTong majiagou group (O_{2s}), FengFeng group (O_{2f}), Carboniferous ZhongTong existing group (C_{2b}), Stockings on Taiyuan formation (C_{3t}), Permian next tasseled Shanxi groups(P_1s), Xiashihezi group (P_1x), Permian stockings on stone box group (P_2s), Shiqianfeng group (P_2sh), Triassic next tasseled Liujiagou group(T_{11}), Heshanggou group (T_{1h}), Zhongtong Ermaying group (T_{2er}), Cainozoic neogene on new stockings group (N_2), Quaternary system next update tasseled (Q_1), Middle update tasseled (Q_2), Upper update tasseled (Q_2), and Brand new tasseled (Q_4). This study area composes of Carboniferous stockings on Taiyuan group and Permian next tasseled Shanxi groups.

6.2.2.2 History matching

In this part, Yan1 well, Yan1-20-10 well and Yan5 well drilled as horizontal well type are chosen for the history matching to verify the accuracy of the model in **Chapter 3**. In addition, sensitivity analysis is made by Yan1 well and the results show that the advanced model can accurately simulate the production of it. History matching results for these wells also indicates that the model proposed in **Chapter 3** can reasonably simulate the field data with branch number 6 and branch angle ranged from 43 degree to 48 degree. What is more, the gas slippage and threshold pressure gradient effects have to be considered for the simulation. The production forecast result from Yan2 well

further explains that the advanced coupled horizontal wellbore model can perfectly forecast the productivity in Yan2 well.

(1) Yan1 well

Parameters		2# coal seam	10# coal seam
Coal thickness (m)		5.6	2.5
Coal depth (m)		1750	1800
Gas content (m^3/t)		20.8	8.7
Reservoir pressure (MPa)		3.6301	3.9541
Critical pressure (MPa)		1.78	1.91
Langmuir pressure(MPa)		2.4	2.70
Langmuir volume (m^3/t)		35.02	35.14
Porosity (fraction)		0.02	0.02
Absolute permeability ($10^{-3}\mu m^2$)	k_x	0.17	0.23
	k_y	0.17	0.23
	k_z	0	0.01
Compressibility factor(MPa^{-1})		0.045	0.045
Skin factor		-3.2	-4.55
Coal density (t/m^3)		1.00	1.00
Wellbore radius (m)		0.108	0.108
Reservoir temperature (℃)		34.6	35
Main stream wellbore radius m		0.08	0.1
Branch wellbore radius m		0.048	0.05
Branch number (Yan1)		6	6
Branch angle degree (Yan1)		44.96	44.8

Table 6.6 Parameters used for simulation and history matching in yanchuan block

The numerical simulation was carried out according to the formation parameters listed above (**Table 6.6**). The purpose for this is to predict the gas production, water production rate and the pressure changes of 2# coal seam and 10# coal seam. The effects of gas slippage and threshold pressure gradient on the gas, water production rates and the pressure were also investigated.

1) Case study 1

Similarly as the Heshun block, case study 1 here for Yanchuan South block is mainly to study the gas and water production rates of 2# and 10# coal seams.

Figure 6.27 and **Figure 6.28** presents the daily gas and total gas production rates under the filed parameters come from 2# and 10# coal seam respectively. As shown in **Figure 6.27**, the maximum daily gas production rate of 2# coal seam is about 150 m^3, while it is only a little more than 100 m^3 for 10# well. What is more, the daily gas production

rate of 2# coal seam keeps higher than that of 10# coal seam in the third stage simulation process.

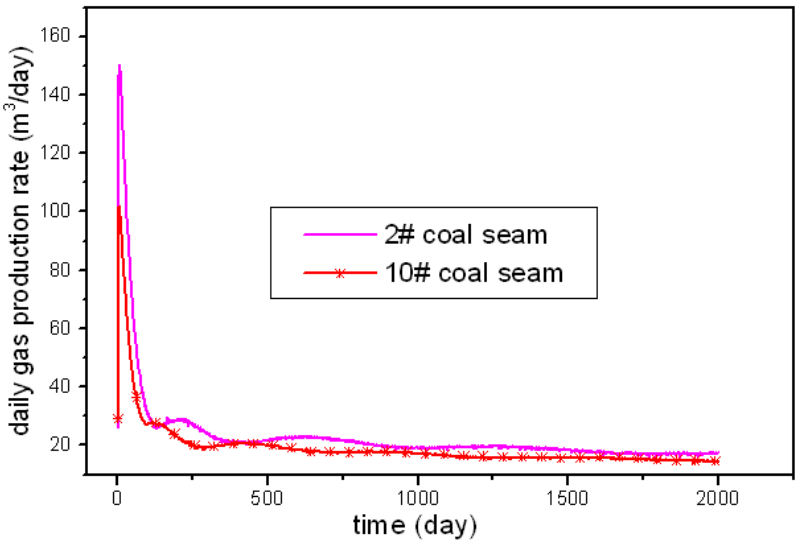

Figure 6.27 Daily gas production rate of 2# and 10# coal seam

As can be seen from **Figure 6.28**, the total gas production rate for 2# and 10# coal seams are straightly increasing. And the gas production rate for 2# coal seam is higher than that of 10# coal seam. This is caused by lower reservoir pressure of 10# coal seam.

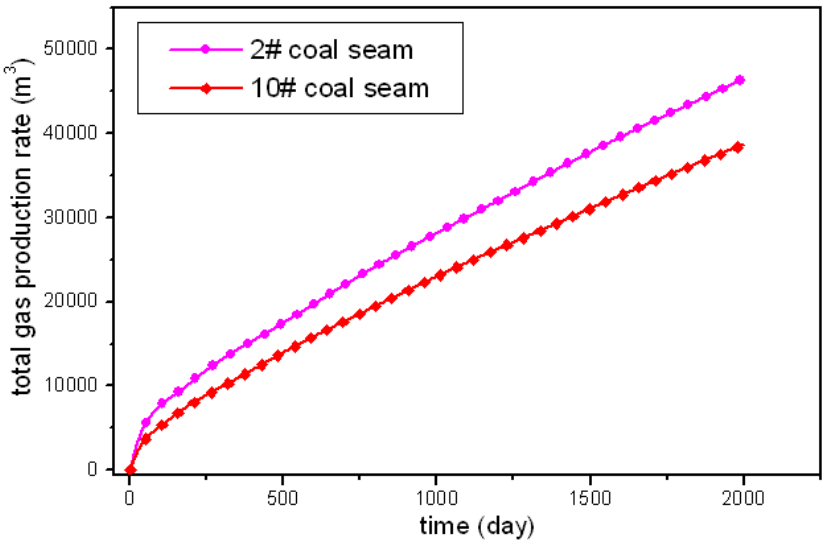

Figure 6.28 Total gas production rate of 2# and 10# coal seam

Figure 6.29 and **Figure 6.30** illustrate the daily water production rate and total water production rate of 2# and 10# coal seam respectively. The highest daily water

production rate for 2# coal seam is about 2.75 m^3/day, and correspondingly the maximum water production rate for 10# coal seam is only about 0.75 m^3/day. What is more, it took longer time for 2# coal seam to reach the minimum daily water production rate than 10# coal seam. In addition, the total water production rate increases with time, as shown in **Figure 6.30**, which is similar to the case for 3# and 15# coal seam in Heshun block.

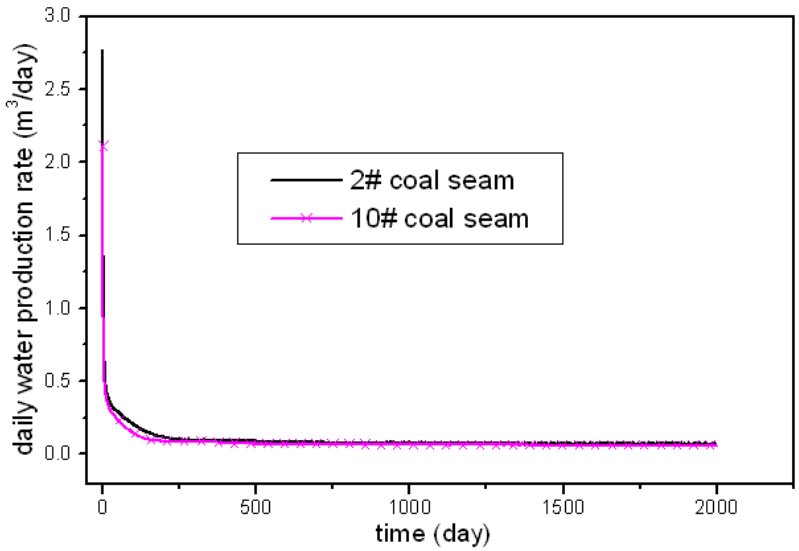

Figure 6.29 Daily water production rate of 2# and 10# coal seam

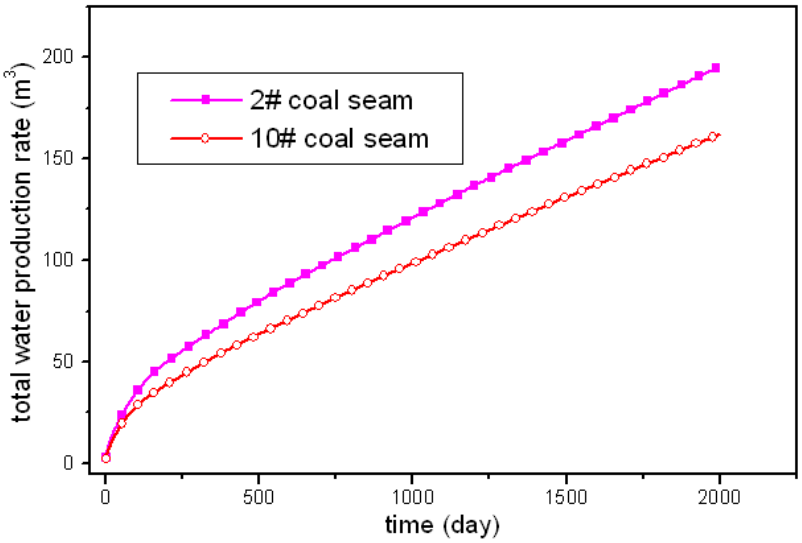

Figure 6.30 Total water production rate of 2# and 10# coal seam

Figure 6.31 presents the pressure changes of 2# and 10# coal seam. The pressure is slowly decreasing with time, the lowest pressure is about 1350 Kpa after producing 250

days for 2# coal seam, and approximately 1600 Kpa after producing about 240 days for 10# coal seam. Since then the pressure kept at a constant level during the simulation days for both 2# coal seam and 10# coal seam. Additionally, the pressure for 10# coal seam is much higher than 2# coal seam pressure in the late stage.

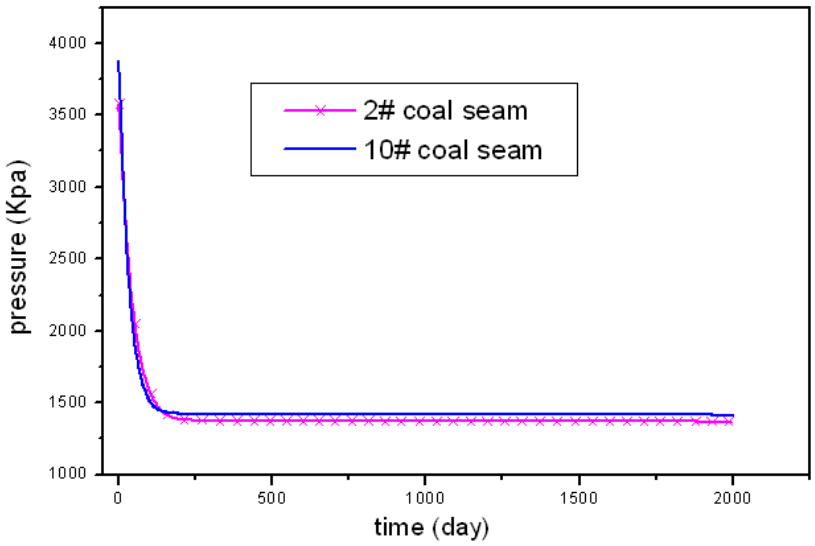

Figure 6.31 Pressure changes of 2# and 10# coal seam

2) Case study 2

This case study is mainly used to study the effects of gas slippage and threshold pressure gradient on the gas, water production rate and the changes of pressure. The comprehensive effects of both threshold pressure gradient and gas slippage effect are both considered. The parameters existed in the gas slippage factor and threshold pressure gradient factor are $\beta_1 = 161, \beta_2 = 0.47, \alpha_1 = 0.002, \alpha_2 = 0.4$.

Figure 6.32 and **Figure 6.33** show the variation of the daily gas production rate and the total gas production rate respectively. From **Figure 6.32** one can see that the daily gas production rate is nearly the same for both cases initially. And the maximum daily gas production rate for both 2# and 10# coal seams are lower when the gas slippage effect and threshold pressure gradient are ignored than the case when the two effects are considered. This indicates that the gas slippage effect performs as the leading role than the threshold pressure gradient during this time. Then the daily gas production rate gradually decreases and keeps at a constant level finally.

As shown in **Figure 6.33**, the total gas production rate is relatively much higher if both the gas slippage effect and threshold pressure gradient effect are considered. The total

gas production rate of 2# coal seam can only reach 38000 m^3 after 2000 days simulation if the two effects are both ignored, however, it can be 200000 m^3 when the two effects are considered. 10# coal seam has the same trend as that of 2# coal seam.

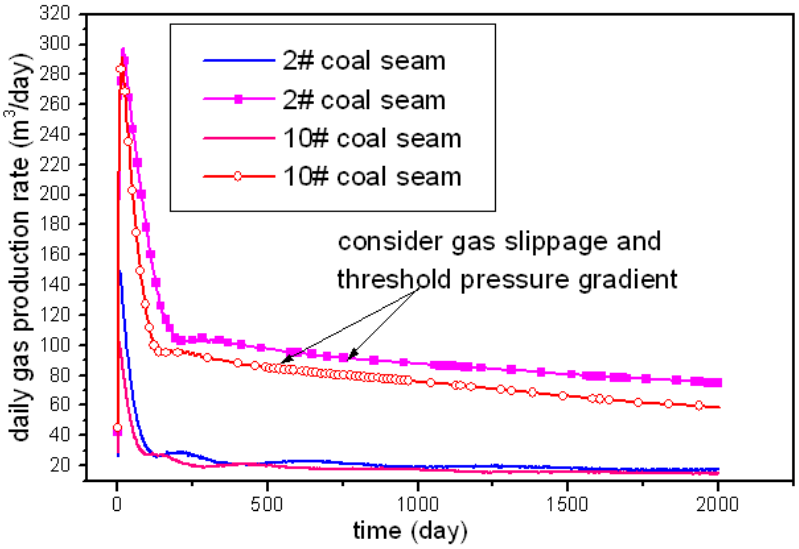

Figure 6.32 Comparison of daily gas production rate for 2# and 10# coal seam

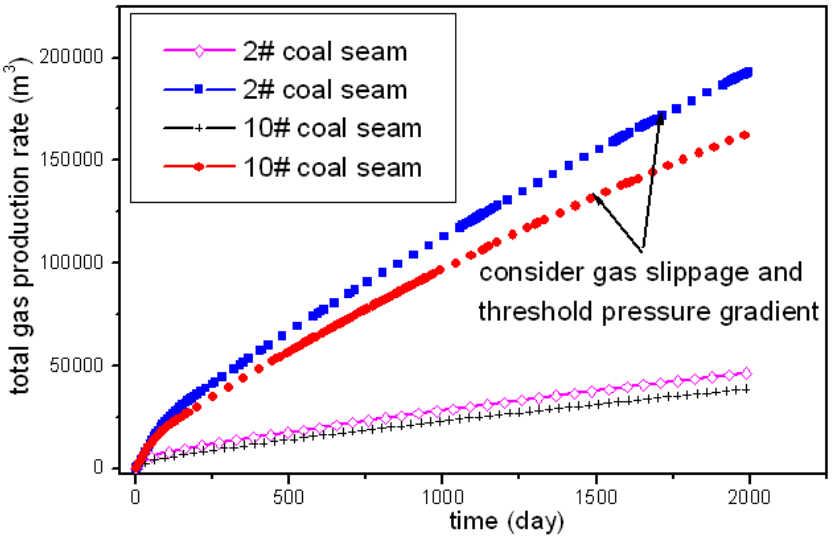

Figure 6.33 Comparison of total gas production rate for 2# and 10# coal seam

Figure 6.34 and **Figure 6.35** present the comparison of daily water and total water production rate respectively. The field data came from 2# and 10# coal seams are used here. It can be seen from **Figure 6.34** that the daily water production rate for both 2# and 10# coal seams are higher when the gas slippage effect and threshold pressure gradient were ignored in the model than the case when the two effects are considered

this is attributed to the fact that the threshold pressure gradient effect is stronger than the gas slippage effect for this simulation stage, which can lower the water production rate. Similar trend can be found in **Figure 6.35**. The difference is that the daily water production rate kept at a constant level after a few hundred days production for all the cases, while the total water production rate increases during the simulation process.

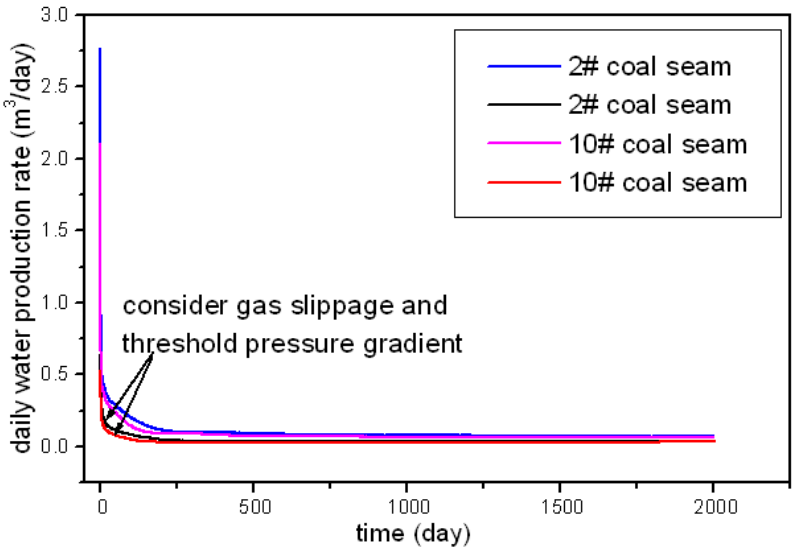

Figure 6.34 Comparison of daily water production rate for 2# and 10# coal seam

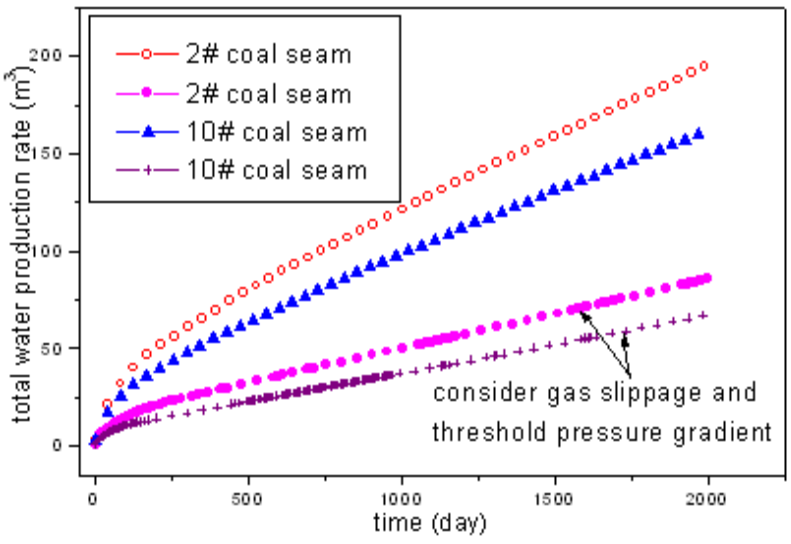

Figure 6.35 Comparison of total water production rate for 2# and 10# coal seam

Figure 6.36 presents the comparison of the pressure changes with time. From the figure it can be seen that the pressure is much lower when the gas slippage effect and threshold pressure gradient were ignored than the case when the two effects are

considered during the whole production process. This is caused by the lower water when the two effects are considered.

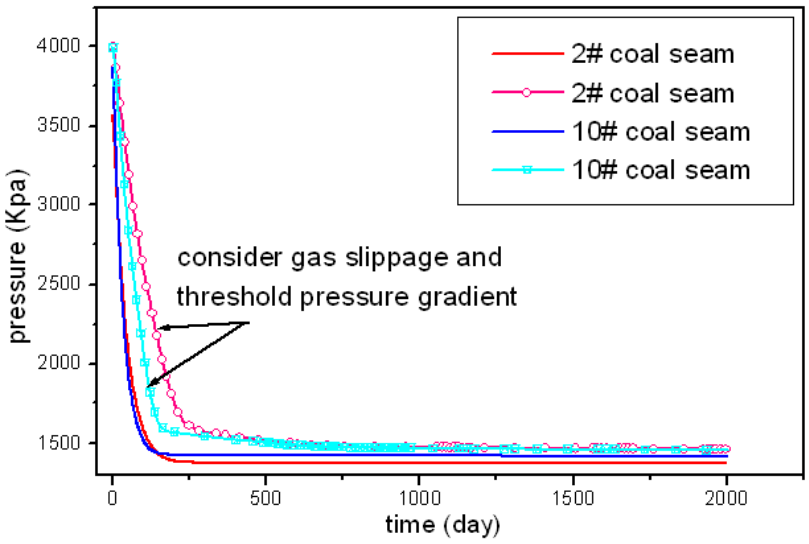

Figure 6.36 Comparison of pressure changes for 2# and 10# coal seam

3) Case study 3

Yan1 well as multi-branch horizontal well type was chosen in Yanchuan South block. The production data from April in 2010 to December in 2010 was used for the history matching, the production days are totally 275 days. The 2# and 10# coal seams are both infinite on plane and saturated by water in natural situation, thus boundary conditions, consisting of constant pressure and saturation at external boundary, and specified pressure for production well were used in the simulation. Here the 10# coal seam is chosen for the study area, which belongs to the carboniferous on stocking Taiyuan group.

The history matching work was done in this stage to further verify the model developed in the study. The permeability in this block is not very low, thus the artificially fracturing work is not considered for this area which can reduce the exploration cost on the region.

The simulated gas production rate, as shown in **Figure 6.37** and **Figure 6.38**, are consistent with the field data observations. Similar conclusion can also be seen in **Figure 6.39**, which illustrates the history matching of pressure. The daily gas production becomes 90 m^3 / day after producing about 125 days (**Figure 6.37**), which

was caused by the shutting well for reproduction, and this is also why there exists pressure buildup and drawdown (**Figure 6.39**).

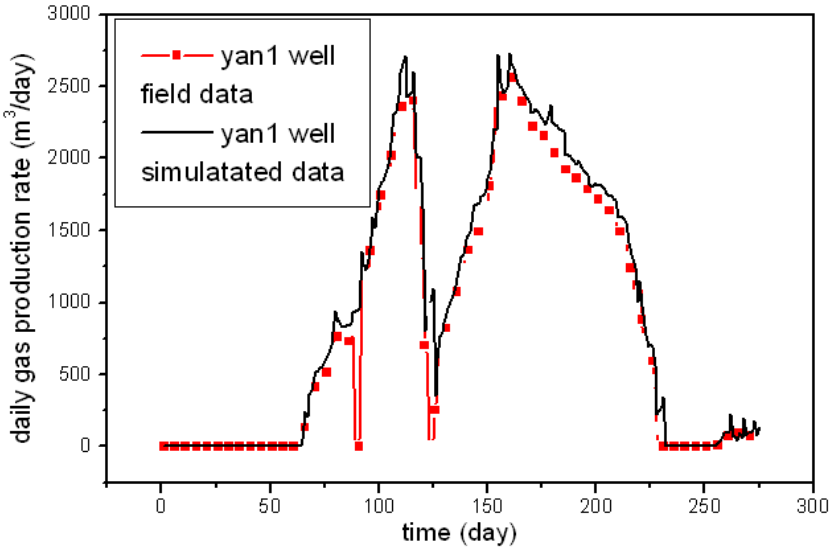

Figure 6.37 History matching curves of daily gas production rate for yan1 well

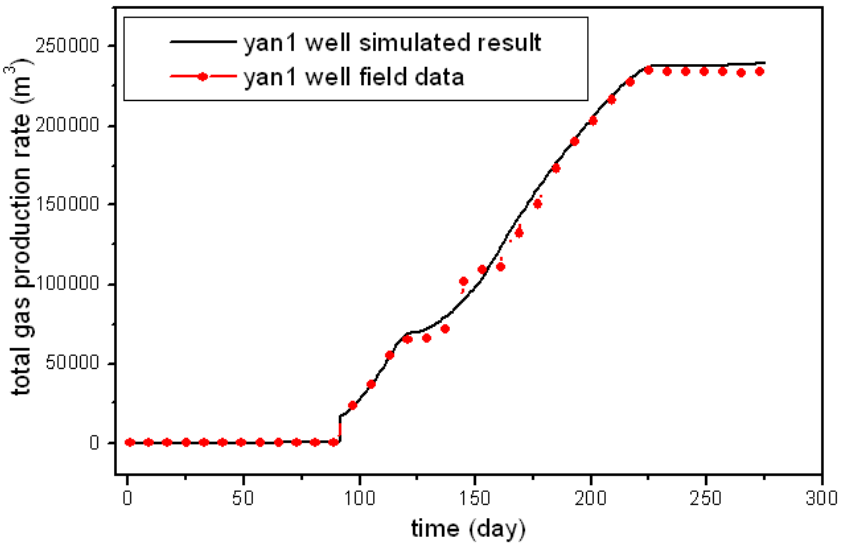

Figure 6.38 History matching curves of total gas production rate for yan1 well

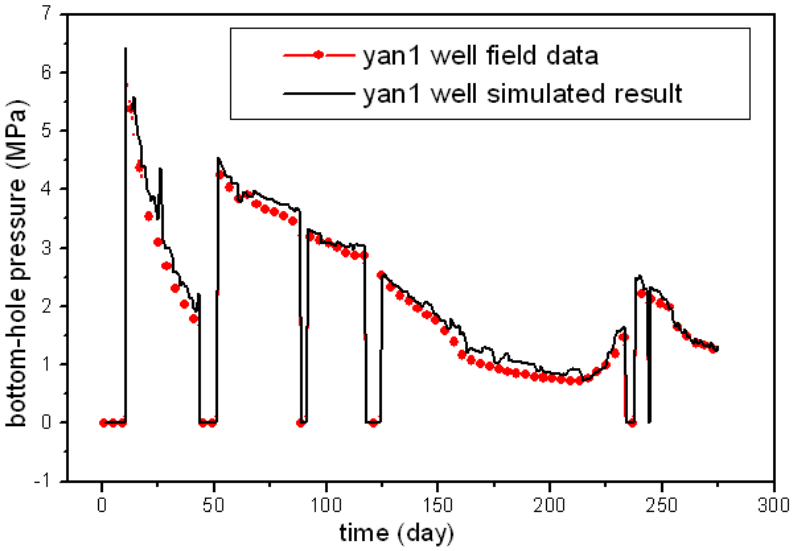

Figure 6.39 History matching curves of BHP for yan1 well

Figure 6.40 and **Figure 6.41** give the history matching result for water production rates of Yan1 well. The simulated result shows good agreement with the observed result. It is also obviously to see that the water production was suddenly reduced to zero on 125 day (**Figure 6.40)**, and then reproduction again, which is caused by a few days of repairing well. The result also indicates that 10# coal seam is the main layer to produce water, which means 10# coal seam should be plugged first to exploit 2# coal seam.

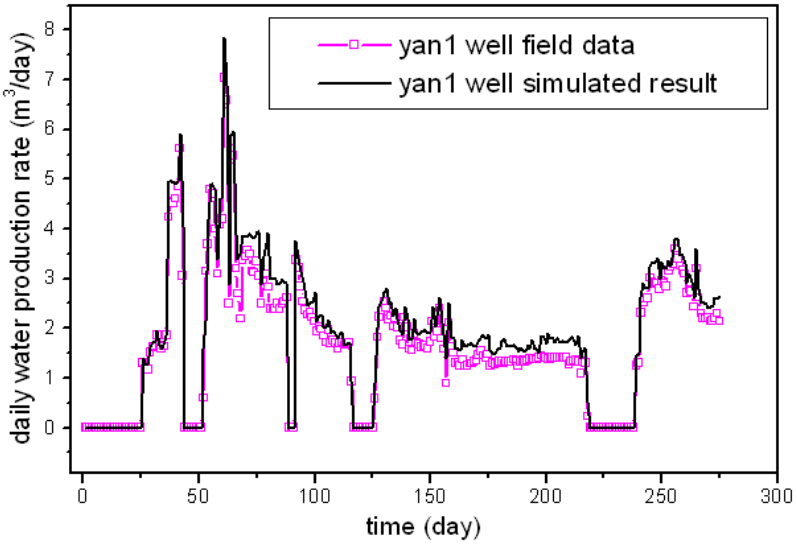

Figure 6.40 History matching curves of daily water production rate for yan1 well

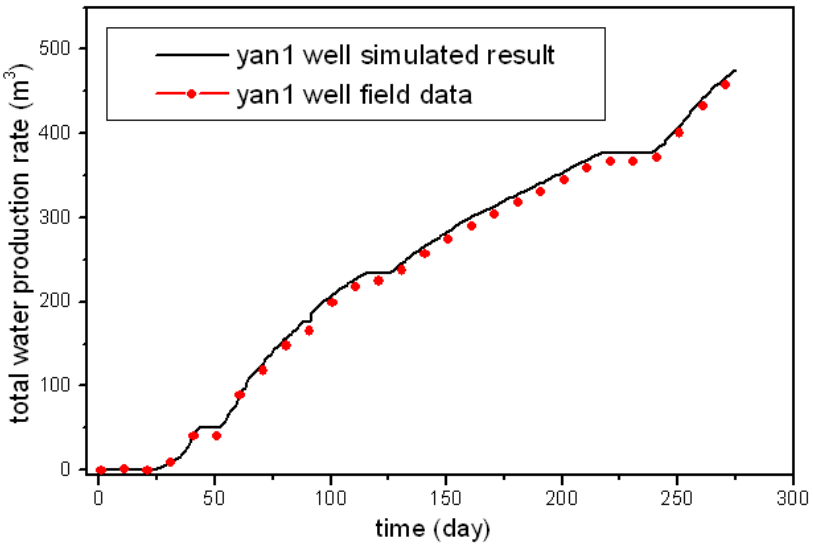

Figure 6.41 History matching curves of total water production rate for yan1 well

In addition, the good history matching results are achieved with branch number 6, branch angle 45 degree, and the following parameters:

Coal thickness	Porosity	Cleat permeability	Skin facor
7.62m	0.02	2.1md	-3.4

(2) Yan1-20-10 well

Yan1-20-10 well is a multi-branch horizontal type parameter well located around Yan1 well. Its drilling branch number is 6 and branch angle is 47.89 degree. The basic well parameters are the same as Yan1 well. History matching is made with the parameters in **Table 6.6** as input and with the simulator developed in **Chapter 3**.

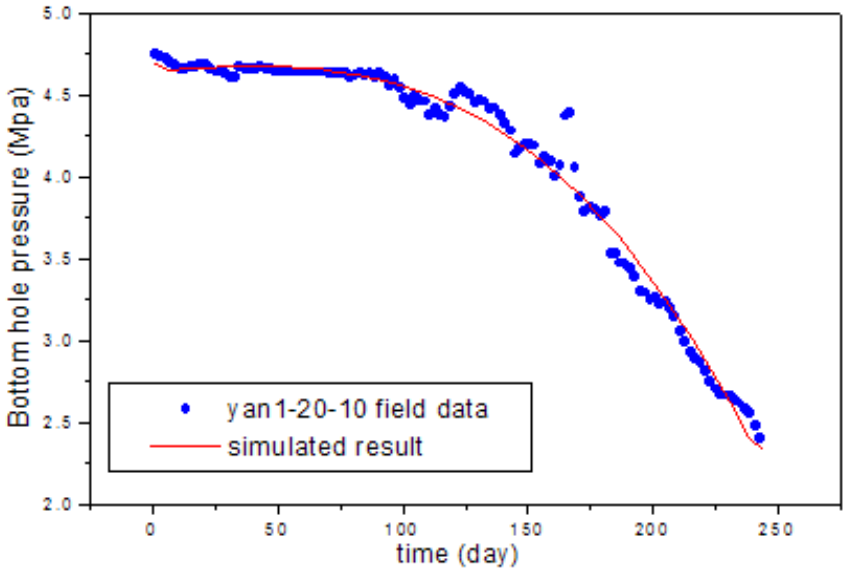

Figure 6.42 History matching of bottom-hole pressure

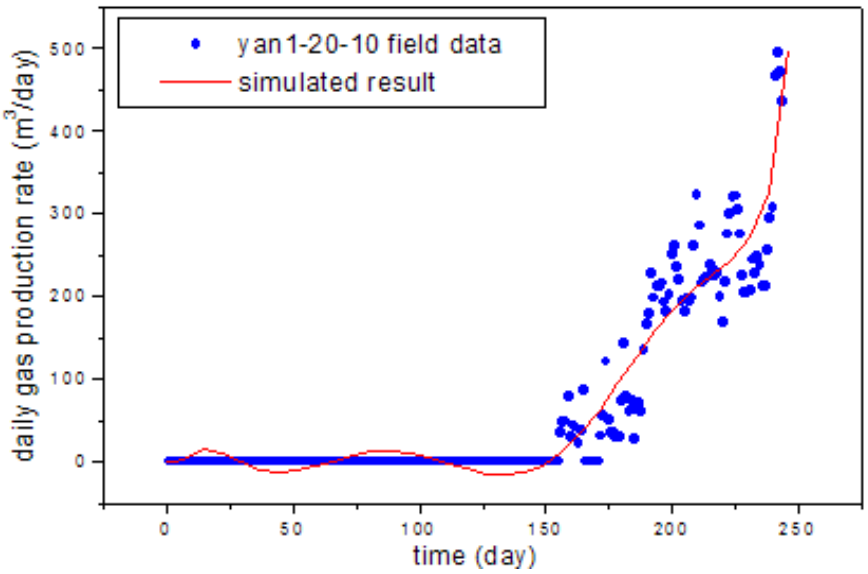

Figure 6.43 History matching of daily gas rate

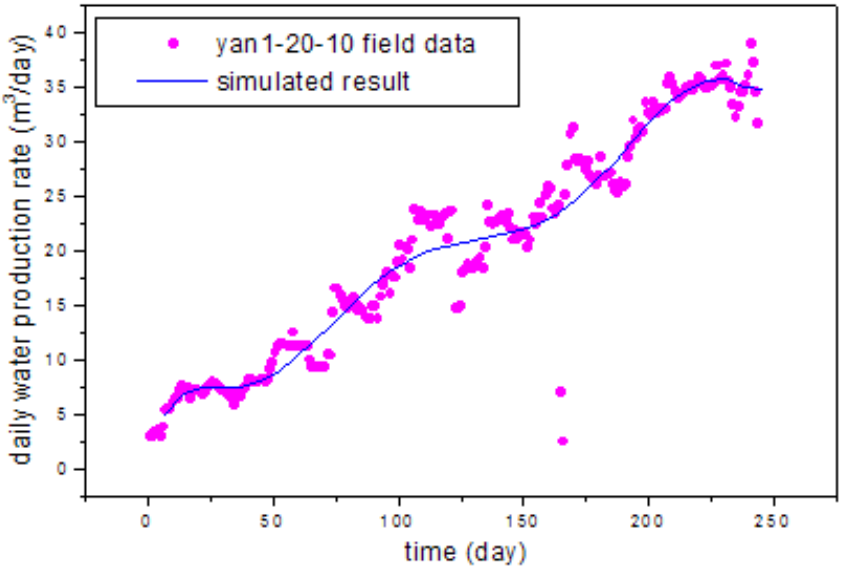

Figure 6.44 History matching of daily water rate

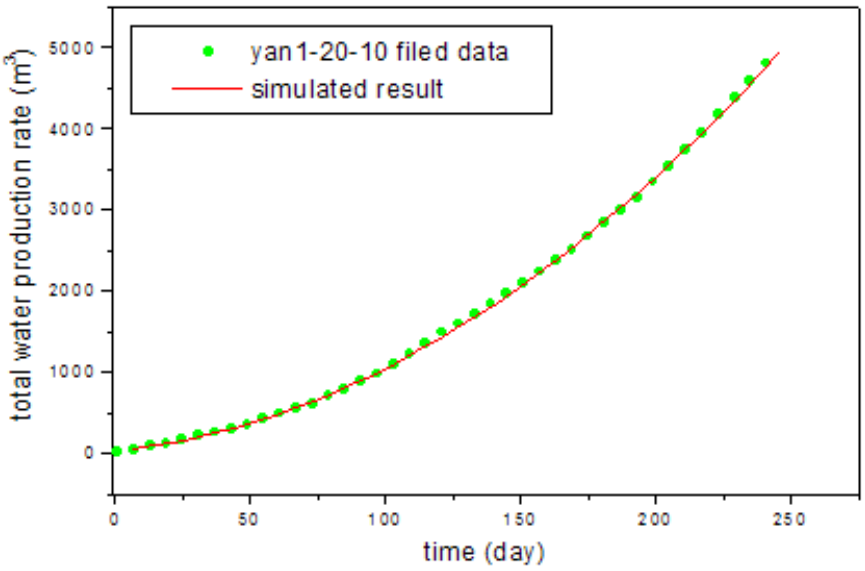

Figure 6.45 History matching of total water rate

Figure 6.42-Figure 6.45 gives the history matching of pressure, gas and water rate for Yan1-20-10 well. During the history matching process, it was found that the matching results are the best when the branch number is 6, branch angle is 48 degree which are the very close to the input branch number and branch angle, and the following fluid parameters:

Coal thickness	Porosity	Cleat permeability	Skin factor
4.562	0.02	0.75	-2.28

These history matched parameters can be guided for the future production of the well, for the tested parameters are not existed yet for Yan1-20-10.

(3) Yan5 well

Yan5 well is a multi-branch horizontal type parameter well deployed by Sinopec Huadong Company. Its drilling branch number is 6 and branch angle is 42.98, and it is located in the Ordos basin in Shanxi province. The main production layer for it is 2# coal seam, and the basic parameters are got through the stress test and well test, as shown in **Table 6.7**. The history matching is done by the information provided, and the simulator developed in **Chapter 3**. In addition, the history matched parameters can be treated as reference for the next stage exploration of this well.

No	Layer	Depth/m	Coal thickness/m	Well type
Yan5	2	878.80-882.50	3.7	horizontal

Table 6.7 Parameters for yan5 well through well test

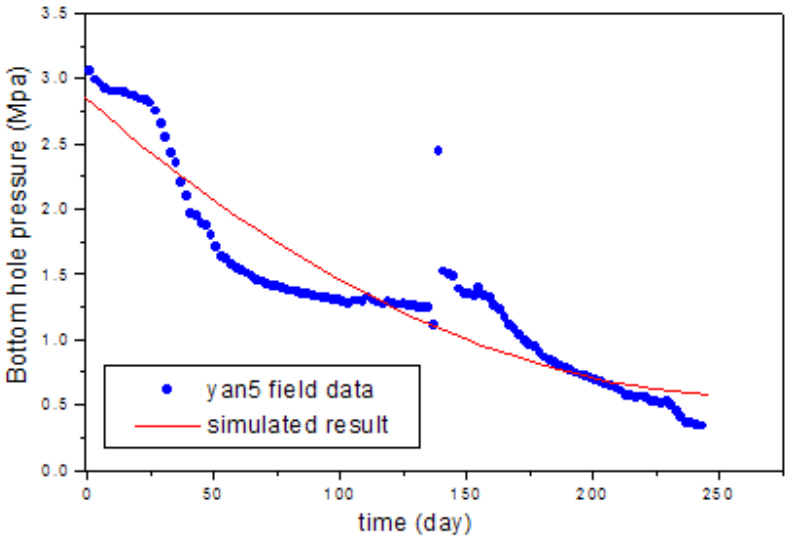

Figure 6.46 History matching of bottom-hole pressure for yan5 well

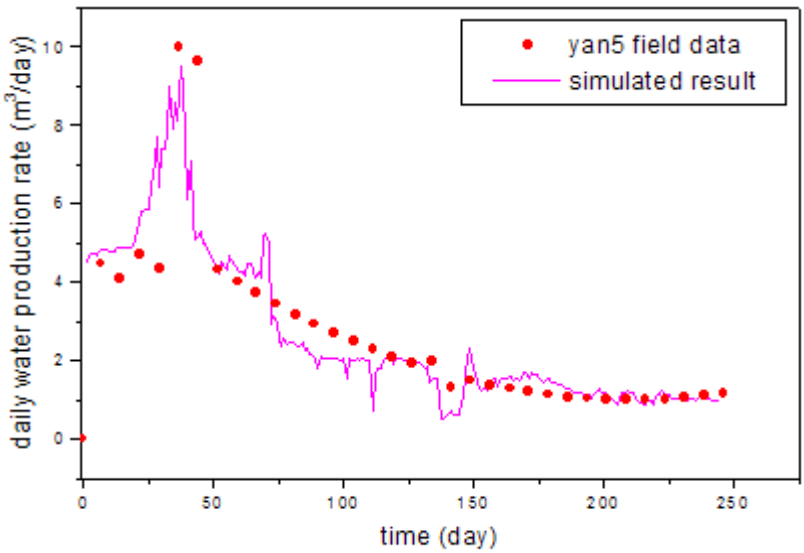

Figure 6.47 History matching of daily water rate for yan5 well

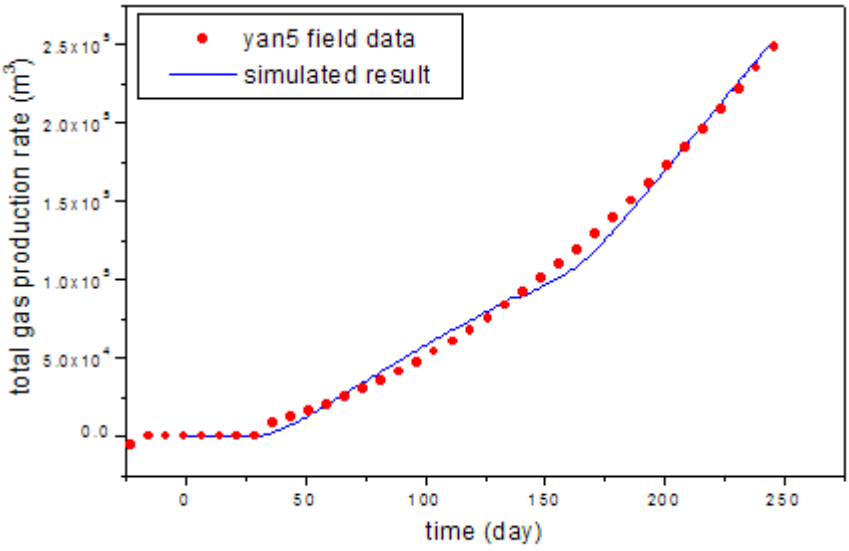

Figure 6.48 History matching of total gas rate of yan5 well

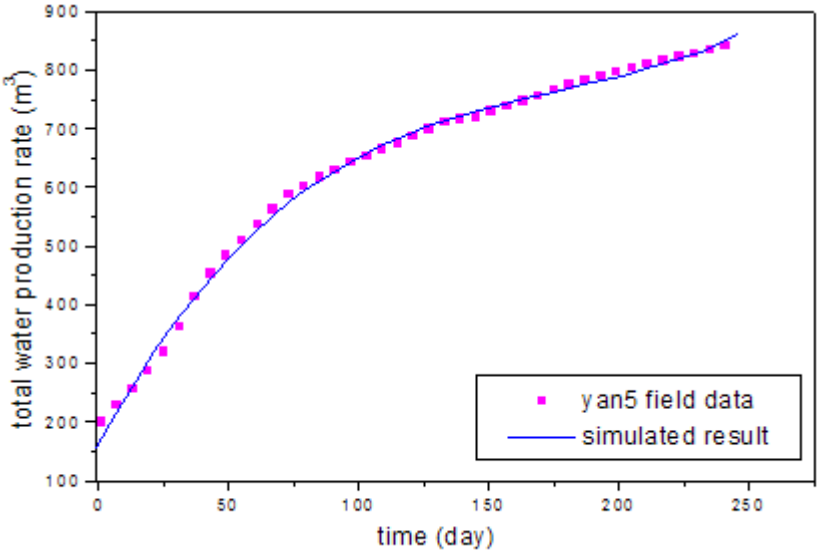

Figure 6.49 History matching of total water rate for yan5 well

Figure 6.46-**Figure 6.49** shows a good history matching result of pressure, gas and water rate. It is achieved with branch angle 43 degree and branch number 6 which fits the input drilling type very well, and the following parameters:

Coal thickness	Porosity	Cleat permeability	Skin factor
4.0m	0.02	0.058md	-4.46

The coal seam thickness is the only parameter one can get through the field data, which is 3.7 m. And the relative error between the input value and history matched value is 7.5%, which is in a reasonable extent to validate the accuracy of the model proposed in **Chapter 3**. And the other interpreted parameters such as porosity, cleat permeability and skin factor can guide the future production for the field.

6.2.2.3 Productivity forecast

Yan2 well is utilized for the productivity forecast, it is a horizontal type parameter well deployed in Ordos basin by Sinopec Huadong Company. And its drilling branch number is 6, and drilling branch angle is 44.68 degree. The main production layer for it is the 2# coal seam in Shanxi group and 10# coal seam in Taiyuan group. The designed drilling layer for Yan2 well is located in Majiagou group with drilling depth of 935m, and it shouldn't stop finishing drilling until it reached the 10# coal seam of Shanxi group. **Table 6.8** gives the basic information for the productivity forecast of Yan2 well.

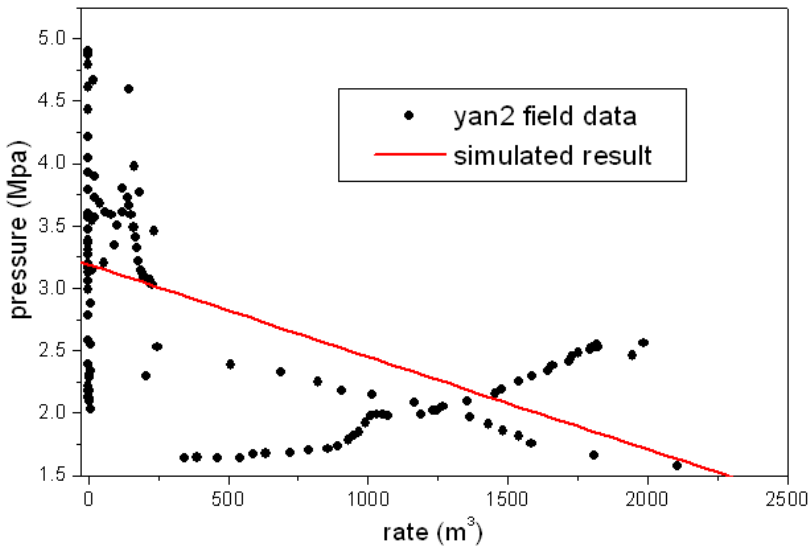

Figure 6.50 Forecast curve for yan2 well

The predicted gas rate for Yan2 well is around 2400 m^3/day, and the field gas rate is 2107 m^3/day, as shown in **Figure 6.18**, the relative error between them is 12.2%. The

agreement of field data and simulation result is very good if comparing every point between them. The whole relative error is around 27.8%, which shows good prediction of the gas rate.

Well type		Horizontal							
Formation section	section	Quaternary system	Liujiagou grouop	Shiqianfeng group	Upper stone box group	Down stone box group	Shanxi group	Taiyuan group	Benxi group
	depth(m)	108	244	374	709	834	913	951	956
height		1.2m							

Table 6.8 Basic information for yan2 well

6.2.3 Zhijin block

The model proposed in **Chapter 4** is used for the history matching of Zhijin block, for the gas component in this block is variety, and the well type for this block is multi-branch horizontal well type.

6.2.3.1 Zhi2 well

Zhi2 well is a CBM multi-branch parameter well located in Zhijin-Langdai-Anshun district. And it is explored by Sinopec Huadong Company. In addition, its dirlling branch number is 8 and branch angle is 43.98 degree. The main production layer for it is the 6#, 7#, 16# and 23# coal seam in Longtan group. Here, the 23# coal seam is chosen as the study zone, **Table 6.9** shows the basic parameters achieved from well testing analysis.

No	Depth/m	Struction/m	Type/°	Thickness/m	Radius/mm
$23^{\#}$	430.45～432.30	1.85	horizontal	1.85	215.9

Table 6.9 Parameters for zhi2 well

The history matching result for the gas and water rate is better than expected by using the multi-branch horizontal well type model in **Chapter 4** with branch number 8, and branch angle 44 degree (**Figure 6.51** and **Figure 6.52**). The history matched parameters are shown as follows:

Matrix porosity	Cleat porosity	Matrix permeability	Cleat permeability
0.014	0.02	1.4md	2.4

While the input value for Zhi2 well is shown as:

Matrix porosity	Cleat porosity	Matrix permeability	Cleat permeability
0.0139	0.02	1.429md	2.28

The relative error between the history matched value and input value for the matrix porosity, cleat porosity, matrix permeability and cleat permeability are 0.7%, 0%, 2.07% and 5% respectively. From this one can see that the relative error for the permeability is becoming much smaller, the interpreted cleat permeability as well the input cleat permeability is both big enough to explain the 3000 m^3 daily gas rate. From this point, one can conclude the accuracy and reasonablility of the model developed in **Chapter 4**. Thus, the history matched parameters can be used for further field production.

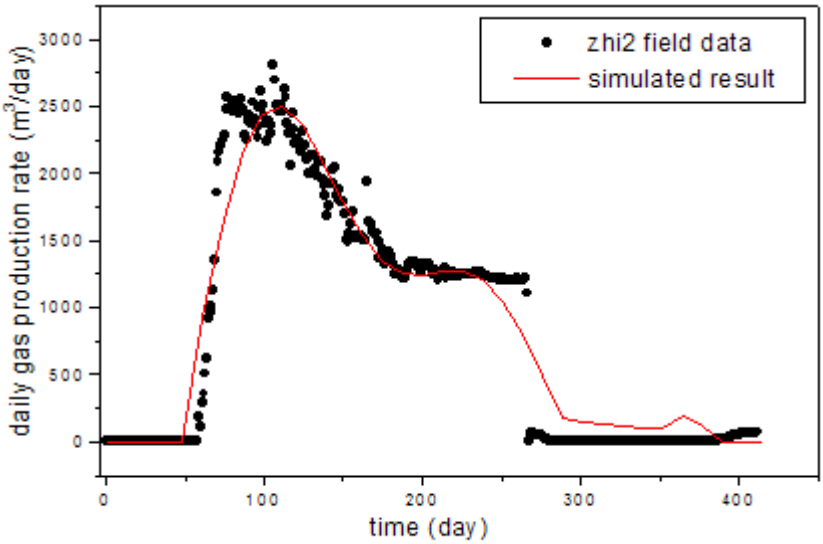

Figure 6.51 History matching of daily gas rate for zhi2 well

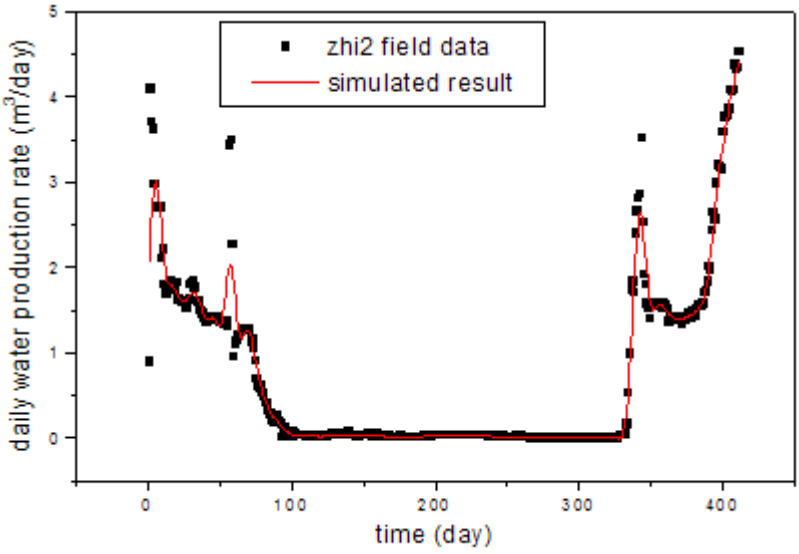

Figure 6.52 History matching of daily water rate for zhi2 well

6.2.3.2 Zhi3 well

Zhi3 well is also a multi-branch parameter CBM well located in Zhijin-Langdai-Anshun district, deployed by the Sinopec huadong company, with its drilling branch number is

8, and branch angle is 44.99 degree. The main production layer for it is 16# coal seam in Longtan group. **Table 6.10** gives the basic parameters for Zhi3 well.

No	Depth/m	Type/°	Thickness/m	Radius/mm
16#	735.90-738.05m	horizontal	2.15	215.9

Table 6.10 Parameters for zhi3 well

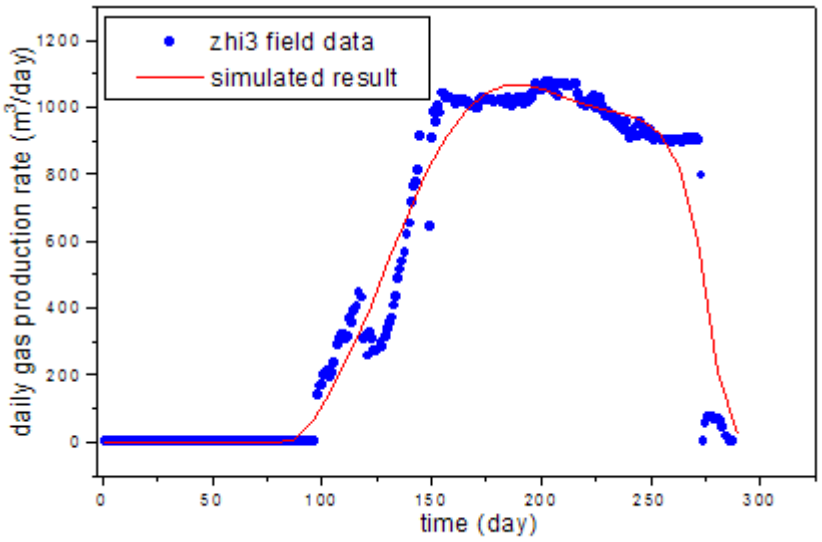

Figure 6. 53 History matching of daily gas rate for zhi3 well

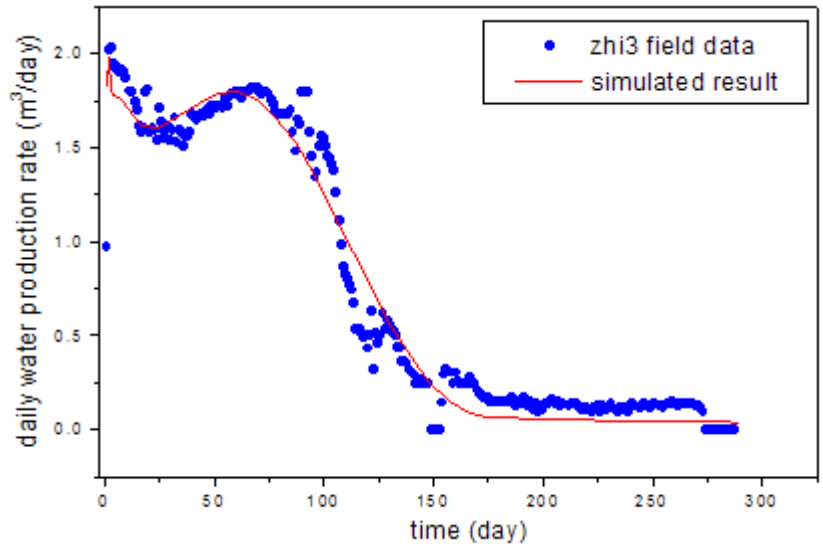

Figure 6.54 History matching of daily water rate for zhi3 well

Figure 6.53 and **Figure 6.54** show the history matching of gas and water rate for Zhi3 well with branch number 8 and branch angle 45 degree which is nearly exactly the same as the drilling branch number and branch angle. Moreover, the other history matched parameters are as follows:

Matrix porosity	Cleat porosity	Matrix permeability	Cleat permeability
0.018	0.02	0.8 md	1.7

While the input value that comes from well test analysis is shown as:

Matrix porosity	Cleat porosity	Matrix permeability	Cleat permeability
0.0178	0.02	0.827md	1.68

The relative error between matrix porosity, cleat porosity, matrix permeability and cleat permeability is 1%, 0%, 3.4%, 1.17%. One can see that the relative error for permeability has good agreement with the input value, which just reflect the high gas production rate (1000 m^3/day or more). This indicates that triple porosity model gives better matched result compared with dual porosity model if the gas slippage effect, threshold pressure gradient effect and matrix shrinkage effect are all considered. Thus the history matched result from the simulator in this study should be used for future exploration in Zhi3 well.

6.3 Chapter conclusion

(1) Comparisons of gas and water production rates between the case that ignores the gas slippage and threshold pressure gradient effects and the case that takes the two effects into consideration are made for He2 well and Yan1 well, the purpose to do this is to investigate the influence of the two effects on the production rate, and which one is dominant during the simulation process.

(2) The gas slippage effect on the gas production rate is stronger than threshold pressure gradient effect for He2 well in Heshun block, while it has weaker effect on water production rate and pressure changes than threshold pressure gradient. Similar effect can be found when simulating Yan1 well in Yanchuan Southern block.

(3) The result of 3# and 15# coal seam in heshun block indicates that 3# coal seam can produce much more gas than 15# coal seam. While for Yanchuan South block, 2# coal seam is easier to produce gas and its gas production rate is higher than the 10# coal seam, which means that 3# coal seam in Heshun block and 2# coal seam in Yanchuan South block should be the layer chosen for developing.

(4) The history matching work was done according to the observation data of Heshun block, Yanchuan Southern block and Zhijin block to validate the accuracy of the model as well as the necessity for considering the effects of gas slippage, threshold pressure gradient and matrix shrinkage.

(5) He2 well, He2-3 well and He2-5-1 well are used for the history matching in heshun block as vertical well type using the model developed in **Chapter 2**. The simulated results have good agreement with the field data, but the history matched permeability

value is much bigger than the field tested value. However, the history matched value is more reasonable to explain the gas production rate, which means the matched permeability value is more accurate for future field exploitation.

(6) Yan1, Yan1-20-10 and Yan5 well are chosen for the history matching in Yanchuan southern block as multi-branch horizontal well type using the model built in **Chapter 3**. The best history matching results achieved with branch number 6 and branch angle ranging from 43 degree to 48 degree. In addition, the permeability relative error between history matched value and input value is the biggest, while the history matched result is much more accurate according to the gas production rate, which is similar to the interpretation for Heshun block. Otherwise, the daily gas production rate could not reach more than 1000 m^3 if the permeability as low as the input value.

(7) The best history matching results achieved for Zhi2 well and Zhi3 well with branch number 8 and branch angle around 45 degree using the simulator developed in **Chapter 4**. Additionally, the history matched permeability value has better agreement with the observed permeability value than expected, which can both be used for the future well exploration, because they can best describe the high field gas and water production rate. Also, Zhijin block shows potential production ability, so it should be explored further. In addition, from the relative error point of view, the triple porosity model built in **Chapter 4** can better matching the field production data compared with the dual porosity model developed in **Chapter 3** if gas slippage effect, matrix shrinkage effect and threshold pressure gradient effect are all considered**.**

(8) The productivity forecast value for He2-2 well is 375.6 m^3/day, which shows good agreement with its reservoir production characteristic. And the predicted gas rate for Yan2 well is around 2400 m^3/day, while the gas rate from the field data is 2107 m^3/day. Thus, the relative error for it is 12.2%, and the whole relative error is around 27.8% if comparing every point in the figure, which shows the reasonability for field data prediction by using the models in this thesis.

Chapter 7 Conclusions and recommendations for future work

Firstly, this chapter provides a summary of the key results of the thesis, presents the main conclusions got from the CBM reservoir simulation and well testing method. In brief, the novel dual porosity and triple porosity models are developed in this study, and the corresponding new well testing methods are investigated, which have great significance and guidance in the future development of unconventional gas reservoir. Finally, the original objectives listed in **Chapter 1** have been achieved. Secondly, the recommendations for future work are described in details.

7.1 Conclusions

7.1.1 Motivation

7.1.1.1 Problems of the conventional simulation method

Many mathematical simulation models both with vertical well type and horizontal well types that are used in the oil and gas field as well as the CBM reservoir have been developed. The gas slippage and threshold pressure gradient are both considered in some conventional oil and gas reservoir. The matrix shrinkage effect is also taken into consideration for some specified CBM reservoir. However, they exists the following problems:

(1) The gas slippage and threshold pressure gradient effect as the whole part is not considered in the CBM reservoir primary production process yet, which sometimes results in overestimating the gas production rate and underestimating the water production rate, and can't exactly be used for the history matching of field data.

(2) The permeability model developed currently has a lot of limitations and shortcomings, they can only be applied for particular CBM fields, and sometimes the forecast results are not good enough.

Owing to the problems listed above, the novel and comprehensive mathematical models are driven to be developed for better evaluating and forecasting the field production.

7.1.1.2 Problems of Enhanced CBM method

A lot of achievements and improvements have been got in enhancing the CBM reservoir production. While they still have some shortcomings that need to be optimized for better simulating the actual field production.

In addition, an advanced coupled compositional triple porosity dual permeability model considering the gas slippage effect and threshold pressure gradient effects has not been developed for enhanced CBM reservoir simulation, which can best accurately simulate the enhancing process of CBM reservoir.

Also, the proper permeability model that can be incorporated with the advanced coupled compositional triple porosity permeability model has not been studied yet.

7.1.1.3 Problems of the well testing method

Water occupied the cleat system initially in the CBM reservoir, so the well testing fluid for CBM reservoir is the water in the initial stage, while the natural gas that existed in the sandstone is the testing object for the conventional gas reservoir. Thus there exits big difference between the natural gas and CBM reservoir in the following aspects:

(1) Well test fluid

(2) Fluid characteristics

(3) Different well test object and analyzing method

Currently, the published well testing method for CBM reservoir is mainly characterized into two types: modified P-M method, Pseudo pressure method. These methods have great strengths in interpreting the parameters in CBM reservoir, take pseudo pressure method (**Kamal, M.M. and Six, J.L., 1989[23]**) as an example:

(1) It enables the interpretation engineer to calculate the absolute permeability at any time even when both gas and water are being produced.

(2) It was verified successfully by analyzing simulated tests from a rigorous coal degasification numerical simulator.

However, they have a lot of limitations:

(1) Only the total mobility value λ_t can be interpreted if the modified P-M method for CBM is used due to the difficulty in getting accurate relative permeability data.

(2) Pseudo pressure method can only limited to the situation when the gas desorption is very fast, and also need the isothermal adsorption data for the interpretation, which is very difficult to get in CBM reservoir.

There is another traditional pressure square method used for multiphase well test analysis in conventional oil and gas reservoir, which has much less limitations. However, in case that CBM reservoir is different from the common oil reservoir, the pressure squared method proposed by AI-Khalifah (**AI-Khalifah, A-J.A., et al., 1987[22]**) can't be directly applied to the gas and water two phase CBM reservoir. So it has to be modified for the well testing interpretation of CBM reservoir. Thus, a new pressure square method that is suited for triple porosity dual permeability CBM reservoir needs to be developed in this thesis.

7.1.2 Key findings and Conclusions

Owing to the problems found above, the key findings and main conclusions are shown as follows:

7.1.2.1 Dual porosity single permeability model

(1) Vertical well model

A new three dimensional, dual porosity, single permeability, non-equilibrium adsorption, gas and water two phase flow, pseudo-steady state mathematical model was developed, which reflects the concrete influence factors in low permeability CBM reservoirs, and it was followed by a new theoretical formulation of permeability and porosity including the effect of matrix shrinkage. The breakthrough of this model is that it is beyond the limitation of researches nowadays that the gas slippage effect model is only applied to single phase permeability research.

A computer programme called COAFOR has been developed for this model. Three synthetic cases were studied, which proved that the developed algorithm works well for solving the problem stated above. The good agreement between the results that come from COAFOR and Eclipse under the same parameters further validates the accurate of the model in this chapter.

The gas and water rate increases with Langmuir pressure, while decreases with Langmuir volume, which means the larger the Langmuir volume, the lower the gas rate. Moreover, larger desorption time can lower the desorption rate, thus the gas and water rate drops with the increasing of desorption time. In addition, the stronger the heterogeneous of the reservoir, the earlier for the gas to reach its maximum, and the bigger the gas rate, however, this effect reversed for the late stage production.

What is more, there exist three stages in coal de-watering and production processes. The existence of threshold pressure gradient can largely reduce the gas and water production rate, so is total gas and water production rate. The gas slippage factor can increase gas and water production rate at the initial and middle stage of production, and lower the bottom-hole pressure. In addition, the matrix shrinkage effect can largely increase the gas rate owing to the enhanced permeability caused by the leading role of the matrix shrinkage effect.

(3) Single and multi-branch horizontal well model

The advanced coupled horizontal wellbore models of single and multi-branch well considering the effects of threshold pressure gradient and gas slippage are developed. The matrix shrinkage effect is modelled using a new developed permeability model. The models are solved using the IMPES method, and a program is coded using Fortran. Results show that the coupled multi-branch horizontal wellbore model can largely enhance the gas and water production rates, which has great significance in guiding the industry development.

The gas slippage factor is determined by β_1 and β_2, based on this, two cases are studied here: set β_1 and β_2 as constant respectively. Results showed that the gas and water production rate increase with the increasing of gas slippage factor, while the average pressure decreases with the rising of gas slippage factor.

The threshold pressure gradient plays an important role in the development of horizontal CBM reservoir. Gas threshold pressure is determined by α_1 and α_2, when α_1 is set at a given value, the water and gas production rate nearly converge to one point at the initial stage, and decrease with the increasing of α_2 at the late stage. While α_2 has an opposite effect on the pressure changes: the average reservoir increases with the rising value of α_2. This is because of the lower gas and water production rate. Similar trend can be found when α_2 is set as constant.

Water threshold pressure gradient effect is determined by α_3 and α_4. The daily gas production rate increases with the water threshold pressure gradient before gas production rate reaches its maximum, while this effect is reversed after this period. And the total water production rate decreases with the increasing of water threshold pressure

gradient during the whole simulation process. What is more, the average pressure increases with the rising of water threshold pressure gradient.

The daily gas production rate increases with the Langmuir pressure and decreases with Langmuir volume, which are attributed to the higher desorption rate with higher Langmuir pressure and lower Langmuir volume.

The gas production rate increases with the branch number, while the increasing speed of water production rate becomes slower once the branch number goes from 6 to 8 than from 4 to 6. So it is not always the bigger the branch number the better for the well production. In addition, branch angle 45 degree is the best choice for the well production pattern.

7.1.2.1 Triple porosity dual permeability model

A novel permeability model was developed based on the surface energy theories, to focus on the impact of matrix shrinkage/swelling on ECBM production, followed that a coupled compositional triple porosity horizontal wellbore model for CBM reservoir, considering the gas slippage and threshold pressure gradient effects is proposed. And it is solved through modified IMPES method originally used for block oil model. Then the simulator called TRIPLE-COAL is developed using Fortran program.

The triple porosity model has great superiority than the dual porosity model for the simulation, which can much more accurately simulate the field data. In addition, the multi-branch well type model can largely enhance the gas and water rate, especial when the branch number is chosen as 8 and branch angle is 45 degree.

The gas production rate decreases with the cleat porosity before it reaches its maximum rate, while the trend is reversed after this. Because the initial water content is lower with smaller porosity than with larger porosity, and the residual gas content is bigger with larger cleat porosity. Additionally, the gas production rate increases with the cleat permeability owing to the larger flowing path for the gas provided by bigger cleat permeability. Bigger desorption rate can enhance the gas rate, and it increases with Langmuir pressure, while decreases with Langmuir volume, thus the gas rate rises with the increasing of Langmuir pressure and drops with the increasing of Langmuir volume.

The gas slippage effect can only improve the gas and water rate in the early and middle stage, while the threshold pressure gradient effect can influence the pressure during the whole production process. The larger the threshold pressure gradient, the slower the

pressure drop. Moreover, the gas molar fraction rising speed is faster when the permeability model is applied to the advance coupled triple porosity model after around 100 days' production, which means the matrix shrinkage effect is stronger than the stress effect during this process. The critical fracture porosity ranging from 0.2 to 0.45 has dramatic effect on the permeability for injection well, while relative marginal effect for production well.

It was found that the critical fracture porosity 0.2, the gas slippage factor $\beta_1 = 165, \beta_2 = 0.123$ and the threshold pressure gradient factor $\alpha_1 = 0.002, \alpha_2 = 0.4,$ $\alpha_2 = 0.65, \alpha_2 = 0.16$, branch number 8, branch angle 45 degree give the best overall match through history matching of injection well bottom hole pressure, which further validate the accuracy of the model proposed in this Chapter. What is more, the history matching results for gas and water rate in the production well show excellent agreement between simulated result and observed data, which again validates the accuracy of the model developed in this Chapter. In addition, the well block permeability behavior for production well further validates the accuracy of the permeability model proposed in this study.

7.1.2.2 Well testing model

A pressure square method for the triple porosity model of CBM reservoir is proposed. Neither the relative permeability curve nor the variation of the pressure gradient is needed for the well test interpretation in this method, only the gas saturation gradient for the two phase flow needs to be considered. Thus this method has its great superiority over the other well testing methods.

The well testing data for the case study comes from the Eclipse simulation result, and the interpreted result has better agreement than expected. Thus this method can be applied to the field for well testing interpretation.

7.1.2.3 Field application

Comparisons of gas and water production rates between the case that ignores the gas slippage and threshold pressure gradient effects and the case that takes the two effects into consideration are made for He2 well and Yan1 well, the purpose to do this is to investigate the influence of the two effects on the production rate, and which one is dominant during the simulation process.

The gas slippage effect on the gas production rate is stronger than threshold pressure gradient effect for He2 well in Heshun block, while it has weaker effect on water production rate and pressure changes than threshold pressure gradient. Similar effect can be found when simulating Yan1 well in Yanchuan Southern block.

The result of 3# and 15# coal seam in heshun block indicates that 3# coal seam can produce much more gas than 15# coal seam. While for Yanchuan South block, 2# coal seam is easier to produce gas and its gas production rate is higher than the 10# coal seam, which means that 3# coal seam in Heshun block and 2# coal seam in Yanchuan South block should be the layer chosen for developing.

The history matching work was done according to the observation data of Heshun block, Yanchuan Southern block and Zhijin block to validate the accuracy of the model as well as the necessity for considering the effects of gas slippage, threshold pressure gradient and matrix shrinkage.

He2 well, He2-3 well and He2-5-1 well are used for the history matching in heshun block as vertical well type using the model developed in **Chapter 2**. The simulated results have good agreement with the field data, but the history matched permeability value is much bigger than the field tested value. However, the history matched value is more reasonable to explain the gas production rate, which means the matched permeability value is more accurate for future field exploitation.

Yan1, Yan1-20-10 and Yan5 well are chosen for the history matching in Yanchuan southern block as multi-branch horizontal well type using the model built in **Chapter 3**. The best history matching results achieved with branch number 6 and branch angle ranging from 43 degree to 48 degree. In addition, the permeability relative error between history matched value and input value is the biggest, while the history matched result is much more accurate according to the gas production rate, which is similar to the interpretation for Heshun block. Otherwise, the daily gas production rate could not reach more than 1000 m^3 if the permeability as low as the input value.

The best history matching results achieved for Zhi2 well and Zhi3 well with branch number 8 and branch angle around 45 degree using the simulator developed in **Chapter 4**. Additionally, the history matched permeability value has better agreement with the observed permeability value than expected, which can both be used for the future well exploration, because they can best describe the high field gas and water production rate. Also, Zhijin block shows potential production ability, so it should be explored further.

In addition, from the relative error point of view, the triple porosity model built in **Chapter 4** can better matching the field production data compared with the dual porosity model developed in **Chapter 3** if gas slippage effect, matrix shrinkage effect and threshold pressure gradient effect are all considered**.**

The productivity forecast value for He2-2 well is 375.6m^3/day, which shows good agreement with its reservoir production characteristic. And the predicted gas rate for Yan2 well is around 2400 m^3/day, while the gas rate from the field data is 2107 m^3/day. Thus, the relative error for it is 12.2%, and the whole relative error is around 27.8% if comparing every point in the figure, which shows the reasonability for field data prediction by using the models in this thesis.

7.2 Future work

As illustrated in this study, the new dual porosity single permeability model considering the gas slippage and threshold pressure gradient effects with vertical well production type, the advanced non-analytical coupled CBM model for predicting the flux and pressure in the CBM reservoir and single or multi-branch wellbore simultaneously, and a coupled compositional triple porosity horizontal wellbore model for CBM reservoir, considering the gas slippage and threshold pressure gradient effect with the new developed permeability model all have good capability in the simulating and forecasting of CBM reservoir production. With these models, the relative error of the history matched parameters is small enough for the guidance of future production.

However, the simulator coded in this thesis only uses the simple gridding method, this means that the grid around the wellbore is not refined, which will make great simulation error in some field in the future simulation and exploration process. Thus infilling the near wellbore grid should be done for even better CBM reservoir simulation.

In addition, the new models in this study are only being applied to the single well field forecasting, evaluation and exploration. While it is not applicable for the well blocks or well groups case. Thus the method about how apply the new single well models into the well groups' or well blocks' evaluation, forecasting and exploration in CBM reservoir should be investigated in the future.

Also, some field drilled a lot of wells for production in the CBM field to check where is much more productive, and to study the effects of the well interference. So the multi-wells interference effect on the CBM reservoir production and exploration under the

impact of matrix shrinkage, gas slippage and threshold pressure gradient should be a very interesting point for the future study, and also has great significance for the multiple wells field development and production. Thus, it needs further investigation in the future.

Another point is that only the vertical well type and horizontal or multi-branch horizontal well type are considered in this theis, while other drilling well type such as U shape, C shape or other more complexed drilling well shape is not investigated, which results in the models' limitation when being applied to some unconventional gas fields with irregular shapes around the world. It is a good point to extend the current model for evaluation and forecasting the wells' production with different shapes.

What is more, the temperature in some unconventional gas fields changes all the time, while it is not taken into consideration in this study. Thus, the application of temperature field into the CBM reservoir model should make the study much more suitable and reasonable for the practical field exploration and development. Then the effect of the temperature on the reservoir parameters, such as permeability, porosity, adsorption time etc, and how the CBM reservoir production changes under the variation of these parameters can be investigate.

Finally, the pressure squared well testing method for the triple porosity dual permeability model is investigated in this thesis. Neither the relative permeability curve nor the variation of the pressure gradient is needed for the well test interpretation in this method, only the gas saturation gradient for the two phase flow needs to be ignored. Thus this method has its great superiority over the other well testing methods, and it can also be applied to the field for well testing interpretation. However, the new numerical well testing technology for the CBM reservoir that can interpret the reservoir parameters in a different way is not mentioned in this thesis, which is very important for the future field production guidance. So this should be studied in the future.

Appendix A: Transportation equation derivation

In this appendix, the derivation process for the transportation equation in CBM reservoir that considering the gas slippage and threshold pressure gradient is briefly illustrated.

Appendix A.1 Derivation of the Continuity Equation

A differential equation can be developed to model a two-phase fluid flow in a coal seam by conducting a mass balance on a differential volume element (**Figure A.1**). A general mass balance for a volume element over the time interval Δt:

$$[in]-[out]\pm[generation|consumption]=[accumulation] \tag{A.1}$$

Take out a small control volume from one Hexahedron in coal seam with coordinate (x,y,z), its length, width, height are $\Delta x,\Delta y,\Delta z$ respectively. The fluid flows from front, followed by out; left into and right out; bottom inflow and top surface outflow. The velocity, density and saturation, porosity of the fluid is (x,y,z), $\rho(x,y,z)$, $S(x,y,z)$, ϕ. Suppose that the gas inflow and outflow rate in x,y,z direction are $V_{fx}\big|_{x+\Delta x/2}$ and $V_{fx}\big|_{x-\Delta x/2}$; $V_{fy}\big|_{y+\Delta y/2}$ and $V_{fy}\big|_{y-\Delta y/2}$; $V_{fz}\big|_{z+\Delta z/2}$ and $V_{fz}\big|_{z-\Delta z/2}$.

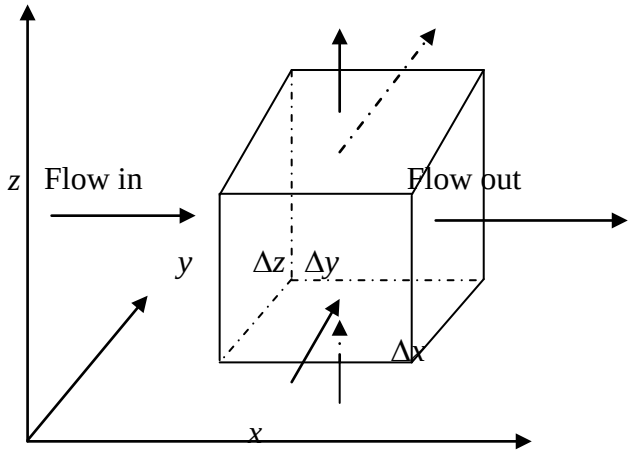

Figure A.1 Differential volume element of the CBM reservoir

The mass flux entering the control volume in the direction of x, y and z within Δt is:

$$m_{fx}=(\rho_f V_{fx})\big|_x\,\Delta y\Delta z\Delta t \tag{A.2}$$

$$m_{fy}=(\rho_f V_{fy})\big|_y\,\Delta x\Delta z\Delta t \tag{A.3}$$

$$m_{fz}=(\rho_f V_{fz})\big|_z\,\Delta x\Delta y\Delta t \tag{A.4}$$

And the corresponding flowing out mass flux is:

$$m_{fx+\Delta x} = (\rho_f V_{fx})\big|_{x+\Delta x}\,\Delta y\Delta z\Delta t \tag{A.5}$$

$$m_{fy+\Delta y} = (\rho_f V_{fy})\big|_{y+\Delta y}\,\Delta x\Delta z\Delta t \tag{A.6}$$

$$m_{fz+\Delta z} = (\rho_f V_{fz})\big|_{z+\Delta z}\,\Delta x\Delta y\Delta t \tag{A.7}$$

The gas saturation change in the control volume during the period of Δt is:

$$(s_f \rho_f \phi)\Delta x\Delta y\Delta z\big|_{t+\Delta t} - (s_f \rho_f \phi)\Delta x\Delta y\Delta z\big|_t \tag{A.8}$$

By substituting **Equation (A.2) - Equation (A.8)** into **Equation (A.1)** yields:

$$-[(\rho_f V_{fx})\big|_{x+\Delta x} - (\rho_f V_{fx})]\Delta y\Delta z\Delta t - [(\rho_f V_{fy})\big|_{y+\Delta y} - (\rho_f V_{fy})]\Delta x\Delta z\Delta t - [(\rho_f V_{fz})\big|_{z+\Delta z} - (\rho_f V_{fz})]\Delta x\Delta y\Delta t + q_{vg} + q_{mfg} = (s_f \rho_f \phi)\Delta x\Delta y\Delta z\big|_{t+\Delta t} - (s_f \rho_f \phi)\Delta x\Delta y\Delta z\big|_t \tag{A.9}$$

Dividing **Equation (A.9)** by the differential volume $V_b = \Delta x\Delta y\Delta z$, and suppose that $\Delta x \to 0, \Delta y \to 0, \Delta z \to 0$, then there is:

$$-\nabla \cdot \left(\rho_f \vec{v}_f\right) + Q_{vf}\ / V_b + Q_{mf}\ / V_b = \frac{\partial}{\partial t}\left(\phi \rho_g s_g\right) \tag{A.10}$$

Equation (A.10) is known as the continuity equation for fluid flow in three-dimensional coordinates.

The flow stream in cleats include the simultaneous flow of gas, dissolved gas in water, water, and water in gas phase. The water in gas phase at in-seam condition is much smaller and can be ignored in the derivations. Although the dissolved gas in water is small comparing to the free gas phase in the cleat porosity, it is included in the model equations. **Equation (A.10)** can be modified for the flow of gas, the dissolved gas in water, and the water in the cleat system as follows:

For gas phase

$$-\nabla \cdot \left(\rho_g \vec{v}_g + r_{sw}\rho_w \vec{v}_w\right) + Q_{vf}\ / V_b + Q_{mf}\ / V_b = \frac{\partial}{\partial t}\left(\phi \rho_g s_g + r_{sw}\phi \rho_w s_w\right) \tag{A.11}$$

For water phase

$$-\nabla\cdot\left(\rho_w\vec{v}_w\right)+q_{vw}=\frac{\partial}{\partial t}\left(\phi\rho_w s_w\right) \tag{A.12}$$

The density of the gas phase can be obtained from the real gas equation:

$$\rho_g=\frac{MP_g}{zRT} \tag{A.13}$$

The density of the water phase is shown as:

$$\rho_w=\frac{\rho_{wsc}}{B_w} \tag{A.14}$$

Substituting **Equation (A.13)** and **Equation (A.14)** into **Equation (A.11)** and **Equation (A.12)** respectively, and dividing **Equation (A.11)** and **Equation (A.12)** by constants M/RT and ρ_{wsc}, respectively, then the water and gas transport equation can be shown as:

$$\begin{aligned}&-\nabla\cdot\left(\frac{p_g}{z}\vec{v}_g+r_{sw}\frac{RT}{M}\frac{\rho_{wsc}}{B_w}\vec{v}_w\right)+\frac{RT}{M}(Q_{vg}+Q_{mg})/V_b\\&=\frac{\partial}{\partial t}\left(\phi\frac{p_g}{z}s_g+r_{sw}\frac{RT}{M}\frac{\rho_{wsc}}{B_w}\phi s_w\right)\end{aligned} \tag{A.15}$$

$$-\nabla\cdot\left(\frac{\vec{v}_w}{B_w}\right)+q_{vw}=\frac{\partial}{\partial t}\left(\phi s_w\frac{1}{B_w}\right) \tag{A.16}$$

The transport of water is assumed to obey the Darcy's Law. Here, both consider the gravity and capillary pressure, then, the superficial velocity for water phase in **Equation (A.16)** is:

$$\vec{v}_w=-\frac{k_f k_{rw}}{\mu_w}\nabla(p_w-\rho_w gH) \tag{A.17}$$

The transport of compressible gas is assumed to be under the influence of two fields, the potential field and the concentration field. Velocity through the potential field is laminar flow process and can be described by Darcy's Law (here also consider both the gravity and capillary pressure):

$$\vec{v}_g{}^D=-\frac{k_f k_{rg}}{\mu_g}\nabla(p_g-\rho_g gH) \tag{A.18}$$

Appendix A: Tansportation equation derivation

The velocity through the concentration gradient field is a diffusion (i.e. Knudsen diffusion) process and can be described by Fick's law of diffusion:

$$\vec{v}_g^{\,F} = -\frac{MD_a}{\rho_g}\nabla(C_a) \tag{A.19}$$

The concentration can be described as the function of density and saturation:

$$C_a = \frac{\rho_g}{M}S_g \tag{A.20}$$

From the definition of the gas density (**Equation (A.13)**) and concentration (**Equation (A.20)**), **Equation (A.19)** becomes:

$$\vec{v}_g^{\,F} = -D_a\frac{z}{p_g}\nabla(\frac{p_g}{z}s_g) \tag{A.21}$$

Hence, the velocity of the compressible gas phase is derived by adding the two velocities together:

$$\vec{v}_g = -\frac{k_f k_{rg}}{\mu_g}\nabla(p_g - \rho_g gH) - D_a\frac{z}{p_g}\nabla(\frac{p_g}{z}s_g) \tag{A.22}$$

The non-ideality of the gas phase can be accounted by assigning the volume formation factor for gas, which is defined as the volume of the gas in the reservoir condition divided by its volume at the surface conditions, at the standard pressure, p_{sc}, and standard temperature, T_{sc}:

$$B_g = \frac{(zRT/p)}{(zRT/p)_{sc}} = \frac{zT}{p}(\frac{p_{sc}}{T_{sc}}) \tag{A.23}$$

Substituting **Equation (A.22)** and **Equation (A.23)** into **Equation (A.15)** for gas phase and **Equation (A.17)** into **Equation (A.16)** for the water phase, then dividing by Tp_{sc}/T_{sc}. The material balance equations for gas and water phase in the cleat system becomes (Owing to the fact that the gas dissolved in the water is very small, so the dissolved gas is ignored from the equations):

$$\nabla\cdot\left(\frac{k_f k_{rg}}{\mu_g B_g}\nabla(p_g - \rho_g gH) + D_a\nabla(\frac{s_g}{B_g})\right) - q_{vg} + q_{mfg} = \frac{\partial}{\partial t}\left(\frac{\phi s_g}{B_g}\right) \tag{A.24}$$

$$\nabla \cdot \left(\frac{k_f k_{rw}}{\mu_w B_w} \nabla (p_w - \rho_w g H) \right) - q_{vw} = \frac{\partial}{\partial t} \left(\frac{\phi s_w}{B_w} \right) \tag{A.25}$$

Here, take gas slippage effect into consideration, the relative permeability functions $k_{rw}(s_w, p_w)$ and $k_{rg}(s_g, p_g)$ will take place of the relative permeability functions $k_{rw}(s_w)$ and $k_{rg}(s_g)$ in the conventional kinematic equation. Then the gas, water kinematic equation that considers gas slippage effect is obtained. While gas slippage effect will not have impact on the flow of water, so there is: $k_{rw}(s_w, p_w) = k_{rw\infty}(s_w)$.

Thus the gas and water phase velocity equation can be shown as:

$$\begin{cases} \vec{v}_g = -\dfrac{k_f k_{rg\infty}(s_g)}{\mu_g} (1 + \alpha_1 (\dfrac{k_f k_{rg\infty}(s_g)}{\phi_g})^{-\alpha_2} / p_m) \ \nabla (p_g - \rho_g g H) - D_a \nabla (\dfrac{s_g}{B_g}) \\ \vec{v}_w = -\dfrac{k_f k_{rw\infty}}{\mu_w} \nabla (p_w - \rho_w g H) \end{cases} \tag{A.26}$$

Appendix A.2 Kinematic equations of gas and water phase by considering threshold pressure gradient

The total pressure drop should be equal to the pressure drop of fluid flow and the threshold pressure according to the definition of threshold pressure gradient, that is:

$$\nabla \Phi_l = \frac{\mu_l}{k_{rl} k_f} v_l + \lambda_{bl}, \ l = w, g \tag{A.27}$$

Rearranging **Equation (A.27)**, there is

$$v_l = \frac{k_{rl} k_f}{\mu_l} (\nabla \Phi_l - \lambda_{bl}), l = w, g \tag{A.28}$$

Thus the synthetic kinematic equations of gas and water considering both threshold pressure gradient and gas slippage effect have the following forms:

For gas phase:

$$\begin{cases} \vec{v}_g = -\dfrac{k_f k_{rg\infty}(s_g)}{\mu_g} (1 + \alpha_1 (\dfrac{k_f k_{rg\infty}(s_g)}{\phi_g})^{-\alpha_2} / p_m) (\nabla (p_g - \rho_g g H) - \lambda_{bg}) - D_a \nabla (\dfrac{s_g}{B_g}) & \nabla (p_g - \rho_g g H) \geq \lambda_{bg} \\ \vec{v}_g = 0 & \nabla (p_g - \rho_g g H) \leq \lambda_{bg} \end{cases} \tag{A.29}$$

For water phase:

$$\begin{cases} \vec{v}_w = -\dfrac{k_f k_{rw\infty}}{\mu_w}(\nabla(p_w - \rho_w g H) - \lambda_{bw}) & \nabla(p_w - \rho_w g H) \geq \lambda_{bw} \\ \vec{v}_w = 0 & \nabla(p_w - \rho_w g H) \leq \lambda_{bw} \end{cases} \tag{A.30}$$

Substituting **Equation (A.29)** into **Equation (A.24)** for gas phase and **Equation (A.30)** into **Equation (A.25)** for the water phase, the material balance equations for gas and water phase in the cleat system becomes:

$$\begin{aligned} &\nabla \cdot \left(\frac{k_f k_{rg\infty}}{\mu_g B_g}(1+\alpha_1(\frac{k_f k_{rg\infty}(s_g)}{\phi_g})^{-\alpha_2} / p_m)(\nabla(p_g - \rho_g g H) - \lambda_{bg}) + D_a \nabla(\frac{s_g}{B_g}) \right) \\ &-q_{vg} + q_{mfg} = \frac{\partial}{\partial t}\left(\frac{\phi s_g}{B_g} \right) \end{aligned} \tag{A.31}$$

$$\nabla \cdot \left(\frac{k_f k_{rw\infty}}{\mu_w B_w}(\nabla(p_w - \rho_w g H) - \lambda_{bw}) \right) - q_{vw} = \frac{\partial}{\partial t}\left(\frac{\phi s_w}{B_w} \right) \tag{A.32}$$

Appendix A.3 Calculation of the Flow Rates at the Wells

Appendix A.3.1 Water phase flow rate calculation

Taking threshold pressure gradient into consideration, the superficial velocity for the water phase can be derived as:

$$\vec{v}_w = \frac{q_{vw} B_w}{2\pi r h} = -\frac{k k_{rw\infty}}{\mu_w}(\frac{\partial p}{\partial r} - \lambda_{bw}) \tag{A.33}$$

Suppose $p(p) = p - \lambda_{bw} r$, then separating the variables, and integrating both side of the equation:

$$\frac{q_{vw}}{2\pi h}\int_{r_w}^{r_e}\frac{dr}{r} = -\int_{p_{wf}}^{p_e}\frac{k k_{rw\infty}}{\mu_w B_w}dp \tag{A.34}$$

Thus, the rate of water flow can be expressed as

$$q_{vw} = \frac{2\pi h k k_{rw\infty}}{\mu_w B_w \ln(\frac{r_e}{r_w} + s)}[(p_{fw} - \lambda_{bw} r_w) - (p_{wf} - \lambda_{bw} r_e)] \tag{A.35}$$

Appendix A.3.2 Gas phase flow rate calculation

The derivation of the gas flow rate at the well needs special attention. Because the gas phase is compressible, it expands as the pressure drops; the velocity becomes greater at the downstream end than at the upstream end, and consequently the pressure gradient increases toward the downstream end. The most important thing is that when the threshold pressure gradient and gas slippage effects were all taken into consideration, the flow of CBM becomes high velocity, non-Darcy flow.

The extended high velocity and non-Darcy gas flow equation for CBM reservoir that considering the gas slippage effect and threshold pressure gradient can be expressed as:

$$\frac{\partial p}{\partial r} - \lambda_g = \frac{\mu_g}{k k_{rg\infty}} v_g + \beta \rho_g v_g^{\ 2} \tag{A.36}$$

Here, introduce $p^{'}(p) = p - \lambda_{bw} r$, and assuming a steady-state flow at the well and considering the gas volume factor $B_g = \frac{zTp_{sc}}{T_{sc} p}$. Then **Equation (A.36)** can be written as:

$$\frac{dp^{'}}{dr} = \frac{\mu_g}{k_g} \frac{q_{vg}}{2\pi r h} \frac{zTp_{sc}}{T_{sc} p} + \beta \rho_g \left(\frac{q_{vg}}{2\pi r h} \frac{zTp_{sc}}{T_{sc} p}\right)^2 \tag{A.37}$$

Define the psedo-pressure $m(p^{'}) = 2\int_{p_0^{'}}^{p^{'}} \frac{p^{'}}{\mu_g z} dp^{'}$. Integrating **Equation (A.37)**:

$$\begin{aligned} m - m_w &= \frac{1}{\pi k h} \frac{Tp_{sc}}{T_{sc} p} q_{vg} \left(p \ln\left(\frac{r}{r_w}\right) - \lambda_g (r - r^w)\right) \\ &+ \frac{\beta \rho_g}{2\pi^2 h^2} \frac{zT^2 p_{sc}^{\ 2}}{T_{sc}^{\ 2} \mu_g p_g^{\ 2}} q_{vg}^{\ 2} \left(p\left(\frac{1}{r_w} - \frac{1}{r}\right) - \lambda_g \ln\left(\frac{r}{r_w}\right)\right) \end{aligned} \tag{A.38}$$

Study had shown that the product of compressibility factor and the gas viscosity $z\mu_g$ were shown to be nearly constant at pressures less than 13.6MPa; whereas $p / z\mu_g$ is nearly constant at pressures greater than 13.6MPa **(Craft., B.C., et al., 1991[153])**. Therefore, $z\mu_g$ can be withdrawn from the integrals by using its average value:

$$m - m_w = \frac{2}{\overline{\mu z}} \left((p^{'})^2 - (p_w^{'})^2\right) \tag{A.39}$$

Substituting **Equation (A.39)** into **Equation (A.38)**, rearranging:

$$(p')^2-(p_w')^2=\frac{\overline{\mu z}}{2\pi kk_{rg\infty}h}\frac{p_{sc}T}{T_{sc}}q_{vg}(\ln\frac{r}{r_w}+s') \tag{A.40}$$

According to the equals mentioned above, the gas flow rate considering the effect of threshold pressure gradient has the following form:

$$q_{vg}=\frac{2\pi hkk_{rg\infty}}{\mu_g B_g\ln(\frac{r_e}{r_w}+s')}[(p_{fg}-\lambda_{bg}r_e)^2-(p_{wf}-\lambda_{bg}r_w)^2] \tag{A.41}$$

Where: $s'=s+s_{sp}+D_{sp}Q_g$, it is seen as skin factor, $s_{sp}=-\frac{\lambda_{bg}}{p}(r-r_w)$; $D_{sp}=\frac{\beta\rho_g}{2\pi h}\frac{zT}{T_{sc}}$;

$\frac{k_g}{\mu_g}(\frac{1}{r_w}-\frac{1}{r}\frac{\lambda_g}{p}\ln\frac{r}{r_w})$; $\Delta p'=(p')^2-(p_w')^2=(p-\lambda_{bg}r)^2-(p_{wf}-\lambda_{bg}r_w)^2$, $psia^2$.

Appendix B: Source code

Appendix B.1 Basic transportation equation solution module

```
SUBROUTINE XATRIX()

 PARAMETER(NNX=60,NNY=60,NNK=10,NNN=NNX*NNY*NNK,NNW=30)

COMMON /CCOM/ II,JJ,KK,NW,NWP,NWI,DELT,IOCODE,IHEDIN(80)
COMMON /CGRID/ DX(NNX,NNY,NNK),DY(NNX,NNY,NNK,),DZ(NNX,NNY,N
NK)&,EL(NNX,NNY,NNK)

COMMON /CPARM/ VPN(NNX,NNY,NNK), VP(NNX,NNY,NNK),VPM(NNX,NN
VPN(NNX,NNY,NNK),VP(NNX,NNY,NNK),VPM(NNX,NNY,NNK)&,KX(NNX,N
NY,NNK),KY(NNX,NNY,NNK),KZ(NNX,NNY,NNK)&,DFX(NNX,NNY,NNK),DF
Y(NNX,NNY,NNK),DFZ(NNX,NNY,NNK)

COMMON/CTRAN/TX(NNX+1,NNY,NNK),TY(NNX,NNY+1,NNK),TZ(NNX,NNY
,NNK+1) &,TDX(NNX+1,NNY,NNK),TDY(NNX,NNY+1,NNK),TDZ(NNX,NNY,N
NK+1)
COMMON/CTABL/SAT(25),KRWT(25),KRGT(25),PCGWT(25),PWT(25),MUWT(2
5)&,BWT(25),BWPT(25),PGT(25),MUGT(25),BGT(25),BGPT(25),CRT(25)&,RHOS
SCG,RHOSCW,MSAT,MPWT,MPGT

 REAL KRWT,KRGT,MUWT,MUGT

COMMON/CCODE/NN,FACT1,FACT2,TMAX,GWRMAX,PAMIN,PAMAX,DSMA
X,&DPMAX,VL,PL,FG,TAO,BETA,KCOFF,&KMTRX,KSOL,MITER,OMEGA,TO
L,TOL1,EFC,KNK,TCR,PCR,T

COMMON/PRSTC/PN(NNX,NNY,NNK),SWN(NNX,NNY,NNK),SGN(NNX,NNY,
NNK),&PMN(NNX,NNY,NNK),CMN(NNX,NNY,NNK),P(NNX,NNY,NNK),SW(N
NX,NNY,NNK),&SG(NNX,NNY,NNK),PM(NNX,NNY,NNK),CM(NNX,NNY,NNK)
,QMFG(NNX,NNY,NNK)

COMMON/CBWBG/BWN(NNX,NNY,NNK),BW(NNX,NNY,NNK),BGN(NNX,NN
Y,NNK),& BG(NNX,NNY,NNK),BGM(NNX,NNY,NNK),CT(NNX,NNY,NNK)

COMMON /WRATE/QG(NNX,NNY,NNK),QW(NNX,NNY,NNK),WELLS(NNW),&
IQN1(NNW),IQN2(NNW),IQN3(NNW),LAYER(NNW),KIP(NNW),QVW(NNW),&
```

```
QVG(NNW),PWFX(NNW),PID(NNW,NNK),PWF(NNW,NNK),PWFC(NNW,NNK),
&IQNEND(NNW),NEP(NNW),HPID(NNW,NNX),HPWF(NNW,NNX),HPWFX(NN
W)&  ,HPWFN(NNW,NNX),HRW(NNW)

CHARACTER*5 WELLS

COMMON/COEFF/AW(NNX+1,NNY,NNK),AE(NNX+1,NNY,NNK),AS(NNX,NNY
+1,NNK)&,AN(NNX,NNY+1,NNK),AT(NNX,NNY,NNK+1),AB(NNX,NNY,NNK+1
)&,WW(NNX+1,NNY,NNK),WE(NNX+1,NNY,NNK),WS(NNX,NNY+1,NNK)&,W
N(NNX,NNY+1,NNK),WT(NNX,NNY,NNK+1),WB(NNX,NNY,NNK+1)&,E(NNX,
NNY,NNK),B(NNX,NNY,NNK),GWWT(NNX,NNY,NNK)&,GGWT(NNX,NNY,NN
K)

COMMON/PD/PDES,DE(NNN),UL1(NNN),UL2(NNN),UL3(NNN),&U1(NNN),U2(
NNN),U3(NNN),DEE(NNN)

REAL STPW1,STPW2,STPG1,STPG2

REAL KX,KY,KZ

REALMUW1,MUG1,MUW2,MUG2,MUW3,MUG3,MUW4,MUG4,MUW5,MUG5,
MUW6,MUG6&,MUW,MUG,KRW1,KRG1,KRW2,KRG2,KRW3,KRG3,KRW4,KR
G4,KRW5,KRG5,KRW6&,KRG6,MW1,MG1,MW2,MG2,MW3,MG3,MW4,MG4,M
W5,MG5,MW6,MG6

REAL LAMDAW2,LAMDAW3,LAMDAW4, LAMDAW5,LAMDAW6, LAMDAG1,
LAMDAG2,& LAMDAG3,LAMDAG4,LAMDAG5,LAMDAG6

    DIV1=1.0/DELT

    SFC=0.0864

    RECD=1.0E6

    RHOSCW1=9.8*RHOSCW*(1E-3)

    RHOSCG1=9.8*RHOSCG*(1E-3)

    DO 200 K=1,KK

    DO 200 J=1,JJ

    DO 200 I=1,II
```

```
SB=SG(I,J,K)/BG(I,J,K)

PP=P(I,J,K)

!Invoke the interpolation funtion

CALL INTERP(PWT,MUWT,MPWT,PP,MUW)

CALL INTERP(PGT,MUGT,MPGT,PP,MUG)

SSW=SW(I,J,K)

CALL INTERP(SAT,PCGWT,MSAT,SSW,PCGW)

RW=RHOSCW1/BW(I,J,K)

RG=RHOSCG1/BG(I,J,K)

! initial value of the threshold pressure gradient and gas slippage effect experimental factor

STPW1=0.0

STPW2=0.0

STPG1=0

STPG2=0

SLE1=161

SLE2=0.47

IF(I.EQ.1)GOTO 115

    SBX1= SG(I-1,J,K)/BG(I-1,J,K)

    P1=P(I-1,J,K)

    CALL INTERP(PWT,MUWT,MPWT,P1,MUW1)

    CALL INTERP(PGT,MUGT,MPGT,P1,MUG1)

    SW1=SW(I-1,J,K)

    CALL INTERP(SAT,PCGWT,MSAT,SW1,PCGW1)
```

```
        RW1=RHOSCW1/BW(I-1,J,K)
        RG1=RHOSCG1/BG(I-1,J,K)
         FACT=-(EL(I-1,J,K)-EL(I,J,K))
! the difference equation (x direction) for gravity and capillary pressure
        GWW1=0.5*(RW1+RW)*FACT + PCGW-PCGW1
        GGW1=0.5*(RG1+RG)*FACT
        P11=P1-PP
        HW1=P11+GWW1
        HG1=P11+GGW1
        IF(HW1.GE.0.) THEN
              CALL INTERP(SAT,KRWT,MSAT,SW1,KRW1)
              LAMDAW1=-DX(I-1,J,K)*STPW1/(KX(I-1,J,K)*KRW1/MUW1)**ST
              PW2
        END IF
        IF(HW1.LT.0.) THEN
              CALL INTERP(SAT,KRWT,MSAT,SSW,KRW1)
              LAMDAW1=DX(I,J,K)*STPW1/(KX(I,J,K)*KRW1/MUW1)**STPW2
        END IF
        IF(HG1.GE.0.) THEN
              CALL INTERP(SAT,KRGT,MSAT,SW1,KRG1)
              LAMDAG1=-DX(I-1,J,K)*(STPG1/(KX(I-1,J,K)*KRG1*0.987E-3)+ST
              PG2)
              HG=HG1+LAMDAG1
              QQ1=KX(I-1,J,K)*KRG1*DY(I-1,J,K)*DZ(I-1,J,K)*ABS(HG)/MUG1
```

```
                RECL=QQ1*RHOSCG*(KX(I-1,J,K)*KRG1)**0.5/(MUG1*VP(I-1,J,
                K)& *DZ(I-1,J,K)*DY(I-1,J,K))
                IF((RECL.GE.0).AND.(RECL.LT.RECD))THEN
                        KRG1=KRG1*(1+SLE1*(KX(I-1,J,K)*KRG1/
                        &(VP(I-1,J,K)*(1-SW1)))**SLE2)/P1
                END IF
        END IF
        IF(HG1.LT.0.) THEN
                CALL INTERP(SAT,KRGT,MSAT,SSW,KRG1)
                LAMDAG1=DX(I,J,K)*(STPG1/(KX(I,J,K)*KRG1*0.987E-3)+STPG2)
                HG=HG1+LAMDAG1
                QQ1=KX(I,J,K)*KRG1*DY(I,J,K)*DZ(I,J,K)*ABS(HG)/MUG
                RECL=QQ1*RHOSCG*(KX(I,J,K)*KRG1)**0.5/(MUG*VP(I,J,K)
                &*DZ(I,J,K)*DY(I,J,K))
                IF((RECL.GE.0).AND.(RECL.LT.RECD))THEN
                        KRG1=KRG1*(1+SLE1*(KX(I,J,K)*KRG1/
                        &(VP(I,J,K)*(1-SSW)))**SLE2)/PP
                END IF
        END IF
! Variable Kr/(B*MU) in the transmissibility coefficient
        MW1=4.0*KRW1/((BW(I-1,J,K)+BW(I,J,K)) * (MUW1+MUW))
        MG1=4.0*KRG1/((BG(I-1,J,K)+BG(I,J,K)) * (MUG1+MUG))
! Transmissibility coefficient
115   AWW=TX(I,J,K)*MW1
```

```
AGW=TX(I,J,K)*MG1
IF((ABS(HG1)-ABS(LAMDAG1))<=0) AGW=0
IF((ABS(HW1)-ABS(LAMDAW1))<=0) AWW=0
ADW=TDX(I,J,K)*(SBX1-SB)
IF(I.EQ.II)GOTO 125
    SBX2= SG(I+1,J,K)/BG(I+1,J,K)
    P2=P(I+1,J,K)
    CALL INTERP(PWT,MUWT,MPWT,P2,MUW2)
    CALL INTERP(PGT,MUGT,MPGT,P2,MUG2)
    SW2=SW(I+1,J,K)
    CALL INTERP(SAT,PCGWT,MSAT,SW2,PCGW2)
    RW2=RHOSCW1/BW(I+1,J,K)
    RG2=RHOSCG1/BG(I+1,J,K)
    FACT=-(EL(I+1,J,K)-EL(I,J,K))
    GWW3=0.5*(RW2+RW)*FACT + PCGW-PCGW2
    GGW3=0.5*(RG2+RG)*FACT
    P22=P2-PP
    HW2=P22+GWW2
    HG2=P22+GGW2
    IF(HW2.GE.0.)THEN
        CALL INTERP(SAT,KRWT,MSAT,SW2,KRW2)
        LAMDAW2=-DX(I+1,J,K)*STPW1/(KX(I+1,J,K)*KRW2/MUW2)
        **STPW2
    END IF
```

```
IF(HW2.LT.0.) THEN
    CALL INTERP(SAT,KRWT,MSAT,SSW,KRW2)
    LAMDAW2=DX(I,J,K)*STPW1/(KX(I,J,K)*KRW2/MUW2)**STPW2
END IF
IF(HG2.GE.0.) THEN
    CALL INTERP(SAT,KRGT,MSAT,SW2,KRG2)
    LAMDAG2=-DX(I+1,J,K)*(STPG1/(KX(I+1,J,K)*KRG2*0.987E-3)
    +STPG2)
    HG=HG2+LAMDAG2
    QQ2=KX(I+1,J,K)*KRG2*DY(I+1,J,K)*DZ(I+1,J,K)*ABS(HG)/
    MUG2
    RECL=QQ2*RHOSCG*(KX(I+1,J,K)*KRG2)**0.5/(MUG2*VP(I+1
    ,J,K)&*DZ(I+1,J,K)*DY(I+1,J,K))
    IF((RECL.GE.0).AND.(RECL.LT.RECD))THEN
        KRG2=KRG2*(1+SLE1*(KX(I+1,J,K)*KRG2/
        &(VP(I+1,J,K)*(1-SW2)))**SLE2)/P2
    END IF
END IF
IF(HG2.LT.0.) THEN
    CALL INTERP(SAT,KRGT,MSAT,SSW,KRG2)
    LAMDAG2=DX(I,J,K)*(STPG1/(KX(I,J,K)*KRG2*0.987E-3)+STPG2)
    HG=HG2+LAMDAG2
    QQ2=KX(I,J,K)*KRG2*DY(I,J,K)*DZ(I,J,K)*ABS(HG)/MUG
    RECL=QQ2*RHOSCG*(KX(I,J,K)*KRG2)**0.5/(MUG*VP(I,J,K)
```

```
                &*DZ(I,J,K)*DY(I,J,K))
                IF((RECL.GE.0).AND.(RECL.LT.RECD))THEN
                    KRG2=KRG2*(1+SLE1*(KX(I,J,K)*KRG2/
                    & (VP(I,J,K)*(1-SSW)))**SLE2)/PP
                END IF
            END IF
            MW2=4.0*KRW2/((BW(I+1,J,K)+BW(I,J,K)) * (MUW2+MUW))
            MG2=4.0*KRG2/((BG(I+1,J,K)+BG(I,J,K)) * (MUG2+MUG))
125     AWE=TX(I+1,J,K)*MW2
        AGE=TX(I+1,J,K)*MG2
        IF((ABS(HG2)-ABS(LAMDAG2))<=0) AGE=0
        IF((ABS(HW2)-ABS(LAMDAW2))<=0) AWE=0
        ADE=TDX(I+1,J,K)*(SBX2-SB)
        IF(J.EQ.1)GOTO 135
            SBY1= SG(I,J-1,K)/BG(I,J-1,K)
            P3=P(I,J-1,K)
            CALL INTERP(PWT,MUWT,MPWT,P3,MUW3)
            CALL INTERP(PGT,MUGT,MPGT,P3,MUG3)
            SW3=SW(I,J-1,K)
            CALL INTERP(SAT,PCGWT,MSAT,SW3,PCGW3)
            RW3=RHOSCW1/BW(I,J-1,K)
            RG3=RHOSCG1/BG(I,J-1,K)
            FACT=-(EL(I,J-1,K)-EL(I,J,K))
            GWW3=0.5*(RW3+RW)*FACT + PCGW-PCGW3
```

```
GGW3=0.5*(RG3+RG)*FACT
P33=P3-PP
HW3=P33+GWW3
HG3=P33+GGW3
IF(HW3.GE.0.) THEN
    CALL INTERP(SAT,KRWT,MSAT,SW3,KRW3)
    LAMDAW3=-DY(I,J-1,K)*STPW1/(KY(I,J-1,K)*KRW3/MUW3)
    **STPW2
END IF
IF(HW3.LT.0.) THEN
    CALL INTERP(SAT,KRWT,MSAT,SSW,KRW3)
    LAMDAW3=DY(I,J,K)*STPW1/(KY(I,J,K)*KRW3/MUW3)**STPW2
END IF
IF(HG3.GE.0.) THEN
    CALL INTERP(SAT,KRGT,MSAT,SW3,KRG3)
    LAMDAG3=-DY(I,J-1,K)*(STPG1/(KY(I,J-1,K)*KRG3*0.987E-3)
    +STPG2)
    HG=HG3+LAMDAG3
    QQ3=KY(I,J-1,K)*KRG3*DX(I,J-1,K)*DZ(I,J-1,K)*ABS(HG)/MUG3
    RECL=QQ3*RHOSCG*(KY(I,J-1,K)*KRG3)**0.5/(MUG3*
    VP(I,J-1,K)&*DZ(I,J-1,K)*DX(I,J-1,K))
    IF((RECL.GE.0).AND.(RECL.LT.RECD))THEN
        KRG3=KRG3*(1+SLE1*(KY(I,J-1,K)*KRG3/
        &(VP(I,J-1,K)*(1-SW3)))**SLE2)/P3
```

```
                END IF
            END IF
            IF(HG3.LT.0.) THEN
                CALL INTERP(SAT,KRGT,MSAT,SSW,KRG3)
                LAMDAG3=DY(I,J,K)*(STPG1/(KY(I,J,K)*KRG3*0.987E-3)+STPG2)
                HG=HG3+LAMDAG3
                QQ3=KY(I,J,K)*KRG3*DX(I,J,K)*DZ(I,J,K)*ABS(HG)/MUG
                RECL=QQ3*RHOSCG*(KY(I,J,K)*KRG3)**0.5/(MUG*VP(I,J,K)
                &*DZ(I,J,K)*DX(I,J,K))
                IF((RECL.GE.0).AND.(RECL.LT.RECD))THEN
                    KRG3=KRG3*(1+SLE1*(KY(I,J,K)*KRG3/
                    &(VP(I,J,K)*(1-SSW)))**SLE2)/PP
                END IF
            END IF
            MW3=4.0*KRW3/((BW(I,J-1,K)+BW(I,J,K)) * (MUW3+MUW))
            MG3=4.0*KRG3/((BG(I,J-1,K)+BG(I,J,K)) * (MUG3+MUG))
135     AWS=TY(I,J,K)*MW3
        AGS=TY(I,J,K)*MG3
      IF((ABS(HG3)-ABS(LAMDAG3))<=0) AGS=0
      IF((ABS(HW3)-ABS(LAMDAW3))<=0) AWS=0
      ADS=TDY(I,J,K)*(SBY1-SB)
      IF(J.EQ.JJ)GOTO 140
          SBY2= SG(I,J+1,K)/BG(I,J+1,K)
          P4=P(I,J+1,K)
```

```
CALL INTERP(PWT,MUWT,MPWT,P4,MUW4)

CALL INTERP(PGT,MUGT,MPGT,P4,MUG4)

SW4=SW(I,J+1,K)

CALL INTERP(SAT,PCGWT,MSAT,SW4,PCGW4)

RW4=RHOSCW1/BW(I,J+1,K)

RG4=RHOSCG1/BG(I,J+1,K)

FACT=-(EL(I,J+1,K)-EL(I,J,K))

GWW4=0.5*(RW4+RW)*FACT + PCGW-PCGW4

GGW4=0.5*(RG4+RG)*FACT

P44=P4-PP

HW4=P44+GWW4

HG4=P44+GGW4

IF(HW4.GE.0.) THEN

    CALL INTERP(SAT,KRWT,MSAT,SW4,KRW4)

    LAMDAW4=-DY(I,J+1,K)*STPW1/(KY(I,J+1,K)*KRW4/MUW4)

    **STPW2

END IF

IF(HW4.LT.0.) THEN

    CALL INTERP(SAT,KRWT,MSAT,SSW,KRW4)

    LAMDAW4=DY(I,J,K)*STPW1/(KY(I,J,K)*KRW4/MUW4)**STPW2

END IF

IF(HG4.GE.0.)THEN

    CALL INTERP(SAT,KRGT,MSAT,SW4,KRG4)

    LAMDAG4=-DY(I,J+1,K)*(STPG1/(KY(I,J+1,K)*KRG4*0.987E-3)
```

```
            +STPG2)
            HG=HG4+LAMDAG4
            QQ4=KY(I,J+1,K)*KRG4*DX(I,J+1,K)*DZ(I,J+1,K)*ABS(HG)
            /MUG4
            RECL=QQ4*RHOSCG*(KY(I,J+1,K)*KRG4)**0.5/(MUG4*
            VP(I,J+1,K)&*DZ(I,J+1,K)*DX(I,J+1,K))
            IF((RECL.GE.0).AND.(RECL.LT.RECD))THEN
                  KRG4=KRG4*(1+SLE1*(KY(I,J+1,K)*KRG4/
                  &(VP(I,J+1,K)*(1-SW4)))**SLE2)/P4
            END IF
      END IF
      IF(HG4.LT.0.)THEN
            CALL INTERP(SAT,KRGT,MSAT,SSW,KRG4)
            LAMDAG4=DY(I,J,K)*(STPG1/(KY(I,J,K)*KRG4*0.987E-3)+STPG2)
            HG=HG4+LAMDAG4
            QQ4=KY(I,J,K)*KRG4*DX(I,J,K)*DZ(I,J,K)*ABS(HG)/MUG
            RECL=QQ4*RHOSCG*(KY(I,J,K)*KRG4)**0.5/(MUG*VP(I,J,K)
            &*DZ(I,J,K)*DX(I,J,K))
            IF((RECL.GE.0).AND.(RECL.LT.RECD))THEN
                  KRG4=KRG4*(1+SLE1*(KY(I,J,K)*KRG4/
                  &(VP(I,J,K)*(1-SSW)))**SLE2)/PP
            END IF
      END IF
      MW4=4.0*KRW4/((BW(I,J+1,K)+BW(I,J,K)) * (MUW4+MUW))
```

```
        MG4=4.0*KRG4/((BG(I,J+1,K)+BG(I,J,K)) * (MUG4+MUG))
140   AWN=TY(I,J+1,K)*MW4
      AGN=TY(I,J+1,K)*MG4
      IF((ABS(HG4)-ABS(LAMDAG4))<=0) AGN=0
      IF((ABS(HW4)-ABS(LAMDAW4))<=0) AWN=0
      ADN=TDY(I,J+1,K)*(SBY2-SB)
       IF(K.EQ.1)GOTO 145
          SBZ1=SG(I,J,K-1)/BG(I,J,K-1)
          P5=P(I,J,K-1)
          CALL INTERP(PWT,MUWT,MPWT,P5,MUW5)
          CALL INTERP(PGT,MUGT,MPGT,P5,MUG5)
          SW5=SW(I,J,K-1)
          CALL INTERP(SAT,PCGWT,MSAT,SW5,PCGW5)
          RW5=RHOSCW1/BW(I,J,K-1)
          RG5=RHOSCG1/BG(I,J,K-1)
          FACT=-(EL(I,J,K-1)-EL(I,J,K))
          GWW5=0.5*(RW5+RW)*FACT + PCGW-PCGW5
          GGW5=0.5*(RG5+RG)*FACT
          P55=P5-PP
          HW5=P55+GWW5
          HG5=P55+GGW5
          IF(HW5.GE.0.) THEN
                CALL INTERP(SAT,KRWT,MSAT,SW5,KRW5)
                LAMDAW5=-DZ(I,J,K-1)*STPW1/(KZ(I,J,K-1)*KRW5/MUW5)
```

```
            **STPW2
        END IF
        IF(HW5.LT.0.) THEN
            CALL INTERP(SAT,KRWT,MSAT,SSW,KRW5)
            LAMDAW5=DZ(I,J,K)*STPW1/(KZ(I,J,K)*KRW5/MUW5)**STPW2
        END IF
        IF(HG5.GE.0.) THEN
            CALL INTERP(SAT,KRGT,MSAT,SW5,KRG5)
            LAMDAG5=-DZ(I,J,K-1)*(STPG1/(KZ(I,J,K-1)*KRG5*0.987E-3)
            +STPG2)
            HG=HG5+LAMDAG5
            QQ5=KZ(I,J,K-1)*KRG5*DX(I,J,K-1)*DY(I,J,K-1)*ABS(HG)/MUG5
            RECL=QQ5*RHOSCG*(KZ(I,J,K-1)*KRG5)**0.5/(MUG5*
            VP(I,J,K-1)&*DY(I,J,K-1)*DX(I,J,K-1))
            IF((RECL.GE.0).AND.(RECL.LT.RECD))THEN
                KRG5=KRG5*(1+SLE1*(KZ(I,J,K-1)*KRG5/
                &(VP(I,J,K-1)*(1-SW5)))**SLE2)/P5
            END IF
        END IF
        IF(HG5.LT.0.) THEN
            CALL INTERP(SAT,KRGT,MSAT,SSW,KRG5)
            LAMDAG5=DZ(I,J,K)*(STPG1/(KZ(I,J,K)*KRG5*0.987E-3)+STPG2)
            HG=HG5+LAMDAG5
            QQ5=KZ(I,J,K)*KRG5*DX(I,J,K)*DY(I,J,K)*ABS(HG)/MUG
```

```
                RECL=QQ5*RHOSCG*(KZ(I,J,K)*KRG5)**0.5/(MUG*VP(I,J,K)
                &*DY(I,J,K)*DX(I,J,K))
                IF((RECL.GE.0).AND.(RECL.LT.RECD))THEN
                    KRG5=KRG5*(1+SLE1*(KZ(I,J,K)*KRG5/
                    &(VP(I,J,K)*(1-SSW)))**SLE2)/PP
                END IF
            END IF
            MW5=4.0*KRW5/((BW(I,J,K-1)+BW(I,J,K)) * (MUW5+MUW))
            MG5=4.0*KRG5/((BG(I,J,K-1)+BG(I,J,K)) * (MUG5+MUG))
145     AWT=TZ(I,J,K)*MW5
        AGT=TZ(I,J,K)*MG5
        IF((ABS(HG5)-ABS(LAMDAG5))<=0) AGT=0
        IF((ABS(HW5)-ABS(LAMDAW5))<=0) AWT=0
        ADT=TDZ(I,J,K)*(SBZ1-SB)
        IF(K.EQ.KK)GOTO 150
            SBZ2=SG(I,J,K+1)/BG(I,J,K+1)
            P6=P(I,J,K+1)
            CALL INTERP(PWT,MUWT,MPWT,P6,MUW6)
            CALL INTERP(PGT,MUGT,MPGT,P6,MUG6)
            SW6=SW(I,J,K+1)
            CALL INTERP(SAT,PCGWT,MSAT,SW6,PCGW6)
            RW6=RHOSCW1/BW(I,J,K+1)
            RG6=RHOSCG1/BG(I,J,K+1)
            FACT=-(EL(I,J,K+1)-EL(I,J,K))
```

```
GWW6=0.5*(RW6+RW)*FACT + PCGW-PCGW6
GGW6=0.5*(RG6+RG)*FACT
P66=P6-PP
HW6=P66+GWW6
HG6=P66+GGW6
IF(HW6.GE.0.)THEN
    CALL INTERP(SAT,KRWT,MSAT,SW6,KRW6)
    LAMDAW6=-DZ(I,J,K+1)*STPW1/(KZ(I,J,K+1)*KRW6/MUW6)
    **STPW2
END IF
IF(HW6.LT.0.) THEN
    CALL INTERP(SAT,KRWT,MSAT,SSW,KRW6)
    LAMDAW6=DZ(I,J,K)*STPW1/(KZ(I,J,K)*KRW6/MUW6)**STPW2
END IF
IF(HG6.GE.0.) THEN
    CALL INTERP(SAT,KRGT,MSAT,SW6,KRG6)
    LAMDAG6=-DZ(I,J,K+1)*(STPG1/(KZ(I,J,K+1)*KRG6*0.987E-3)
    +STPG2)
    HG=HG6+LAMDAG6
    QQ6=KZ(I,J,K+1)*KRG6*DX(I,J,K+1)*DY(I,J,K+1)*ABS(HG)/
    MUG6
    RECL=QQ6*RHOSCG*(KZ(I,J,K+1)*KRG6)**0.5/(MUG6*
    VP(I,J,K+1)&*DY(I,J,K+1)*DX(I,J,K+1))
    IF((RECL.GE.0).AND.(RECL.LT.RECD))THEN
```

```
                    KRG6=KRG6*(1+SLE1*(KZ(I,J,K+1)*KRG6/
                    &(VP(I,J,K+1)*(1-SW6)))**SLE2)/P6
                END IF
            END IF
            IF(HG6.LT.0.) THEN
                CALL INTERP(SAT,KRGT,MSAT,SW6,KRG6)
                LAMDAG6=DZ(I,J,K)*(STPG1/(KZ(I,J,K)*KRG6*0.987E-3)+STPG2)
                HG=HG6+LAMDAG6
                QQ6=KZ(I,J,K)*KRG6*DX(I,J,K)*DY(I,J,K)*ABS(HG)/MUG
                RECL=QQ6*RHOSCG*(KZ(I,J,K)*KRG6)**0.5/(MUG*VP(I,J,K)
                &*DY(I,J,K)*DX(I,J,K))
                IF((RECL.GE.0).AND.(RECL.LT.RECD))THEN
                    KRG6=KRG6*(1+SLE1*(KZ(I,J,K)*KRG6/
                    &(VP(I,J,K)*(1-SSW)))**SLE2)/PP
                END IF
            END IF
            MW6=4.0*KRW6/((BW(I,J,K+1)+BW(I,J,K)) * (MUW6+MUW))
            MG6=4.0*KRG6/((BG(I,J,K+1)+BG(I,J,K)) * (MUG6+MUG))
150     AWB=TZ(I,J,K+1)*MW6
        AGB=TZ(I,J,K+1)*MG6
        IF((ABS(HG6)-ABS(LAMDAG6))<=0) AGB=0
        IF((ABS(HW6)-ABS(LAMDAW6))<=0) AWB=0
        ADB=TDZ(I,J,K+1)*(SBZ2-SB)
        AG1=AGW*(GGW1+LAMDAG1)
```

```
AG2=AGE*(GGW2+LAMDAG2)

AG3=AGS*(GGW3+LAMDAG3)

AG4=AGN*(GGW4+LAMDAG4)

AG5=AGT*(GGW5+LAMDAG5)

AG6=AGB*(GGW6+LAMDAG6)

AW1=AWW*(GWW1+LAMDAW1)

AW2=AWE*(GWW2+LAMDAW2)

AW3=AWS*(GWW3+LAMDAW3)

AW4=AWN*(GWW4+LAMDAW4)

AW5=AWT*(GWW5+LAMDAW5)

AW6=AWB*(GWW6+LAMDAW6)

! Gravity item on the left hand side of the equation, contains capillary pressure

GGWT(I,J,K)= (AG1 + AG2 + AG3 + AG4 + AG5 + AG6)*SFC

GWWT(I,J,K)= (AW1 + AW2 + AW3 + AW4 + AW5 + AW6)*SFC

AW(I,J,K)=(BW(I,J,K)* AWW+ BG(I,J,K)*AGW)*SFC

AE(I,J,K)=(BW(I,J,K)* AWE+ BG(I,J,K)*AGE)*SFC

AS(I,J,K)=(BW(I,J,K)* AWS+ BG(I,J,K)*AGS)*SFC

AN(I,J,K)=(BW(I,J,K)* AWN+ BG(I,J,K)*AGN)*SFC

AT(I,J,K)=(BW(I,J,K)* AWT+ BG(I,J,K)*AGT)*SFC

AB(I,J,K)=(BW(I,J,K)* AWB+ BG(I,J,K)*AGB)*SFC

SBQR=ADW+ADE+ADS+ADN+ADT+ADB

WW(I,J,K)=AWW*SFC

WE(I,J,K)=AWE*SFC

WS(I,J,K)=AWS*SFC
```

```
      WN(I,J,K)=AWN*SFC

      WT(I,J,K)=AWT*SFC

      WB(I,J,K)=AWB*SFC

      IF(KCOFF.NE.1)GOTO 200

          WRITE(IOCODE,33)

          WRITE(IOCODE,4)

          WRITE(IOCODE,2)I,J,K,AT(I,J,K),AS(I,J,K),AW(I,J,K),E(I,J,K),

          &AE(I,J,K) ,AN(I,J,K),AB(I,J,K),B(I,J,K)

200   CONTINUE

2     FORMAT(1X,'(',3I3,')',8E15.6)

4     FORMAT(//T3,'NODE       AT(I,J,K)     AS(I,J,K)       AW(I,J,K)',

     &'      E(I,J,K)     AE(I,J,K)       AN(I,J,K)      AB(I,J,K)',

     &'      B(I,J,K)'/)

33    FORMAT(//)
```

Appendix B.2 Single branch horizontal wellbore model solution module

```
SUBROUTINE  HWELLP()
PARAMETER(NNX=60,NNY=60,NNK=10,NNN=NNX*NNY*NNK,NNW=30)

COMMON /CCOM/ II,JJ,KK,NW,NWP,NWI,DELT,IOCODE,IHEDIN(80)

COMMON/CTABL/SAT(25),KRWT(25),KRGT(25),PCGWT(25),PWT(25),MUWT(2
5)&,BWT(25),BWPT(25),PGT(25),MUGT(25),BGT(25),BGPT(25),CRT(25)&,RHOS
CG,RHOSCW,MSAT,MPWT,MPGT

REAL KRWT,KRGT,MUWT,MUGT

COMMON /WRATE/QG(NNX,NNY,NNK),QW(NNX,NNY,NNK),WELLS(NNW),&
IQN1(NNW),IQN2(NNW),IQN3(NNW),LAYER(NNW),KIP(NNW),QVW(NNW),&
QVG(NNW),PWFX(NNW),PID(NNW,NNK),PWF(NNW,NNK),PWFC(NNW,NNK),
```

```
&IQNEND(NNW),NEP(NNW),HPID(NNW,NNX),HPWF(NNW,NNX),HPWFX(NNW)& ,HPWFN(NNW,NNX),HRW(NNW)

CHARACTER*5 WELLS

COMMON/PRSTC/PN(NNX,NNY,NNK),SWN(NNX,NNY,NNK),SGN(NNX,NNY,NNK),&PMN(NNX,NNY,NNK),CMN(NNX,NNY,NNK),P(NNX,NNY,NNK),SW(NNX,NNY,NNK),&SG(NNX,NNY,NNK),PM(NNX,NNY,NNK),CM(NNX,NNY,NNK),QMFG(NNX,NNY,NNK)

REAL RHO(NNW,NNX),MUI(NNW,NNX),REY(NNW,NNX),REYW(NNW,NNX)

REAL FRAC(NNW,NNX),FRAC0

INTEGER IQ1,IQ2,IQ3,IQ4,I

REAL HDIA

REAL QWGMAIN(NNW,NNX),QWG(NNW,NNX)

REAL MUW, MUG

! Horizontal wellbore diameter

HDIA=0.2

! Calculate QW and QG

CALL WERATE()

! Calculate the intermediate variable

    DO N=1,NW

        IQ1=IQN1(N)

        IQ2=IQN2(N)

        IQ3=IQN3(N)

        IQ4=IQNEND(N)

        HDIA=2*HRW(N)

        DO I=IQ1,IQ4
```

```
!Calculate the density and viscosity in the horizontal wellbore
        FACG=RHOSCG*QG(I,IQ2,IQ3)
        FACW=RHOSCW*QW(I,IQ2,IQ3)
        RHO(N,I)=(FACW+FACG)/(QG(I,IQ2,IQ3)+QW(I,IQ2,IQ3))
        PP=P(I,IQ2,IQ3)
        CALL INTERP(PWT,MUWT,MPWT,PP,MUW)
        CALL INTERP(PGT,MUGT,MPGT,PP,MUG)
        FAC1=FACW/(FACW+FACG)
        MUI(N,I)=(MUW**FAC1)*(MUG**(1-FAC1))
        !Calculate the wellbore wall flux and main flux
        QWG(N,I)=QG(I,IQ2,IQ3)+QW(I,IQ2,IQ3)
ENDDO
QWGMAIN(N,IQ4)=QWG(N,IQ4)
DO I=IQ4-1,IQ1,-1
        QWGMAIN(N,I)=QWG(N,I)+QWGMAIN(N,I+1)
ENDDO
!Calculate Re number
DO I=IQ1,IQ4
        REYW(N,I)=RHO(N,I)*QWG(N,I)/3.1416/HDIA
        REY(N,I)=4*QWGMAIN(N,I)*RHO(N,I)/3.1416/HDIA/MUI(N,I)
!Calculate the friction coefficient
        IF(REY(N,I)<2100)THEN
                FRAC(N,I)=16/REY(N,I)*(1+0.04304*REYW(N,I)**0.6142)
        ELSE
```

```
                    FRAC0=2.28-4*LOG10(21.25/(REY(N,I)**0.9))
                    FRAC0=1/(FRAC0*FRAC0)
                    FRAC(N,I)=FRAC0*(1-0.0153*REYW(N,I)**0.3978)
                ENDIF
            ENDDO
! Calculate the wellbore pressure
            HPWF(N,IQ1)=HPWFX(N)+0.4053*RHO(N,IQ1)/HDIA**4*((FRAC(N,IQ1)
            &/HDIA-2)*QWGMAIN(N,IQ1)*QWGMAIN(N,IQ1)+2*
            &(QWGMAIN(N,IQ1)+QWG(N,IQ1))*(QWGMAIN(N,IQ1)
            &+QWG(N,IQ1)))/74.6496E11
            DO I=IQ1+1,IQ4
                QM1=RHO(N,I-1)*QWGMAIN(N,I-1)*QWGMAIN(N,I-1)
                QM2=RHO(N,I)*QWGMAIN(N,I)*QWGMAIN(N,I)
                QM3=2*RHO(N,I-1)*(QWGMAIN(N,I-1)+QWG(N,I-1))*
                &(QWGMAIN(N,I-1)+QWG(N,I-1))
                QM4=2*RHO(N,I)*(QWGMAIN(N,I)+QWG(N,I))*
                &(QWGMAIN(N,I)+QWG(N,I))
                QM=(QM1+QM2+QM3+QM4)/74.6496E11
                HPWF(N,I)=HPWF(N,I-1)+0.4053/HDIA**4*QM
            ENDDO
        ENDDO
END
```

Appendix B.3 Coupled Multibranch horizontal wellbore solution module

```
SUBROUTINE  HWELLP()
PARAMETER(NNX=60,NNY=60,NNK=10,NNN=NNX*NNY*NNK,NNW=30)

COMMON /CCOM/ II,JJ,KK,NW,NWP,NWI,DELT,IOCODE,IHEDIN(80)

COMMON/CTABL/SAT(25),KRWT(25),KRGT(25),PCGWT(25),PWT(25),MUWT(2
5)&,BWT(25),BWPT(25),PGT(25),MUGT(25),BGT(25),BGPT(25),CRT(25)&,RHOS
CG,RHOSCW,MSAT,MPWT,MPGT

REAL KRWT,KRGT,MUWT,MUGT

COMMON/WRATE/QG(NNX,NNY,NNK),QW(NNX,NNY,NNK),WELLS(NNW),&I
QN1(NNW),IQN2(NNW),IQN3(NNW),LAYER(NNW),KIP(NNW),QVW(NNW),&Q
VG(NNW),PWFX(NNW),PID(NNW,NNK),PWF(NNW,NNK),PWFC(NNW,NNK),&
IQNEND(NNW),NEP(NNW),HPID(NNW,NNX),HPWF(NNW,NNX),HPWFX(NNW
)&,HPWFN(NNW,NNX),HRW(NNW)

CHARACTER*5 WELLS

COMMON/PRSTC/PN(NNX,NNY,NNK),SWN(NNX,NNY,NNK),SGN(NNX,NNY,
NNK),&PMN(NNX,NNY,NNK),CMN(NNX,NNY,NNK),P(NNX,NNY,NNK),SW(N
NX,NNY,NNK),&SG(NNX,NNY,NNK),PM(NNX,NNY,NNK),CM(NNX,NNY,NNK)
,QMFG(NNX,NNY,NNK)

COMMON/BRANCH/ANGLE(NNW),NUMBRAN(NNW),BANGLE(NNW,20),BRW
(NNW,20),&IQNB1(NNW,20),IQNB2(NNW,20),IQNB3(NNW,20),IQNENDB(NNW,
20),&BPID(NNW,20,20),BQW(NNW,20),BQG(NNW,20),BNEP(NNW,20),&BLEN(
NNW,20),SBRAN(NNW,20),BHPWF(NNW,20,20)

REAL RHO(NNW,NNX),MUI(NNW,NNX),REY(NNW,NNX),REYW(NNW,NNX)

REAL FRAC(NNW,NNX),FRAC0

INTEGER IQ1,IQ2,IQ3,IQ4,I

REAL HDIA

REAL QWG, MAIN(NNW,NNX),QWG(NNW,NNX)

REAL MUW,MUG
```

```
REAL BRHO(NNW,20,20),BMUI(NNW,20,20)
REAL BQMAIN(NNW,20,20),BQWG(NNW,20,20),QBRA(NNW,NNX)
REAL BREY(NNW,20,20),BREYW(NNW,20,20)
REAL BFRAC(NNW,20,20)
!Calculating the horizontal wellbore diameter
HDIA=0.2
!Calculating QW and QG
CALL WERATE()
!Calculating the intermediate variable
DO N=1,NW
    IQ1=IQN1(N)
    Q2=IQN2(N)
    IQ3=IQN3(N)
    IQ4=IQNEND(N)
    HDIA=2*HRW(N)
    DO I=IQ1,IQ4
    ! Calculating the density and viscosity in the horizontal wellbore
        IF(QG(I,IQ2,IQ3)+QW(I,IQ2,IQ3)/=0)THEN
                FACG=RHOSCG*QG(I,IQ2,IQ3)
                FACW=RHOSCW*QW(I,IQ2,IQ3)
                RHO(N,I)=(FACW+FACG)/(QG(I,IQ2,IQ3)+QW(I,IQ2,IQ3))
                PP=P(I,IQ2,IQ3)
                CALL INTERP(PWT,MUWT,MPWT,PP,MUW)
                CALL INTERP(PGT,MUGT,MPGT,PP,MUG)
```

```
                FAC1=FACW/(FACW+FACG)
                MUI(N,I)=(MUW**FAC1)*(MUG**(1-FAC1))
            ENDIF
        ! Calculating the wellbore wall fluc and main flux
            QWG(N,I)=QG(I,IQ2,IQ3)+QW(I,IQ2,IQ3)
        ENDDO
        ! Calculating the density and viscosity for the branch well
        DO I=1,NUMBRAN(N)
            IQB1=IQNB1(N,I)
            IQB2=IQNB2(N,I)
            IQB3=IQNB3(N,I)
            BQW(N,I)=0
            BQG(N,I)=0
            DO K=0,BNEP(N,I)-1
                IF(QG(IQB1,IQB2,IQB3)+QW(IQB1,IQB2,IQB3)/=0)THEN
                    FACG=RHOSCG*QG(IQB1,IQB2,IQB3)
                    FACW=RHOSCW*QW(IQB1,IQB2,IQB3)
                    BRHO(N,I,K+1)=(FACW+FACG)/(QG(IQB1,IQB2,IQB3)+
                    &QW(IQB1,IQB2,IQB3))
                    PP=P(IQB1,IQB2,IQB3)
                    CALL INTERP(PWT,MUWT,MPWT,PP,MUW)
                    CALL INTERP(PGT,MUGT,MPGT,PP,MUG)
                    FAC1=FACW/(FACW+FACG)
                    BMUI(N,I,K+1)=(MUW**FAC1)*(MUG**(1-FAC1))
```

```
            ENDIF
        ! Calculating the wellbore wall fluc and main flux
            BQWG(N,I,K+1)=QG(IQB1,IQB2,IQB3)+QW(IQB1,IQB2,IQB3)
            BQW(N,I)=BQW(N,I)+QW(IQB1,IQB2,IQB3)
            BQG(N,I)=BQG(N,I)+QG(IQB1,IQB2,IQB3)
            IF(BANGLE(N,I)<90)THEN
                IQB1=IQB1+1
                IQB2=IQB2-1
            ELSEIF(BANGLE(N,I)==90)THEN
                IQB1=IQB1
                IQB2=IQB2-1
            ELSEIF(BANGLE(N,I)<180)THEN
                IQB1=IQB1-1
                IQB2=IQB2-1
            ELSEIF(BANGLE(N,I)==180)THEN
                IQB1=IQB1-1
                IQB2=IQB2
            ELSEIF(BANGLE(N,I)<270)THEN
                IQB1=IQB1-1
                IQB2=IQB2+1
            ELSEIF(BANGLE(N,I)==270)THEN
                IQB1=IQB1
                IQB2=IQB2+1
            ELSE
```

```
                IQB1=IQB1+1
                IQB2=IQB2+1
            ENDIF
        ENDDO
        BQMAIN(N,I,BNEP(N,I))=BQWG(N,I,BNEP(N,I))
        DO K=BNEP(N,I)-1,1,-1
            BQMAIN(N,I,K)=BQMAIN(N,I,K+1)+BQWG(N,I,K)
        ENDDO
        QBRA(N,IQNB1(N,I)-IQ1+1)=BQMAIN(N,I,1)
        ! Calculating Re number
        DO K=1,BNEP(N,I)
            BREYW(N,I,K)=BRHO(N,I,K)*BQWG(N,I,K)/6.2832/BRW(N,I)
            BREY(N,I,K)=4*BQMAIN(N,I,K)*BRHO(N,I,K)/6.2832/BRW(N,I)/
            &BMUI(N,I,K)
            ! Calculating the friction coefficient
            IF(BREY(N,I,K)==0)THEN
                BFRAC(N,I,K)=0
            ELSEIF(BREY(N,I,K)<2100)THEN
                BFRAC(N,I,K)=16/BREY(N,I,K)*(1+0.04304*BREYW(N,I,K)
                & **0.6142)
            ELSE
                FRAC0=2.28-4*LOG10(21.25/(BREY(N,I,K)**0.9))
                FRAC0=1/(FRAC0*FRAC0)
                BFRAC(N,I,K)=FRAC0*(1-0.0153*BREYW(N,I,K)**0.3978)
```

```
                ENDIF
            ENDDO
        ENDDO
        QWGMAIN(N,IQ4)=QWG(N,IQ4)+QBRA(N,IQ4)
        DO I=IQ4-1,IQ1,-1
            QWGMAIN(N,I)=QWG(N,I)+QWGMAIN(N,I+1)+QBRA(N,I)
        ENDDO
        ! Calculating Re number
        DO I=IQ1,IQ4
            IF(QWGMAIN(N,I)==0)THEN
                REY(N,I)=0
            ELSE
                REYW(N,I)=RHO(N,I)*QWG(N,I)/3.1416/HDIA
                REY(N,I)=4*QWGMAIN(N,I)*RHO(N,I)/3.1416/HDIA/MUI(N,I)
            ENDIF
! Calculating friction coefficient
            IF(REY(N,I)==0)THEN
                FRAC(N,I)=0
            ELSEIF(REY(N,I)<2100)THEN
                FRAC(N,I)=16/REY(N,I)*(1+0.04304*REYW(N,I)**0.6142)
            ELSE
                FRAC0=2.28-4*LOG10(21.25/(REY(N,I)**0.9))
                FRAC0=1/(FRAC0*FRAC0)
                FRAC(N,I)=FRAC0*(1-0.0153*REYW(N,I)**0.3978)
```

```
        ENDIF
    ENDDO
! Calculating the wellbore pressure
    HPWF(N,IQ1)=HPWFX(N)+0.4053*RHO(N,IQ1)/HDIA**4*((FRAC(N,IQ1)
    &/HDIA-2)*QWGMAIN(N,IQ1)*QWGMAIN(N,IQ1)+2*
    &(QWGMAIN(N,IQ1)+QWG(N,IQ1)+QBRA(N,IQ1))*
    &(QWGMAIN(N,IQ1)+QWG(N,IQ1)+QBRA(N,IQ1)))/74.6496E11
    DO I=IQ1+1,IQ4
        QM1=RHO(N,I-1)*QWGMAIN(N,I-1)*QWGMAIN(N,I-1)
        QM2=RHO(N,I)*QWGMAIN(N,I)*QWGMAIN(N,I)
        QM3=2*RHO(N,I-1)*(QWGMAIN(N,I-1)+QWG(N,I-1)+QBRA(N,I-1))*
        &(QWGMAIN(N,I-1)+QWG(N,I-1)+QBRA(N,I-1))
        QM4=2*RHO(N,I)*(QWGMAIN(N,I)+QWG(N,I)+QBRA(N,I))*
        &(QWGMAIN(N,I)+QWG(N,I)+QBRA(N,I))
        QM=(QM1+QM2+QM3+QM4)/74.6496E11
        HPWF(N,I)=HPWF(N,I-1)+0.4053/HDIA**4*QM
    ENDDO
! Calculating the branch wellbore pressure
    DO I=1,NUMBRAN(N)
        IQB1=IQNB1(N,I)
        IQB2=IQNB2(N,I)
        IQB3=IQNB3(N,I)
        BHPWF(N,I,1)=HPWF(N,IQB1-IQ1+1)+0.4053*BRHO(N,I,1)/16/
        &BRW(N,I)**4*((BFRAC(N,I,1)/2/BRW(N,I)-2)*BQAMIN(N,I,
```

```
        1)*&BQMAIN(N,I,1)+2*(BQMAIN(N,I,1)+BQWG(N,I,1))*(BQMAIN
        (N,I,1)&          +BQWG(N,I,1)))/74.6496E11
        DO K=2,BNEP(N,I)
            QBM1=BRHO(N,I,K-1)*BQMAIN(N,I,K-1)*BQMAIN(N,I,K-1)
            QBM2=BRHO(N,I,K)*BQMAIN(N,I,K)*BQMAIN(N,I,K)
            QBM3=2*BRHO(N,I,K-1)*(BQMAIN(N,I,K-1)+BQWG(N,I,K-1))*
            &(BQMAIN(N,I,K-1)+BQWG(N,I,K-1))
            QBM4=2*BRHO(N,I,K)*(BQMAIN(N,I,K)+BQWG(N,I,K))*
            &(BQMAIN(N,I,K)+BQWG(N,I,K))
            QBM=(QBM1+QBM2+QBM3+QBM4)/74.6496E11
            BHPWF(N,I,K)=BHPWF(N,I,K-1)+0.4053/16/BRW(N,I)**4*QBM
        ENDDO
    ENDDO
ENDDO
END
```

Appendix B.4 Triple porosity model solution module

```
subroutine coefficients(div1,d288,temp1,cefg0)
!=================
! this subroutine computes pressure equation coefficients
!============================================================
use declarations
implicit none
real div1,d288,temp1,cefg0
```

```
real sb,fssw,fssg,pcgw,pfcgw,ho1,hw1,hg1,ggwi,gwwi,pp,& ssw,ssg,krw,krg,muw,mug
!pcgwi,sswi,ssgi

real mwc,mgc,mtc,acp,f1,f2,f3,td2

real act(nx,ny,nk),amt(nx,ny,nk)

real rrw,rrg,sbx1,p1,sw1,sg1,rw1,rg1,ffact, gww1, ggw1, pcgw1, p11, mw1, mg1, aww,
agw,adw,krw1,krg1,mug1,muw1,&rw2,rg2,sbx2,p2,sw2,sg2,gww2,pcgw2,ggw2,p22,h
w2,hg2,mw2,krw2,muw2,mg2,krg2,mug2,awe,age,ade,&rw3,rg3,sby1,p3,sw3,sg3,gww
3,pcgw3,ggw3,p33,hw3,hg3,mw3,krw3,muw3,mg3,krg3,mug3,aws,ags,ads,&rw4,rg4,s
by2,p4,sw4,sg4,gww4,pcgw4,ggw4,p44,hw4,hg4,mw4,krw4,muw4,mg4,krg4,mug4,aw
n,agn,adn,&rw5,rg5,sbz1,p5,sw5,sg5,gww5,pcgw5,ggw5,p55,hw5,hg5,mw5,krw5,muw
5,mg5,krg5,mug5,awt,agt,adt,&rw6,rg6,sbz2,p6,sw6,sg6,gww6,pcgw6,ggw6,p66,hw6,h
g6,mw6,krw6,muw6,mg6,krg6,mug6,awb,agb,adb

real ag1,ag2,ag3,ag4,ag5,ag6,aw1,aw2,aw3,aw4,aw5,aw6,sbqr,fsbqr

real stpw1, stpw2,stpg1, stpg2, sle1,sle2

real lamdaw1,lamdaw2,lamdaw3,lamdaw4,lamdaw5,lamdaw6,lamdag1,lamdag2, lamda
g3,lamdag4,lamdag5,lamdag6

integer i,j,k

do k=1,kk

 do j=1,jj

  do i=1,ii

        if(mp(i,j,k)/=0)then ! if there is matrix porosity

            sb=sg(i,j,k)/bg(i,j,k)

              pp=p(i,j,k)

              call interp(pwt,muwt,mpwt,pp,muw)

              call interp(pgt,mugt,mpgt,pp,mug)

              ssw=sw(i,j,k)

              ssg=sg(i,j,k)
```

```
call interp(sat,pcgwt,msat,ssw,pcgw)

if(fp(i,j,k)/=0)then !if there is fracture porosity

!----------------mass transfer transmissibility calculation

 fssw=fsw(i,j,k)

 fssg=fsg(i,j,k)

 call interp(fsat,fpcgwt,fmsat,fssw,pfcgw)

 gwwi=pfcgw-pcgw ! gravity effects

 ggwi=0.0

 ho1=pp-pf(i,j,k)

 hw1=ho1+gwwi

 hg1=ho1+ggwi

 if(iflow/=0)then

  !thomas et al.(1983)approach

      !if(hw1>=0)call interp(sat,krwt,msat,ssw,krw)

      !if(hw1<0)then

       ! pcgwi=0.0  !capillary pressure at the matrix/fracture interface

        !call interpc(pcgwt,sat,msat,pcgwi,sswi)

        !call interp(sat,krwt,msat,sswi,krw)

        !krw=krw*fssw

      !end if

      !if(hg1>=0)call interp(sat,krgt,msat,ssg,krg)

      !if(hg1<0)then

        !ssgi=1-swc !gas saturation at the matrix/fracture interface

        !call interp(sat,krgt,msat,ssgi,krg)
```

```
                !krg=krg*fssg
              !end if
              !upstream weighting approach
              if(hw1>=0)call interp(sat,krwt,msat,ssw,krw)
              if(hw1<0)call interp(fsat,fkrwt,fmsat,fssw,krw)
              if(hg1>=0)call interp(sat,krgt,msat,ssg,krg)
              if(hg1<0)call interp(fsat,fkrgt,fmsat,fssg,krg)
              mwc=krw/muw
              mgc=krg/mug
              mtc=mwc+mgc
              acp=mwc*gwwi+mgc*ggwi
              amt(i,j,k)=tm(i,j,k)*mtc ! transmissibility for mass transfer
              act(i,j,k)=tm(i,j,k)*acp !capillary pressure effects in mass transfer
            else
             !using time dependent fx for interporosity rate(gas/water system)
              f1=1 !no time dependent effects for single-phase fc
              if(fssw>0)then
               if(ts(i,j,k)/=0)then
               !ts(i,j,k)at which fc starts to vary in two-phase flow
              td2=0.006328*ka(i,j,k)*krdp*(ft-
              ts(i,j,k))/mp(i,j,k)/muw/l(i,j,k)**2
                 if(td2<0.000001) td2=0.000001 !correlation lower limit
                 if(td2<tdt)then        !tdt dimensionless transition time
                  f2=fkn*(1/td2+0.00001/td2**2)**0.5
```

```
                else
                  f2=1+473.04/td2**0.75
                end if
                f3=1+0.004433/td2**0.5
              else
                f2=1
              end if
            end if
            ffg(i,j,k)=f1*fssg*krgi+f2*fssw*krgg
            !ffg()time dependent oil mobility term
            !krgi initial gas rel.perm at the matrix/fracture interface
            !krgg  gas rel perm at the matrix/fracture interface
            ffw(i,j,k)=f3*fssw*krwi
            mgc=ffg(i,j,k)/mug
            mwc=ffw(i,j,k)/muw
            mtc=mgc+mwc
            acp=mwc*gwwi
            amt(i,j,k)=tm(i,j,k)*mtc
            act(i,j,k)=tm(i,j,k)*acp
          end if
        end if
        rrw=rhoscw/bw(i,j,k)
        rrg=rhoscg/bg(i,j,k)
```

! initial value of the threshold pressure gradient and gas slippage effect experimental factor

```
stpw1=0.0
stpw2=0.0
stpg1=0
stpg2=0
sle1=161
sle2=0.47
if(i/=1)then
 sbx1=sg(i-1,j,k)/bg(i-1,j,k)
  p1=p(i-1,j,k)
  call interp(pwt,muwt,mpwt,p1,muw1)
  call interp(pgt,mugt,mpgt,p1,mug1)
  sw1=sw(i-1,j,k)
  sg1=sg(i-1,j,k)
  call interp(sat,pcgwt,msat,sw1,pcgw1)
  rw1=rhoscw/bw(i-1,j,k)
  rg1=rhoscg/bg(i-1,j,k)
  ffact=-d288*(el(i-1,j,k)-el(i,j,k))
  gww1=(rw1+rrw)*ffact+pcgw-pcgw1
  ggw1=(rg1+rrg)*ffact
  p11=p1-pp
  hw1=p11+gww1
  hg1=p11+ggw1
```

```
if(hw1>=0) then
    call interp(sat,krwt,msat,sw1,krw1)
    lamdaw1=-dx(i-1,j,k)*stpw1/(kx(i-1,j,k)*krw1/muw1)**stpw2
end if
if(hw1<0) then
    call interp(sat,krwt,msat,ssw,krw1)
    lamdaw1=dx(i,j,k)*stpw1/(kx(i,j,k)*krw1/muw1)**stpw2
end if
if(hg1>=0) then
    call interp(sat,krgt,msat,sg1,krg1)
    lamdag1=-dx(i-1,j,k)*(stpg1/(kx(i-1,j,k)*krg1*0.987E-
    3)+stpg2)
    hg=hg1+lamdag1
    qq1=kx(i-1,j,k)*krg1*dy(i-1,j,k)*dz(i-1,j,k)*abc(hg)/mug1
    recl=qq1*rhoscg*(kx(i-1,j,k)*krg1)**0.5/(mug1*vp(i-1,j,k)
    &*dz(i-1,j,k)*dy(i-1,j,k))
    if((recl>=0).and.(recl<=recd))then
        krg1=krg1*(1+sle1*(kx(i-1,j,k)*krg1/
        & (vp(i-1,j,k)*(1-sw1)))**sle2)/p1
    end if
end if
if(hg1<0) then
    call interp(sat,krgt,msat,ssg,krg1)
    lamdag1=dx(i,j,k)*(stpg1/(kx(i,j,k)*krg1*0.987E-3)+stpg2)
```

```
            hg=hg1+lamdag1
            qq1=kx(i,j,k)*krg1*dy(i,j,k)*dz(i,j,k)*abc(hg)/mug
            recl=qq1*rhoscg*(kx(i,j,k)*krg1)**0.5/(mug*vp(i,j,k)
            &*dz(i,j,k)*dy(i,j,k))
            if((recl>=0).and.(recl<=recd))then
                krg1=krg1*(1+sle1*(kx(i,j,k)*krg1/
                &(vp(i,j,k)*(1-ssw)))**sle2)/pp
            end if
          end if
          mw1=4.0*krw1/((bw(i-1,j,k)+bw(i,j,k))*(muw1+muw))
          mg1=4.0*krg1/((bg(i-1,j,k)+bg(i,j,k))*(mug1+mug))
        end if
        aww=tx(i,j,k)*mw1
        agw=tx(i,j,k)*mg1
        if((abs(hg1)-abs(lamdag1))<=0) agw=0
        if((abs(hw1)-abs(lamdaw1))<=0) aww=0
        adw=tdx(i,j,k)*(sbx1-sb)
        if(i/=ii)then
          sbx2=sg(i+1,j,k)/bg(i+1,j,k)
          p2=p(i+1,j,k)
          call interp(pwt,muwt,mpwt,p2,muw2)
          call interp(pgt,mugt,mpgt,p2,mug2)
          sw2=sw(i+1,j,k)
          sg2=sg(i+1,j,k)
```

```
call interp(sat,pcgwt,msat,sw2,pcgw2)
rw2=rhoscw/bw(i+1,j,k)
rg2=rhoscg/bg(i+1,j,k)
ffact=-d288*(el(i+1,j,k)-el(i,j,k))
gww2=(rw2+rrw)*ffact+pcgw-pcgw2
ggw2=(rg2+rrg)*ffact
p22=p2-pp
hw2=p22+gww2
hg2=p22+ggw2
if(hw2>=0) then
    call interp(sat,krwt,msat,sw2,krw2)
    lamdaw2=-dx(i+1,j,k)*stpw1/(kx(i+1,j,k)*krw2/muw2)**stpw2
end if
if(hw2<0) then
    call interp(sat,krwt,msat,ssw,krw2)
    lamdaw2=dx(i,j,k)*stpw1/(kx(i,j,k)*krw2/muw2)**stpw2
end if
if(hg2>=0) then
    call interp(sat,krgt,msat,sg2,krg2)
    lamdag2=-dx(i+1,j,k)*(stpg1/(kx(i+1,j,k)*krg2*0.987E-3)
    +stpg2)
    hg=hg2+lamdag2
    qq2=kx(i+1,j,k)*krg2*dy(i+1,j,k)*dz(i+1,j,k)*abc(hg)/mug2
    recl=qq2*rhoscg*(kx(i+1,j,k)*krg2)**0.5/(mug2*vp(i,j,k)
```

```
                &*dz(i+1,j,k)*dy(i+1,j,k))
                if((recl>=0).and.(recl<=recd))then
                    krg2=krg2*(1+sle1*(kx(i+1,j,k)*krg2/
                    &(vp(i+1,j,k)*(1-sw2)))**sle2)/p2
                end if
            end if
            if(hg2<0) then
                call interp(sat,krgt,msat,ssg,krg2)
                lamdag2=dx(i,j,k)*(stpg1/(kx(i,j,k)*krg2*0.987E-3)+stpg2)
                hg=hg2+lamdag2
                qq2=kx(i,j,k)*krg2*dy(i,j,k)*dz(i,j,k)*abc(hg)/mug
                recl=qq2*rhoscg*(kx(i,j,k)*krg2)**0.5/(mug*vp(i,j,k)
                &*dz(i,j,k)*dy(i,j,k))
                if((recl>=0).and.(recl<=recd))then
                    krg2=krg2*(1+sle1*(kx(i,j,k)*krg2/
                    &(vp(i,j,k)*(1-ssw)))**sle2)/pp
                end if
            end if
            mw2=4.0*krw2/((bw(i+1,j,k)+bw(i,j,k))*(muw2+muw))
            mg2=4.0*krg2/((bg(i+1,j,k)+bg(i,j,k))*(mug2+mug))
        end if
        awe=tx(i+1,j,k)*mw2
        age=tx(i+1,j,k)*mg2
        if((abs(hg2)-abs(lamdag2))<=0) age=0
```

```
if((abs(hw2)-abs(lamdaw2))<=0) awe=0
ade=tdx(i+1,j,k)*(sbx2-sb)
if(j/=1)then
 sby1=sg(i,j-1,k)/bg(i,j-1,k)
 p3=p(i,j-1,k)
 call interp(pwt,muwt,mpwt,p3,muw3)
 call interp(pgt,mugt,mpgt,p3,mug3)
 sw3=sw(i,j-1,k)
 sg3=sg(i,j-1,k)
 call interp(sat,pcgwt,msat,sw3,pcgw3)
 rw3=rhoscw/bw(i,j-1,k)
 rg3=rhoscg/bg(i,j-1,k)
 ffact=-d288*(el(i,j-1,k)-el(i,j,k))
 gww3=(rw3+rrw)*ffact+pcgw-pcgw3
 ggw3=(rg3+rrg)*ffact
 p33=p3-pp
 hw3=p33+gww3
 hg3=p33+ggw3
 if(hw3>=0) then
        call interp(sat,krwt,msat,sw3,krw3)
        lamdaw3=-dy(i,j-1,k)*stpw1/(ky(i,j-1,k)*krw3/muw3)**stpw2
 end if
 if(hw3<0) then
        call interp(sat,krwt,msat,ssw,krw3)
```

```
            lamdaw3=dy(i,j,k)*stpw1/(ky(i,j,k)*krw3/muw3)**stpw2
        end if
        if(hg3>=0) then
            call interp(sat,krgt,msat,sg3,krg3)
            lamdag3=-dy(i,j-1,k)*(stpg1/(ky(i,j-1,k)*krg3*0.987E-3)
            +stpg2)
            hg=hg3+lamdag3
            qq3=ky(i,j-1,k)*krg3*dx(i,j-1,k)*dz(i,j-1,k)*abc(hg)/mug3
            recl=qq3*rhoscg*(ky(i,j-1,k)*krg3)**0.5/(mug3*vp(i,j-1,k)
            &*dz(i,j-1,k)*dx(i,j-1,k))
            if((recl>=0).and.(recl<=recd))then
                krg3=krg3*(1+sle1*(ky(i,j-1,k)*krg3/
                &(vp(i,j-1,k)*(1-sw3)))**sle2)/p3
            end if
        end if
        if(hg3<0) then
            call interp(sat,krgt,msat,ssg,krg3)
            lamdag3=dy(i,j,k)*(stpg1/(ky(i,j,k)*krg3*0.987E-3)+stpg2)
            hg=hg3+lamdag3
            qq3=ky(i,j,k)*krg3*dx(i,j,k)*dz(i,j,k)*abc(hg)/mug
            recl=qq3*rhoscg*(ky(i,j,k)*krg3)**0.5/(mug*vp(i,j,k)
            &*dz(i,j,k)*dx(i,j,k))
            if((recl>=0).and.(recl<=recd))then
                krg3=krg3*(1+sle1*(ky(i,j,k)*krg3/
```

```
                    &(vp(i,j,k)*(1-ssw)))**sle2)/pp
            end if
          end if
          mw3=4.0*krw3/((bw(i,j-1,k)+bw(i,j,k))*(muw3+muw))
          mg3=4.0*krg3/((bg(i,j-1,k)+bg(i,j,k))*(mug3+mug))
        end if
        aws=ty(i,j,k)*mw3
        ags=ty(i,j,k)*mg3
        if((abs(hg3)-abs(lamdag3))<=0) ags=0
        if((abs(hw3)-abs(lamdaw3))<=0) aws=0
        ads=tdy(i,j,k)*(sby1-sb)
        if(j/=jj)then
          sby2=sg(i,j+1,k)/bg(i,j+1,k)
          p4=p(i,j+1,k)
          call interp(pwt,muwt,mpwt,p4,muw4)
          call interp(pgt,mugt,mpgt,p4,mug4)
          sw4=sw(i,j+1,k)
          sg4=sg(i,j+1,k)
          call interp(sat,pcgwt,msat,sw4,pcgw4)
          rw4=rhoscw/bw(i,j+1,k)
          rg4=rhoscg/bg(i,j+1,k)
          ffact=-d288*(el(i,j+1,k)-el(i,j,k))
          gww4=(rw4+rrw)*ffact+pcgw-pcgw4
          ggw4=(rg4+rrg)*ffact
```

```
p44=p4-pp
hw4=p44+gww4
hg4=p44+ggw4
if(hw4>=0) then
    call interp(sat,krwt,msat,sw4,krw4)
    lamdaw4=-dy(i,j+1,k)*stpw1/(ky(i,j+1,k)*krw4/muw4)**stpw2
end if
if(hw4<0) then
    call interp(sat,krwt,msat,ssw,krw4)
    lamdaw4=dy(i,j,k)*stpw1/(ky(i,j,k)*krw4/muw4)**stpw2
end if
if(hg4>=0)then
    call interp(sat,krgt,msat,sg4,krg4)
    lamdag4=-dy(i,j+1,k)*(stpg1/(ky(i,j+1,k)*krg4*0.987E-3)
    +stpg2)
    hg=hg4+lamdag4
    qq4=ky(i,j+1,k)*krg4*dx(i,j+1,k)*dz(i,j+1,k)*abc(hg)/mug4
    recl=qq4*rhoscg*(ky(i,j+1,k)*krg4)**0.5/(mug4*vp(i,j+1,k)
    &*dz(i,j+1,k)*dx(i,j+1,k))
    if((recl>=0).and.(recl<=recd))then
        krg4=krg4*(1+sle1*(ky(i,j+1,k)*krg4/
        &(vp(i,j+1,k)*(1-sw4)))**sle2)/p4
    end if
end if
```

```
        if(hg4<0) then
                call interp(sat,krgt,msat,ssg,krg4)
                lamdag4=dy(i,j,k)*(stpg1/(ky(i,j,k)*krg4*0.987E-3)+stpg2)
                hg=hg4+lamdag4
                qq4=ky(i,j,k)*krg4*dx(i,j,k)*dz(i,j,k)*abc(hg)/mug
                recl=qq4*rhoscg*(ky(i,j,k)*krg4)**0.5/(mug*vp(i,j,k)
                &*dz(i,j,k)*dx(i,j,k))
                if((recl>=0).and.(recl<=recd))then
                        krg4=krg4*(1+sle1*(ky(i,j,k)*krg4/
                        &(vp(i,j,k)*(1-ssw)))**sle2)/pp
                end if
        end if
        mw4=4.0*krw4/((bw(i,j+1,k)+bw(i,j,k))*(muw4+muw))
        mg4=4.0*krg4/((bg(i,j+1,k)+bg(i,j,k))*(mug4+mug))
end if
awn=ty(i,j+1,k)*mw4
agn=ty(i,j+1,k)*mg4
if((abs(hg4)-abs(lamdag4))<=0) agn=0
if((abs(hw4)-abs(lamdaw4))<=0) awn=0
adn=tdy(i,j+1,k)*(sby2-sb)
if(k/=1)then
        sbz1=sg(i,j,k-1)/bg(i,j,k-1)
        p5=p(i,j,k-1)
        call interp(pwt,muwt,mpwt,p5,muw5)
```

```
call interp(pgt,mugt,mpgt,p5,mug5)

sw5=sw(i,j,k-1)

sg5=sg(i,j,k-1)

call interp(sat,pcgwt,msat,sw5,pcgw5)

rw5=rhoscw/bw(i,j,k-1)

rg5=rhoscg/bg(i,j,k-1)

ffact=-d288*(el(i,j,k-1)-el(i,j,k))

gww5=(rw5+rrw)*ffact+pcgw-pcgw5

ggw5=(rg5+rrg)*ffact

p55=p5-pp

hw5=p55+gww5

hg5=p55+ggw5

if(hw5>=0) then

        call interp(sat,krwt,msat,sw5,krw5)

        lamdaw5=-dz(i,j,k-1)*stpw1/(kz(i,j,k-1)*krw5/muw5)**stpw2

end if

if(hw5<0) then

        call interp(sat,krwt,msat,ssw,krw5)

        lamdaw5=dz(i,j,k)*stpw1/(kz(i,j,k)*krw5/muw5)**stpw2

end if

if(hg5>=0) then

        call interp(sat,krgt,msat,sg5,krg5)

        lamdag5=-dz(i,j,k-1)*(stpg1/(kz(i,j,k-1)*krg5*0.987E-3)+stpg2)

        hg=hg5+lamdag5
```

```
                qq5=kz(i,j,k-1)*krg5*dx(i,j,k-1)*dy(i,j,k-1)*abc(hg)/mug5
                recl=qq5*rhoscg*(kz(i,j,k-1)*krg5)**0.5/(mug5*vp(i,j,k-1)
                &*dy(i,j,k-1)*dx(i,j,k-1))
                if((recl>=0).and.(recl<=recd))then
                        krg5=krg5*(1+sle1*(kz(i,j,k-1)*krg5/
                        &(vp(i,j,k-1)*(1-sw5)))**sle2)/p5
                end if
            end if
            if(hg5<0) then
                call interp(sat,krgt,msat,ssg,krg5)
                lamdag5=dz(i,j,k)*(stpg1/(kz(i,j,k)*krg5*0.987E-3)+stpg2)
                hg=hg5+lamdag5
                qq5=kz(i,j,k)*krg5*dx(i,j,k)*dy(i,j,k)*abc(hg)/mug
                recl=qq5*rhoscg*(kz(i,j,k)*krg5)**0.5/(mug*vp(i,j,k)
                &*dy(i,j,k)*dx(i,j,k))
                if((recl>=0).and.(recl<=recd))then
                        krg5=krg5*(1+sle1*(kz(i,j,k)*krg5/
                &(vp(i,j,k)*(1-ssw)))**sle2)/pp
                end if
            end if
            mw5=4.0*krw5/((bw(i,j,k-1)+bw(i,j,k))*(muw5+muw))
            mg5=4.0*krg5/((bg(i,j,k-1)+bg(i,j,k))*(mug5+mug))
        end if
        awt=tz(i,j,k)*mw5
```

```
agt=tz(i,j,k)*mg5

if((abs(hg5)-abs(lamdag5))<=0) agt=0

if((abs(hw5)-abs(lamdaw5))<=0) awt=0

adt=tdz(i,j,k)*(sbz1-sb)

if(k/=kk)then

 sbz2=sg(i,j,k+1)/bg(i,j,k+1)

 p6=p(i,j,k+1)

 call interp(pwt,muwt,mpwt,p6,muw6)

 call interp(pgt,mugt,mpgt,p6,mug6)

 sw6=sw(i,j,k+1)

 sg6=sg(i,j,k+1)

 call interp(sat,pcgwt,msat,sw6,pcgw6)

 rw6=rhoscw/bw(i,j,k+1)

 rg6=rhoscg/bg(i,j,k+1)

 ffact=-d288*(el(i,j,k+1)-el(i,j,k))

 gww6=(rw6+rrw)*ffact+pcgw-pcgw6

 ggw6=(rg6+rrg)*ffact

 p66=p6-pp

 hw6=p66+gww6

 hg6=p66+ggw6

 if(hw6>=0) then

        call interp(sat,krwt,msat,sw6,krw6)

        lamdaw6=-dz(i,j,k+1)*stpw1/(kz(i,j,k+1)*krw6/muw6)**stpw2

 end if
```

```
if(hw6<0) then
    call interp(sat,krwt,msat,ssw,krw6)
    lamdaw6=dz(i,j,k)*stpw1/(kz(i,j,k)*krw6/muw6)**stpw2
end if
if(hg6>=0) then
    call interp(sat,krgt,msat,sg6,krg6)
    lamdag6=-dz(i,j,k+1)*(stpg1/(kz(i,j,k+1)*krg6*0.987E-3)
    +stpg2)
    hg=hg6+lamdag6
    qq6=kz(i,j,k+1)*krg6*dx(i,j,k+1)*dy(i,j,k+1)*abc(hg)/mug6
    recl=qq6*rhoscg*(kz(i,j,k+1)*krg6)**0.5/(mug6*vp(i,j,k+1)
    &*dy(i,j,k+1)*dx(i,j,k+1))
    if((recl>=0).and.(recl<=recd))then
        krg6=krg6*(1+sle1*(kz(i,j,k+1)*krg6/
        &(vp(i,j,k+1)*(1-sw6)))**sle2)/p6
    end if
end if
if(hg6<0) then
    call interp(sat,krgt,msat,ssg,krg6)
    lamdag6=dz(i,j,k)*(stpg1/(kz(i,j,k)*krg6*0.987E-3)+stpg2)
    hg=hg6+lamdag6
    qq6=kz(i,j,k)*krg6*dx(i,j,k)*dy(i,j,k)*abc(hg)/mug
    recl=qq6*rhoscg*(kz(i,j,k)*krg6)**0.5/(mug*vp(i,j,k)
    &*dy(i,j,k)*dx(i,j,k))
```

```
            if((recl>=0).and.(recl<=recd))then
                krg6=krg6*(1+sle1*(kz(i,j,k)*krg6/
                &(vp(i,j,k)*(1-ssw)))**sle2)/pp
            end if
          end if
          mw6=4.0*krw6/((bw(i,j,k+1)+bw(i,j,k))*(muw6+muw))
          mg6=4.0*krg6/((bg(i,j,k+1)+bg(i,j,k))*(mug6+mug))
        end if
        awb=tz(i,j,k+1)*mw6
        agb=tz(i,j,k+1)*mg6
        if((abs(hg6)-abs(lamdag6))<=0) agb=0
        if((abs(hw6)-abs(lamdaw6))<=0) awb=0
        adb=tdz(i,j,k+1)*(sbz2-sb)
        ag1=agw*(ggw1+lamdag1)
        ag2=age*(ggw2+lamdag2)
        ag3=ags*(ggw3+lamdag3)
        ag4=agn*(ggw4+lamdag4)
        ag5=agt*(ggw5+lamdag5)
        ag6=agb*(ggw6+lamdag6)
        aw1=aww*(gww1+lamdaw1)
        aw2=awe*(gww2+lamdaw2)
        aw3=aws*(gww3+lamdaw3)
        aw4=awn*(gww4+lamdaw4)
        aw5=awt*(gww5+lamdaw5)
```

```
            aw6=awb*(gww6+lamdaw6)
            ggwt(i,j,k)=ag1+ag2+ag3+ag4+ag5+ag6
            gwwt(i,j,k)=aw1+aw2+aw3+aw4+aw5+aw6
            if(iflow/=0)then
              qgm(i,j,k)=0.0 !gas flow rate transferred to the fracture system
              qwm(i,j,k)=0.0 !water flow rate transferred to the fracture system
            end if
            qwg(i,j,k)=bw(i,j,k)*(-gwwt(i,j,k)+qw(i,j,k)+qwm(i,j,k))&
                    +bg(i,j,k)*(-ggwt(i,j,k)+qg(i,j,k)+qgm(i,j,k)-qmag(i,j,k))
            aw(i,j,k)=bw(i,j,k)*aww+bg(i,j,k)*agw
            ae(i,j,k)=bw(i,j,k)*awe+bg(i,j,k)*age
            as(i,j,k)=bw(i,j,k)*aws+bg(i,j,k)*ags
            an(i,j,k)=bw(i,j,k)*awn+bg(i,j,k)*agn
            at(i,j,k)=bw(i,j,k)*awt+bg(i,j,k)*agt
            ab(i,j,k)=bw(i,j,k)*awb+bg(i,j,k)*agb
            sbqr=adw+ade+ads+adn+adt+adb
            ww(i,j,k)=aww
            we(i,j,k)=awe
            ws(i,j,k)=aws
            wn(i,j,k)=awn
            wt(i,j,k)=awt
            wb(i,j,k)=awb
        end if
        !-------------------------------------------------------------------------
```

```
!for fracture system

if(fp(i,j,k)/=0) then  !if there is fracture porosity

sb=fsg(i,j,k)/fbg(i,j,k)

pp=pf(i,j,k)

call interp(pwt,muwt,mpwt,pp,muw)

call interp(pgt,mugt,mpgt,pp,mug)

ssw=fsw(i,j,k)

ssg=fsg(i,j,k)

call interp(fsat,fpcgwt,fmsat,ssw,pcgw)

rrw=rhoscw/fbw(i,j,k)

rrg=rhoscg/fbg(i,j,k)

if(i/=1.and.fp(i-1,j,k)/=0)then

 sbx1=fsg(i-1,j,k)/fbg(i-1,j,k)

 p1=pf(i-1,j,k)

 call interp(pwt,muwt,mpwt,p1,muw1)

 call interp(pgt,mugt,mpgt,p1,mug1)

 sw1=fsw(i-1,j,k)

 sg1=fsg(i-1,j,k)

 call interp(fsat,fpcgwt,fmsat,sw1,pcgw1)

 rw1=rhoscw/fbw(i-1,j,k)

 rg1=rhoscg/fbg(i-1,j,k)

 ffact=-d288*(el(i-1,j,k)-el(i,j,k))

 gww1=(rw1+rrw)*ffact+pcgw-pcgw1

 ggw1=(rg1+rrg)*ffact
```

```
p11=p1-pp

hw1=p11+gww1

hg1=p11+ggw1
```

! initial value of the threshold pressure gradient and gas slippage effect experimental factor

```
stpw1=0.0

stpw2=0.0

stpg1=0

stpg2=0

sle1=161

sle2=0.47

 if(hw1>=0) then

        call interp(fsat,fkrwt,fmsat,sw1,krw1)

        lamdaw1=-dx(i-1,j,k)*stpw1/(kx(i-1,j,k)*krw1/muw1)**stpw2

 end if

 if(hw1<0) then

        call interp(fsat,fkrwt,fmsat,ssw,krw1)

        lamdaw1=dx(i,j,k)*stpw1/(kx(i,j,k)*krw1/muw1)**stpw2

 end if

 if(hg1>=0) then

        call interp(fsat,fkrgt,fmsat,sg1,krg1)

        lamdag1=-dx(i-1,j,k)*(stpg1/(kx(i-1,j,k)*krg1*0.987E-3)

        +stpg2)

        hg=hg1+lamdag1
```

```
                qq1=kx(i-1,j,k)*krg1*dy(i-1,j,k)*dz(i-1,j,k)*abc(hg)/mug1
                recl=qq1*rhoscg*(kx(i-1,j,k)*krg1)**0.5/(mug1*vp(i-1,j,k)
                &*dz(i-1,j,k)*dy(i-1,j,k))
                if((recl>=0).and.(recl<=recd))then
                        krg1=krg1*(1+sle1*(kx(i-1,j,k)*krg1/
                        &(vp(i-1,j,k)*(1-sw1)))**sle2)/p1
                end if
        end if
        if(hg1<0) then
                call interp(fsat,fkrgt,fmsat,ssg,krg1)
                lamdag1=dx(i,j,k)*(stpg1/(kx(i,j,k)*krg1*0.987E-3)+stpg2)
                hg=hg1+lamdag1
                qq1=kx(i,j,k)*krg1*dy(i,j,k)*dz(i,j,k)*abc(hg)/mug
                recl=qq1*rhoscg*(kx(i,j,k)*krg1)**0.5/(mug*vp(i,j,k)
                &*dz(i,j,k)*dy(i,j,k))
                if((recl>=0).and.(recl<=recd))then
                        krg1=krg1*(1+sle1*(kx(i,j,k)*krg1/
                        &(vp(i,j,k)*(1-ssw)))**sle2)/pp
                end if
        end if
        mw1=4.0*krw1/((fbw(i-1,j,k)+fbw(i,j,k))*(muw1+muw))
        mg1=4.0*krg1/((fbg(i-1,j,k)+fbg(i,j,k))*(mug1+mug))
    end if
    aww=ftx(i,j,k)*mw1
```

```
agw=ftx(i,j,k)*mg1
 if((abs(hg1)-abs(lamdag1))<=0) agw=0
 if((abs(hw1)-abs(lamdaw1))<=0) aww=0
adw=ftdx(i,j,k)*(sbx1-sb)
if(i/=ii.and.fp(i+1,j,k)/=0)then
 sbx2=fsg(i+1,j,k)/fbg(i+1,j,k)
 p2=pf(i+1,j,k)
 call interp(pwt,muwt,mpwt,p2,muw2)
 call interp(pgt,mugt,mpgt,p2,mug2)
 sw2=fsw(i+1,j,k)
 sg2=fsg(i+1,j,k)
 call interp(fsat,fpcgwt,fmsat,sw2,pcgw2)
 rw2=rhoscw/fbw(i+1,j,k)
 rg2=rhoscg/fbg(i+1,j,k)
 ffact=-d288*(el(i+1,j,k)-el(i,j,k))
 gww2=(rw2+rrw)*ffact+pcgw-pcgw2
 ggw2=(rg2+rrg)*ffact
 p22=p2-pp
 hw2=p22+gww2
 hg2=p22+ggw2
 if(hw2>=0) then
        call interp(fsat,fkrwt,fmsat,sw2,krw2)
        lamdaw2=-dx(i+1,j,k)*stpw1/(kx(i+1,j,k)*krw2/muw2)**stpw2
 end if
```

```
        if(hw2<0) then
            call interp(fsat,fkrwt,fmsat,ssw,krw2)
            lamdaw2=dx(i,j,k)*stpw1/(kx(i,j,k)*krw2/muw2)**stpw2
        end if
        if(hg2>=0) then
            call interp(fsat,fkrgt,fmsat,sg2,krg2)
            lamdag2=-dx(i+1,j,k)*(stpg1/(kx(i+1,j,k)*krg2*0.987E-3)
            +stpg2)
            hg=hg2+lamdag2
            qq2=kx(i+1,j,k)*krg2*dy(i+1,j,k)*dz(i+1,j,k)*abc(hg)/mug2
            recl=qq2*rhoscg*(kx(i+1,j,k)*krg2)**0.5/(mug2*vp(i,j,k)
            &*dz(i+1,j,k)*dy(i+1,j,k))
            if((recl>=0).and.(recl<=recd))then
                krg2=krg2*(1+sle1*(kx(i+1,j,k)*krg2/
                &(vp(i+1,j,k)*(1-sw2)))**sle2)/p2
            end if
        end if
        if(hg2<0) then
            call interp(fsat,fkrgt,fmsat,ssg,krg2)
            lamdag2=dx(i,j,k)*(stpg1/(kx(i,j,k)*krg2*0.987E-3)+stpg2)
            hg=hg2+lamdag2
            qq2=kx(i,j,k)*krg2*dy(i,j,k)*dz(i,j,k)*abc(hg)/mug
            recl=qq2*rhoscg*(kx(i,j,k)*krg2)**0.5/(mug*vp(i,j,k)
            &*dz(i,j,k)*dy(i,j,k))
```

```
            if((recl>=0).and.(recl<=recd))then
                krg2=krg2*(1+sle1*(kx(i,j,k)*krg2/
                &(vp(i,j,k)*(1-ssw)))**sle2)/pp
            end if
          end if
          mw2=4.0*krw2/((fbw(i+1,j,k)+fbw(i,j,k))*(muw2+muw))
          mg2=4.0*krg2/((fbg(i+1,j,k)+fbg(i,j,k))*(mug2+mug))
        end if
        awe=ftx(i+1,j,k)*mw2
        age=ftx(i+1,j,k)*mg2
        if((abs(hg2)-abs(lamdag2))<=0) age=0
        if((abs(hw2)-abs(lamdaw2))<=0) awe=0
        ade=ftdx(i+1,j,k)*(sbx2-sb)
        if(j/=1.and.fp(i,j-1,k)/=0)then
          sby1=fsg(i,j-1,k)/fbg(i,j-1,k)
          p3=pf(i,j-1,k)
          call interp(pwt,muwt,mpwt,p3,muw3)
          call interp(pgt,mugt,mpgt,p3,mug3)
          sw3=fsw(i,j-1,k)
          sg3=fsg(i,j-1,k)
          call interp(fsat,fpcgwt,fmsat,sw3,pcgw3)
          rw3=rhoscw/fbw(i,j-1,k)
          rg3=rhoscg/fbg(i,j-1,k)
          ffact=-d288*(el(i,j-1,k)-el(i,j,k))
```

```
gww3=(rw3+rrw)*ffact+pcgw-pcgw3

ggw3=(rg3+rrg)*ffact

p33=p3-pp

hw3=p33+gww3

hg3=p33+ggw3

if(hw3>=0) then

    call interp(fsat,fkrwt,fmsat,sw3,krw3)

    lamdaw3=-dy(i,j-1,k)*stpw1/(ky(i,j-1,k)*krw3/muw3)**stpw2

end if

if(hw3<0) then

    call interp(fsat,fkrwt,fmsat,ssw,krw3)

    lamdaw3=dy(i,j,k)*stpw1/(ky(i,j,k)*krw3/muw3)**stpw2

end if

if(hg3>=0) then

    call interp(fsat,fkrgt,fmsat,sg3,krg3)

    lamdag3=-dy(i,j-1,k)*(stpg1/(ky(i,j-1,k)*krg3*0.987E-3)

    +stpg2)

    hg=hg3+lamdag3

    qq3=ky(i,j-1,k)*krg3*dx(i,j-1,k)*dz(i,j-1,k)*abc(hg)/mug3

    recl=qq3*rhoscg*(ky(i,j-1,k)*krg3)**0.5/(mug3*vp(i,j-1,k)

    &*dz(i,j-1,k)*dx(i,j-1,k))

    if((recl>=0).and.(recl<=recd))then

        krg3=krg3*(1+sle1*(ky(i,j-1,k)*krg3/

        &(vp(i,j-1,k)*(1-sw3)))**sle2)/p3
```

```
            end if
        end if
        if(hg3<0) then
            call interp(fsat,fkrgt,fmsat,ssg,krg3)
            lamdag3=dy(i,j,k)*(stpg1/(ky(i,j,k)*krg3*0.987E-3)+stpg2)
            hg=hg3+lamdag3
            qq3=ky(i,j,k)*krg3*dx(i,j,k)*dz(i,j,k)*abc(hg)/mug
            recl=qq3*rhoscg*(ky(i,j,k)*krg3)**0.5/(mug*vp(i,j,k)
            &*dz(i,j,k)*dx(i,j,k))
            if((recl>=0).and.(recl<=recd))then
                krg3=krg3*(1+sle1*(ky(i,j,k)*krg3/
                &(vp(i,j,k)*(1-ssw)))**sle2)/pp
            end if
        end if
        mw3=4.0*krw3/((fbw(i,j-1,k)+fbw(i,j,k))*(muw3+muw))
        mg3=4.0*krg3/((fbg(i,j-1,k)+fbg(i,j,k))*(mug3+mug))
    end if
    aws=fty(i,j,k)*mw3
    ags=fty(i,j,k)*mg3
    if((abs(hg3)-abs(lamdag3))<=0) ags=0
    if((abs(hw3)-abs(lamdaw3))<=0) aws=0
    ads=ftdy(i,j,k)*(sby1-sb)
    if(j/=jj.and.fp(i,j+1,k)/=0)then
        sby2=fsg(i,j+1,k)/fbg(i,j+1,k)
```

```
p4=pf(i,j+1,k)
call interp(pwt,muwt,mpwt,p4,muw4)
call interp(pgt,mugt,mpgt,p4,mug4)
sw4=fsw(i,j+1,k)
sg4=fsg(i,j+1,k)
call interp(fsat,fpcgwt,fmsat,sw4,pcgw4)
rw4=rhoscw/fbw(i,j+1,k)
rg4=rhoscg/fbg(i,j+1,k)
ffact=-d288*(el(i,j+1,k)-el(i,j,k))
gww4=(rw4+rrw)*ffact+pcgw-pcgw4
ggw4=(rg4+rrg)*ffact
p44=p4-pp
hw4=p44+gww4
hg4=p44+ggw4
if(hw4>=0) then
    call interp(fsat,fkrwt,fmsat,sw4,krw4)
    lamdaw4=-dy(i,j+1,k)*stpw1/(ky(i,j+1,k)*krw4/muw4)**stpw2
end if
if(hw4<0) then
    call interp(fsat,fkrwt,fmsat,ssw,krw4)
    lamdaw4=dy(i,j,k)*stpw1/(ky(i,j,k)*krw4/muw4)**stpw2
end if
if(hg4>=0) then
    call interp(fsat,fkrgt,fmsat,sg4,krg4)
```

```
                lamdag4=-dy(i,j+1,k)*(stpg1/(ky(i,j+1,k)*krg4*0.987E-3)
                +stpg2)
                hg=hg4+lamdag4
                qq4=ky(i,j+1,k)*krg4*dx(i,j+1,k)*dz(i,j+1,k)*abc(hg)/mug4
                recl=qq4*rhoscg*(ky(i,j+1,k)*krg4)**0.5/(mug4*vp(i,j+1,k)
                &*dz(i,j+1,k)*dx(i,j+1,k))
                if((recl>=0).and.(recl<=recd))then
                        krg4=krg4*(1+sle1*(ky(i,j+1,k)*krg4/
                        &(vp(i,j+1,k)*(1-sw4)))**sle2)/p4
                end if
        end if
        if(hg4<0) then
                call interp(fsat,fkrgt,fmsat,ssg,krg4)
                lamdag4=dy(i,j,k)*(stpg1/(ky(i,j,k)*krg4*0.987E-3)+stpg2)
                hg=hg4+lamdag4
                qq4=ky(i,j,k)*krg4*dx(i,j,k)*dz(i,j,k)*abc(hg)/mug
                recl=qq4*rhoscg*(ky(i,j,k)*krg4)**0.5/(mug*vp(i,j,k)
                &*dz(i,j,k)*dx(i,j,k))
                if((recl>=0).and.(recl<=recd))then
                        krg4=krg4*(1+sle1*(ky(i,j,k)*krg4/
                        &(vp(i,j,k)*(1-ssw)))**sle2)/pp
                end if
        end if
        mw4=4.0*krw4/((fbw(i,j+1,k)+fbw(i,j,k))*(muw4+muw))
```

```
  mg4=4.0*krg4/((fbg(i,j+1,k)+fbg(i,j,k))*(mug4+mug))
end if
awn=fty(i,j+1,k)*mw4
agn=fty(i,j+1,k)*mg4
if((abs(hg4)-abs(lamdag4))<=0) agn=0
if((abs(hw4)-abs(lamdaw4))<=0) awn=0
adn=ftdy(i,j+1,k)*(sby2-sb)
if(k/=1.and.fp(i,j,k-1)/=0)then
  sbz1=fsg(i,j,k-1)/fbg(i,j,k-1)
  p5=pf(i,j,k-1)
  call interp(pwt,muwt,mpwt,p5,muw5)
  call interp(pgt,mugt,mpgt,p5,mug5)
  sw5=fsw(i,j,k-1)
  sg5=fsg(i,j,k-1)
  call interp(fsat,fpcgwt,fmsat,sw5,pcgw5)
  rw5=rhoscw/fbw(i,j,k-1)
  rg5=rhoscg/fbg(i,j,k-1)
  ffact=-d288*(el(i,j,k-1)-el(i,j,k))
  gww5=(rw5+rrw)*ffact+pcgw-pcgw5
  ggw5=(rg5+rrg)*ffact
  p55=p5-pp
  hw5=p55+gww5
  hg5=p55+ggw5
  if(hw5>=0) then
```

```
            call interp(fsat,fkrwt,fmsat,sw5,krw5)
            lamdaw5=-dz(i,j,k-1)*stpw1/(kz(i,j,k-1)*krw5/muw5)**stpw2
        end if
        if(hw5<0) then
            call interp(fsat,fkrwt,fmsat,ssw,krw5)
            lamdaw5=dz(i,j,k)*stpw1/(kz(i,j,k)*krw5/muw5)**stpw2
        end if
        if(hg5>=0) then
            call interp(fsat,fkrgt,fmsat,sg5,krg5)
            lamdag5=-dz(i,j,k-1)*(stpg1/(kz(i,j,k-1)*krg5*0.987E-3)+stpg2)
            hg=hg5+lamdag5
            qq5=kz(i,j,k-1)*krg5*dx(i,j,k-1)*dy(i,j,k-1)*abc(hg)/mug5
            recl=qq5*rhoscg*(kz(i,j,k-1)*krg5)**0.5/(mug5*vp(i,j,k-1)
            &*dy(i,j,k-1)*dx(i,j,k-1))
            if((recl>=0).and.(recl<=recd))then
                krg5=krg5*(1+sle1*(kz(i,j,k-1)*krg5/
                &(vp(i,j,k-1)*(1-sw5)))**sle2)/p5
            end if
        end if
        if(hg5<0) then
            call interp(fsat,fkrgt,fmsat,ssg,krg5)
            lamdag5=dz(i,j,k)*(stpg1/(kz(i,j,k)*krg5*0.987E-3)+stpg2)
            hg=hg5+lamdag5
            qq5=kz(i,j,k)*krg5*dx(i,j,k)*dy(i,j,k)*abc(hg)/mug
```

```
                recl=qq5*rhoscg*(kz(i,j,k)*krg5)**0.5/(mug*vp(i,j,k)
                &*dy(i,j,k)*dx(i,j,k))
                if((recl>=0).and.(recl<=recd))then
                    krg5=krg5*(1+sle1*(kz(i,j,k)*krg5/
                    &(vp(i,j,k)*(1-ssw)))**sle2)/pp
                end if
            end if
            mw5=4.0*krw5/((fbw(i,j,k-1)+fbw(i,j,k))*(muw5+muw))
            mg5=4.0*krg5/((fbg(i,j,k-1)+fbg(i,j,k))*(mug5+mug))
        end if
        awt=ftz(i,j,k)*mw5
        agt=ftz(i,j,k)*mg5
        if((abs(hg5)-abs(lamdag5))<=0) agt=0
        if((abs(hw5)-abs(lamdaw5))<=0) awt=0
        adt=ftdz(i,j,k)*(sbz1-sb)
        if(k/=kk.and.fp(i,j,k+1)/=0)then
            sbz2=fsg(i,j,k+1)/fbg(i,j,k+1)
            p6=pf(i,j,k+1)
            call interp(pwt,muwt,mpwt,p6,muw6)
            call interp(pgt,mugt,mpgt,p6,mug6)
            sw6=fsw(i,j,k+1)
            sg6=fsg(i,j,k+1)
            call interp(fsat,fpcgwt,fmsat,sw6,pcgw6)
            rw6=rhoscw/fbw(i,j,k+1)
```

```
rg6=rhoscg/fbg(i,j,k+1)
ffact=-d288*(el(i,j,k+1)-el(i,j,k))
gww6=(rw6+rrw)*ffact+pcgw-pcgw6
ggw6=(rg6+rrg)*ffact
p66=p6-pp
hw6=p66+gww6
hg6=p66+ggw6
if(hw6>=0) then
    call interp(fsat,fkrwt,fmsat,sw6,krw6)
    lamdaw6=-dz(i,j,k+1)*stpw1/(kz(i,j,k+1)*krw6/muw6)**stpw2
end if
if(hw6<0) then
    call interp(fsat,fkrwt,fmsat,ssw,krw6)
    lamdaw6=dz(i,j,k)*stpw1/(kz(i,j,k)*krw6/muw6)**stpw2
end if
if(hg6>=0) then
    call interp(fsat,fkrgt,fmsat,sg6,krg6)
    lamdag6=-dz(i,j,k+1)*(stpg1/(kz(i,j,k+1)*krg6*0.987E-3)
    +stpg2)
    hg=hg6+lamdag6
    qq6=kz(i,j,k+1)*krg6*dx(i,j,k+1)*dy(i,j,k+1)*abc(hg)/mug6
    recl=qq6*rhoscg*(kz(i,j,k+1)*krg6)**0.5/(mug6*vp(i,j,k+1)
    &*dy(i,j,k+1)*dx(i,j,k+1))
    if((recl>=0).and.(recl<=recd))then
```

```
                krg6=krg6*(1+sle1*(kz(i,j,k+1)*krg6/
                &(vp(i,j,k+1)*(1-sw6)))**sle2)/p6
            end if
        end if
        if(hg6<0) then
            call interp(fsat,fkrgt,fmsat,ssg,krg6)
            lamdag6=dz(i,j,k)*(stpg1/(kz(i,j,k)*krg6*0.987E-3)+stpg2)
            hg=hg6+lamdag6
            qq6=kz(i,j,k)*krg6*dx(i,j,k)*dy(i,j,k)*abc(hg)/mug
            recl=qq6*rhoscg*(kz(i,j,k)*krg6)**0.5/(mug*vp(i,j,k)
            &*dy(i,j,k)*dx(i,j,k))
            if((recl>=0).and.(recl<=recd))then
                krg6=krg6*(1+sle1*(kz(i,j,k)*krg6/
                &(vp(i,j,k)*(1-ssw)))**sle2)/pp
            end if
        end if
        mw6=4.0*krw6/((fbw(i,j,k+1)+fbw(i,j,k))*(muw6+muw))
        mg6=4.0*krg6/((fbg(i,j,k+1)+fbg(i,j,k))*(mug6+mug))
    end if
    awb=ftz(i,j,k+1)*mw6
    agb=ftz(i,j,k+1)*mg6
    if((abs(hg6)-abs(lamdag6))<=0) agb=0
    if((abs(hw6)-abs(lamdaw6))<=0) awb=0
    adb=ftdz(i,j,k+1)*(sbz2-sb)
```

```
ag1=agw*(ggw1+lamdag1)

ag2=age*(ggw2+lamdag2)

ag3=ags*(ggw3+lamdag3)

ag4=agn*(ggw4+lamdag4)

ag5=agt*(ggw5+lamdag5)

ag6=agb*(ggw6+lamdag6)

aw1=aww*(gww1+lamdaw1)

aw2=awe*(gww2+lamdaw2)

aw3=aws*(gww3+lamdaw3)

aw4=awn*(gww4+lamdaw4)

aw5=awt*(gww5+lamdaw5)

aw6=awb*(gww6+lamdaw6)

fgwwt(i,j,k)=aw1+aw2+aw3+aw4+aw5+aw6

fggwt(i,j,k)=ag1+ag2+ag3+ag4+ag5+ag6

fqwg(i,j,k)=fbw(i,j,k)*(-fgwwt(i,j,k)+fqw(i,j,k)-qwm(i,j,k))&

        +fbg(i,j,k)*(-fggwt(i,j,k)+fqg(i,j,k)-qgm(i,j,k))

faw(i,j,k)=fbw(i,j,k)*aww+fbg(i,j,k)*agw

fae(i,j,k)=fbw(i,j,k)*awe+fbg(i,j,k)*age

fas(i,j,k)=fbw(i,j,k)*aws+fbg(i,j,k)*ags

fan(i,j,k)=fbw(i,j,k)*awn+fbg(i,j,k)*agn

fat(i,j,k)=fbw(i,j,k)*awt+fbg(i,j,k)*agt

fab(i,j,k)=fbw(i,j,k)*awb+fbg(i,j,k)*agb

fsbqr=adw+ade+ads+adn+adt+adb

fww(i,j,k)=aww
```

```
                fwe(i,j,k)=awe

                fws(i,j,k)=aws

                fwn(i,j,k)=awn

                fwt(i,j,k)=awt

                fwb(i,j,k)=awb

          end if


        end do

  end do

end do

!-------------------------calculate main diagonal and rhs vector

do k=1,kk

  do j=1,jj

    do i=1,ii

          if(mp(i,j,k)/=0)then !if there is matrix porosity

            sum1(i,j,k)=aw(i,j,k)+ae(i,j,k)+as(i,j,k)+an(i,j,k)+at(i,j,k)+ab(i,j,k)

                gam(i,j,k)=mpv(i,j,k)*ct(i,j,k)*div1

                e(i,j,k)=-sum1(i,j,k)-gam(i,j,k)

                b(i,j,k)=qwg(i,j,k)-gam(i,j,k)*p(i,j,k)-sbqr

                !------------------consider the desorption rate from the micropore system

                e(i,j,k)=e(i,j,k)+temp1/2.0*vl(k)*pl(k)/(pl(k)+p(i,j,k))**2

                b(i,j,k)=b(i,j,k)-temp1*(cefg0-

                cmn(i,j,k))+temp1/2.0*vl(k)*pl(k)/(pl(k)+pn(i,j,k))**2*pn(i,j,k)

          end if
```

```
            if(fp(i,j,k)/=0)then !if there is fracture porosity
              fsum(i,j,k)=faw(i,j,k)+fae(i,j,k)+fas(i,j,k)+fan(i,j,k)+fat(i,j,k)+fab(i,j,k)
                    fgam(i,j,k)=fpv(i,j,k)*fct(i,j,k)*div1
                    fe(i,j,k)=-fsum(i,j,k)-fgam(i,j,k)
                    fb(i,j,k)=fqwg(i,j,k)-fgam(i,j,k)*pf(i,j,k)-fsbqr
                    !-----------------consider the desorption rate from the micropore system
                    !fe(i,j,k)=fe(i,j,k)-temp1/2.0*vl(k)*pl(k)/(pl(k)+p(i,j,k))**2
                    !fb(i,j,k)=fb(i,j,k)+temp1*(cefg0-cmn(i,j,k))-
temp1/2.0*vl(k)*pl(k)/(pl(k)+pn(i,j,k))**2*pn(i,j,k)
                    if(mp(i,j,k)/=0)then !if there is mass transfer
                      e(i,j,k)=e(i,j,k)-amt(i,j,k)
                      b(i,j,k)=b(i,j,k)+act(i,j,k)
                      f(i,j,k)=amt(i,j,k)
                      fe(i,j,k)=fe(i,j,k)-amt(i,j,k)
                      fb(i,j,k)=fb(i,j,k)-act(i,j,k)
                      ff(i,j,k)=amt(i,j,k)
                    end if
              end if
            end do
  end do
end do
end subroutine
```

References

[1] Langmuir, I., 1916. The constitution and fundamental properties of solids and liquids. Part I. Solids. Journal of the American Chemical Society, 38(11), 2221-2295.

[2] Manik, J., 1999. Compositional modeling of enhanced coalbed methane recovery. PhD thesis, Petroleum and Natural Gas Engineering, Pennsylvania State University, Pennsylvania.

[3] Manik, J., Ertekin, T. and Kohler, T.E., 2000. Development and validation of a compositional Coalbed simulator. Paper 2000-44, The Petroleum Society's Canadian International Petroleum Conference, Calgary, Alberta, Canada, June, 4-8.

[4] Law, D.H.-S., van der Meer, L.G.H. and Gunter, W.D., 2002. Numerical simulator comparison study for enhanced coalbed methane recovery process, part I: pure carbon dioxide injection. Paper SPE 75669, The SPE Gas Technology Symposium, Calgary, Alberta, Canada, April, 30-May, 2.

[5] Clarkson, C.R. and Bustin, R.M., 1999. The effect of pore structure and gas pressure upon the transport properties of coal: a laboratory and modelling study. 1. Isotherms and pore volume distributions. Fuel, 78(11), 1333-1344.

[6] Shi, J.Q. and Durucan, S., 2003. A bidisperse pore diffusion model for methane displacement desorption in coal by CO_2 injection. Fuel, 82(10), 1219-1229.

[7] Cui, X.J., Bustin, R.M. and Dipple, G., 2004. Selective transport of CO_2, CH_4 and N_2 in coals: insights from modelling of experimental gas adsorption data. Fuel, 83(3), 293-303.

[8] Siemons, N., Busch, A., Bruining, H. and Krooss, B., 2003. Accessing the kinetics and capacity of gas adsorption in coals by a combined adsorption/diffusion method. Paper SPE 84340, The SPE Annual Technical Conference and Exhibition, Denver, Colorado, U.S.A., October, 5-8.

[9] King, G.R., 1990. Material Balance Techniques for Coal-Seam and Devonian Shale Gas Reservoirs. Paper SPE 20730, The 65th Annual Technical Conference and Exhibition of Petroleum Engineers, New Orleans, LA., September, 23-26.

[10] Seidle, J.P., 1999. A Modified p/Z Method for Coal Wells. Paper SPE 55605, The 1999 Rocky Mountain Regional Meeting, Gillette, Wyoming, May, 15-18.

[11] Ahmed, T., Centilmen, A. and Roux, B., 2006. A Generalized Material Balance Equation for coalbed methane Reservoirs. Paper SPE 102638, The 2006 SPE Annual Technical Conference and Exhibition, San Antonio, Texas, U.S.A., September, 24-27.

[12] Xue, ChengGang, Cao, WenJiang and Zhong, Ying, 2000. Derivation of material balance equation and reserve calculation, 23(4): 44-49.

[13] Chen, YuanQian and Hu, JiangGuo, 2008. Determination of saturated CBM reservoir geological reserve, recoverable reserve and recovery and its application.Oil and gas geology, 29(1):151-156.

[14] Mattar, L. and McNeil, R., 1998. The "Flowing" Gas Material Balance. The Journal of Canadian Petroleum Technology, 37(2):52-55.

[15] Agarwal, R.G., Gardner, D.C., Kleinsteiber, S.W., Fussell, D.D., 1998. Analyzing Well Production Data Using Combined Type-Curve and Decline-Curve Analysis Concepts. Paper SPE 49222, The 1998 SPE Annual Technical Conference and Exhibition, New Orleans, Louisiana, September, 27-30.

[16] Mattar, L. and Anderson, D., 2005. Dynamic Material Balance (Oil or Gas-In-Place without Shut-Ins). Paper 2005-113, The Petroleum Society's 6th Canadian International Petroleum conference (56th Annual Technical Meeting), Calgary, Alberta, Canada, June 7-9.

[17] Gerami, S., Pooladi-Darvish, M., Morad, K., and Mattar, L., 2007. Type Curves for Dry CBM Reservoirs With Equilibrium Desorption. Paper 2007-011, The Petroleum Society's Canadian Petroleum Conference, Calgary, June, 12-14.

[18] Clarkson, C.R., Jordan, C.L., Gierhart, R.R. and Seidle, J.P., 2008. Production Data analysis of Coalbed-Methane Wells. Paper SPE 107705, The SPE Rocky Mountain Oil and Gas Technology Symposium, Denver, April, 16-18.

[19] Morad, K. and Clarkson, C.R., 2008. Application of Flowing p/Z* Material Balance for Dry Coalbed-Methane Reservoirs. Paper SPE 114995, The CIPC/SPE Gas Technology Symposium 2008 Joint Conference, Calgary, Alberta, Canada, Jun, 16-19.

[20] Handy, L.L., 1957. Effect of local high gas saturations on productivity indices. Paper 57-111, The Spring meeting of the Pacific Coast District, Division of Production, Los Angeles, Calif, May.

[21] Fetkovich, M.J., 1973. The isochronal testing of oil wells. Paper SPE 4529, The 48th Annual Fall Meeting of the Society of Petroleum Engineers of AIME, Las Vegas, Nev., September, 30-October, 3.

[22] Al-Khalifah, A-J.A., Aziz, K. and Horne, R.N., 1987. A new approach to multiphase well test analysis. Paper SPE 16743, The 62th Annual Technical Conference and Exhibition, Dallas, TX, September, 27-30.

[23] Kamal, M.M. and Six, J.L., 1989. Pressure transient testing of methane producing coalbeds. Paper SPE 19789, The 64th Annual Technical Conference and Exhibition of the Society of Petroleum Engineers, San Antonio, TX, October, 8-11.

[24] Jochen, V.A., Lee, W.J. and Semmelbeck, M.E., 1994. Determining Permeability in Coalbed Methane Reservoirs. Paper SPE 28584, The SPE 69th Annual Technical Conference and Exhibition, New Orieans, U.S.A., September, 25-28.

[25] Perrine, R.L., 1956. Analysis of pressure-buildup curves. Paper 56-482, The spring meeting of the Pacific Coast District, Division of Production, Los Angeles, California Research Corp, La Habra, Calif, May.

[26] Martin, J.C., 1959. Simplified equations of flow in gas drive reservoirs and the theoretical foundation of multiphase pressure buildup analysis, Trans., AIME, 216,309-320.

[27] Ayan, C. and Lee, W.J., 1988. The effects of multiphase flow on the interpretation of pressure-buildup tests. SPE Formation Evaluation, 3(2), 459-466.

[28] Raghavan, R., 1975. Well test analysis: wells producing by solution gas drive. Paper SPE 5588, The SPE-AIME 50th Annual Fall Technical Conference and Exhibition, Dallas, September, 28-October, 1.

[29] Raghavan, R., 1989. Well test analysis for multiphase flow. SPE formation evaluation, 4(4), 585-594.

[30] Klinkenberg, L.J., 1941. The permeability of porous media to liquids and gases. Paper 41-200, American Petroleum Institute, The Eleventh Mid Year Meeting, Tulsa, Okla, May.

[31] Rushing, J.A., Newsham, K.E. and Van Fraassen, K.C., 2003. Measurement of the two phase gas slippage phenomenon and its effect on gas relative permeability in tight

gas sands. Paper SPE 84297, The SPE Annual Technical Conference and Exhibition, Denver, Colorado, U.S.A., October, 5-8.

[32] Li, K. and Horne, R.N., 2001. Gas slippage in two-phase flow and the effect of temperature. Paper SPE 68778, The SPE Western Regional Meeting, Bakersfield, California, March, 26-30.

[33] Ertekin, T., King, G.R. and Schwerer, F.C., 1986. Dynamic gas slippage: a unique dual-mechanism approach to the flow of gas in tight formations. SPE formation Evaluation, 1(1), 43-52.

[34] Estes, K.R., and Fulton, F.P., 1956. Gas slippage and permeability measurements. Journal of Petroleum Technology, 8(10), 69-73.

[35] Jones, F.O. and Owens, W.W., 1980. A laboratory study of low-permeability gas sands. Journal of petroleum Technology, 32(9), 1631-1640.

[36] Sampath, K. and William, K.C., 1982. Factors affecting gas slippage in tight sandstones of cretaceous age in the Uinta Basin. Journal of Petroleum Technology, 34(11), 2715-2720.

[37] Rushing, J.A., Newsham, K.E., Lasswell, P.M. and Blasingame, T.A., 2004. Klinkenberg-corrected permeability measurements in tight gas sands: steady-state versus unsteady-state techniques. Paper SPE 89867, The SPE Annual Technical Conference and Exhibition, Houston, Texas, U.S.A., September, 26-29.

[38] Thomas, L.K., Katz, D.L. and Tek, M.R., 1968. Threshold Pressure Phenomena in Porous Media. SPE Journal, 8(2), 174-184.

[39] Wu, Fan, Sun, LiJuan and Qiao, GuoAn, 2001. A research on gas flow property and starting pressure phenomenon. Natural Gas Industry, 82-84.

[40] Vinsome, P.K.W., 1976. Orthomin, an Iterative Method for Solving Sparse Sets of Simultaneous Linear Equations. Paper SPE 5729, The fourth symposium of numerical simulation of reservoir performance of the society of petroleum engineers of AIME, Los Angeles, Calif, February, 19-20.

[41] Ancell, K.L., Lambert, S. and Johnson, F.S., 1980. Analysis of the coalbed degasification process at a seventeen well pattern in the Warrior Basin of Alabama. Paper SPE/DOE 8971, SPE/DOE Symposium on Unconventional Gas Recovery,

Pittsburgh, Pennsylvania, May, 18-21.

[42] Bayles, G.A. and Reznik, A.A., 1986. Pressure transient analysis of methane production from Coal Beds: an analytical approach. Paper SPE 15226, The Unconventional Gas Technology Symposium of the Society of Petroleum Engineers, Louisville, KY, May, 18-21.

[43] King, R.G., Ertekin, T. and Schwerer, C.F., 1986. Numerical simulation of the transient behavior of Coal Seam degasification wells. SPE Formation Evaluation, 1(2), 165-183.

[44] Bumb, A.C. and McKee, C.R., 1988. Gas-Well testing in the presence of desorption for Coalbed Methane and Devonian shale. SPE Formation Evaluation, 3(1), 179-185.

[45] Ertekin, T. and Sung, W., 1989. Pressure transient analysis of Coal Seams in the presence of multi-mechanistic flow and sorption phenomena. Paper SPE 19102, The SPE Gas Technology Symposium, Dallas, Texas, June, 7-9.

[46] Sarkar, P.S. and Rajtar, J.M., 1994. Transient Well Testing of Coalbed Methane Reservoirs with Horizontal Wells. Paper SPE 27681, The 1994 SPE Permian Basin Oil and Gas Recovery Conference, Midland, Texas, March,16-18.

[47] Kamal, M.M. and Six, J.L., 1993. Pressure Transient Testing of Methane Producing Coalbeds. SPE Advanced Technology Series, 1(1), 195-203.

[48] Zhang, X.M. and Tong, D.K., 2008. The Coalbed Methane transport model and its application in the presence of matrix shrinkage. Science in China Series E: Technological Sciences, 51(7), 968-974.

[49] Zheng, S.Y. and Xue, L.L., 2011. Modelling and simulation of a new dual porosity CBM reservoir model with an improved permeability model through horizontal wells. Paper SPE 141118, The SPE Middle East Unconventional Gas Conference and Exhibition, Muscat, Oman, January,31-February,2.

[50] Ozdemir, E., 2009. Modeling of coal bed methane (CBM) production and CO_2 sequestration in coal seams. International Journal of Coal Geology, 77(1-2), 145-152.

[51] Scott, R. and Larry, P., 2001. Advanced Reservoir Modeling In Desorption-Controlled Reservoirs. Paper SPE 71090, The SPE Rocky Mountain Petroleum Technology Conference, Keystone, Colorado, May, 21-23.

[52] Douglas, M.S. and Williams, F.L., 1984. Diffusional effects in the recovery of methane from Coalbeds. SPE Journal, 24(5), 529-535.

[53] Wei, X.R., Wang, G.X., Massarotto, P., Golding, S.D. and Rudolph, V., 2007. Numerical simulation of multicomponent gas diffusion and flow in coals for CO_2 enhanced Coalbed Methane recovery. Chemical Engineering Science, 62(16), 4193-4203.

[54] Shi, J.Q. and Durucan, S., 2008. Modeling of mixed-gas adsorption and diffusion in Coalbed reservoirs. Paper SPE 114197, The 2008 SPE Unconventional Reservoirs Conference, Keystone, Colorado, U.S.A., February, 10-12.

[55] Kolesar, J.E., Ertekin, T. and Obut, S.T., 1990. The Unsteady-State nature of sorption and diffusion phenomena in the micropore structure of coal: Part 1-Theory and Mathematical formulation. SPE Formation Evaluation, 5(1), 81-88.

[56] Gray, I., 1987. Reservoir Engineering in Coal Seams: Part 1- The physical Process of Gas Storage and Movement in Coal Seams. SPE Reservoir Engineering, 2(1), 28-34.

[57] Somerton, W.H., Soylemezoglu, I.M. and Dudley, R.C., 1975. Effect of stress on permeability of coal. International Journal of Rock Mechanics and Mineral Science & Geomechanics, 12(5-6), 129-145.

[58] Harpalania, S. and Schraufnagel, A.R., 1990. Shrinkage of coal matrix with release of gas and its impact on permeability of coal. Fuel, 69(5), 551-556.

[59] McKee, C.R, Bumb, A.C., and Koenig, R. A., 1988. Stress-Dependent Permeability of Coal and porosity of coal and Other Geologic Formations. SPE Journal of Formation Evaluation, 3(1), 81-91.

[60] Seidle, J.P. and Huitt, L.G., 1995. Experimental measurement of coal matrix shrinkage due to gas desorption and implications for cleat permeability increases. Paper SPE 30010, The international Meeting on Petroleum Engineering, Beijing, PR China, November, 14-17.

[61] Palmer, I. and Mansoori, J., 1998. How permeability depends on stress and pore pressure in coalbeds: a new model. SPE Reservoir Evaluation and Engineering, 1(6), 539-544.

[62] Shi, J.Q. and Durucan, S., 2005. A Model for Changes in Coalbed Permeability during Primary and Enhanced Methane Recovery. Journal of SPE Reservoir Evaluation & Engineering (SPEREE), 8(4), 291-299.

[63] Pan, Z.J. and Connell, D.L., 2007. A theoretical model for gas adsorption-induced coal swelling. International Journal of Coal Geology, 69(4), 243-252.

[64] Robertson, E.P. and Christiansen, R.L., 2008. A permeability model for Coal and other fractured, sorptive-elastic media. SPE Journal, 13(3), 314-324.

[65] Robertson, E.P., 2008. Improvements in measuring sorption-induced strain and permeability in coal. Paper SPE 116259, The 2008 SPE Eastern Regional/AAPG Eastern Section Joint Meeting, Pittsburgh, Pennsylvania, USA, October, 11-15.

[66] Shedid, A.S. and Rahman, K., 2009. Experimental Investigation of stress-dependent petrophysical properties of Coalbed Methane (CBM). Paper SPE 119998, The 2009 SPE Middle East Oil & Gas Show and Conference, Bahrain International Exhibition Centre, Kingdom of Bahrain, March, 15-18.

[67] Clarkson, C.R., Pan, Z., Palmer, I. and Harpalani, S., 2010. Predicting sorption-induced strain and permeability increase with depletion for Coalbed-Methane reservoirs. SPE Journal, 15(1), 152-159.

[68] Bansal, P.P., Harper, J.L., Mcdonald, A.E., Moreland, E.E., Odeh, A.S. and Trimble, R.H., 1979. A strongly coupled, fully implicit, three dimensional, three phase reservoir simulator. Paper SPE 8329, The 54th Annual Fall Technical Conference and Exhibition of the Society of Petroleum Engineers of AIME, Las Vegas, Nevada, September, 23-25.

[69] Cheshire, M.I., Appleyard, R.J., Banks, D., Crozier, J.R. and Holmes, A.J., 1980. An efficient fully implicit simulator. EUR 179, European Offshore Petroleum Conference and Exhibition, London, England, October 21-24.

[70] Folefac, A.N., 1988. Reservoir simulation of heavy oil recovery by hot fluid injection in horizontal wells. PhD Thesis, Imperial College, London.

[71] Folefac, A.N., Archer, J.S., Issa, R.I. and Arshad, A.M., 1991. Effect of pressure drop along horizontal wellbores on well performance. Paper SPE 23094, The Offshore Europe Conference, Aberdeen, September, 3-6.

[72] Arshad, A.M., 1990. Private communication.

[73] Brekke, K., Johansen, T.E. and Olufsen, R., 1993. A new modular approach to comprehensive simulation of horizontal wells. Paper SPE 26518, The 68th Annual Technical Conference and Exhibition of the Society of Petroleum Engineers, Houston, Texas, October, 3-6.

[74] Al, Attas, M.O., 1996. Horizontal drilling performance analysis. Paper SPE # 36251, The 7th Abu Dhabi International Petroleum Exhibition Conference (ADIPEC) held in Abu Dhabi, U.A.E., October, 13-16.

[75] Holmes, J.A., 1983. Enhancements to the strongly coupled, fully implicit well model: wellbore crossflow modeling and collective well control. Paper SPE 12259, The Reservoir simulation Symposium, San Francisco, CA, November, 15-18.

[76] Holmes, J.A., Barkve, T. and Lund, O., 1998. Application of a multisegment well model to simulate flow in advanced wells. Paper SPE 50646, The 1998 SPE European Petroleum Conference, the Hague, the Netherlands, October 20-22.

[77] Dikken, J.B., 1990. Pressure drop in horizontal wells and its effect on production performance. Journal of petroleum technology, 42(11), 1426-1433.

[78] Borisov, J.P., 1964. Oil production using horizontal and multiple deviation wells. Nedra, Moscow.

[79] Joshi, S.D., 1991. Horizontal well technology. Tulsa, Oklahoma, Penn Well Books.

[80] Babu, D.K., Odeh, A.S., Al-Khalifa, A.J. and McCann, R.C., 1991. Numerical simulation of horizontal wells. Paper SPE 21425, The SPE Middle East Oil Show, Bahrain, November, 16-19.

[81] Goode, P.A. and Wilkinson, D.J., 1991. Inflow performance of partially open horizontal wells. Journal of Petroleum Technolgoy, 43(8), 983-987.

[82] Mutalik, P.N., Godbole, S.P. and Joshi, S.D., 1988. Effect of drainage area shapes on the productivity of horizontal wells. Paper SPE 18301, The 63rd Annual Technical

Conference and Exhibition of the Society of Petroleum Engineers, Houston, TX, October, 2-5.

[83] Zhang, L. and Dusseault, M.B., 1994. Are horizontal wells always better producers than vertical wells?. Paper HWC94-27, The Canadian SPE/CIM/CANMET International Conference on recent Advances in Horizontal Well Applications, Calgary, Canada, March, 20-23.

[84] Penmatcha, V.R. and Aziz, K., 1998. A comprehensive reservoir/wellbore model for horizontal wells. Paper SPE 39521, The SPE India Oil and Gas Conference and Exhibition, New Delhi, India, February, 17-19.

[85] Giger, F.M., Reiss, L.H. and Jourdan, A.P., 1984. The reservoir engineering aspects of horizontal drilling. Paper SPE 13024, The 59th Annual Technical Conference and Exhibition held in Houston, Texas, September, 16-19.

[86] Furui, K.J., Zhu, D. and Hill, A.D., 2003. A rigorous formation damage skin factor and reservoir inflow model for a horizontal well. SPE production & Facilities, 18(3), 151-157.

[87] Hagoort, J., 2009. A simplified analytical method for estimating the productivity of a horizontal well producing at constant rate or constant pressure. Journal of Petroleum Science and Engineering, 64(1-4), 77-87.

[88] Ozkan, E., Sarica, C. and Haci, M., 1999. Influence of pressure drop along the wellbore on horizontal-well productivity. SPE Journal, 4(3), 288-301.

[89] Vicente, R., Sarica, C. and Ertekin, T., 2003. Horizontal well design optimization: a study of the parameters affecting the productivity and flux distribution of a horizontal well. Paper SPE 84194, The SPE Annual Technical Conference and Exhibition, Denver, Colorado, U.S.A., October, 5-8.

[90] Augustine, R.J., 2002. An investigation of the economic benefit of inflow control devices on horizontal well completions using a reservoir-wellbore coupled model. Paper SPE 78293, The SPE 13th European Petroleum Conference, Aberdeen, Scotland, U.K., October, 29-31.

[91] Ouyang, L.-B. and Huang, B., 2005. An evaluation of well completion impacts on the performance of horizontal and multilateral wells. Paper SPE 96530, The SPE

Annual Technical Conference and Exhibition held in Dallas, Texas, U.S.A., October, 9-12.

[92] Kabir, A., 2006. An algorithm for coupling reservoir and wellbore simulators. An internal document of department of Petroleum Engineering, Curtin University of Technology, Perth.

[93] Kabir, A. and Sanchez, G., 2009. Accurate inflow profile prediction of horizontal wells through coupling of a reservoir and a wellbore simulator. Paper SPE 119095, The SPE Reservoir Simulation Symposium, The Woodlands, Texas, USA, February 2-4.

[94] Kabir, A. and Jose, A.V., 2010. Accurate inflow profile prediction of horizontal wells using a newly developed coupled reservoir and wellbore flow equations. Paper SPE 129038, The SPE Oil and Gas India Conference and Exhibition, Mumbai, India, January, 20-22.

[95] Gui, P., Cunha, J.C. and Cunha, L.B., 2006. A coupled model to simulate the fluid flow in the reservoir and horizontal wellbore. Paper 2006-124, the 7th Canadian International Petroleum Conference (57th Annual Technical Meeting), Calgary, Alberta, Canada, June, 13-15.

[96] Chen, C.-C. and Raghavan, R., 1997. A multiply-fractured horizontal well in a rectangular drainage region. SPE Journal, 2(4), 455-465.

[97] Wan, J. and Aziz, K., 2002. Semi-analytical well model of horizontal wells with multiple hydraulic fractures. SPE Journal, 7(4), 437-445.

[98] Guo, B.Y. and Yu, X.C., 2008. A simple and accurate mathematical model for predicting productivity of multifractured horizontal wells. Paper SPE 114452, The CIPC/SPE Gas Technology Symposium 2008 Joint Conference, Calgary, Alberta, Canada, June, 16-19.

[99] Lin, J.J. and Zhu, D., 2010. Modeling well performance for fractured horizontal gas wells. CPS/SPE International Oil & Gas Conference and Exhibition, Beijing, China, June, 8-10.

[100] Cai, W.B., Li, Z.M., Zhang, X.L., Zhang, B. and Zhang, Q., 2009. Horizontal well fracturing technology for reservoirs with low permeability. Petroleum exploration and development, 36(1), 80-85.

[101] Belyadi, A., Aminian, K., Ameri, S. and Light-Foot Boston, A., 2010. Performance of the hydraulically fractured horizontal wells in low permeability formation. Paper SPE 139082, The SPE Eastern Regional Meeting held in Morgantown, West Virginia, USA, October, 12-14.

[102] Briceno, M., Summers, L.E. and Quijada, O.J., 2002. Horizontal wells pressure build up analysis in Orinoco heavy oil Belt. Paper SPE/Petroleum Society of CIM/CHOA 78969, The 2002 SPE International Thermal Operations and Heavy Oil Symposium and International Horizontal Well Technology Conference, Calgary, Alberta, Canada, November,4-7.

[103] Al-Mohannadi, N., Ozkan, E. and Kazemi, H., 2004. Grid system requirements in numerical modeling of pressure transient tests in horizontal wells. Paper SPE 92041, The 2004 SPE International Petroleum Conference in Mexico, Puebla, Mexico, November, 8-9.

[104] Al-Thawad, F., Agyapong, D., Banerjee, R. and Issaka, M.B., 2004. Pressure transient analysis of horizontal wells in a fractured reservoir; Gridding between art and science. Paper SPE 87013, The 2004 Asia Pacific Conference on Integrated Modelling for Asset Management, Kuala Lumpur, Malaysia, March 29-30.

[105] Ertekin, T., Sung, W. and Schwerer, C.F., 1988. Production performance analysis of horizontal drainage wells for the degasification of coal seams. Journal of Petroleum Technology, 40(5), 625-632.

[106] Osisanya, O.S. and Schaffitzel, F.R., 1996. A review of horizontal drilling and completion techniques for recovery of Coalbed Methane. Paper SPE 37131, The 1996 SPE International Conference on Horizontal Well Technology, Calgary, Canada, November, 18-20.

[107] Mutalik, P.N. and Magness, W.D., 2006. Production data analysis of Horizontal CBM wells in Arkoma Basin. Paper SPE 103206, The SPE Annual Technical Conference and Exhibition, San Antonio, Texas, U.S.A., September, 24-27.

[108] Clarkson, C.R., Jordan, C.L. and Blasingame, T.A., 2009. Production data analysis of fractured and horizontal CBM wells. Paper SPE 125929, The SPE Eastern Regional Meeting, Charleston, West Virginia, USA, September, 23-25.

[109] Meszaros, G., 2007. Geosteering horizontal Coalbed Methane reservoirs: A case study. Paper SPE 107714, The SPE Rocky Mountain Oil & Gas Technology Symposium, Denver, Colorado, U.S.A., April, 16-18.

[110] Lehocky, N. and Jonkers, J., 2008. CBM coal fracture orientation in vertical and horizontal wellbores from electrical images to optimize horizontal well placement. SPWLA 49th Annual Logging Symposium, Edinburgh, Scotland, UK, May, 25-28.

[111] Soliman, M.Y., Miranda, C. and Wang, H.M., 2010. Application of after closure analysis to a dual porosity formation, to CBM, and to a fractured horizontal well. SPE production & operations, 25(4), 472-483.

[112] Sani, M.A. and Ejefodomi, A.E., 2011. Horizontal wells drilling activity in South Texas unconventional gas resources and microseismic hydraulic fracturing monitoring application to reduce risk and increases the success rate. Paper SPE 149061, The SPE/DGS Saudi Arabia Section Technical Symposium and Exhibition, Al-Khobar, Saudi Arabia, May, 15-18.

[113] Maricic, N., Mohaghegh, S.D. and Artun, E., 2005. A parametric study on the benefits of drilling horizontal and multilateral wells in Coalbed Methane reservoirs. Paper SPE 96018, The SPE Annual Technical Conference and Exhibition, Dallas, Texas, October, 9-12.

[114] Konopczynski, M.R., Hughes, J. and Best, J.E., 1995. A novel approach to initiating multi-lateral horizontal wells. SPE/IADC 29385, The SPE/IADC Drilling Conference, Amsterdam, February, 26-March, 2.

[115] Vo, D.T. and Madden, M.V., 1995. Performance evaluation of trilateral wells: field examples. SPE Reservoir Engineering, 10(1), 22-28.

[116] Winton, J.A.C., Lodder, R.J. and Smit, A.L., 1998. Multi-lateral well construction: A multi-benefit drilling technology. Paper IADC/SPE 39353, IADC/SPE Drilling Conference, Dallas, Texas, March, 3-6.

[117] Ross, B., 1996. Three methods of achieving a true hydraulic seal/control across a junction in a multilateral well. Paper SPE 36993, The SPE Asia Pacific Oil & Gas Conference, Adelaide, Australia, October, 28-31.

[118] Zhu, D., Hill, A.D. and Landrum, W.R., 2002. Evaluation of crossflow effects in multilateral wells. Paper SPE 75250, The SPE/DOE Improved Oil Recovery Symposium, Tulsa, Oklahoma, April, 13-17.

[119] DeMong, K. and Rivenbark, M., 2000. Recent case histories of offshore dual multilateral completion systems in the Middle East. Paper SPE 87243, The 9th Abu Dhabi International Petroleum Exhibition and Conference, Abu Dhabi, U.A.E., October, 15-18.

[120] Hembling, D., Salamy, S., Qatani, A., Carter, N. and Jacob, S., 2006. Swell packers: Enabling openhole intelligent and multilateral well completions for enhanced oil recovery. Paper IADC/SPE 100824, IADC/SPE Asia Pacific Drilling Technology Conference and Exhibition, Bangkok, Thailand, November, 13-15.

[121] Mohamed, M.G. and Monhamed, B.E., 2008. Multi lateral horizontal well application for improving the oil recovery of a mature field, Intisar N. Field, Concession 103-Libya. Paper SPE 112125, The SPE North Africa Technical Conference and Exhibition, Marrakech, Morocco, March, 12-14.

[122] Salameh, A.L., 2001. Improved oil recovery by new horizontalization strategy in giant carbonate reservoir. Paper SPE 68075, The SPE Middle East Oil Show, Bahrain, March, 17-20.

[123] Yurkiw, F.J., Gilmour, S.G., Barrenechea, P.J., Wasslen, R.D., Churcher, P.L. and Pustanyk, R.H., 1996. Multi-Lateral underbalanced drilling for field optimization: Weyburn Unit, Saskatchewan, Canada. Paper SPE 37064, The SPE International Conference on Horizontal Well Technology, Calgary, Canada, November, 18-20.

[124] Retnanto, A., Frick, T.P., Brand, C.W. and Economides, M.J., 1996. Optimal configurations of multiple-lateral horizontal wells. Paper SPE 35712, The SPE Western Regional Meeting, Anchorage, U.S.A., May, 22-24.

[125] Lee, S.S., Veeken, C.A.M. and Frens, M.A., 2001. Multi-lateral well modelling to optimise well design and cost. Paper 68728, The SPE Asia Pacific Oil and Gas Conference and Exhibition, Jakarta, Indonesia, April, 17-19.

[126] Joshi, S., 2000. Horizontal and multi-lateral wells: performance analysis-an art or a science? JCPT, 39(10), 19-23.

[127] Tabatabaei, M. and Ghalambor, A., 2009. A new method to predict performance of horizontal and multilateral wells. Paper IPTC 13122, The International Petroleum Technology Conference, Doha, Qatar, December, 7-9.

[128] Thomas, E. and Suhy, P.E., 2009. Plugging and abandoning multilateral horizontal CBM wells for safe mine through operations. Paper 125734, The SPE Eastern Regional Meeting, Charleston, West Virginia, USA, September, 23-25.

[129] Kikuchi, S. and Fada'q, S.A., 2006. Challenges, lessons learned, and successful implementations of multilateral completion technology offshore Abu Dhabi. Paper SPE 101385, The Abu Dhabi International Petroleum Exhibition and Conference, Abu Dhabi, U.A.E., November, 5-8.

[130] Patching, T.H., 1970. Retention and release of gas in coal-a review. Canadian Mining and Metallurgical Bulletin, 63(703), 1302-1308.

[131] Smith, H.D., Bromhal, G., Neal Sams, W., Jikich, S. and Ertekin, T., 2005. Simulating carbon dioxide sequestration/ECBM production in coal seams: effects of permeability anisotropies and the diffusion-time constant. SPE Reservoir Evaluation & Engineering, 8(2), 156-163.

[132] Balan, H.O. and Gumrah, F., 2009. Enhanced Coalbed Methane recovery with respect to physical properties of coal and operational parameters. Journal of Canadian Petroleum Technology, 48(8), 56-61.

[133] Wang, G. X., Wei, X.R., Rudolph, V., Wei, C.T. and Qin, Y., 2009. A multi-scale model for CO_2 sequestration enhanced Coalbed Methane recovery. Chemical engineering, 3(1), 20-25.

[134] Ronny, P., Giuseppe, S. and Marco, M., 2011. A model for enhanced coal bed methane recovery aimed at carbon dioxide storage. Adsorption, 17(5), 889-900.

[135] Shimada, S., Li, H.Y., Oshima, Y. and Adachi, K., 2005. Displacement behavior of CH_4 adsorbed on coals by injecting pure CO_2, N_2 and CO_2–N_2 mixture. Environmental Geology, 49(1), 44-52.

[136] Mazumder, S., Karnik, A. and Wolf, K.H., 2006. Swelling of coal in response to CO_2 Sequestration for ECBM and its effect on fracture permeability. SPE Journal, 11(3), 390-398.

[137] Jessen, K., Tang, G.Q. and Kovscek, R.A., 2008. Laboratory and simulation investigation of enhanced Coalbed Methane recovery by gas injection. Transport in Porous Media, 73(2), 141-159.

[138] Shi, J.Q., Mazumder, S. and Wolf, K.H., 2008. Competitive methane desorption by supercritical CO_2 injection in Coal. Transport in Porous Media, 75(1), 35-54.

[139] Gorucu, B.F., Jikich, A.S., Bromhal, S.G., Neal, S.W., Ertekin, T. and Smith, H.D., 2007. Effects of matrix shrinkage and swelling on the economics of Enhanced Coalbed Methane Production and CO_2 sequestration in coal. SPE Reservoir Evaluation & Engineering, 10(4), 382-392.

[140] Mitra, A. and Harpalani, S., 2007. Modeling incremental swelling of coal matrix with CO_2 Injection in Coalbed Methane reservoirs. Paper SPE 111184, The SPE Eastern Regional Meeting, Lexington, Kentucky, U.S.A., October, 17-19.

[141] Lin, W., Tang, G.-Q. and Kovscek ,A.R., 2008. Sorption induced permeability change of coal during gas injection processes. SPE Reservoir Evaluation & Engineering, 11(4), 792-802.

[142] Mazumder, S. and Wolf, K.H., 2008. Differential swelling and permeability change of coal in response to CO_2 injection for ECBM. Paper SPE 114791, The SPE Asia Pacific Oil & Gas Conference and Exhibition, Perth, Australia, October, 20-22.

[143] Jessen, K., Lin W.J. and Kovscek R.A., 2007. Multicomponent sorption modeling in ECBM displacement calculations. Paper SPE 110258, The SPE Annual Technical Conference and Exhibition, Anaheim, California, U.S.A., November, 11-14.

[144] Sinayuc, C. and Gumrah, F., 2008. Modelling of ECBM recovery from Amasra coalbed in Zonguldak basin, Turkey. Paper SPE 2008-081, The Canadian International Petroleum Conference/SPE Gas Technology Symposium 2008 Joint Conference (the Petroleum Society's 59th Annual Technical Meeting), Calgary, Alberta, Canada, June, 17-19.

[145] Calderon, C.E., Mohaghegh, S.D. and Bromhal, G., 2010. Characterization and simulation of ECBM: history matching of forecasting CO_2 sequestration in Marshal County, West Virginia. Paper SPE 139034, The SPE Eastern Regional Meeting, Morganotwn, West Virginia, USA, October, 12-14.

[146] Wu, J., 1994. Coal Absorption Method of Calculating Coal Surface Energy and It's Significance. Coal Geology & Exploration (in Chinese), 22 (2):18-23.

[147] Govier, G.W. and Aziz K., 1973. The flow of Complex Mixtures in Pipes. Journal of Applied Mechanics, 40(2), 404.

[148] Ouyang, Liang B., Aziz, K., 1998. A simplified Approach to Couple Wellbore Flow and Reservoir Inflow for Arbitrary Well Configurations. Paper SPE 48936-MS, SPE Annual Technical Conference and Exhibition, New Orleans, Louisiana, September, 27-30.

[149] Abou-Kassem, J.H., Mattar, L and Dranchuk, P.M, 1990. Computer calculations of compressibility of natural gas[J]. The Journal of Canadian Petroleum Technology, Vol 29, No. 5, 105-108.

[150] Arri, L.E., Yee, D., Morgan, W.D. and Jeansonne, M.W., 1992. Modeling Coalbed Methane production with binary gas sorption. The SPE Rocky Mountain Regional Meeting, Casper, Wyoming, May, 18-21.

[151] Scherer, G.W., 1986. Dilation of porous glass. Journal of the American Ceramic Society, 69(6), 473-480.

[152] Hu, X.H., Zheng, S.Y., Hu, S.M., Zhang, D.L. and Huo, Y.Y., 2011.Well testing interpretation for two phase CBM reservoir through pressure square method. Journal of Oil and Gas Technology, 33(2), 118-122.

[153] Craft, B.C., Hawkins, M.F. and Terry, R.E., 1991. Applied Petroleum Reservoir Engineering. Old Tappan, NJ (USA); Prentice Hall Inc, 424p.